Cell Metabolism

Best of 2014

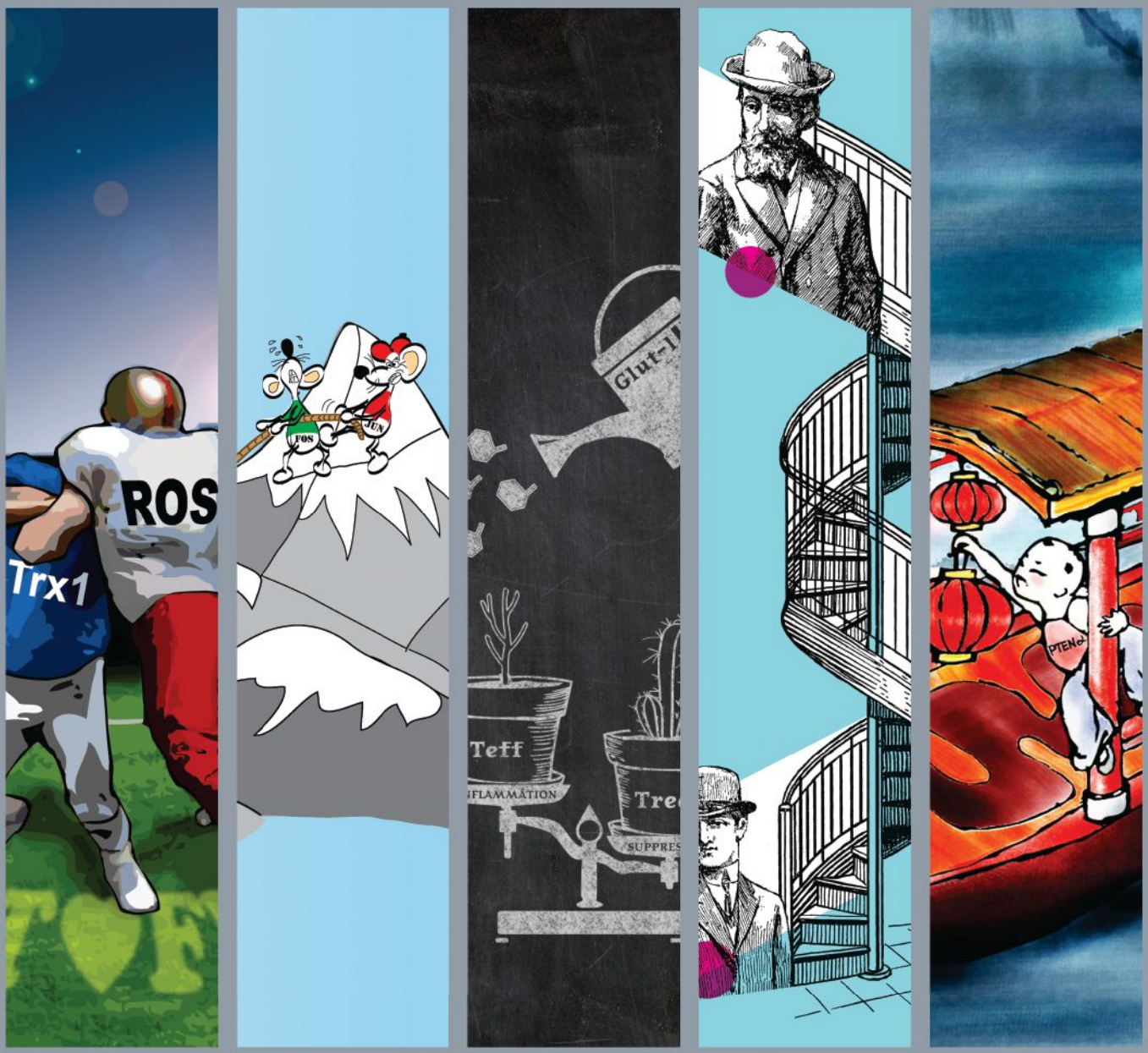

Featuring a *Cell Metabolism* SnapShot

CellPress
www.cell.com

Introducing

bio-techne®

HIGHEST QUALITY PRODUCT PORTFOLIO

TRUSTED GLOBAL BRANDS

R&D systems NOVUS BIOLOGICALS™ TOCRIS

bio-techne® LEARN MORE bio-techne.com/launch

Building Innovation Opportunities

bio-techne.com	North America	Europe • Middle East • Africa	China	Rest of World
info@bio-techne.com techsupport@bio-techne.com	TEL 800 343 7475	TEL +44 (0)1235 529449	info.cn@bio-techne.com TEL +86 (21) 52380373	bio-techne.com/find-us/distributors TEL +1 612 379 2956

Bio-Techne is a trading name for R&D Systems

“ WE’RE BRINGING A NEW PERSPECTIVE TO

cancer metabolism research

XF technology provides the easiest and most comprehensive assessment of cancer cell metabolism, measuring glucose and glutamine metabolism, and fatty acid oxidation of cancer cells in a microplate, in real time! ”

— Kacey Caradonna PhD,
Applications Scientist
Seahorse Bioscience

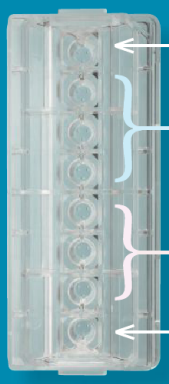

The Seahorse XFp Extracellular Flux Analyzer

Measurements of cellular glycolysis are essential to understanding cancer. The XFp Analyzer and XFp Glycolysis Stress Test Kit make it easy to measure the three key parameters of cellular glycolysis in a microplate: glycolysis, glycolytic capacity, and glycolytic reserve, revealing critical information not evident in mitochondrial respiration measurements alone.

See what’s possible.

Scan this QR code to view videos and see what the XF technology can achieve. Visit www.seahorsebio.com/cancercell for more information!

Seahorse Bioscience

MBL International Corporation

PCSK9 Screening *Made Easy*

MBL International Corporation manufactures a broad portfolio of ELISA kits for research related to atherosclerosis and coronary heart disease. Proprotein convertase subtilisin/kexin type 9 (PCSK9) has become clinically relevant as a therapeutic target for hypercholesterolemia. Since 2008, MBLI has provided optimized PCSK9 Human ELISA and PCSK9-LDLR *in vitro* binding kits as screening and discovery tools for the scientific community.

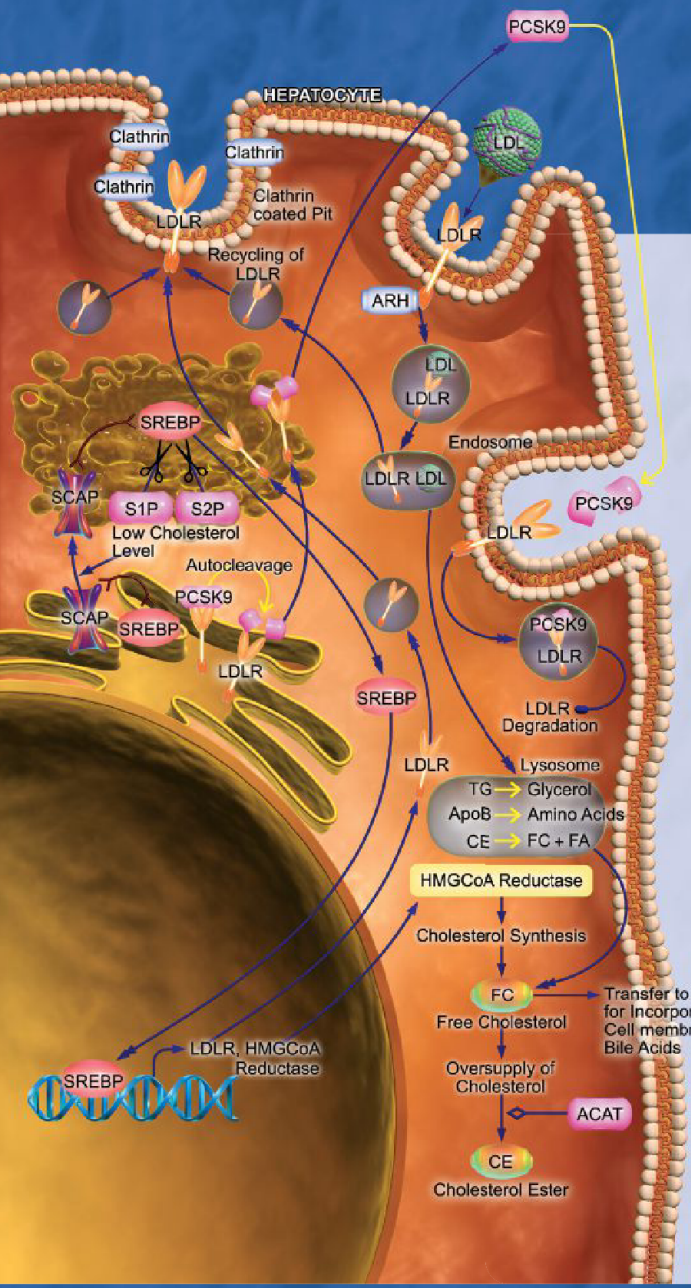

PCSK9-LDLR Binding Assay
(Code No. CY-8150)

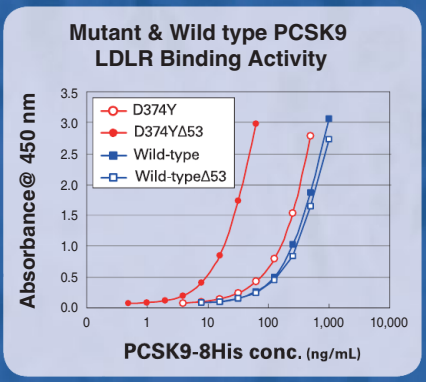

Total PCSK9 Assay (Code No. CY-8079)

Effect of inhibitors on secretion of PCSK9 in A431

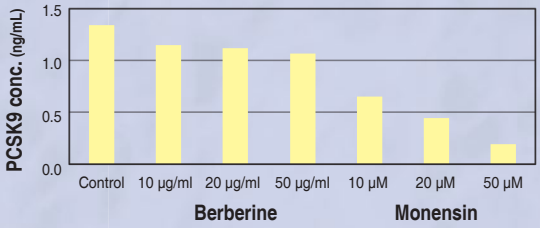

Effect of inhibitors on secretion of PCSK9 in SW480

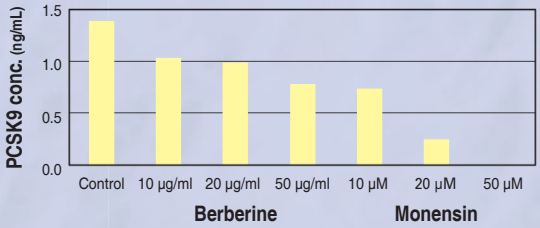

References

Lambert G, et al, J. Am. Coll. Cardiol., in press
Abujrad H, et al, Atherosclerosis, 233, 123-129 (2014)
Lee CJ, et al, Metabolism, 62, 845-850 (2013)
Cameron J, et al, Transl. Res., 160, 125-130 (2012)

Contact MBL International today to learn more about our products and how we can help you discover ways to make your science more efficient and effective.

mblintl.com • 800-200-5459 • 781-939-6963

life.science.discovery.™

MC-RUO-017

Foreword

Three years ago, Cell Press launched the "Best of" reprint collections across a number of our journals, including *Cell Metabolism*. This remarkably popular series highlights some of the most noteworthy papers published in the previous calendar year. We proudly welcome you to the 2014 edition of *Best of Cell Metabolism*. In looking back at the papers published during 2014, we wanted to provide our readers with a sense of the various topics and findings in which they and their colleagues have shown significant interest. *Cell Metabolism* is published monthly in two volumes each year, with each volume covering 6 months. In order to take into consideration the amount of time since publication, we have selected nine of the most-accessed articles from volumes 19 and 20, which cover the first and second halves of 2014, respectively. We use the number of requests for PDF and full-text HTML versions of a given article up through the end of June 2014 to determine the most-accessed articles, with attention and weighting given to the time since publication. We acknowledge that no single measurement can truly be indicative of "the best" research papers over a given period of time. This is especially true when sufficient time has not necessarily passed to allow one to fully appreciate the relative importance of a discovery. That said, we think it is still informative to look back at what the community found most interesting in *Cell Metabolism* over the course of 2014.

In this reprint collection, we present a review and several short and full-length articles. Throughout the collection, you will see a range of exciting topics, including the molecular mechanisms and clinical applications of fasting, analysis of white to brown fat energy expenditure in cancer-associated cachexia, and an examination of the role of adipocyte inflammation in tissue expansion in remodeling. We've also included a SnapShot focusing on Sirtuins, NAD, and aging.

We hope that you will enjoy reading this special collection and that you will visit www.cell.com/cell-metabolism/home to check out the latest findings that we have had the privilege to publish.

We invite you to join us as *Cell Metabolism* celebrates 10 years! For a decade, *Cell Metabolism* has been publishing novel reports in metabolic biology, from molecular and cellular biology to translational studies. Check out www.cell.com/cell-metabolism/ten to see how we are commemorating the milestones, breakthroughs, and achievements of the last 10 years and looking forward to new challenges in the decade to come.

Also, be sure to visit www.cell.com to find other high-quality papers published in the full collection of Cell Press journals.

Finally, we are grateful for the generosity of our sponsors, who helped to make this reprint collection possible.

Cell Metabolism

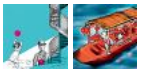

For information for the Best of Series, please contact:
Jonathan Christison
Program Director, Best of Cell Press
e: jchristison@cell.com
p: 617-397-2893
t: @CellPressBiz

Cell Metabolism

Best of 2014

Review

Articles

Cell Metabolism
Review

Fasting: Molecular Mechanisms and Clinical Applications

Valter D. Longo[1,*] and Mark P. Mattson[2,3,*]
[1]Longevity Institute, Davis School of Gerontology and Department of Biological Sciences, University of Southern California, Los Angeles, CA 90089-2520, USA
[2]National Institute on Aging Intramural Research Program, National Institutes of Health, Baltimore, Maryland 21224, USA
[3]Department of Neuroscience, Johns Hopkins University School of Medicine, Baltimore, Maryland 21205, USA
*Correspondence: vlongo@usc.edu (V.D.L.), mark.mattson@nih.gov (M.P.M.)
http://dx.doi.org/10.1016/j.cmet.2013.12.008

Fasting has been practiced for millennia, but, only recently, studies have shed light on its role in adaptive cellular responses that reduce oxidative damage and inflammation, optimize energy metabolism, and bolster cellular protection. In lower eukaryotes, chronic fasting extends longevity, in part, by reprogramming metabolic and stress resistance pathways. In rodents intermittent or periodic fasting protects against diabetes, cancers, heart disease, and neurodegeneration, while in humans it helps reduce obesity, hypertension, asthma, and rheumatoid arthritis. Thus, fasting has the potential to delay aging and help prevent and treat diseases while minimizing the side effects caused by chronic dietary interventions.

Introduction

In humans, fasting is achieved by ingesting no or minimal amounts of food and caloric beverages for periods that typically range from 12 hr to 3 weeks. Many religious groups incorporate periods of fasting into their rituals including Muslims, who fast from dawn until dusk during the month of Ramadan, and Christians, Jews, Buddhists, and Hindus, who traditionally fast on designated days of the week or calendar year. In many clinics, patients are now monitored by physicians while undergoing water only or very low calorie (less than 200 kcal/day) fasting periods lasting from 1 week or longer for weight management and for disease prevention and treatment. Fasting is distinct from caloric restriction (CR), in which the daily caloric intake is reduced chronically by 20%–40%, but meal frequency is maintained. Starvation is instead a chronic nutritional insufficiency that is commonly used as a substitute for the word fasting, particularly in lower eukaryotes, but is also used to define extreme forms of fasting, which can result in degeneration and death. We now know that fasting results in ketogenesis; promotes potent changes in metabolic pathways and cellular processes such as stress resistance, lipolysis, and autophagy; and can have medical applications that, in some cases, are as effective as those of approved drugs such as the dampening of seizures and seizure-associated brain damage and the amelioration of rheumatoid arthritis (Bruce-Keller et al., 1999; Hartman et al., 2012; Müller et al., 2001). Findings from well-controlled investigations in experimental animals, and emerging human studies, indicate that fasting may provide effective strategies to reduce weight, delay aging, and optimize health. Here we review the fascinating and potent effects of different forms of fasting, including intermittent fasting (IF, including alternate day fasting or 2 days a week fasting, for example) and periodic fasting (PF) lasting three days or longer every 2 or more weeks. We focus on fasting and minimize the discussion of CR, a topic reviewed elsewhere (Fontana et al., 2010; Masoro, 2005).

Lessons from Simple Organisms

The remarkable effects of the typical 20%–40% CR on aging and diseases in mice and rats are often viewed as responses evolved in mammals to adapt to periods of limited availability of food (Fontana and Klein, 2007; Fontana et al., 2010; Masoro, 2005; Weindruch and Walford, 1988). However, the cellular and molecular mechanisms responsible for the protective effects of CR have likely evolved billions of years earlier in prokaryotes attempting to survive in an environment largely or completely devoid of energy sources while avoiding age-dependent damage that could compromise fitness. In fact, *E. coli* switched from a nutrient-rich broth to a calorie-free medium survive four times longer, an effect reversed by the addition of various nutrients—but not acetate, a carbon source associated with starvation conditions (Figure 1A) (Gonidakis et al., 2010). The effect of rich medium, but not acetate, in reducing longevity raises the possibility that a ketone-body-like carbon source such as acetate may be part of an "alternate metabolic program" that evolved billions of years ago in microorganisms and that now allows mammals to survive during periods of food deprivation by obtaining much of the energy by catabolizing fatty acids and ketone bodies, including acetoacetate and β-hydroxybutyrate (Cahill, 2006).

In the yeast *S. cerevisiae*, switching cells from standard growth medium to water also causes a consistent 2-fold chronological lifespan extension as well, as a major increase in the resistance to multiple stresses (Figure 1B) (Longo et al., 1997, 2012). The mechanisms of food-deprivation-dependent lifespan extension involve the downregulation of the amino acid response Tor-S6K (Sch9) pathway, as well as of the glucose-responsive Ras-adenylate cyclase-PKA pathway, resulting in the activation of the serine/threonine kinase Rim15, a key enzyme coordinating the protective responses (Fontana et al., 2010). The inactivation of Tor-S6K and Ras-AC-PKA and activation of Rim15 results in increased transcription of genes, including superoxide dismutases and heat shock proteins controlled by stress-responsive transcription factors Msn2, Msn4, and Gis1, required for the

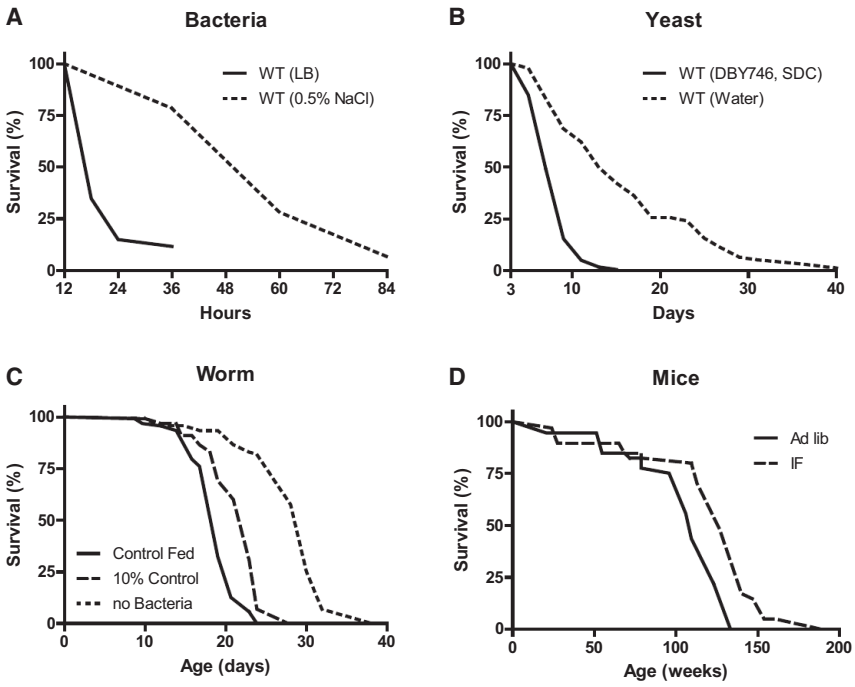

Figure 1. Fasting Extends Lifespans of Bacteria, Yeast, Worms, and Mice

(A) Lifespan of *E. coli* incubated in either LB medium or nutrient-free NaCl (Gonidakis et al., 2010).

(B) Lifespan of *S. cerevisiae* incubated in either nutrient-rich medium or water (Wei et al., 2008).

(C) Lifespan of *C. elegans* in standard nutrient-rich medium or in medium with a 90% reduction or complete removal of bacterial food (Kaeberlein et al., 2006).

(D) Lifespan of mal C57BL/6J mice on alternating day fasting initiated at 1–2 month of age (Goodrick et al., 1990).

majority of the protective effects caused by food deprivation (Wei et al., 2008). Notably, when switched to food deprivation conditions, both bacteria and yeast enter a hypometabolic mode that allows them to minimize the use of reserve carbon sources and can also accumulate high levels of the ketone-body-like acetic acid, analogously to mammals.

Another major model organism in which fasting extends lifespan is the nematode *C. elegans*. Food deprivation conditions achieved by feeding worms little or no bacteria lead to a major increase in lifespan (Figure 1C) (Kaeberlein et al., 2006; Lee et al., 2006), which requires AMPK as well as the stress resistance transcription factor DAF-16, similar to the role of transcription factors Msn2/4 and Gis1 in yeast and FOXOs in flies and mammals (Greer et al., 2007). Intermittent food deprivation also extends lifespan in *C. elegans* by a mechanism involving the small GTPase RHEB-1 (Honjoh et al., 2009).

In flies, most studies indicate that intermittent food deprivation does not affect lifespan (Grandison et al., 2009). However, food reduction or food dilution have been consistently shown to extend *Drosophila* longevity (Piper and Partridge, 2007), suggesting that flies can benefit from dietary restriction but may be sensitive to even short starvation periods.

Together, these results indicate not only that food deprivation can result in prolongevity effects in a wide variety of organisms but also underline that different organisms have different responses to fasting.

Adaptive Responses to Fasting in Mammals

In most mammals, the liver serves as the main reservoir of glucose, which is stored in the form of glycogen. In humans, depending upon their level of physical activity, 12 to 24 hr of fasting typically results in a 20% or greater decrease in serum glucose and depletion of the hepatic glycogen, accompanied by a switch to a metabolic mode in which nonhepatic glucose, fat-derived ketone bodies, and free fatty acids are used as energy sources (Figures 2 and 3). Whereas most tissues can utilize fatty acids for energy, during prolonged periods of fasting, the brain relies on the ketone bodies β-hydroxybutyrate and acetoacetate, in addition to glucose, for energy consumption (Figure 3B). Ketone bodies are produced in hepatocytes from the acetyl-CoA generated from β-oxidation of fatty acids released into the bloodstream by adipocytes, and also by the conversion of ketogenic amino acids. After hepatic glycogen depletion, ketone bodies, fat-derived glycerol, and amino acids account for the gluconeogenesis-dependent generation of approximately 80 g/day of glucose, which is mostly utilized by the brain. Depending on body weight and composition, the ketone bodies, free fatty acids, and gluconeogenesis allow the majority of human beings to survive 30 or more days in the absence of any food and allow certain species, such as king penguins, to survive for over 5 months without food (Eichhorn et al., 2011) (Figure 3C). In humans, during prolonged fasting, the plasma levels of 3-β-hydroxybutyrate are about five times those of free fatty acids and acetoacetic acid (Figure 3A and 3B). The brain and other organs utilize ketone bodies in a process termed ketolysis, in which acetoacetic acid and 3-β-hydroxybutyrate are converted into acetoacetyl-CoA and then acetyl-CoA. These metabolic adaptations to fasting in mammals are reminiscent of those described earlier for *E. coli* and yeast, in which acetic acid accumulates in response to food deprivation (Gonidakis et al., 2010; Longo et al., 2012). In yeast, glucose, acetic acid, and ethanol, but not glycerol, which in fasting mammals is generated from the breakdown of fats, accelerate aging (Fabrizio et al., 2005; Wei et al., 2009). Thus, glycerol functions as a carbon source that does not activate the proaging nutrient signaling pathways but can be catabolized by cells. It will be important to understand how the different carbon sources generated during fasting affect cellular protection and aging, and to determine whether glycerol, specific ketone bodies, or fatty acids can provide nourishment while reducing cellular aging in mammals, a possibility suggested by beneficial effects of a dietary ketone precursor in a mouse model of Alzheimer's disease (Kashiwaya et al., 2013). It will also be important to study, in various model organisms and humans, how high intake of specific types of fats (medium- versus long-chain fatty acids, etc.) in

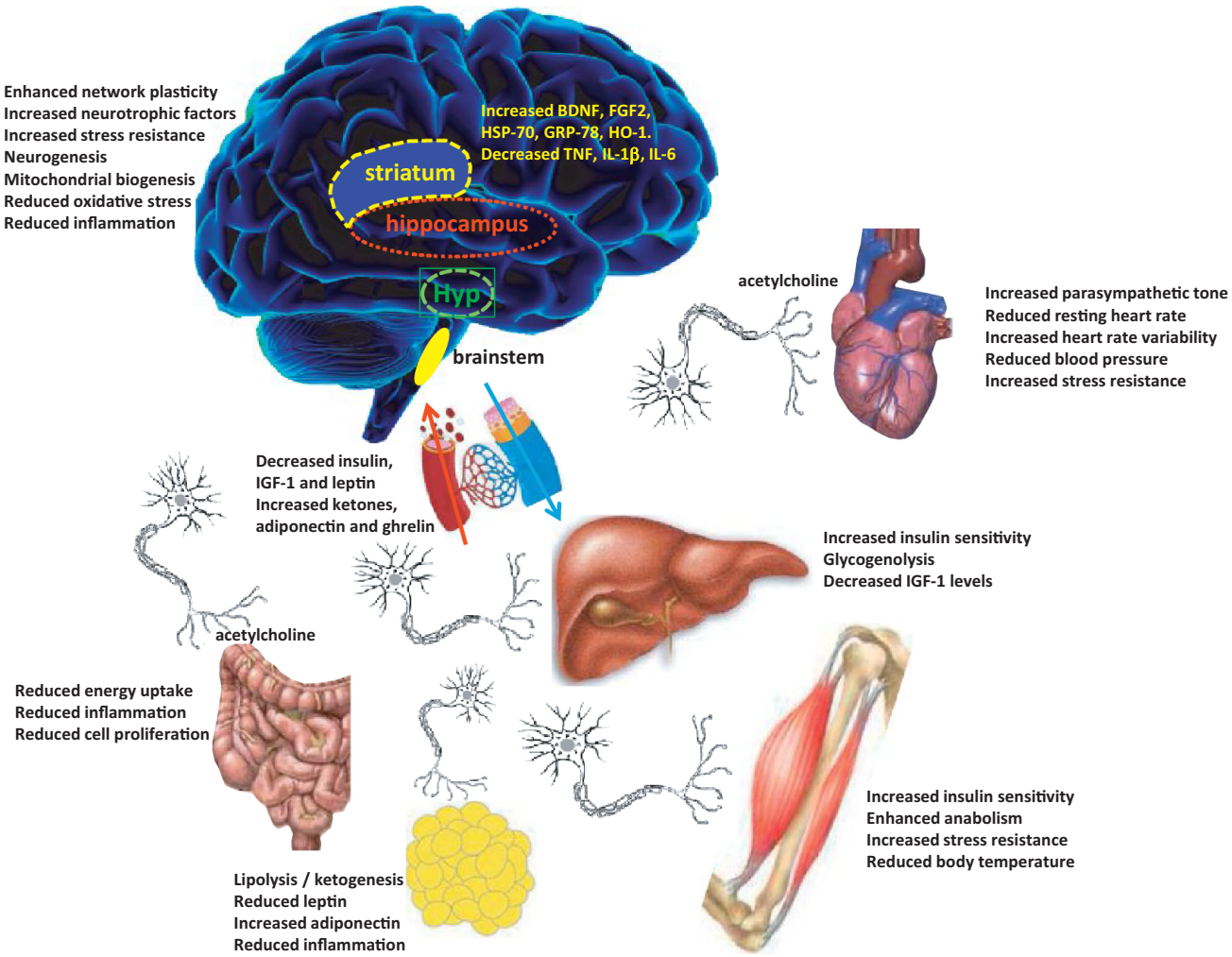

Figure 2. Pivotal Roles of the Nervous and Endocrine Systems as Mediators of Adaptive Responses of Major Organ Systems to Intermittent Fasting

IF modifies brain neurochemistry and neuronal network activity in ways that optimize brain function and peripheral energy metabolism. Four brain regions that are particularly important in adaptive responses to IF include the hippocampus (cognitive processing), striatum (control of body movements), hypothalamus (Hyp, control of food intake and body temperature), and brainstem (control of cardiovascular and digestive systems). The brain communicates with all of the peripheral organs involved in energy metabolism. IF enhances parasympathetic activity (mediated by the neurotransmitter acetylcholine) in the autonomic neurons that innervate the gut, heart, and arteries, resulting in improved gut motility and reduced heart rate and blood pressure. By depleting glycogen from liver cells, fasting results in lipolysis and the generation of ketone bodies, causing a reduction in body fat. IF enhances insulin sensitivity of muscle and liver cells and reduces IGF-1 production. Levels of oxidative stress and inflammation are reduced throughout the body and brain in response to IF.

substitution of carbohydrates and proteins influences gluconeogenesis and glucose levels as well as aging and diseases.

Fasting and the Brain

In mammals, severe CR/food deprivation results in a decrease in the size of most organs except the brain, and the testicles in male mice (Weindruch and Sohal, 1997). From an evolutionary perspective, this implies that maintenance of a high level of cognitive function under conditions of food scarcity is of preeminent importance. Indeed, a highly conserved behavioral trait of all mammals is to be active when hungry and sedentary when satiated. In rodents, alternating days of normal feeding and fasting (IF) can enhance brain function, as indicated by improvements in performance on behavioral tests of sensory and motor function (Singh et al., 2012) and learning and memory (Fontán-Lozano et al., 2007). The behavioral responses to IF are associated with increased synaptic plasticity and increased production of new neurons from neural stem cells (Lee et al., 2002).

Particularly interesting with regard to adaptive responses of the brain to limited food availability during human evolution is brain-derived neurotrophic factor (BDNF). The genes encoding BDNF and its receptor, TrkB, appeared in genomes relatively recently, as they are present in vertebrates, but absent from worms, flies, and lower species (Chao, 2000). The prominent roles of BDNF in the regulation of energy intake and expenditure in mammals is highlighted by the fact that the receptors for both BDNF and insulin are coupled to the highly conserved PI3-kinase-Akt and MAP kinase signaling pathways (Figure 4). Studies of rats and mice have shown that running wheel exercise and IF increase BDNF expression in several regions of the brain,

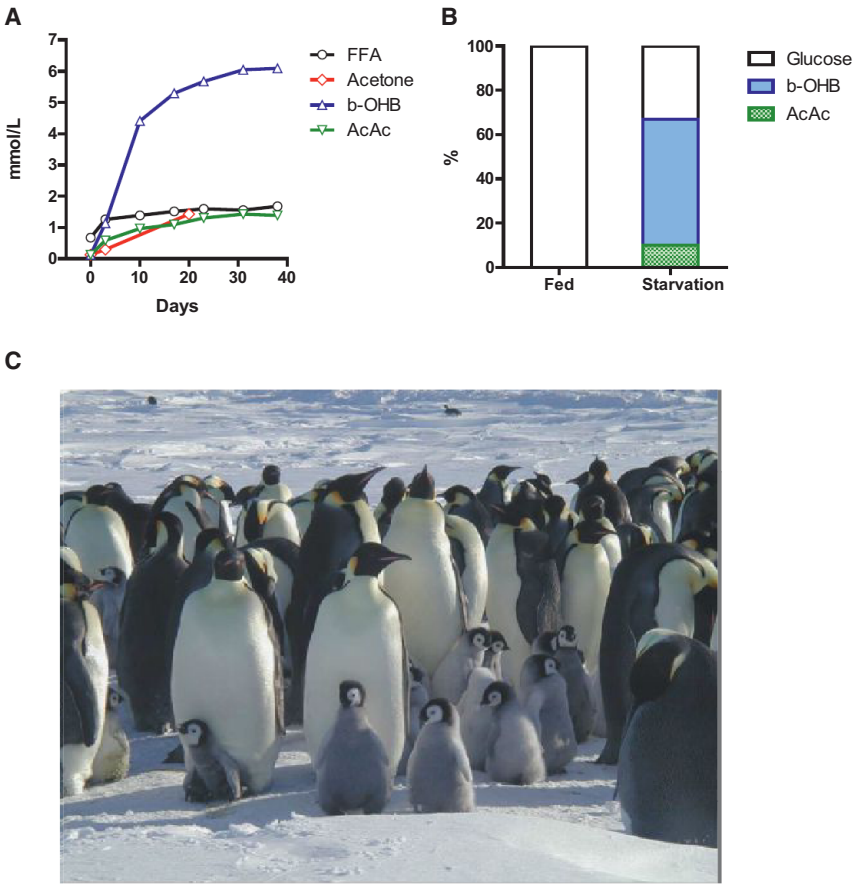

Figure 3. Fasting in Mammals

(A) Concentrations of ketone bodies (acetone, β-hydroxybutyric acid, and acetoacetic acid) and plasma free fatty acids (FFA) during 40 days of fasting in humans. Note the more than three orders of magnitude change in β-hydroxybutyrate and the doubling of FFA.

(B) Brain substrate utilization in three fasting obese volunteers after several weeks of food deprivation. Many studies suggest that human brain cells can survive with little to no glucose, but this has not been clearly demonstrated (redrawn from Cahill [2006]).

(C) Emperor penguins can fast for periods lasting for over 5 months. The picture shows Emperor penguins and their chicks a few weeks before fledging (courtesy of Yvone le Maho). The parents go back and forth between the open sea and their colony on sea ice, next to a glacier, which offers protection against wind, to regurgitate food conserved in their stomach to feed their chicks while they are themselves fasting. Fasting penguins undergo three phases (Le Maho et al., 1976; Le Maho et al., 1981; Robin et al., 1987). The first phase (phase I) represents a transition between the fed state and starvation, during which the penguin stops utilizing diet-derived energy. This phase, which lasts between several hours and several days, is characterized by a rapid decrease in protein loss. The following phase (phase II), is a ketotic phase associated with protein sparing, which can last for several days in rats to several months in obese geese, king penguin chicks, bears, and seals (Adams and Costa, 1993; Atkinson and Ramsay, 1995; Castellini and Rea, 1992;Cherel and Groscolas, 1999; Cherel and Le Maho, 1985; Cherel et al., 1988a, 1988b, 1991; Fond et al., 2013; Reilly, 1991; Robin et al., 1987, 1988). Phase III is brief, since the high protein loss leads to death. During phase III, glucose and total plasma protein levels are reduced, and uric acid increases while ketone bodies values remain low. Wild animals that fast for long periods are efficient at sparing proteins during long periods of fasting, with only 2%–10% of total energy coming from proteins versus the 20%–40% in species less adapted to fasting.

and that BDNF in part mediates exercise- and IF-induced enhancement of synaptic plasticity, neurogenesis, and neuronal resistance to injury and disease (see sections on fasting and neurodegeneration below). BDNF signaling in the brain may also mediate behavioral and metabolic responses to fasting and exercise, including regulation of appetite, activity levels, peripheral glucose metabolism, and autonomic control of the cardiovascular and gastrointestinal systems (Mattson, 2012a, 2012b; Rothman et al., 2012).

Hunger is an adaptive response to food deprivation that involves sensory, cognitive, and neuroendocrine changes that motivate and enable food-seeking behaviors. It has been proposed that hunger-related neuronal networks, neuropeptides, and hormones play pivotal roles in the beneficial effects of energy restriction on aging and disease susceptibility. As evidence, when mice in which the hypothalamic ''hunger peptide'' NPY is selectively ablated are maintained on a CR diet, the ability of CR to suppress tumor growth is abolished (Shi et al., 2012). The latter study further showed that the ability of CR to elevate circulating adiponectin levels was also compromised in NPY-deficient mice, suggesting a key role for the central hunger response in peripheral endocrine adaptations to energy restriction. Adiponectin levels increase dramatically in response to fasting; data suggest roles for adiponectin in the beneficial effects of IF on the cardiovascular system (Wan et al., 2010). The hunger response may also improve immune function during aging, as ghrelin-deficient mice exhibit accelerated thymic involution during aging, and treatment of middle-age mice with ghrelin increases thymocyte numbers and improves the functional diversity of peripheral T cell subsets (Peng et al., 2012). In addition to its actions on the hypothalamus and peripheral endocrine cells, fasting may increase neuronal network activity in brain regions involved in cognition, resulting in the production of BDNF, enhanced synaptic plasticity, and improved stress tolerance (Rothman et al., 2012). Thus, hunger may be a critical factor involved in widespread central and peripheral adaptive responses to the challenge of food deprivation for extended time periods.

Fasting, Aging, and Disease in Rodent Models

Different Fasting Methods and Aging

The major differences between IF and PF in mice are the length and the frequency of the fast cycles. IF cycles usually last 24 hr and are 1 to a few days apart, whereas PF cycles last 2 or more days and are at least 1 week apart, which is necessary for mice to regain their normal weight. One difference in the molecular

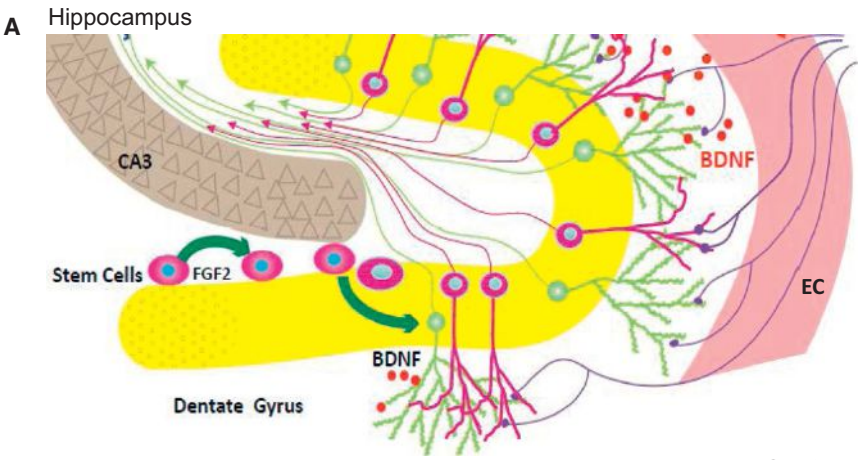

Figure 4. Neural Circuits and Cellular Signaling Pathways that Mediate Adaptive Responses of the Brain to Fasting

(A) Neurons in the hippocampus play critical roles in learning and memory and are vulnerable to dysfunction and degeneration in Alzheimer's disease, stroke, traumatic brain injury, and epilepsy. The dentate gyrus (yellow) contains neurons that receive inputs from neurons in the entorhinal cortex (EC), with the latter brain region serving as a conduit for sensory information from higher cerebral cortical regions involved in responding to sensory inputs and internally generated cognitive processes. Increased activity in these neurons occurs in response to fasting, resulting in the production of brain-derived neurotrophic factor (BDNF). BDNF promotes the growth and maintenance of dendrites and synapses and also enhances the production and survival of new neurons from neural stem cells; the newly generated neurons then integrate into the existing neural circuits. (B) Signaling pathways by which glutamate, BDNF, insulin, and glucagon-like peptide 1 (GLP-1) improve neuronal bioenergetics and protect the neurons against neurodegenerative disease and traumatic injury. Glutamate activates AMPA and N-methyl-D-aspartate (NMDA) receptors, resulting in Ca^{2+} influx and the activation of Ca^{2+}/calmodulin-sensitive (CaM) kinases which, in turn, activate the transcription factors cyclic AMP response-element-binding protein (CREB) and nuclear factor κB (NF-κB). Genes induced by the latter transcription factor include those encoding BDNF, the DNA repair enzyme APE1, the master regulator of mitochondrial biogenesis PGC-1α, and the antioxidant enzyme manganese superoxide dismutase (MnSOD). BDNF and insulin bind their respective receptor tyrosine kinases (trkB and the insulin receptor), resulting in the activation of the PI3 kinase and Akt kinase. BDNF also stimulates mitogen-activated protein kinases (MAPK). Some of the gene targets of BDNF include PGC-1α, APE1, and the antiapoptotic protein Bcl-2. Insulin activates the mammalian target of rapamycin (mTOR) pathway to promote protein synthesis and cell growth. Finally, GLP-1 activates receptors (GLP-1R) coupled to cyclic AMP production, CREB activation, and BDNF production.

changes caused by different fasting regimes is the effect on a variety of growth factors and metabolic markers, with IF causing more frequent but less pronounced changes than PF. It will be important to determine how the frequency of specific changes, such as the lowering of insulin-like growth factor 1 (IGF-1) and glucose, affect cellular protection, diseases, and longevity. The most extensively investigated IF method in animal studies of aging has been alternate day fasting (food is withdrawn for 24 hr on alternate days, with water provided ad libitum) (Varady and Hellerstein, 2007). The magnitude of the effects of alternate day fasting on longevity in rodents depends upon the species and age at regimen initiation, and can range from a negative effect to as much as an 30% lifespan extension (Figure 1D) (Arum et al., 2009; Goodrick et al., 1990). IF every other day extended the lifespan of rats more than fasting every third or fourth day (Carlson and Hoelzel, 1946). Fasting for 24 hr twice weekly throughout adult life resulted in a significant increase in lifespan of black-hooded rats (Kendrick, 1973). In rats, the combination of alternate day fasting and treadmill exercise resulted in greater maintenance of muscle mass than did IF or exercise alone (Sakamoto and Grunewald, 1987). Interestingly, when rats were maintained for 10 weeks on a PF diet in which they fasted 3 consecutive days each week, they were less prone to hypoglycemia during 2 hr of strenuous swimming exercise as a result of their accumulation of larger intramuscular stores of glycogen and triglycerides (Favier and Koubi, 1988). Several major physiological responses to fasting are similar to those caused by regular aerobic exercise, including increased insulin sensitivity and cellular stress resistance, reduced resting blood pressure and heart rate, and increased heart rate variability as a result of increased parasympathetic tone (Figure 2) (Anson et al., 2003; Mager et al., 2006; Wan et al., 2003). Emerging findings suggest that exercise and IF retard aging and some age-related diseases by shared mechanisms involving improved cellular stress adaptation (Stranahan and Mattson, 2012). However, in two different mouse genetic backgrounds, IF did not extend mean lifespan and even reduced lifespan when initiated at 10 months (Goodrick et al., 1990). When initiated at 1.5 months, IF either increased longevity or had no effect (Figure 1D) (Goodrick et al., 1990). These results in rodents point not only to conserved effects of fasting on lifespan but also to the need for a much better understanding of the type of fasting that can maximize its longevity effects and the mechanisms responsible for the detrimental effects that may be counterbalancing antiaging effects. For example, one possibility is that fasting may be consistently protective in young and middle-aged laboratory rodents that are either gaining or maintaining a body weight, but may be detrimental in older animals that, similarly to humans, begin to lose weight at advanced ages. Notably, whereas bacteria, yeast, and humans can survive for several weeks or more without nutrients, most

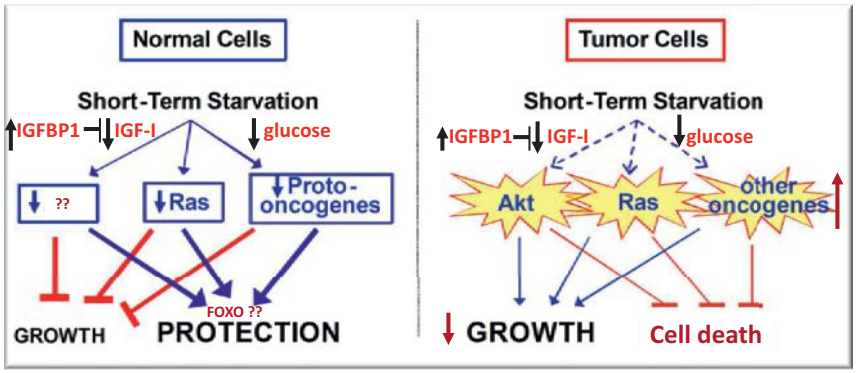

Figure 5. Differential Stress Resistance and Sensitization in Aging, Disease Prevention, and Cancer Treatment

(A) In both mice and humans, fasting for 2 or 5 days, respectively, causes an over 50% decrease in IGF-I, a 30% or more decrease in glucose, and a 5–10-fold increase in the IGF-1 binding protein and inhibitor IGFBP1 (Cahill, 2006; Lee et al., 2012; Raffaghello et al., 2008; Thissen et al., 1994a, 1994b). These and other endocrinological alterations affect the expression of hundreds of genes in many cell types and the consequent reduction or halting of growth and elevation in stress resistance, which may be dependent in part on FOXO and other stress resistance transcription factors. These periodically extreme conditions can promote changes, which are long lasting and delay aging and disease independently of calorie restriction, although the cellular mechanisms responsible for these effects remain poorly understood. In the presence of chemotherapy drugs, fasting can promote the protection of normal, but not cancer, cells (differential stress resistance [DSR]), since oncogenic pathways play central roles in inhibiting stress resistance, and therefore, cancer cells are unable to switch to the stress response mode.

(B) The extreme changes caused by fasting, and particularly the very low IGF-1 and glucose levels and high IGFBP1, also generate a tumor prevention environment that promotes cancer cell death, since transformed cells have acquired a number of mutations that progressively decrease their ability to adapt to extreme environments (differential stress sensitization [DSS]) (Guevara-Aguirre et al., 2011; Lee et al., 2010, 2012).

strains of mice are unable to survive more than 4 or 5 days without food. The age-dependent weight loss may make this sensitivity to long periods of fasting worse.

Fasting and Cancer

Fasting can have positive effects in cancer prevention and treatment. In mice, alternate day fasting caused a major reduction in the incidence of lymphomas (Descamps et al., 2005), and fasting for 1 day per week delayed spontaneous tumorigenesis in p53-deficient mice (Berrigan et al., 2002). However, the major decrease in glucose, insulin, and IGF-1 caused by fasting, which is accompanied by cell death and/or atrophy in a wide range of tissues and organs including the liver and kidneys, is followed by a period of abnormally high cellular proliferation in these tissues, driven in part by the replenishment of growth factors during refeeding. When combined with carcinogens during refeeding, this increased proliferative activity can actually increase carcinogenesis and/or precancerous lesions in tissues including liver and colon (Tessitore et al., 1996). Although these studies underline the need for an in-depth understanding of its mechanisms of action, fasting, when applied correctly even in the presence of carcinogens, is expected to have cancer-preventive effects, as indicated by the studies above and by the findings that multiple cycles of PF can be as effective as toxic chemotherapy in the treatment of some cancers in mice (Lee et al., 2012).

In the treatment of cancer, fasting has been shown to have more consistent and positive effects. PF for 2–3 days was shown to protect mice from a variety of chemotherapy drugs, an effect called differential stress resistance (DSR) to reflect the inability of cancer cells to become protected because oncogenes negatively regulate stress resistance, and prevent cancer cells from becoming protected (Figure 5) (Raffaghello et al., 2008). PF also causes a major sensitization of various cancer cells to chemo treatment, since it fosters an extreme environment in combination with the stress conditions caused by chemotherapy. In contrast to the protected state entered by normal cells during fasting, cancer cells are unable to adapt, a phenomenon called differential stress sensitization (DSS), based on the notion that most mutations are deleterious and that the many mutations accumulated in cancer cells promote growth under standard conditions but render them much less effective in adapting to extreme environments (Lee et al., 2012). In mouse models of metastatic tumors, combinations of fasting and chemotherapy that cause DSR and DSS result in 20%–60% cancer-free survival compared to chemotherapy or fasting alone, which are generally not sufficient to cause any cancer-free survival (Lee et al., 2012; Shi et al., 2012). Thus, the idea that cancer could be treated with weeks of fasting alone, made popular decades ago, may be only partially true, at least for some type of cancers, but is expected to be ineffective or only partially effective for many types of cancers. The efficacy of long-term fasting alone (2 weeks or longer) in cancer treatment will need to be tested in carefully designed clinical trials in which side effects, including malnourishment, cachexia, and possibly a weakened immune system and increased susceptibility to certain infections, are carefully monitored. By contrast, animal data from multiple laboratories indicate that the combination of fasting cycles with chemotherapy is highly and consistently effective in enhancing chemotherapeutic index and has high translation potential. A number of ongoing trials should soon begin to determine the efficacy of fasting in enhancing cancer treatment in the clinic.

Fasting and Neurodegeneration

Compared to ad-libitum-fed controls, rats and mice maintained on an IF diet exhibit less neuronal dysfunction and degeneration and fewer clinical symptoms in models of Alzheimer's disease (AD), Parkinson's disease (PD), and Huntington's disease (HD). These models include transgenic mice expressing mutant human genes that cause dominantly inherited AD (amyloid precursor protein and presenilin-1) and frontotemporal lobe dementia (τ) (Halagappa et al., 2007), PD (α-synuclein) (Griffioen et al., 2012), and HD (huntingtin) (Duan et al., 2003), as well as neurotoxin-based models pertinent to AD, PD, and HD (Bruce-Keller et al., 1999; Duan and Mattson, 1999). Animals on an IF diet also fare better than ad-libitum-fed controls after acute injury, including severe epileptic seizures, stroke, and traumatic brain and spinal cord injuries (Arumugam et al., 2010; Bruce-Keller et al., 1999; Plunet et al., 2008).

Several interrelated cellular mechanisms contribute to the beneficial effects of IF on the nervous system, including reduced

accumulation of oxidatively damaged molecules, improved cellular bioenergetics, enhanced neurotrophic factor signaling, and reduced inflammation (Mattson, 2012a). The latter neuroprotective mechanisms are supported by studies showing that IF diets boost levels of antioxidant defenses, neurotrophic factors (BDNF and FGF2), and protein chaperones (HSP-70 and GRP-78) and reduce levels of proinflammatory cytokines (TNF-α, IL-1β, and IL-6) (Figure 4) (Arumugam et al., 2010). IF may also promote restoration of damaged nerve cell circuits by stimulating synapse formation and the production of new neurons from neural stem cells (neurogenesis) (Lee et al., 2002). Interestingly, while beneficial in models of most neurodegenerative conditions, there is evidence that fasting can hasten neurodegeneration in some models of inherited amyotrophic lateral sclerosis, perhaps because the motor neurons affected in those models are unable to respond adaptively to the moderate stress imposed by fasting (Mattson et al., 2007; Pedersen and Mattson, 1999).

Fasting and the Metabolic Syndrome

Metabolic syndrome (MS), defined as abdominal adiposity, combined with insulin resistance, elevated triglycerides, and/or hypertension, greatly increases the risk of cardiovascular disease, diabetes, stroke, and AD. Rats and mice maintained under the usual ad libitum feeding condition develop an MS-like phenotype as they age. MS can also be induced in younger animals by feeding them a diet high in fat and simple sugars (Martin et al., 2010). IF can prevent and reverse all aspects of the MS in rodents: abdominal fat, inflammation, and blood pressure are reduced; insulin sensitivity is increased; and the functional capacities of the nervous, neuromuscular, and cardiovascular systems are improved (Castello et al., 2010; Wan et al., 2003). Hyperglycemia is ameliorated by IF in rodent models of diabetes (Pedersen et al., 1999), and the heart is protected against ischemic injury in myocardial infarction models (Ahmet et al., 2005). A protective effect of fasting against ischemic renal and liver injury occurs rapidly, with 1–3 days of fasting improving functional outcome and reducing tissue injury and mortality (Mitchell et al., 2010). Six days on a diet missing just a single essential amino acid, such as tryptophan, can also elicit changes in metabolism and stress resistance, similar to those caused by fasting, which are dependent on the amino-acid-sensing kinase Gcn2 (Peng et al., 2012).

Multiple hormonal changes that typify MS in humans are observed in rodents maintained on high-fat and -sugar diets, including elevated levels of insulin and leptin and reduced levels of adiponectin and ghrelin. Elevated leptin levels are typically reflective of a proinflammatory state, whereas adiponectin and ghrelin can suppress inflammation and increase insulin sensitivity (Baatar et al., 2011; Yamauchi et al., 2001). Local inflammation in hypothalamic nuclei that control energy intake and expenditure may contribute to a sustained positive energy balance in MS (Milanski et al., 2012). Fasting results in a lowering of insulin and leptin levels and an elevation of adiponectin and ghrelin levels. By increasing insulin and leptin sensitivity, suppressing inflammation, and stimulating autophagy, fasting reverses all the major abnormalities of the MS in rodents (Singh et al., 2009; Wan et al., 2010). Finally, in addition to its many effects on cells throughout the body and brain, IF may elicit changes in the gut microbiota that protect against MS (Tremaroli and Bäckhed, 2012). Naturally, the challenge of applying fasting-based interventions to treat MS in humans is a major one, as some obese individuals may have difficulties in following IF for long periods.

Fasting, Aging, and Disease in Humans

Fasting and Factors Implicated in Aging

Clinical and epidemiological data are consistent with an ability of fasting to retard the aging process and associated diseases. Major factors implicated in aging whose generation are accelerated by gluttonous lifestyles and slowed by energy restriction in humans include the following: (1) oxidative damage to proteins, DNA, and lipids; (2) inflammation; (3) accumulation of dysfunctional proteins and organelles; and (4) elevated glucose, insulin, and IGF-I, although IGF-1 decreases with aging and its severe deficiency can be associated with certain pathologies (Bishop et al., 2010; Fontana and Klein, 2007). Serum markers of oxidative damage and inflammation, as well as clinical symptoms, are reduced over a period of 2–4 weeks in asthma patients maintained on an alternate day fasting diet (Johnson et al., 2007). Similarly, when on a 2 days/week fasting diet, overweight women at risk for breast cancer exhibited reduced oxidative stress and inflammation (Harvie et al., 2011), and elderly men exhibited reductions in body weight and body fat and improved mood (Teng et al., 2011). Additional effects of fasting in human cells that can be considered as potentially "antiaging" are inhibition the mTOR pathway, stimulation of autophagy, and ketogenesis (Harvie et al., 2011; Sengupta et al., 2010).

Among the major effects of fasting relevant to aging and diseases are changes in the levels of IGF-1, IGFBP1, glucose, and insulin. Fasting for 3 or more days causes a 30% or more decrease in circulating insulin and glucose, as well as rapid decline in the levels of IGF-1, the major growth factor in mammals, which together with insulin is associated with accelerated aging and cancer (Fontana et al., 2010). In humans, 5 days of fasting causes an over 50% decrease in IGF-1 and a 5-fold or higher increase in one of the principal IGF-1-inhibiting proteins, IGFBP1 (Thissen et al., 1994a). This effect of fasting on IGF-1 is mostly due to protein restriction, and particularly to the restriction of essential amino acids, but is also supported by calorie restriction since the decrease in insulin levels during fasting promotes reduction in IGF-1 (Thissen et al., 1994a). Notably, in humans, chronic calorie restriction does not lead to a decrease in IGF-1 unless combined with protein restriction (Fontana et al., 2008).

IF can be achieved in with a minimal decrease in overall calorie intake if the refeeding period in which subjects overeat is considered. Thus, fasting cycles provide a much more feasible strategy to achieve the beneficial effects of CR, and possibly stronger effects, without the burden of chronic underfeeding and some of the potentially adverse effects associated with weight loss or very low BMIs. In fact, subjects who are moderately overweight (BMI of 25–30) in later life can have reduced overall mortality risk compared to subjects of normal weight (Flegal et al., 2013). Although these results may be affected by the presence of many existing or developing pathologies in the low weight control group, they underline the necessity to differentiate between young and middle age individuals and elderly individuals when using CR or fasting to reduce weight or delay aging.

Although extreme dietary interventions during old age may continue to protect from age-related diseases, they could have detrimental effects on the immune system and the ability to respond to certain infectious diseases, wounds, and other challenges (Kristan, 2008; Reed et al., 1996). However, IF or PF designed to avoid weight loss and maximize nourishment have the potential to have beneficial effects even on infectious diseases, wounds, and other insults even in the very old. Studies to test the effect of IF or PF regimens on markers of aging, cancer, cognition and obesity are in progress (V.D.L. and M.P.M., unpublished data).

Fasting and Cancer

Fasting has the potential for applications in both cancer prevention and treatment. Although no human data are available on the effect of IF or PF in cancer prevention, their effect on IGF-1, insulin, glucose/IGFBP1, and ketone body levels could generate a protective environment that reduces DNA damage and carcinogenesis while at the same time creating hostile conditions for tumor and precancerous cells (Figure 5). In fact, elevated circulating IGF-1 is associated with increased risk of developing certain malignancies (Chan et al., 2000; Giovannucci et al., 2000), and individuals with severe IGF-1 deficiency caused by growth hormone receptor deficiency rarely develop cancer (Guevara-Aguirre et al., 2011; Steuerman et al., 2011). Furthermore, the serum from these IGF-1-deficient subjects protected human epithelial cells from oxidative-stress-induced DNA damage. Furthermore, once their DNA became damaged, cells were more likely to undergo programmed cell death (Guevara-Aguirre et al., 2011). Thus, fasting may protect from cancer not only by reducing cellular and DNA damage but also by enhancing the death of precancerous cells.

In a preliminary study of 10 subjects with a variety of malignancies, the combination of chemotherapy with fasting resulted in a decrease in a range of self-reported common side effects caused by chemotherapy compared to the same subjects receiving chemotherapy while on a standard diet (Safdie et al., 2009). The effect of fasting on chemotherapy toxicity and cancer progression is now being tested in clinical trials in both Europe and the US (0S-08-9 and 0S-10-3).

Fasting and Neurodegeneration

Our current understanding of the impact of IF on the nervous system and cognitive functions is largely inferred from animal studies (see above). Interventional studies to determine the impact of fasting on brain function and neurodegenerative disease processes are lacking. After 3–4 months, CR improved cognitive function (verbal memory) in overweight women (Kretsch et al., 1997) and in elderly subjects (Witte et al., 2009). Similarly, when subjects with mild cognitive impairment were maintained for 1 month on a low glycemic diet, they exhibited improved delayed visual memory, cerebrospinal fluid biomarkers of Aβ metabolism and brain bioenergetics (Bayer-Carter et al., 2011). Studies in which cognitive function, regional brain volumes, neural network activity, and biochemical analyses of cerebrospinal fluid are measured in human subjects before and during an extended period of IF should clarify the impact of IF on human brain structure and function.

Fasting, Inflammation, and Hypertension

In humans, one of the best demonstrations of the beneficial effects of long-term fasting lasting 1 to 3 weeks is in the treatment of rheumatoid arthritis (RA). In agreement with the results in rodents, there is little doubt that during the period of fasting both inflammation and pain are reduced in RA patients (Müller et al., 2001). However, after the normal diet is resumed, inflammation returns unless the fasting period is followed by a vegetarian diet (Kjeldsen-Kragh et al., 1991), a combination therapy that has beneficial effects lasting for 2 years or longer (Kjeldsen-Kragh et al., 1994). The validity of this approach is supported by four differently controlled studies, including two randomized trials (Müller et al., 2001). Therefore, fasting combined with a vegetarian diet and possibly with other modified diets provides beneficial effects in the treatment of RA. Alternate day IF also resulted in significant reductions in serum TNF-α and ceramides in asthma patients during a 2 month period (Johnson et al., 2007). The latter study further showed that markers of oxidative stress often associated with inflammation (protein and lipid oxidation) are significantly reduced in response to IF. Thus, for many patients able and willing to endure long-term fasting and to permanently modify their diet, fasting cycles would have the potential not only to augment but also to replace existing medical treatments.

Water-only and other forms of long-term fasting have also been documented to have potent effects on hypertension. An average of 13 days of water-only fasting resulted in the achievement of a systolic blood pressure (BP) below 120 in 82% of subjects with borderline hypertension with a mean 20 mm Hg reduction in BP (Goldhamer et al., 2002). BP remained significantly lower compared to baseline even after subjects resumed the normal diet for an average of 6 days (Goldhamer et al., 2002). A small pilot study of patients with hypertension (140 mm and above systolic BP) also showed that 10–11 days of fasting caused a 37–60 mm decrease in systolic BP (Goldhamer et al., 2001). These preliminary studies are promising but underscore the need for larger controlled and randomized clinical studies that focus on PF strategies that are feasible for a larger portion of the population.

For both hypertension and RA, it will be important to develop PF-mimicking diets that are as effective as the fasting regimens described above but that are also tolerable by the great majority of patients.

Fasting and the MS

PF can reverse multiple features of the MS in humans: it enhances insulin sensitivity, stimulates lipolysis, and reduces blood pressure. Body fat and blood pressure were reduced and glucose metabolism improved in obese subjects in response to an alternate day modified fast (Klempel et al., 2013; Varady et al., 2009). Overweight subjects maintained for 6 months on a twice weekly IF diet in which they consumed only 500–600 calories on the fasting days, lost abdominal fat, displayed improved insulin sensitivity, and reduced blood pressure (Harvie et al., 2011). Three weeks of alternate day fasting resulted in reductions in body fat and insulin levels in normal weight men and women (Heilbronn et al., 2005), and Ramadan fasting (two meals/day separated by approximately 12 hr) in subjects with MS resulted in decreased daily energy intake, decreased plasma glucose levels, and increased insulin sensitivity (Shariatpanahi et al., 2008). Subjects undergoing coronary angiography who reported that they fasted regularly exhibited a lower prevalence of diabetes compared to nonfasters (Horne et al., 2012).

Anti-MS effects of IF were also observed in healthy young men (BMI of 25) after 15 days of alternate day fasting: their whole-body glucose uptake rates increased significantly and levels of plasma ketone bodies and adiponectin were elevated, all of which occurred without a significant decrease in body weight (Halberg et al., 2005). The latter findings are similar to data from animal studies showing that IF can improve glucose metabolism even with little or no weight change (Anson et al., 2003). It will be important to determine if longer fasting periods, which promote a robust switch to a fat breakdown and ketone-body-based metabolism, can cause longer lasting and more potent effects.

Conclusions and Recommendations

Based on the existing evidence from animal and human studies described, we conclude that there is great potential for lifestyles that incorporate IF or PF during adult life to promote optimal health and reduce the risk of many chronic diseases, particularly for those who are overweight and sedentary. Animal studies have documented robust and replicable effects of fasting on health indicators including greater insulin sensitivity and reduced levels of blood pressure, body fat, IGF-I, insulin, glucose, atherogenic lipids, and inflammation. Fasting regimens can ameliorate disease processes and improve functional outcome in animal models of disorders that include cancer, myocardial infarction, diabetes, stroke, AD, and PD. One general mechanism of action of fasting is that it triggers adaptive cellular stress responses, which result in an enhanced ability to cope with more severe stress and counteract disease processes. In addition, by protecting cells from DNA damage, suppressing cell growth, and enhancing apoptosis of damaged cells, fasting could retard and/or prevent the formation and growth of cancers.

However, studies of fasting regimens have not been performed in children, the very old, and underweight individuals, and it is possible that IF and PF would be harmful to these populations. Fasting periods lasting longer than 24 hr, and particularly those lasting 3 or more days, should be done under the supervision of a physician and preferably in a clinic. IF- and PF-based approaches toward combating the current epidemics of overweight, diabetes, and related diseases should be pursued in human research studies and medical treatment plans. Several variations of potential ''fasting prescriptions'' that have been adopted for overweight subjects revolve around the common theme of abstaining from food and caloric beverages for at least 12–24 hr on 1 or more days each week or month, depending on the length, combined with regular exercise. For those who are overweight, physicians could ask their patients to choose a fasting-based intervention that they believe they could comply with based upon their daily and weekly schedules. Examples include the ''5:2'' IF diet (Harvie et al., 2011), the alternate day modified fasting diet (Johnson et al., 2007; Varady et al., 2009), a 4–5 day fast (Lee et al., 2012; Safdie et al., 2009), or low-calorie-but high-nourishment fasting-mimicking diets once every 1–3 months followed by the skipping of one major meal every day if needed (V.D.L., unpublished data). One of the concerns with unbalanced alternating diets, such as those in which low calorie intake is only observed for 2 days a week, are the potential effects on circadian rhythm and the endocrine and gastrointestinal systems, which are known to be influenced by eating habits. During the first 4–6 weeks of implementation of the fasting regimen, a physician or registered dietitian should be in regular contact with the patient to monitor their progress and to provide advice and supervision.

Fasting regimens could also be tailored for specific diseases as stand-alone or adjunct therapies. Results of initial trials of IF (fasting 2 days per week or every other day) in human subjects suggest that there is a critical transition period of 3–6 weeks during which time the brain and body adapt to the new eating pattern and mood is enhanced (Harvie et al., 2011; Johnson et al., 2007). Though speculative, it is likely that during the latter transition period brain neurochemistry changes so that the ''addiction'' to regular consumption of food throughout the day is overcome. Notably, the various fasting approaches are likely to have limited efficacy, particularly on aging and conditions other than obesity, unless combined with high-nourishment diets such as the moderate calorie intake and mostly plant-based Mediterranean or Okinawa low-protein diets (0.8 g protein/kg of body weight), consistently associated with health and longevity.

In the future, it will be important to combine epidemiological data, studies of long-lived populations and their diets, and results from model organisms connecting specific dietary components to proaging and prodisease factors, with data from clinical studies, to design large clinical studies that integrate fasting with diets recognized as protective and enjoyable. A better understanding of the molecular mechanisms by which fasting affects various cell types and organ systems should also lead to the development of novel, FDA-approved prophylactic and preventive and therapeutic interventions for a wide range of disorders.

ACKNOWLEDGMENTS

We thank Min Wei for all the assistance with the preparation of the manuscript. We thank Yvon Le Maho for providing valuable information about fasting and a picture of penguins. We thank Matt Kaeberlein and Matthew Piper for panels for Figure 1. We thank William Mair for helpful discussions on fasting in *Drosophila* and thank Jay Mitchell for helpful comments on the manuscript. This work was supported, in part, by the Intramural Research Program of the National Institute on Aging; by the Glenn Foundation for Medical Research; and by the NIH/NIA grants AG20642, AG025135, and AG034906 to V.D.L.

REFERENCES

Adams, S.H., and Costa, D.P. (1993). Water conservation and protein metabolism in northern elephant seal pups during the postweaning fast. J. Comp. Physiol. B *163*, 367–373.

Ahmet, I., Wan, R., Mattson, M.P., Lakatta, E.G., and Talan, M. (2005). Cardioprotection by intermittent fasting in rats. Circulation *112*, 3115–3121.

Anson, R.M., Guo, Z., de Cabo, R., Iyun, T., Rios, M., Hagepanos, A., Ingram, D.K., Lane, M.A., and Mattson, M.P. (2003). Intermittent fasting dissociates beneficial effects of dietary restriction on glucose metabolism and neuronal resistance to injury from calorie intake. Proc. Natl. Acad. Sci. USA *100*, 6216–6220.

Arum, O., Bonkowski, M.S., Rocha, J.S., and Bartke, A. (2009). The growth hormone receptor gene-disrupted mouse fails to respond to an intermittent fasting diet. Aging Cell *8*, 756–760.

Arumugam, T.V., Phillips, T.M., Cheng, A., Morrell, C.H., Mattson, M.P., and Wan, R. (2010). Age and energy intake interact to modify cell stress pathways and stroke outcome. Ann. Neurol. *67*, 41–52.

Atkinson, S.N., and Ramsay, M.A. (1995). The Effects of Prolonged Fasting of the Body Composition and Reproductive Success of Female Polar Bears (Ursus maritimus). Funct. Ecol. *9*, 559–567.

Baatar, D., Patel, K., and Taub, D.D. (2011). The effects of ghrelin on inflammation and the immune system. Mol. Cell. Endocrinol. *340*, 44–58.

Bayer-Carter, J.L., Green, P.S., Montine, T.J., VanFossen, B., Baker, L.D., Watson, G.S., Bonner, L.M., Callaghan, M., Leverenz, J.B., Walter, B.K., et al. (2011). Diet intervention and cerebrospinal fluid biomarkers in amnestic mild cognitive impairment. Arch. Neurol. *68*, 743–752.

Berrigan, D., Perkins, S.N., Haines, D.C., and Hursting, S.D. (2002). Adult-onset calorie restriction and fasting delay spontaneous tumorigenesis in p53-deficient mice. Carcinogenesis *23*, 817–822.

Bishop, N.A., Lu, T., and Yankner, B.A. (2010). Neural mechanisms of ageing and cognitive decline. Nature *464*, 529–535.

Bruce-Keller, A.J., Umberger, G., McFall, R., and Mattson, M.P. (1999). Food restriction reduces brain damage and improves behavioral outcome following excitotoxic and metabolic insults. Ann. Neurol. *45*, 8–15.

Cahill, G.F., Jr. (2006). Fuel metabolism in starvation. Annu. Rev. Nutr. *26*, 1–22.

Carlson, A.J., and Hoelzel, F. (1946). Apparent prolongation of the life span of rats by intermittent fasting. J. Nutr. *31*, 363–375.

Castellini, M.A., and Rea, L.D. (1992). The biochemistry of natural fasting at its limits. Experientia *48*, 575–582.

Castello, L., Froio, T., Maina, M., Cavallini, G., Biasi, F., Leonarduzzi, G., Donati, A., Bergamini, E., Poli, G., and Chiarpotto, E. (2010). Alternate-day fasting protects the rat heart against age-induced inflammation and fibrosis by inhibiting oxidative damage and NF-kB activation. Free Radic. Biol. Med. *48*, 47–54.

Chan, J.M., Stampfer, M.J., Giovannucci, E., Ma, J., and Pollak, M. (2000). Insulin-like growth factor I (IGF-I), IGF-binding protein-3 and prostate cancer risk: epidemiological studies. Growth Horm. IGF Res. *10* (*Suppl A*), S32–S33.

Chao, M.V. (2000). Trophic factors: An evolutionary cul-de-sac or door into higher neuronal function? J. Neurosci. Res. *59*, 353–355.

Cherel, Y., and Groscolas, R. (1999). Relationships between nutrient storage and nutrient utilisation in long-term fasting birds and mammals. In Proc. 22 Int. Ornithol. Congr., Durban, N.J. Adams and R.H. Slotow, eds. (Johannesburg: BirdLife South Africa), pp. 17–34.

Cherel, Y., and Le Maho, Y. (1985). Five months of fasting in king penguin chicks: body mass loss and fuel metabolism. Am. J. Physiol. *249*, R387–R392.

Cherel, Y., Leloup, J., and Le Maho, Y. (1988a). Fasting in king penguin. II. Hormonal and metabolic changes during molt. Am. J. Physiol. *254*, R178–R184.

Cherel, Y., Robin, J.P., Walch, O., Karmann, H., Netchitailo, P., and Le Maho, Y. (1988b). Fasting in king penguin. I. Hormonal and metabolic changes during breeding. Am. J. Physiol. *254*, R170–R177.

Cherel, Y., Attaix, D., Rosolowska-Huszcz, D., Belkhou, R., Robin, J.P., Arnal, M., and Le Maho, Y. (1991). Whole-body and tissue protein synthesis during brief and prolonged fasting in the rat. Clin. Sci. *81*, 611–619.

Descamps, O., Riondel, J., Ducros, V., and Roussel, A.M. (2005). Mitochondrial production of reactive oxygen species and incidence of age-associated lymphoma in OF1 mice: effect of alternate-day fasting. Mech. Ageing Dev. *126*, 1185–1191.

Duan, W., and Mattson, M.P. (1999). Dietary restriction and 2-deoxyglucose administration improve behavioral outcome and reduce degeneration of dopaminergic neurons in models of Parkinson's disease. J. Neurosci. Res. *57*, 195–206.

Duan, W., Guo, Z., Jiang, H., Ware, M., Li, X.J., and Mattson, M.P. (2003). Dietary restriction normalizes glucose metabolism and BDNF levels, slows disease progression, and increases survival in huntingtin mutant mice. Proc. Natl. Acad. Sci. USA *100*, 2911–2916.

Eichhorn, G., Groscolas, R., Le Glaunec, G., Parisel, C., Arnold, L., Medina, P., and Handrich, Y. (2011). Heterothermy in growing king penguins. Nat. Commun. *2*, 435.

Fabrizio, P., Gattazzo, C., Battistella, L., Wei, M., Cheng, C., McGrew, K., and Longo, V.D. (2005). Sir2 blocks extreme life-span extension. Cell *123*, 655–667.

Favier, R.J., and Koubi, H.E. (1988). Metabolic and structural adaptations to exercise in chronic intermittent fasted rats. Am. J. Physiol. *254*, R877–R884.

Flegal, K.M., Kit, B.K., Orpana, H., and Graubard, B.I. (2013). Association of all-cause mortality with overweight and obesity using standard body mass index categories: a systematic review and meta-analysis. JAMA *309*, 71–82.

Fond, G., Macgregor, A., Leboyer, M., and Michalsen, A. (2013). Fasting in mood disorders: neurobiology and effectiveness. A review of the literature. Psychiatry Res. *209*, 253–258.

Fontán-Lozano, A., Sáez-Cassanelli, J.L., Inda, M.C., de los Santos-Arteaga, M., Sierra-Domínguez, S.A., López-Lluch, G., Delgado-García, J.M., and Carrión, A.M. (2007). Caloric restriction increases learning consolidation and facilitates synaptic plasticity through mechanisms dependent on NR2B subunits of the NMDA receptor. J. Neurosci. *27*, 10185–10195.

Fontana, L., and Klein, S. (2007). Aging, adiposity, and calorie restriction. JAMA *297*, 986–994.

Fontana, L., Weiss, E.P., Villareal, D.T., Klein, S., and Holloszy, J.O. (2008). Long-term effects of calorie or protein restriction on serum IGF-1 and IGFBP-3 concentration in humans. Aging Cell *7*, 681–687.

Fontana, L., Partridge, L., and Longo, V.D. (2010). Extending healthy life span—from yeast to humans. Science *328*, 321–326.

Giovannucci, E., Pollak, M., Platz, E.A., Willett, W.C., Stampfer, M.J., Majeed, N., Colditz, G.A., Speizer, F.E., and Hankinson, S.E. (2000). Insulin-like growth factor I (IGF-I), IGF-binding protein-3 and the risk of colorectal adenoma and cancer in the Nurses' Health Study. Growth Horm. IGF Res. *10* (*Suppl A*), S30–S31.

Goldhamer, A., Lisle, D., Parpia, B., Anderson, S.V., and Campbell, T.C. (2001). Medically supervised water-only fasting in the treatment of hypertension. J. Manipulative Physiol. Ther. *24*, 335–339.

Goldhamer, A.C., Lisle, D.J., Sultana, P., Anderson, S.V., Parpia, B., Hughes, B., and Campbell, T.C. (2002). Medically supervised water-only fasting in the treatment of borderline hypertension. J. Altern. Complement. Med. *8*, 643–650.

Gonidakis, S., Finkel, S.E., and Longo, V.D. (2010). Genome-wide screen identifies Escherichia coli TCA-cycle-related mutants with extended chronological lifespan dependent on acetate metabolism and the hypoxia-inducible transcription factor ArcA. Aging Cell *9*, 868–881.

Goodrick, C.L., Ingram, D.K., Reynolds, M.A., Freeman, J.R., and Cider, N. (1990). Effects of intermittent feeding upon body weight and lifespan in inbred mice: interaction of genotype and age. Mech. Ageing Dev. *55*, 69–87.

Grandison, R.C., Wong, R., Bass, T.M., Partridge, L., and Piper, M.D. (2009). Effect of a standardised dietary restriction protocol on multiple laboratory strains of Drosophila melanogaster. PLoS ONE *4*, e4067.

Greer, E.L., Dowlatshahi, D., Banko, M.R., Villen, J., Hoang, K., Blanchard, D., Gygi, S.P., and Brunet, A. (2007). An AMPK-FOXO pathway mediates longevity induced by a novel method of dietary restriction in C. elegans. Curr. Biol. *17*, 1646–1656.

Griffioen, K.J., Wan, R., Brown, T.R., Okun, E., Camandola, S., Mughal, M.R., Phillips, T.M., and Mattson, M.P. (2012). Aberrant heart rate and brainstem brain-derived neurotrophic factor (BDNF) signaling in a mouse model of Huntington's disease. Neurobiol. Aging *33*, 1481.e1–1481.e5.

Guevara-Aguirre, J., Balasubramanian, P., Guevara-Aguirre, M., Wei, M., Madia, F., Cheng, C.W., Hwang, D., Martin-Montalvo, A., Saavedra, J., Ingles, S., et al. (2011). Growth hormone receptor deficiency is associated with a major reduction in pro-aging signaling, cancer, and diabetes in humans. Sci. Transl. Med. *3*, 70ra13.

Halagappa, V.K., Guo, Z., Pearson, M., Matsuoka, Y., Cutler, R.G., Laferla, F.M., and Mattson, M.P. (2007). Intermittent fasting and caloric restriction ameliorate age-related behavioral deficits in the triple-transgenic mouse model of Alzheimer's disease. Neurobiol. Dis. *26*, 212–220.

Halberg, N., Henriksen, M., Söderhamn, N., Stallknecht, B., Ploug, T., Schjerling, P., and Dela, F. (2005). Effect of intermittent fasting and refeeding on insulin action in healthy men. J. Appl. Physiol. *99*, 2128–2136.

Hartman, A.L., Rubenstein, J.E., and Kossoff, E.H. (2012). Intermittent fasting: A "new" historical strategy for controlling seizures? Epilepsy Res. *104*, 275–279.

Harvie, M.N., Pegington, M., Mattson, M.P., Frystyk, J., Dillon, B., Evans, G., Cuzick, J., Jebb, S.A., Martin, B., Cutler, R.G., et al. (2011). The effects of intermittent or continuous energy restriction on weight loss and metabolic disease risk markers: a randomized trial in young overweight women. Int. J. Obes. (Lond) *35*, 714–727.

Heilbronn, L.K., Smith, S.R., Martin, C.K., Anton, S.D., and Ravussin, E. (2005). Alternate-day fasting in nonobese subjects: effects on body weight, body composition, and energy metabolism. Am. J. Clin. Nutr. *81*, 69–73.

Honjoh, S., Yamamoto, T., Uno, M., and Nishida, E. (2009). Signalling through RHEB-1 mediates intermittent fasting-induced longevity in C. elegans. Nature *457*, 726–730.

Horne, B.D., Muhlestein, J.B., May, H.T., Carlquist, J.F., Lappé, D.L., Bair, T.L., and Anderson, J.L.; Intermountain Heart Collaborative Study Group (2012). Relation of routine, periodic fasting to risk of diabetes mellitus, and coronary artery disease in patients undergoing coronary angiography. Am. J. Cardiol. *109*, 1558–1562.

Johnson, J.B., Summer, W., Cutler, R.G., Martin, B., Hyun, D.H., Dixit, V.D., Pearson, M., Nassar, M., Telljohann, R., Maudsley, S., et al. (2007). Alternate day calorie restriction improves clinical findings and reduces markers of oxidative stress and inflammation in overweight adults with moderate asthma. Free Radic. Biol. Med. *42*, 665–674.

Kaeberlein, T.L., Smith, E.D., Tsuchiya, M., Welton, K.L., Thomas, J.H., Fields, S., Kennedy, B.K., and Kaeberlein, M. (2006). Lifespan extension in Caenorhabditis elegans by complete removal of food. Aging Cell *5*, 487–494.

Kashiwaya, Y., Bergman, C., Lee, J.H., Wan, R., Todd King, M., Mughal, M.R., Okun, E., Clarke, K., Mattson, M.P., and Veech, R.L. (2013). A ketone ester diet exhibits anxiolytic and cognition-sparing properties, and lessens amyloid and tau pathologies in a mouse model of Alzheimer's disease. Neurobiol. Aging, 1530–1539. Published online December 29, 2012. http://dx.doi.org/10.1016/j.neurobiolaging.2012.11.023.

Kendrick, D.C. (1973). The effects of infantile stimulation and intermittent fasting and feeding on life span in the black-hooded rat. Dev. Psychobiol. *6*, 225–234.

Kjeldsen-Kragh, J., Haugen, M., Borchgrevink, C.F., Laerum, E., Eek, M., Mowinkel, P., Hovi, K., and Førre, O. (1991). Controlled trial of fasting and one-year vegetarian diet in rheumatoid arthritis. Lancet *338*, 899–902.

Kjeldsen-Kragh, J., Haugen, M., Borchgrevink, C.F., and Førre, O. (1994). Vegetarian diet for patients with rheumatoid arthritis—status: two years after introduction of the diet. Clin. Rheumatol. *13*, 475–482.

Klempel, M.C., Kroeger, C.M., and Varady, K.A. (2013). Alternate day fasting (ADF) with a high-fat diet produces similar weight loss and cardio-protection as ADF with a low-fat diet. Metabolism *62*, 137–143.

Kretsch, M.J., Green, M.W., Fong, A.K., Elliman, N.A., and Johnson, H.L. (1997). Cognitive effects of a long-term weight reducing diet. Int. J. Obes (Lond). *21*, 14–21.

Kristan, D.M. (2008). Calorie restriction and susceptibility to intact pathogens. Age (Dordr.) *30*, 147–156.

Le Maho, Y., Delclitte, P., and Chatonnet, J. (1976). Thermoregulation in fasting emperor penguins under natural conditions. Am. J. Physiol. *231*, 913–922.

Le Maho, Y., Vu Van Kha, H., Koubi, H., Dewasmes, G., Girard, J., Ferré, P., and Cagnard, M. (1981). Body composition, energy expenditure, and plasma metabolites in long-term fasting geese. Am. J. Physiol. *241*, E342–E354.

Lee, J., Seroogy, K.B., and Mattson, M.P. (2002). Dietary restriction enhances neurotrophin expression and neurogenesis in the hippocampus of adult mice. J. Neurochem. *80*, 539–547.

Lee, G.D., Wilson, M.A., Zhu, M., Wolkow, C.A., de Cabo, R., Ingram, D.K., and Zou, S. (2006). Dietary deprivation extends lifespan in Caenorhabditis elegans. Aging Cell *5*, 515–524.

Lee, C., Safdie, F.M., Raffaghello, L., Wei, M., Madia, F., Parrella, E., Hwang, D., Cohen, P., Bianchi, G., and Longo, V.D. (2010). Reduced levels of IGF-I mediate differential protection of normal and cancer cells in response to fasting and improve chemotherapeutic index. Cancer Res. *70*, 1564–1572.

Lee, C., Raffaghello, L., Brandhorst, S., Safdie, F.M., Bianchi, G., Martin-Montalvo, A., Pistoia, V., Wei, M., Hwang, S., Merlino, A., Emionite, L., de Cabo, R., and Longo, V.D. (2012). Fasting cycles retard growth of tumors and sensitize a range of cancer cell types to chemotherapy. Sci. Transl. Med *4*. Published online March 7, 2012. http://dx.doi.org/10.1126/scitranslmed.3003293.

Longo, V.D., Ellerby, L.M., Bredesen, D.E., Valentine, J.S., and Gralla, E.B. (1997). Human Bcl-2 reverses survival defects in yeast lacking superoxide dismutase and delays death of wild-type yeast. J. Cell Biol. *137*, 1581–1588.

Longo, V.D., Shadel, G.S., Kaeberlein, M., and Kennedy, B. (2012). Replicative and chronological aging in Saccharomyces cerevisiae. Cell Metab. *16*, 18–31.

Mager, D.E., Wan, R., Brown, M., Cheng, A., Wareski, P., Abernethy, D.R., and Mattson, M.P. (2006). Caloric restriction and intermittent fasting alter spectral measures of heart rate and blood pressure variability in rats. FASEB J. *20*, 631–637.

Martin, B., Ji, S., Maudsley, S., and Mattson, M.P. (2010). "Control" laboratory rodents are metabolically morbid: why it matters. Proc. Natl. Acad. Sci. USA *107*, 6127–6133.

Masoro, E.J. (2005). Overview of caloric restriction and ageing. Mech. Ageing Dev. *126*, 913–922.

Mattson, M.P. (2012a). Energy intake and exercise as determinants of brain health and vulnerability to injury and disease. Cell Metab. *16*, 706–722.

Mattson, M.P. (2012b). Evolutionary aspects of human exercise—born to run purposefully. Ageing Res. Rev. *11*, 347–352.

Mattson, M.P., Cutler, R.G., and Camandola, S. (2007). Energy intake and amyotrophic lateral sclerosis. Neuromolecular Med. *9*, 17–20.

Milanski, M., Arruda, A.P., Coope, A., Ignacio-Souza, L.M., Nunez, C.E., Roman, E.A., Romanatto, T., Pascoal, L.B., Caricilli, A.M., Torsoni, M.A., et al. (2012). Inhibition of hypothalamic inflammation reverses diet-induced insulin resistance in the liver. Diabetes *61*, 1455–1462.

Mitchell, J.R., Verweij, M., Brand, K., van de Ven, M., Goemaere, N., van den Engel, S., Chu, T., Forrer, F., Müller, C., de Jong, M., et al. (2010). Short-term dietary restriction and fasting precondition against ischemia reperfusion injury in mice. Aging Cell *9*, 40–53.

Müller, H., de Toledo, F.W., and Resch, K.L. (2001). Fasting followed by vegetarian diet in patients with rheumatoid arthritis: a systematic review. Scand. J. Rheumatol. *30*, 1–10.

Pedersen, W.A., and Mattson, M.P. (1999). No benefit of dietary restriction on disease onset or progression in amyotrophic lateral sclerosis Cu/Zn-superoxide dismutase mutant mice. Brain Res. *833*, 117–120.

Pedersen, C.R., Hagemann, I., Bock, T., and Buschard, K. (1999). Intermittent feeding and fasting reduces diabetes incidence in BB rats. Autoimmunity *30*, 243–250.

Peng, W., Robertson, L., Gallinetti, J., Mejia, P., Vose, S., Charlip, A., Chu, T., and Mitchell, J.R. (2012). Surgical stress resistance induced by single amino acid deprivation requires Gcn2 in mice. Sci Transl. Med. *4*. Published online January 25, 2012. http://dx.doi.org/10.1126/scitranslmed.3002629.

Piper, M.D., and Partridge, L. (2007). Dietary restriction in Drosophila: delayed aging or experimental artefact? PLoS Genet. *3*, e57.

Plunet, W.T., Streijger, F., Lam, C.K., Lee, J.H., Liu, J., and Tetzlaff, W. (2008). Dietary restriction started after spinal cord injury improves functional recovery. Exp. Neurol. *213*, 28–35.

Raffaghello, L., Lee, C., Safdie, F.M., Wei, M., Madia, F., Bianchi, G., and Longo, V.D. (2008). Starvation-dependent differential stress resistance protects normal but not cancer cells against high-dose chemotherapy. Proc. Natl. Acad. Sci. USA *105*, 8215–8220.

Reed, M.J., Penn, P.E., Li, Y., Birnbaum, R., Vernon, R.B., Johnson, T.S., Pendergrass, W.R., Sage, E.H., Abrass, I.B., and Wolf, N.S. (1996). Enhanced cell proliferation and biosynthesis mediate improved wound repair in refed, caloric-restricted mice. Mech. Ageing Dev. *89*, 21–43.

Reilly, J.J. (1991). Adaptations to prolonged fasting in free-living weaned gray seal pups. Am. J. Physiol. *260*, R267–R272.

Robin, J.P., Cherel, Y., Girard, H., Géloen, A., and Le Maho, Y. (1987). Uric acid and urea in relation to protein catabolism in long-term fasting geese. J. Comp. Physiol. B *157*, 491–499.

Robin, J.P., Frain, M., Sardet, C., Groscolas, R., and Le Maho, Y. (1988). Protein and lipid utilization during long-term fasting in emperor penguins. Am. J. Physiol. *254*, R61–R68.

Rothman, S.M., Griffioen, K.J., Wan, R., and Mattson, M.P. (2012). Brain-derived neurotrophic factor as a regulator of systemic and brain energy metabolism and cardiovascular health. Ann. N Y Acad. Sci. *1264*, 49–63.

Safdie, F.M., Dorff, T., Quinn, D., Fontana, L., Wei, M., Lee, C., Cohen, P., and Longo, V.D. (2009). Fasting and cancer treatment in humans: A case series report. Aging (Albany, N.Y. Online) *1*, 988–1007.

Sakamoto, K., and Grunewald, K.K. (1987). Beneficial effects of exercise on growth of rats during intermittent fasting. J. Nutr. *117*, 390–395.

Sengupta, S., Peterson, T.R., Laplante, M., Oh, S., and Sabatini, D.M. (2010). mTORC1 controls fasting-induced ketogenesis and its modulation by ageing. Nature *468*, 1100–1104.

Shariatpanahi, Z.V., Shariatpanahi, M.V., Shahbazi, S., Hossaini, A., and Abadi, A. (2008). Effect of Ramadan fasting on some indices of insulin resistance and components of the metabolic syndrome in healthy male adults. Br. J. Nutr. *100*, 147–151.

Shi, Y., Felley-Bosco, E., Marti, T.M., Orlowski, K., Pruschy, M., and Stahel, R.A. (2012). Starvation-induced activation of ATM/Chk2/p53 signaling sensitizes cancer cells to cisplatin. BMC Cancer *12*, 571.

Singh, R., Kaushik, S., Wang, Y., Xiang, Y., Novak, I., Komatsu, M., Tanaka, K., Cuervo, A.M., and Czaja, M.J. (2009). Autophagy regulates lipid metabolism. Nature *458*, 1131–1135.

Singh, R., Lakhanpal, D., Kumar, S., Sharma, S., Kataria, H., Kaur, M., and Kaur, G. (2012). Late-onset intermittent fasting dietary restriction as a potential intervention to retard age-associated brain function impairments in male rats. Age (Dordr.) *34*, 917–933.

Steuerman, R., Shevah, O., and Laron, Z. (2011). Congenital IGF1 deficiency tends to confer protection against post-natal development of malignancies. Eur. J. Endocrinol. *164*, 485–489.

Stranahan, A.M., and Mattson, M.P. (2012). Recruiting adaptive cellular stress responses for successful brain ageing. Nat. Rev. Neurosci. *13*, 209–216.

Teng, N.I., Shahar, S., Manaf, Z.A., Das, S.K., Taha, C.S., and Ngah, W.Z. (2011). Efficacy of fasting calorie restriction on quality of life among aging men. Physiol. Behav. *104*, 1059–1064.

Tessitore, L., Tomasi, C., Greco, M., Sesca, E., Laconi, E., Maccioni, O., Ramo, R., and Pani, P. (1996). A subnecrogenic dose of diethylnitrosamine is able to initiate hepatocarcinogenesis in the rat when coupled with fasting/refeeding. Carcinogenesis *17*, 289–292.

Thissen, J.P., Ketelslegers, J.M., and Underwood, L.E. (1994a). Nutritional regulation of the insulin-like growth factors. Endocr. Rev. *15*, 80–101.

Thissen, J.P., Pucilowska, J.B., and Underwood, L.E. (1994b). Differential regulation of insulin-like growth factor I (IGF-I) and IGF binding protein-1 messenger ribonucleic acids by amino acid availability and growth hormone in rat hepatocyte primary culture. Endocrinology *134*, 1570–1576.

Tremaroli, V., and Bäckhed, F. (2012). Functional interactions between the gut microbiota and host metabolism. Nature *489*, 242–249.

Varady, K.A., and Hellerstein, M.K. (2007). Alternate-day fasting and chronic disease prevention: a review of human and animal trials. Am. J. Clin. Nutr. *86*, 7–13.

Varady, K.A., Bhutani, S., Church, E.C., and Klempel, M.C. (2009). Short-term modified alternate-day fasting: a novel dietary strategy for weight loss and cardioprotection in obese adults. Am. J. Clin. Nutr. *90*, 1138–1143.

Wan, R., Camandola, S., and Mattson, M.P. (2003). Intermittent fasting and dietary supplementation with 2-deoxy-D-glucose improve functional and metabolic cardiovascular risk factors in rats. FASEB J. *17*, 1133–1134.

Wan, R., Ahmet, I., Brown, M., Cheng, A., Kamimura, N., Talan, M., and Mattson, M.P. (2010). Cardioprotective effect of intermittent fasting is associated with an elevation of adiponectin levels in rats. J. Nutr. Biochem. *21*, 413–417.

Wei, M., Fabrizio, P., Hu, J., Ge, H., Cheng, C., Li, L., and Longo, V.D. (2008). Life span extension by calorie restriction depends on Rim15 and transcription factors downstream of Ras/PKA, Tor, and Sch9. PLoS Genet. *4*, e13.

Wei, M., Fabrizio, P., Madia, F., Hu, J., Ge, H., Li, L.M., and Longo, V.D. (2009). Tor1/Sch9-regulated carbon source substitution is as effective as calorie restriction in life span extension. PLoS Genet. *5*, e1000467.

Weindruch, R., and Sohal, R.S. (1997). Seminars in medicine of the Beth Israel Deaconess Medical Center. Caloric intake and aging. N. Engl. J. Med. *337*, 986–994.

Weindruch, R., and Walford, R.L. (1988). The Retardation of Aging and Disease by Dietary Restriction. (Springfield, Ill., U.S.A.: C.C. Thomas).

Witte, A.V., Fobker, M., Gellner, R., Knecht, S., and Flöel, A. (2009). Caloric restriction improves memory in elderly humans. Proc. Natl. Acad. Sci. USA *106*, 1255–1260.

Yamauchi, T., Kamon, J., Waki, H., Terauchi, Y., Kubota, N., Hara, K., Mori, Y., Ide, T., Murakami, K., Tsuboyama-Kasaoka, N., et al. (2001). The fat-derived hormone adiponectin reverses insulin resistance associated with both lipoatrophy and obesity. Nat. Med. *7*, 941–946.

Cell Metabolism
Article

Low Protein Intake Is Associated with a Major Reduction in IGF-1, Cancer, and Overall Mortality in the 65 and Younger but Not Older Population

Morgan E. Levine,[1,11] Jorge A. Suarez,[1,2,11] Sebastian Brandhorst,[1,2] Priya Balasubramanian,[1,2] Chia-Wei Cheng,[1,2] Federica Madia,[1,3] Luigi Fontana,[4,5,6] Mario G. Mirisola,[1,2,7] Jaime Guevara-Aguirre,[8] Junxiang Wan,[1,2] Giuseppe Passarino,[9] Brian K. Kennedy,[10] Min Wei,[1,2] Pinchas Cohen,[1,2] Eileen M. Crimmins,[1] and Valter D. Longo[1,2,*]
[1]Davis School of Gerontology
[2]Longevity Institute
University of Southern California, Los Angeles, CA 90033, USA
[3]EURL ECVAM, Institute for Health & Consumer Protection, European Commission Joint Research Centre, Ispra (VA) 21027, Italy
[4]Department of Medicine, Washington University in St. Louis, St. Louis, MO 63110, USA
[5]Department of Clinical and Experimental Sciences, Brescia University School of Medicine, Brescia 25123, Italy
[6]CEINGE Biotecnologie Avanzate, Napoli 80145, Italy
[7]Dipartimento di Biopatologia e Metodologie Biomediche, Universita' di Palermo, Palermo 90127, Italy
[8]Universidad San Francisco de Quito & Instituto IEMYR, Quito 17-1200-841, Ecuador
[9]Department of Biology, Ecology and Earth Science, University of Calabria, Rende 87036, Italy
[10]Buck Institute for Research on Aging, Novato, CA 94945, USA
[11]These authors contributed equally to this work
*Correspondence: vlongo@usc.edu
http://dx.doi.org/10.1016/j.cmet.2014.02.006

SUMMARY

Mice and humans with growth hormone receptor/IGF-1 deficiencies display major reductions in age-related diseases. Because protein restriction reduces GHR-IGF-1 activity, we examined links between protein intake and mortality. Respondents aged 50–65 reporting high protein intake had a 75% increase in overall mortality and a 4-fold increase in cancer death risk during the following 18 years. These associations were either abolished or attenuated if the proteins were plant derived. Conversely, high protein intake was associated with reduced cancer and overall mortality in respondents over 65, but a 5-fold increase in diabetes mortality across all ages. Mouse studies confirmed the effect of high protein intake and GHR-IGF-1 signaling on the incidence and progression of breast and melanoma tumors, but also the detrimental effects of a low protein diet in the very old. These results suggest that low protein intake during middle age followed by moderate to high protein consumption in old adults may optimize healthspan and longevity.

INTRODUCTION

Caloric restriction (CR) without malnutrition has been consistently shown to increase longevity in a number of animal models, including yeast, *C. elegans*, and mice (Fontana et al., 2010). However, the effect of CR on the lifespan of nonhuman primates remains controversial and may be heavily influenced by dietary composition (Cava and Fontana, 2013; Colman et al., 2009; Fontana and Klein, 2007; Mattison et al., 2012; Mercken et al., 2013; Stein et al., 2012). The lifespan extension associated with CR in model organisms is believed to operate through its effects on growth hormone (GH) and GH receptor (GHR), leading to subsequent deficiencies in IGF-1 and insulin levels and signaling (Bartke et al., 2001; Bellush et al., 2000; Fontana et al., 2010; Hauck et al., 2002; Wei et al., 2009). The effect of the insulin/IGF-1 pathway on longevity was first described in *C. elegans* by showing that mutations in the insulin/IGF-1 receptor or in the downstream *age-1* gene caused a several-fold increase in lifespan (Johnson, 1990; Kenyon et al., 1993, Kenyon, 2010). Other studies revealed that mutations in orthologs of genes functioning in insulin/IGF-1 signaling, but also activated independently of insulin/IGF-1, including TOR-S6K and RAS-cAMP-PKA, promoted aging in multiple model organisms, thus providing evidence for the conserved regulation of aging by pro-growth nutrient signaling pathways (Fabrizio et al., 2001; Guarente and Kenyon, 2000; Kapahi and Zid, 2004; Kenyon, 2005, 2011; Longo, 1999; Tatar et al., 2001). Not surprisingly, in mice, growth hormone receptor deficiency (GHRD) or growth hormone deficiency (GHD), both of which display low levels of IGF-1 and insulin, cause the strongest lifespan extension but also reduction of age-related pathologies including cancer and insulin resistance/diabetes (Brown-Borg and Bartke, 2012; Brown-Borg et al., 1996; Masternak and Bartke, 2012).

Recently, we showed that humans with growth hormone receptor deficiency (GHRD), also exhibiting major deficiencies in serum IGF-1 and insulin levels, displayed no cancer mortality or diabetes. Despite having a higher prevalence of obesity, combined deaths from cardiac disease and stroke in this group were similar to those in their relatives (Guevara-Aguirre et al., 2011). Similar protection from cancer was also reported in a study that surveyed 230 GHRDs (Steuerman et al., 2011).

Protein restriction or restriction of particular amino acids, such as methionine and tryptophan, may explain part of the effects of calorie restriction and GHRD mutations on longevity and disease risk, since protein restriction is sufficient to reduce IGF-1 levels and can reduce cancer incidence or increase longevity in model organisms, independently of calorie intake (Ayala et al., 2007; Fontana et al., 2008, 2013; Gallinetti et al., 2013; Horáková et al., 1988; Hursting et al., 2007; Leto et al., 1976; Mair et al., 2005; Pamplona and Barja, 2006; Peng et al., 2012; Ross, 1961; Sanz et al., 2006; Smith et al., 1995; Youngman, 1993).

Here, we combined an epidemiological study of 6,381 US men and women aged 50 and above from NHANES III, the only nationally representative dietary survey in the United States, with mouse and cellular studies to understand the link between the level and source of proteins and amino acids, aging, diseases, and mortality.

RESULTS

Human Population

The study population included 6,381 adults ages 50 and over from NHANES III, a nationally representative, cross-sectional study. Our analytic sample had a mean age of 65 years and is representative of the United States population in ethnicity, education, and health characteristics (Table S1).

On average, subjects consumed 1,823 calories, of which the majority came from carbohydrates (51%), followed by fat (33%) and protein (16%), with most of it (11%) derived from animal protein. The percent of calorie intake from protein was used to categorize subjects into a high protein group (20% or more of calories from proteins), a moderate protein group (10%–19% of calories from proteins), and a low protein group (less than 10% of calories from proteins).

Mortality follow-up was available for all NHANES III participants through linkage with the National Death Index up until 2006 (DHHS, 2001). This provided the timing and cause of death. The follow-up period for mortality covered 83,308 total person-years over 18 years, with 40% overall mortality, 19% cardiovascular disease (CVD) mortality, 10% cancer mortality, and about 1% diabetes mortality.

Association between Protein and Mortality

Using Cox Proportional Hazard models, we found that high and moderate protein consumption were positively associated with diabetes-related mortality, but not associated with all-cause, CVD, or cancer mortality when subjects at all the ages above 50 were considered. Results showed that both the moderate and high protein intake groups had higher risks of diabetes mortality compared to participants in the low protein group. Although taken together these results indicate that moderate to high protein intake promotes diabetes mortality, larger studies are necessary to test this possibility further. An alternative explanation for the elevated diabetes mortality in the higher protein group is that, following a diabetes diagnosis, some individuals may switch to a diet comprised of higher protein, lower fat, and low carbohydrates. To test this, we examined the association between protein intake and diabetes mortality in participants who had no prevalence of diabetes at baseline (Table S7).

Among subjects with no diabetes at baseline, those in the high protein group had a 73-fold increase in risk (HR: 73.52; 95% CI: 4.47–1,209.70), while those in the moderate protein category had an almost 23-fold increase in the risk of diabetes mortality (HR: 22.93; 95% CI: 1.31–400.70). We underline that our hazard ratios and confidence intervals may be inflated due to our sample size and the extremely low incidence of diabetes mortality in the low protein group. Overall, there were only 21 diabetes deaths among persons without diabetes at baseline, only 1 of which was from the low protein group. Nevertheless, despite the small sample size, our results still show significant associations between increased protein intake and diabetes-related mortality.

To determine whether the association between protein and mortality differed for middle-aged and older adults, Cox proportional hazard models were rerun, testing for an interaction between protein consumption and age. Significant interactions were found for both all-cause and cancer mortality, indicating that the low protein diet was beneficial in mid-life; however, its benefits declined with age (Figure 1). Based on these results, we stratified the population into two age groups, those ages 50–65 (n = 3,039) and those ages 66+ (n = 3,342), and re-examined relationships between protein and cause-specific mortality. Among those ages 50–65, higher protein levels were linked to significantly increased risks of all-cause and cancer mortality (Table 1). In this age range, subjects in the high protein group had a 74% increase in their relative risk of all-cause mortality (HR: 1.74; 95% CI: 1.02–2.97) and were more than four times as likely to die of cancer (HR: 4.33; 95% CI: 1.96–9.56) when compared to those in the low protein group. None of these associations was significantly affected by controlling for percent calories from total fat or for percent calories from total carbohydrates. However, when the percent calories from animal protein was controlled for, the association between total protein and all-cause or cancer mortality was eliminated or significantly reduced, respectively, suggesting animal proteins are responsible for a significant portion of these relationships. When we controlled for the effect of plant-based protein, there was no change in the association between protein intake and mortality, indicating that high levels of animal proteins promote mortality and not that plant-based proteins have a protective effect (Table S5).

Compared to subjects reporting a low protein diet, subjects who consumed moderate levels of protein also had a 3-fold higher cancer mortality (HR: 3.06; 95% CI: 1.49–6.25), which was not accounted for by either percent calories from fat or percent calories from carbohydrates, but was marginally reduced when controlling for percent calories from animal protein (HR: 2.71; 95% CI: 1.24–5.91), although the size of the effect was not as large as for those in the high protein group. Taken together, these results indicate that respondents ages 50–65 consuming moderate to high levels of animal protein display a major increase in the risks for overall and cancer mortality; however, the risks may be somewhat decreased if protein does not come from an animal source. Similar results were obtained if the population 45–65 was considered, although few deaths occurred in the 45–50 group (data not shown).

In contrast to the findings above, among respondents who were 66 years of age and over at baseline, higher protein levels were associated with the opposite outcomes for overall and cancer mortality but a similar outcome for diabetes mortality

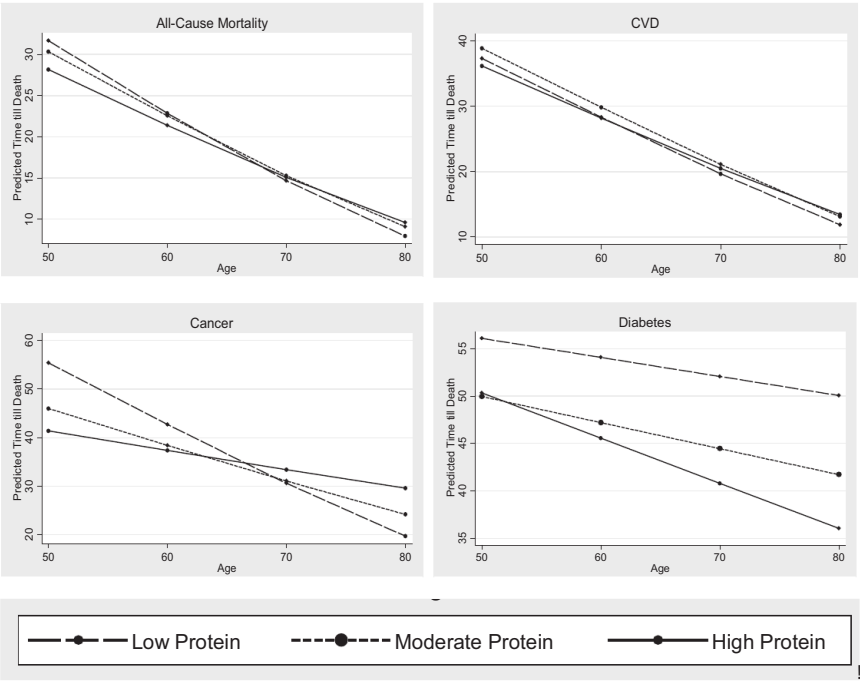

Figure 1. Association between Protein Intake and Mortality

Using Cox proportional hazard models, statistically significant ($p < 0.05$) interactions between age and protein group were found for all-cause and cancer mortality. Based on these models, predicted remaining life expectancy was calculated for each protein group by age at baseline. Overall, low protein appears to have a protective effect against all-cause and cancer mortality prior to age 66, at which point it becomes detrimental. No significant interactions were found for cardiovascular disease (CVD) and diabetes mortality.

(Table 1). When compared to those with low protein consumption, subjects who consumed high amounts of protein had a 28% reduction in all-cause mortality (HR: 0.72; 95% CI: 0.55–0.94), while subjects who consumed moderate amounts of protein displayed a 21% reduction in all-cause mortality (HR: 0.78; 95% CI: 0.62–0.99). Furthermore, this was not affected by percent calories from fat, from carbohydrates, or from animal protein. Subjects with high protein consumption also had a 60% reduction in cancer mortality (HR: 0.40; 95% CI: 0.23–0.71) compared to those with low protein diets, which was also not affected when controlling for other nutrient intake or protein source.

The Influence of IGF-1 on the Association between Protein and Mortality

Adjusted mean IGF-1 levels were positively associated with protein consumption for both age groups (Figure 2). Because IGF-1 was only available for a randomly selected subsample (n = 2,253), we re-examined the age-specific associations between protein and cause-specific mortality in this sample and found them to be similar to what was seen in the full sample, although with somewhat larger effect sizes (Table S3). Next we examined whether IGF-1 acted as a moderator or mediator in the association between protein and mortality. We found that while IGF-1 did not account for the association between protein consumption and mortality (Table S3), it was an important moderator of the association, as indicated by the statistically significant interactions between protein and IGF-1 level (Table S4).

From these models, predicted hazard ratios by IGF-1 and protein group were calculated (Figure S2). Results showed that for every 10 ng/ml increase in IGF-1, the mortality risk of cancer among subjects ages 50–65 increases for the high protein versus the low protein group by an additional 9% ($HR_{high\ protein\ x\ IGF\text{-}1}$: 1.09; 95% CI: 1.01–1.17). In contrast, among older subjects (66+ years), when comparing those in the low protein group, subjects with high or moderate protein diets had a reduced risk of CVD mortality if IGF-1 was also low; however, no benefits were found with increased IGF-1.

Protein Intake, IGF-1, and Cancer in Mice

To verify causation and understand the mechanism that may link proteins to cancer and overall mortality, we studied the effect of a range of protein intake (4%–18%) similar to that of subjects in the NHANES III study on the levels of circulating IGF-1, cancer incidence, and cancer progression in mice. Eighteen-week-old male C57BL/6 mice were fed continuously for 39 days with experimental, isocaloric diets designed to provide either a high (18%) or a low (4%–7%) amount of calories derived from protein, without imposing CR or causing malnutrition (Figures S1A and S1B).

To understand how the different levels of protein and IGF-1 may affect the ability of a newly formed tumor to survive and grow after 1 week on diets containing different protein levels, both groups were implanted subcutaneously with 20,000 syngeneic murine melanoma cells (B16). Tumor measurements began 15 days postimplantation and after 22 days on the diets, at which point incidence was found to be 100% for the high protein level (18%) group but 80% for the low protein level (4%) group (Figure 3A). At day 25, incidence rose to 90% in the low protein group and remained there until the end of the experiment (Figure 3A). From day 22 until the end of the experiment, tumor size was significantly smaller in the group consuming a lower amount of proteins, indicating a much slower tumor progression. At day 39 the mean tumor size was 78% larger in the high compared to the low protein group (day 36, $p = 0.0001$; day 39, $p < 0.0001$) (Figure 3B). To test the hypothesis that GHR signaling may be involved in this effect of protein levels, blood samples were obtained and analyzed at day 16 to determine the levels of IGF-1 and the IGF-1 inhibitory protein IGFBP-1 (Wolpin et al., 2007). Serum IGF-1 was 35% lower ($p = 0.0004$) in the low protein group when compared to animals fed the high protein diet (Figure 3C). Conversely, serum IGFBP-1 was 136% higher ($p = 0.003$) in the low protein group compared to the high protein group (Figure 3D).

To test further the hypothesis that the GHR-IGF-1 axis promotes cancer progression, we implanted subcutaneous

Table 1. Associations between Mortality and Protein Intake

	Hazard Ratio (95% CI)							
	Ages 50–65 (N = 3,039)				Ages 66+ (N = 3,342)			
	Model 1	Model 2	Model 3	Model 4	Model 1	Model 2	Model 3	Model 4
All-Cause Mortality								
Moderate protein (n = 4,798)	1.34 (0.81–2.22)	1.37 (0.82–2.27)	1.35 (0.80–2.29)	1.15 (0.67–1.96)	0.79 (0.62–0.99)	0.79 (0.62–0.99)	0.79 (0.62–0.99)	0.79 (0.61–1.01)
High protein (n = 1,146)	1.74 (1.02–2.97)	1.77 (1.03–3.03)	1.74 (0.99–3.05)	1.18 (0.60–2.31)	0.72 (0.55–0.94)	0.73 (0.56–0.95)	0.72 (0.55–0.94)	0.72 (0.50–1.02)
% kcal fat	–	0.99 (0.98–1.01)	–	–	–	1.00 (0.99–1.01)	–	–
% kcal carbs	–	–	1.00 (0.99–1.01)	–	–	–	1.00 (0.99–1.00)	–
% kcal animal protein	–	–	–	1.03 (1.00–1.06)	–	–	–	1.00 (0.98–1.02)
CVD Mortality								
Moderate protein (n = 4,798)	0.79 (0.40–1.54)	0.83 (0.43–1.60)	0.81 (0.41–1.62)	0.61 (0.29–1.29)	0.80 (0.57–1.12)	0.80 (0.57–1.12)	0.80 (0.57–1.12)	0.80 (0.56–1.14)
High protein (n = 1,146)	1.03 (0.51–2.09)	1.08 (0.54–2.15)	1.10 (0.52–2.31)	0.55 (0.19–1.62)	0.78 (0.54–1.14)	0.79 (0.54–1.15)	0.78 (0.53–1.15)	0.77 (0.48–1.25)
% kcal fat	–	0.99 (0.97–1.01)	–	–	–	1.00 (0.99–1.01)	–	–
% kcal carbs	–	–	1.00 (0.99–1.02)	–	–	–	1.00 (0.99–1.01)	–
% kcal animal protein	–	–	–	1.04 (0.99–1.11)	–	–	–	1.00 (0.98–1.02)
Cancer Mortality								
Moderate protein (n = 4,798)	3.06 (1.49–6.25)	3.13 (1.52–6.44)	3.56 (1.65–7.65)	2.71 (1.24–5.91)	0.67 (0.43–1.06)	0.67 (0.43–1.06)	0.67 (0.42–1.05)	0.66 (0.40–1.07)
High protein (n = 1,146)	4.33 (1.96–9.56)	4.42 (2.01–9.74)	4.98 (2.13–11.66)	3.19 (1.21–8.35)	0.40 (0.23–0.71)	0.41 (0.23–0.73)	0.39 (0.22–0.69)	0.38 (0.17–0.82)
% kcal fat	–	0.99 (0.98–1.01)	–	–	–	1.02 (1.01–1.03)	–	–
% kcal carbs	–	–	1.00 (0.98–1.01)	–	–	–	1.00 (0.99–1.01)	–
% kcal animal protein	–	–	–	1.02 (0.97–1.07)	–	–	–	1.00 (0.97–1.04)
Diabetes Mortality								
Moderate protein (n = 4,798)	3.43 (0.69–17.02)	3.36 (0.67–16.96)	3.41 (0.67–17.36)	2.99 (0.58–15.31)	5.38 (0.95–30.49)	5.05 (0.93–27.34)	4.93 (0.89–27.35)	6.20 (0.35–37.01)
High protein (n = 1,146)	3.93 (0.73–21.07)	3.88 (0.71–21.17)	3.90 (0.67–22.84)	2.77 (0.24–31.73)	10.64 (1.85–61.31)	10.42 (1.88–57.87)	9.07 (1.49–55.30)	15.16 (1.93–118.9)
% kcal fat	–	1.01 (0.97–1.05)	–	–	–	–	–	–
% kcal carbs	–	–	1.00 (0.96–1.04)	–	–	–	–	–
% kcal animal protein	–	–	–	1.02 (0.92–1.14)	–	–	–	–

Reference = low protein (n = 437 in both age groups). Model 1 (baseline model): Adjusted for age, sex, race/ethnicity, education, waist circumference, smoking, chronic conditions (diabetes, cancer, myocardial infarction), trying to lose weight in the last year, diet changed in the last year, reported intake representative of typical diet, and total calories. Model 2: Adjusted for covariates and % kcals from total fat. Model 3: Adjusted for covariates and % kcals from total carbohydrates. Model 4: Adjusted for covariates and % kcals from animal protein.

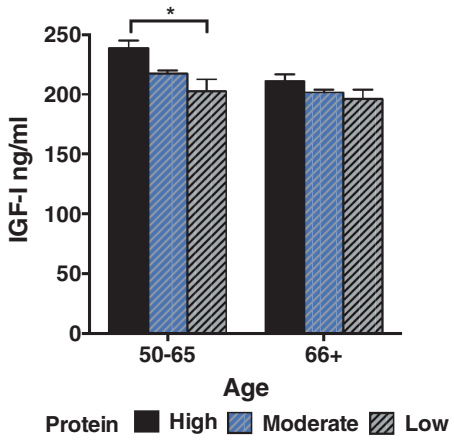

Figure 2. Serum IGF-1 Levels in Respondents 50–65 and 66+ Reporting Low, Moderate, or High Protein Intake

IGF-1 in respondents ages 50–65 is significantly lower among those with low protein intake when compared to high ($p = 0.004$). For those ages 66+ the difference between high and low intake becomes marginally significant ($p = 0.101$). The cohort for which IGF-1 levels were calculated includes 2,253 subjects. Of those ages 50–65 (n = 1,125), 89 were in the low protein category, 854 were in the moderate protein category, and 182 were in the high protein category. Of those ages 66+ (n = 1,128), 80 were in the low protein category, 867 were in the moderate protein category, and 181 were in the high protein category. Data points represent the mean ± SEM. *$p < 0.01$.

melanoma (B16) into GHR/IGF-1-deficient GHRKO mice and their respective age- and sex-matched littermate controls (18-week-old male C57BL/6 mice). Tumor measurements began 10 days postimplantation and continued until day 18. The data show that tumor progression is strongly inhibited in the GHRKO mice when compared to progression in the control group (Figures 3E and S1L; $p < 0.01$).

We also tested the effect of protein intake on breast cancer incidence and progression in a mouse model. Twelve-week-old female BALB/c mice were placed under the same dietary regimen as described for C57BL/6 mice, except that the mice had to be switched from a 4% to a 7% kcal from protein diet within the first week in order to prevent weight loss (Figures S1E and S1F). After a week of feeding on these diets, mice were implanted subcutaneously with 20,000 cells of syngeneic, murine breast cancer (4T1), and 15 days later animals were assessed for tumors. On day 18 postimplantation (day 25 on the diet), tumor incidence was 100% in the high protein (18%) group but only 70% in the low protein (7%) group. The incidence in the low protein group rose to 80% at day 39, where it remained until the end of the experiment (Figure 3F). A 45% smaller mean tumor size was also observed in the low protein group compared to the high protein group at the end of the experiment at day 53 ($p = 0.0038$) (Figure 3G). As for C57BL/6 mice, IGF-1 was measured after 16 days from the switch to different protein levels. In the low protein intake group, IGF-1 levels were reduced by 30% compared to those in the high level group ($p < 0.0001$) (Figure 3H). Additionally, a low protein intake also caused an IGFBP-1 increase of 84% ($p = 0.001$) (Figure 3I), similar to what was observed in the C57BL/6 genetic background (Figure 3D). Analogously, when soy protein intake was reduced from high levels to low levels, we observed a 30% decrease in IGF-1 ($p < 0.0001$) (Figure 3J) and a 140% increase in IGFBP-1 ($p < 0.0001$) (Figure 3K). Although there was a trend for an effect of substituting the same level of animal protein with plant protein on IGF-1 and IGFBP-1, the differences were not significant. These data suggest that lower protein intake may play a role in decreasing cancer incidence and/or progression in part by decreasing IGF-1 and increasing the IGF-1 inhibitor IGFBP-1. Additional studies on various types of animal- versus plant-based proteins are necessary to determine their effect on cancer, IGF-1, and IGFBP-1.

Cellular Studies

To test the hypothesis that there is a fundamental link between the level of amino acids and lifespan, the impact of the presence of specific concentrations of amino acids on yeast survival and mutation rate was assayed. A wild-type DBY746 *S. cerevisiae* strain was grown in the presence of half (0.5×), standard (1×), and double (2×) amino acid concentrations with all other nutrients maintained constant. Survival was measured at days 1, 3, 5, and 8. No survival differences were observed during days 1 and 3. At day 5, the two highest amino acid concentrations showed a trend for increased mortality, which resulted in a 10-fold decrease in surviving cells by day 8 (Figure 3L).

In order to assess the relationship between amino acids, aging, and age-dependent DNA damage, we used aging *S. cerevisiae* to measure spontaneous mutation rate (Madia et al., 2007). The mutation rate was 3- and 4-fold higher in 5-day-old but not young cells exposed to 1× and 2× amino acid levels, respectively, compared to cells exposed to a 0.5× amino acid concentration (Figure 3M). These results indicate that even in unicellular organisms, amino acids can promote cellular aging and age-dependent genomic instability.

To further discern the pathways involved in promoting age-dependent genomic instability, we measured the induction of stress responsive genes regulated by the Ras-PKA-Msn2/4 and Tor-Sch9-Gis1 pathways in the presence or absence of amino acids. For cells grown in control media containing only tryptophan (Trp), leucine (Leu), and histidine (His) (essential for growth in this strain), the presence of all amino acids in the media reduced the induction of stress resistance transcription factors Msn2/4 (STRE) and Gis1 (PDS), indicating that the addition of amino acids was sufficient to inhibit cellular protection (Figure 3N).

The Tor-Sch9 pathway extends longevity but also promotes DNA mutations (Madia et al., 2009; Wei et al., 2008). To determine whether Ras-cAMP-PKA signaling also regulates age-dependent genomic instability, we studied Ras2-deficient mutants. We confirmed that *ras2Δ* mutants are long-lived (Figure S1H) but also show that inactivation of Ras signaling attenuated age- and oxidative stress-dependent genomic instability (Figures S1I, S1J, 3O, and S1K). Together, these results indicate a mechanism where amino acids are able to affect mutation frequency and thus genomic instability, at least in part, by activation of the Tor-Sch9 and Ras/PKA pathways and decreased stress resistance (Figure 3P).

Low Protein Intake and Weight Maintenance in Old Mice

Based on the observed opposite effects of a low protein diet in subjects 50–65 years old versus those 66 and older and on the major drop in BMI and IGF-1 levels after age 65, we

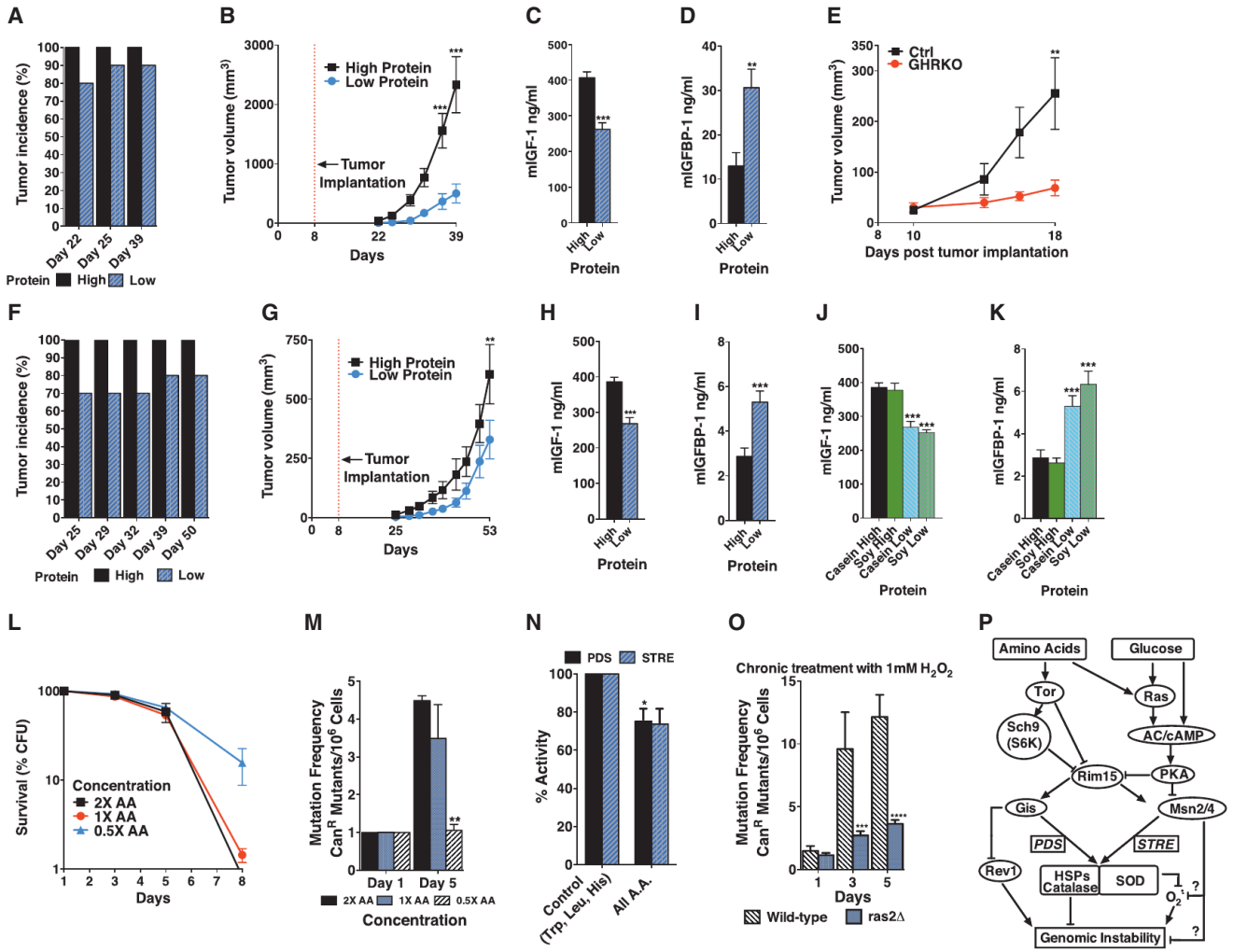

Figure 3. Effects of Proteins and Amino Acids on Tumor Progression or DNA Damage in Mouse and *S. cerevisiae* Models

(A) Tumor incidence in 18-week-old male C57BL/6 mice implanted with 20,000 melanoma (B16) cells and fed either a high protein (18%; n = 10) or low protein (4%; n = 10) diet.

(B) B16 tumor volume progression in 18-week-old male C57BL/6 mice fed either a high protein (n = 10) or low protein (n = 10) diet.

(C) IGF-1 at day 16 in 18-week-old male C57BL/6 mice fed either a high protein (n = 5) or low protein (n = 5) diet.

(D) IGFBP-1 at day 16 in 18-week-old male C57BL/6 mice fed either a high protein (n = 10) or low protein (n = 10) diet.

(E) B16 melanoma tumor progression in 10-month-old female GHRKO mice (n = 5) versus age-matched littermate controls (Ctrl; n = 7).

(F) Tumor incidence in 12-week-old female BALB/c mice implanted with 20,000 breast cancer (4T1) cells and fed either a high protein (18%; n = 10) or low protein (7%; n = 10) diet.

(G) 4T1 breast cancer progression in 12-week-old female BALB/c mice fed either a high protein (n = 10) or low protein (n = 10) diet.

(H) IGF-1 at day 16 in 12-week-old female BALB/c mice fed either a high animal protein (n = 5) or low animal protein (n = 5) diet.

(I) IGFBP-1 at day 16 in 12-week-old female BALB/c mice fed either a high animal protein (n = 10) or low animal protein (n = 10) diet.

(J) IGF-1 at day 16 in 12-week-old female BALB/c mice fed either a high soy protein (n = 5) or low soy protein (n = 5) diet.

(K) IGFBP-1 at day 16 in 12-week-old female BALB/c mice fed either high soy protein (n = 10) or low soy protein (n = 10) diet.

(L and M) Survival (L) and DNA mutation frequency (M) of yeast exposed to a 0.5×, 1×, or 2× concentration of a standard amino acid mix.

(N) PDS and STRE activity in yeast grown in media containing only Trp, Leu, and His compared to those grown in the presence of all amino acids.

(O) *RAS2* deletion protects against oxidative stress-induced genomic instability measured as DNA mutation frequency (Can^r) in wild-type (DBY746) and *ras2Δ* mutants chronically exposed to 1 mM H_2O_2.

(P) A model for the effect of amino acids on aging and genomic instability in *S. cerevisiae*. Amino acids activate the Tor-Sch9 and Ras-cAMP-PKA pathway also activated by glucose and promote age- and oxidative stress-dependent genomic instability in part via reduced activity of Gis1 and Msn2/4. In all graphs, data points represent the mean of the biological replicates ± SEM. *p < 0.05, **p < 0.01, ***p < 0.001.

hypothesized that older subjects on a low protein diet may become malnourished and unable to absorb or process a sufficient level of amino acids. To test this possibility in mice, we fed young mice (18 weeks old) and old mice (24 months old) with isocaloric diets containing either 18% or 4% animal protein. A very low protein diet was purposely selected to reveal any sensitivity to protein restriction in an old organism. Whereas old mice maintained on a high protein diet for 30 days gained

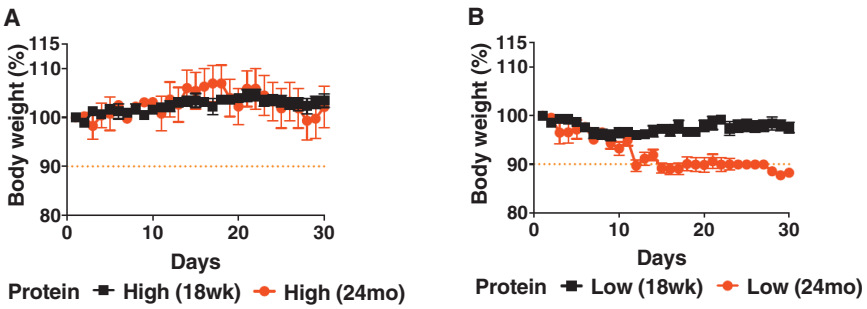

Figure 4. Effect of Protein Intake on Body Weight in Young and Old Mice

(A) Young (18-week-old; n = 10) and old (24-month-old; n = 6) C57BL/6 mice fed a high (18%) protein diet.

(B) Young (18-week-old; n = 10) and old (24-month-old; n = 6) C57BL/6 mice fed a low (4%) protein diet. Data points represent mean ± SEM.

weight, old but not young mice on a low protein diet lost 10% of their weight by day 15 (Figures 4A and 4B), in agreement with the effect of aging on turning the beneficial effects of protein restriction on mortality into negative effects.

DISCUSSION

Here, using a major nationally representative study of nutrition in the United States population, our results show that among those ages 50 and above, the level of protein intake is associated with increased risk of diabetes mortality, but not associated with differences in all-cause, cancer, or CVD mortality. Nevertheless, we found an age interaction for the association between protein consumption and mortality, both overall and from cancer, with subjects ages 50–65 years potentially experiencing benefits from low protein intake, and subjects ages 66+ experiencing detriments. This may explain why previously the strong association between protein intake, IGF-1, disease, and mortality has been poorly understood and controversial (Saydah et al., 2007). Furthermore, among 2,253 subjects, the risks of all-cause and cancer mortality for those with high protein intake compared to the low protein intake group were increased even further for those who also had high levels of IGF-1. This is in agreement with previous studies associating IGF-1 levels to various types of cancer (Giovannucci et al., 2003; Guevara-Aguirre et al., 2011; Pollak et al., 2004).

Notably, our results showed that the amount of proteins derived from animal sources accounted for a significant proportion of the association between overall protein intake and all-cause and cancer mortality. These results are in agreement with recent findings on the association between red meat consumption and death from all-cause and cancer (Fung et al., 2010; Pan et al., 2012). Previous studies in the U.S. have found that a low carbohydrate diet is associated with an increase in overall mortality and showed that when such a diet is from animal-based products, the risk of overall as well as cancer mortality is increased even further (Fung et al., 2010; Lagiou et al., 2007). Our study indicates that high levels of animal proteins, promoting increases in IGF-1 and possibly insulin, is one of the major promoters of mortality for people age 50–65 in the 18 years following the survey assessing protein intake.

Our results from yeast and mice may explain at least part of the fundamental connection between protein intake, cancer, and overall mortality by providing a link between amino acids, stress resistance, DNA damage, and cancer incidence/progression. In mice, the changes caused by reduced protein levels had an effect potent enough to prevent the establishment of 10%–30% of tumors, even when 20,000 tumor cells were already present at a subcutaneous site. Furthermore, the progression of both melanoma and breast cancer was strongly attenuated by the low protein diet, indicating that low protein diets may have applications in both cancer prevention and treatment, in agreement with previous studies (Fontana et al., 2006, 2008; McCarty, 2011; Youngman, 1993).

Although protein intake is associated with increased mortality for adults who were middle-aged at baseline, there was also evidence that a low protein diet may be hazardous for older adults. Both high and moderate protein intake in the elderly were associated with reduced mortality compared to that in the low protein group, suggesting that protein intake representing at least 10% of the calories consumed may be necessary after age 65 to reduce age-dependent weight loss and prevent an excessive loss of IGF-1 and of other important factors. In fact, previous studies have noted that an increased protein intake and the resulting increase in IGF-1 may prove beneficial in older adults (Heaney et al., 1999), and the switch from the protective to the detrimental effect of the low protein diet coincides with a time at which weight begins to decline. Based on previous longitudinal studies, weight tends to increase up until age 50–60, at which point it becomes stable before beginning to decline steadily by an average of 0.5% per year for those over age 65 (Villareal et al., 2005; Wallace et al., 1995). We speculate that frail subjects who have lost a significant percentage of their body weight and have a low BMI may be more susceptible to protein malnourishment. It is also possible that other factors such as inflammation or genetic factors may contribute to the sensitivity to protein restriction in elderly subjects, in agreement with our mouse studies.

Although other studies have noted age-associated declines of nutrient absorption in rodents related to changes in the pH microclimate, impaired adaptive response in the aged gut, and changes in the morphology of the intestine, there is still no clear association between food absorption and mortality (Chen et al., 1990; Woudstra and Thomson, 2002). In humans, some studies have shown that dietary protein digestion and absorption kinetics are not impaired in vivo in healthy, elderly men. However, these studies have also reported increased splanchnic extraction of amino acids, which might result in decreased availability to peripheral tissues, and speculated that in the case of low protein intake or increased protein requirement, the limited systemic availability of dietary amino acids may contribute to decreased muscle protein synthesis (Boirie et al., 1997; Koopman et al., 2009). Furthermore, in humans factors like poor dentition, medication, and psychosocial

issues also play a significant role in rates of malnourishment (Woudstra and Thomson, 2002).

IGF-1 has been previously shown to decrease at older ages (Iranmanesh et al., 1991), possibly increasing the risk of frailty (Lamberts et al., 1997) and mortality (Cappola et al., 2003). Thus our findings may explain the controversy related to IGF-1 and mortality indicating that a minimum level of proteins and possibly IGF-1 is important in the elderly, or that low circulating IGF-1 reflects a state of malnourishment, frailty, and/or morbidity (Maggio et al., 2007). In fact, inflammation and other disorders are known to decrease IGF-1 levels, raising the possibility that the low protein and low IGF-1 group may contain a significant number of both malnourished and frail individuals having or in the process of developing major diseases (Fontana et al., 2012).

There are some limitations to our study, which should be acknowledged. First, the use of a single 24 hr dietary recall followed by up to 18 years of mortality assessment has the potential of misclassifying dietary practice if the 24 hr period was not representative of a participant's normal day. However, 93% of our sample reported that the 24 hr period represented a normal day. We also include this variable as a control in our analysis. Furthermore, the 24 hr dietary recall has been shown to be a valid approach to identify the ''usual diet'' of subjects (Blanton et al., 2006; Conway et al., 2004; Coulston and Boushey, 2008; Prentice et al., 2011). While we must admit that the lack of longitudinal data on dietary consumption is a potential limitation of our study, study of dietary consistency over six years among older people revealed little change over time in dietary habits (Garry et al., 1989). Another study looking at dietary habits over 20 years showed that while energy intake decreased for protein, fat, and carbohydrates as people aged, the decreases were equal across the three types (Flynn et al., 1992).

Another limitation of our study is classification of respondents into protein intake groups and small sample sizes, especially for analyses involving diabetes mortality among persons without diabetes at baseline, or participants in the IGF-1 subsample. As a result, our hazard ratios and 95% confidence intervals may be much larger than what would have been seen with a larger sample size. Nevertheless, one would expect a small sample size to decrease statistical power and make it harder to detect associations. Therefore, our ability to detect significance indicates that the associations between protein and mortality are robust. Furthermore, the lower limits of the 95% confidence intervals from our mortality analyses were well above 1.0, signifying that the increased risk is probably large. Finally, given these limitations, our study was strengthened by its use of reliable cause-specific mortality data, as well as its inclusion of a large nationally representative sample, a feature often missing from the previous literature.

Overall, our human and animal studies indicate that a low protein diet during middle age is likely to be beneficial for the prevention of cancer, overall mortality, and possibly diabetes through a process that may involve, at least in part, regulation of circulating IGF-1 and possibly insulin levels. In agreement with other epidemiological and animal studies (Estruch et al., 2013; Linos and Willett, 2007; Michaud et al., 2001; Willett, 2006), our findings suggest that a diet in which plant-based nutrients represent the majority of the food intake is likely to maximize health benefits in all age groups. However, we propose that up to age 65 and possibly 70, depending on health status, the 0.7 to 0.8 g of proteins/kg of body weight/day reported by the Food and Nutrition Board of the Institute of Medicine, currently viewed as a minimum requirement, should be recommended instead of the 1.0–1.3 g grams of proteins/kg of body weight/day consumed by adults ages 19–70 (Fulgoni, 2008). We also propose that at older ages, it may be important to avoid low protein intake and gradually adopt a moderate to high protein, preferably mostly plant-based consumption to allow the maintenance of a healthy weight and protection from frailty (Bartali et al., 2006; Ferrucci et al., 2003; Kobayashi et al., 2013).

EXPERIMENTAL PROCEDURES

Nutrient Intake for Human Data

Nutrient intake data are based on reports of food and beverage intake during a 24 hr period. Data were collected via an automated, microcomputer-based coding system, with information on over 80 nutrients. There are several advantages to using this method for collecting dietary data. Given that the time elapsing between consumption and recall is short, participants are typically able to recall more information. Also, unlike many other reporting methods, 24 hr dietary recall relies on data collection after consumption, reducing the potential for assessment to alter dietary behaviors (Coulston and Boushey, 2008). Furthermore, 24 hr recalls have been shown to be a stronger estimate of total energy and protein consumption compared to the commonly used food frequency questionnaires (Prentice et al., 2011), and have also been shown to be a more valid measure of total energy and nutrient intake than both the Block food-frequency questionnaire and the National Cancer Institute's Diet History Questionnaire (Blanton et al., 2006). Finally, this approach has been found to accurately assess energy, protein, fat, and carbohydrate intake, regardless of body mass index (Conway et al., 2004).

Epidemiological Mortality Follow-Up

Mortality data were available from the National Death Index. Information for 113 potential underlying causes of death (UCOD-113) was used to determine all-cause mortality, cardiovascular mortality, cancer mortality, and diabetes mortality.

Statistical Analysis for Human Data

Cox proportional hazard models were used to estimate the association between intake of calories from protein on subsequent all-cause, CVD, cancer, and diabetes mortality, with the latter three run using competing-risks structures. Next we tested the interaction between age and protein consumption on the association with mortality. Based on these results, we categorized subjects into two age groups (50–65 years and 66+ years), which were used in the remainder of the analyses. age-stratified proportional hazard models were used to estimate the association of percent calories from protein with mortality within the two age groups and examine whether the relationship was influenced by percent of calories from fat, percent of calories from carbohydrates, or animal protein. Hazard models were re-estimated for the IGF-1 subsample to determine whether including IGF-1 changed the association between protein intake and mortality. Finally, proportional hazard models were used to examine the interaction between protein and IGF-1 and to calculate predicted hazard ratios for each protein group at various IGF-1 levels, to determine whether protein intake is differentially associated with mortality depending on levels of IGF-1. All analyses were run using sample weights, accounting for sampling design, and controlling for age, race/ethnicity, education, sex, disease status, smoking, dietary changes, attempted weight loss, and total calorie consumption.

Cancer Models in Mice

All animal experiments were performed according to procedures approved by USC's Institutional Animal Care and Use Committee. To establish a subcutaneous cancer mouse model, we injected 18-week-old male C57BL/6 mice as well as 10-month-old GHRKO mice, age-matched littermate control mice with B16 melanoma cells, and 12-week-old female BALB/c with 4T1 breast

cancer cells. Before injection, cells in log phase of growth were harvested and suspended in serum-free, high-glucose Dulbecco's modified Eagle's medium (DMEM) at 2×10^5 or 2×10^6 cells/ml, and 100 μl (2×10^4 cells per C57BL/6 or BALB/c mouse; 2×10^5 cells per GHRKO mouse) was subsequently injected subcutaneously in the lower back. All mice were shaved before subcutaneous tumor injection. Tumor incidence was determined by palpation of the injected area, and tumor size was measured using a digital Vernier caliper starting 10–15 days postimplantation. The experiments for C57BL/6 and BALB/c mice ended at different time points based on USC IACUC-approved humane endpoint criteria for tumor size and ulceration.

SUPPLEMENTAL INFORMATION

Supplemental Information includes two figures, seven tables, Supplemental Results, and Supplemental Experimental Procedures and can be found with this article online at http://dx.doi.org/10.1016/j.cmet.2014.02.006.

ACKNOWLEDGMENTS

GHRKO (C57BL/6 background) mice were kindly provided by J.J. Kopchick (Ohio University). This work was funded by NIH/NIA grants (AG20642, AG025135, and AG034906) to V.D.L., NIH/NIA grants (P30AG017265 and T32AG0037) to E.M.C., and a USC Norris Cancer Center pilot grant to V.D.L. The funding sources had no involvement in study design; in the collection, analysis and interpretation of data; in the writing of the report; and in the decision to submit the article for publication. V.D.L. has equity interest in L-Nutra, a company that develops medical food. The other authors declare that they have no conflicts of interest.

Received: December 4, 2013
Revised: January 24, 2014
Accepted: February 10, 2014
Published: March 4, 2014

REFERENCES

Ayala, V., Naudí, A., Sanz, A., Caro, P., Portero-Otin, M., Barja, G., and Pamplona, R. (2007). Dietary protein restriction decreases oxidative protein damage, peroxidizability index, and mitochondrial complex I content in rat liver. J. Gerontol. A Biol. Sci. Med. Sci. *62*, 352–360.

Bartali, B., Frongillo, E.A., Bandinelli, S., Lauretani, F., Semba, R.D., Fried, L.P., and Ferrucci, L. (2006). Low nutrient intake is an essential component of frailty in older persons. J. Gerontol. A Biol. Sci. Med. Sci. *61*, 589–593.

Bartke, A., Brown-Borg, H., Mattison, J., Kinney, B., Hauck, S., and Wright, C. (2001). Prolonged longevity of hypopituitary dwarf mice. Exp. Gerontol. *36*, 21–28.

Bellush, L.L., Doublier, S., Holland, A.N., Striker, L.J., Striker, G.E., and Kopchick, J.J. (2000). Protection against diabetes-induced nephropathy in growth hormone receptor/binding protein gene-disrupted mice. Endocrinology *141*, 163–168.

Blanton, C.A., Moshfegh, A.J., Baer, D.J., and Kretsch, M.J. (2006). The USDA Automated Multiple-Pass Method accurately estimates group total energy and nutrient intake. J. Nutr. *136*, 2594–2599.

Boirie, Y., Gachon, P., and Beaufrère, B. (1997). Splanchnic and whole-body leucine kinetics in young and elderly men. Am. J. Clin. Nutr. *65*, 489–495.

Brown-Borg, H.M., and Bartke, A. (2012). GH and IGF1: roles in energy metabolism of long-living GH mutant mice. J. Gerontol. A Biol. Sci. Med. Sci. *67*, 652–660.

Brown-Borg, H.M., Borg, K.E., Meliska, C.J., and Bartke, A. (1996). Dwarf mice and the ageing process. Nature *384*, 33.

Cappola, A.R., Xue, Q.L., Ferrucci, L., Guralnik, J.M., Volpato, S., and Fried, L.P. (2003). Insulin-like growth factor I and interleukin-6 contribute synergistically to disability and mortality in older women. J. Clin. Endocrinol. Metab. *88*, 2019–2025.

Cava, E., and Fontana, L. (2013). Will calorie restriction work in humans? Aging (Albany, N.Y. Online) *5*, 507–514.

Chen, T.S., Currier, G.J., and Wabner, C.L. (1990). Intestinal transport during the life span of the mouse. J. Gerontol. *45*, B129–B133.

Colman, R.J., Anderson, R.M., Johnson, S.C., Kastman, E.K., Kosmatka, K.J., Beasley, T.M., Allison, D.B., Cruzen, C., Simmons, H.A., Kemnitz, J.W., and Weindruch, R. (2009). Caloric restriction delays disease onset and mortality in rhesus monkeys. Science *325*, 201–204.

Conway, J.M., Ingwersen, L.A., and Moshfegh, A.J. (2004). Accuracy of dietary recall using the USDA five-step multiple-pass method in men: an observational validation study. J. Am. Diet. Assoc. *104*, 595–603.

Coulston, A.M., and Boushey, C. (2008). Nutrition in the prevention and treatment of disease. (Amsterdam, Boston: Academic Press).

DHHS (2001). U.S. Department of Health and Human Services (DHHS). National Center for Health Statistics. Third National Health and Nutrition Examination Survey, 1988-1994, NHANES III. (Hyattsville, MD: Centers for Disease Control and Prevention).

Estruch, R., Ros, E., Salas-Salvadó, J., Covas, M.I., Corella, D., Arós, F., Gómez-Gracia, E., Ruiz-Gutiérrez, V., Fiol, M., Lapetra, J., et al.; PREDIMED Study Investigators (2013). Primary prevention of cardiovascular disease with a Mediterranean diet. N. Engl. J. Med. *368*, 1279–1290.

Fabrizio, P., Pozza, F., Pletcher, S.D., Gendron, C.M., and Longo, V.D. (2001). Regulation of longevity and stress resistance by Sch9 in yeast. Science *292*, 288–290.

Ferrucci, L., Guralnik, J.M., Cavazzini, C., Bandinelli, S., Lauretani, F., Bartali, B., Repetto, L., and Longo, D.L. (2003). The frailty syndrome: a critical issue in geriatric oncology. Crit. Rev. Oncol. Hematol. *46*, 127–137.

Flynn, M.A., Nolph, G.B., Baker, A.S., and Krause, G. (1992). Aging in humans: a continuous 20-year study of physiologic and dietary parameters. J. Am. Coll. Nutr. *11*, 660–672.

Fontana, L., and Klein, S. (2007). Aging, adiposity, and calorie restriction. JAMA *297*, 986–994.

Fontana, L., Klein, S., and Holloszy, J.O. (2006). Long-term low-protein, low-calorie diet and endurance exercise modulate metabolic factors associated with cancer risk. Am. J. Clin. Nutr. *84*, 1456–1462.

Fontana, L., Weiss, E.P., Villareal, D.T., Klein, S., and Holloszy, J.O. (2008). Long-term effects of calorie or protein restriction on serum IGF-1 and IGFBP-3 concentration in humans. Aging Cell *7*, 681–687.

Fontana, L., Partridge, L., and Longo, V.D. (2010). Extending healthy life span—from yeast to humans. Science *328*, 321–326.

Fontana, L., Vinciguerra, M., and Longo, V.D. (2012). Growth factors, nutrient signaling, and cardiovascular aging. Circ. Res. *110*, 1139–1150.

Fontana, L., Adelaiye, R.M., Rastelli, A.L., Miles, K.M., Ciamporcero, E., Longo, V.D., Nguyen, H., Vessella, R., and Pili, R. (2013). Dietary protein restriction inhibits tumor growth in human xenograft models. Oncotarget *4*, 2451–2461.

Fulgoni, V.L., 3rd. (2008). Current protein intake in America: analysis of the National Health and Nutrition Examination Survey, 2003-2004. Am. J. Clin. Nutr. *87*, 1554S–1557S.

Fung, T.T., van Dam, R.M., Hankinson, S.E., Stampfer, M., Willett, W.C., and Hu, F.B. (2010). Low-carbohydrate diets and all-cause and cause-specific mortality: two cohort studies. Ann. Intern. Med. *153*, 289–298.

Gallinetti, J., Harputlugil, E., and Mitchell, J.R. (2013). Amino acid sensing in dietary-restriction-mediated longevity: roles of signal-transducing kinases GCN2 and TOR. Biochem. J. *449*, 1–10.

Garry, P.J., Rhyne, R.L., Halioua, L., and Nicholson, C. (1989). Changes in dietary patterns over a 6-year period in an elderly population. Ann. N Y Acad. Sci. *561*, 104–112.

Giovannucci, E., Pollak, M., Liu, Y., Platz, E.A., Majeed, N., Rimm, E.B., and Willett, W.C. (2003). Nutritional predictors of insulin-like growth factor I and their relationships to cancer in men. Cancer Epidemiol. Biomarkers Prev. *12*, 84–89.

Guarente, L., and Kenyon, C. (2000). Genetic pathways that regulate ageing in model organisms. Nature *408*, 255–262.

Guevara-Aguirre, J., Balasubramanian, P., Guevara-Aguirre, M., Wei, M., Madia, F., Cheng, C.W., Hwang, D., Martin-Montalvo, A., Saavedra, J., Ingles, S., et al. (2011). Growth hormone receptor deficiency is associated with a major reduction in pro-aging signaling, cancer, and diabetes in humans. Sci. Transl. Med. *3*, 70ra13.

Hauck, S.J., Aaron, J.M., Wright, C., Kopchick, J.J., and Bartke, A. (2002). Antioxidant enzymes, free-radical damage, and response to paraquat in liver and kidney of long-living growth hormone receptor/binding protein gene-disrupted mice. Horm. Metab. Res. *34*, 481–486.

Heaney, R.P., McCarron, D.A., Dawson-Hughes, B., Oparil, S., Berga, S.L., Stern, J.S., Barr, S.I., and Rosen, C.J. (1999). Dietary changes favorably affect bone remodeling in older adults. J. Am. Diet. Assoc. *99*, 1228–1233.

Horáková, M., Deyl, Z., Hausmann, J., and Macek, K. (1988). The effect of low protein-high dextrin diet and subsequent food restriction upon life prolongation in Fischer 344 male rats. Mech. Ageing Dev. *45*, 1–7.

Hursting, S.D., Lashinger, L.M., Colbert, L.H., Rogers, C.J., Wheatley, K.W., Nunez, N.P., Mahabir, S., Barrett, J.C., Forman, M.R., and Perkins, S.N. (2007). Energy balance and carcinogenesis: underlying pathways and targets for intervention. Curr. Cancer Drug Targets *7*, 484–491.

Iranmanesh, A., Lizarralde, G., and Veldhuis, J.D. (1991). Age and relative adiposity are specific negative determinants of the frequency and amplitude of growth hormone (GH) secretory bursts and the half-life of endogenous GH in healthy men. J. Clin. Endocrinol. Metab. *73*, 1081–1088.

Johnson, T.E. (1990). Increased life-span of age-1 mutants in Caenorhabditis elegans and lower Gompertz rate of aging. Science *249*, 908–912.

Kapahi, P., and Zid, B. (2004). TOR pathway: linking nutrient sensing to life span. Sci. SAGE KE *2004*, PE34.

Kenyon, C. (2005). The plasticity of aging: insights from long-lived mutants. Cell *120*, 449–460.

Kenyon, C.J. (2010). The genetics of ageing. Nature *464*, 504–512.

Kenyon, C. (2011). The first long-lived mutants: discovery of the insulin/IGF-1 pathway for ageing. Philos. Trans. R. Soc. Lond. B Biol. Sci. *366*, 9–16.

Kenyon, C., Chang, J., Gensch, E., Rudner, A., and Tabtiang, R. (1993). A C. elegans mutant that lives twice as long as wild type. Nature *366*, 461–464.

Kobayashi, S., Asakura, K., Suga, H., and Sasaki, S.; Three-generation Study of Women on Diets and Health Study Group (2013). High protein intake is associated with low prevalence of frailty among old Japanese women: a multicenter cross-sectional study. Nutr. J. *12*, 164.

Koopman, R., Walrand, S., Beelen, M., Gijsen, A.P., Kies, A.K., Boirie, Y., Saris, W.H., and van Loon, L.J. (2009). Dietary protein digestion and absorption rates and the subsequent postprandial muscle protein synthetic response do not differ between young and elderly men. J. Nutr. *139*, 1707–1713.

Lagiou, P., Sandin, S., Weiderpass, E., Lagiou, A., Mucci, L., Trichopoulos, D., and Adami, H.O. (2007). Low carbohydrate-high protein diet and mortality in a cohort of Swedish women. J. Intern. Med. *261*, 366–374.

Lamberts, S.W., van den Beld, A.W., and van der Lely, A.J. (1997). The endocrinology of aging. Science *278*, 419–424.

Leto, S., Kokkonen, G.C., and Barrows, C.H., Jr. (1976). Dietary protein, lifespan, and biochemical variables in female mice. J. Gerontol. *31*, 144–148.

Linos, E., and Willett, W.C. (2007). Diet and breast cancer risk reduction. J. Natl. Compr. Canc. Netw. *5*, 711–718.

Longo, V.D. (1999). Mutations in signal transduction proteins increase stress resistance and longevity in yeast, nematodes, fruit flies, and mammalian neuronal cells. Neurobiol. Aging *20*, 479–486.

Madia, F., Gattazzo, C., Fabrizio, P., and Longo, V.D. (2007). A simple model system for age-dependent DNA damage and cancer. Mech. Ageing Dev. *128*, 45–49.

Madia, F., Wei, M., Yuan, V., Hu, J., Gattazzo, C., Pham, P., Goodman, M.F., and Longo, V.D. (2009). Oncogene homologue Sch9 promotes age-dependent mutations by a superoxide and Rev1/Polzeta-dependent mechanism. J. Cell Biol. *186*, 509–523.

Maggio, M., Lauretani, F., Ceda, G.P., Bandinelli, S., Ling, S.M., Metter, E.J., Artoni, A., Carassale, L., Cazzato, A., Ceresini, G., et al. (2007). Relationship between low levels of anabolic hormones and 6-year mortality in older men: the aging in the Chianti Area (InCHIANTI) study. Arch. Intern. Med. *167*, 2249–2254.

Mair, W., Piper, M.D., and Partridge, L. (2005). Calories do not explain extension of life span by dietary restriction in Drosophila. PLoS Biol. *3*, e223.

Masternak, M.M., and Bartke, A. (2012). Growth hormone, inflammation and aging. Pathobiol Aging Age Relat Dis *2*, http://dx.doi.org/10.3402/pba.v2i0.17293.

Mattison, J.A., Roth, G.S., Beasley, T.M., Tilmont, E.M., Handy, A.M., Herbert, R.L., Longo, D.L., Allison, D.B., Young, J.E., Bryant, M., et al. (2012). Impact of caloric restriction on health and survival in rhesus monkeys from the NIA study. Nature *489*, 318–321.

McCarty, M.F. (2011). mTORC1 activity as a determinant of cancer risk—rationalizing the cancer-preventive effects of adiponectin, metformin, rapamycin, and low-protein vegan diets. Med. Hypotheses *77*, 642–648.

Mercken, E.M., Crosby, S.D., Lamming, D.W., JeBailey, L., Krzysik-Walker, S., Villareal, D.T., Capri, M., Franceschi, C., Zhang, Y., Becker, K., et al. (2013). Calorie restriction in humans inhibits the PI3K/AKT pathway and induces a younger transcription profile. Aging Cell *12*, 645–651.

Michaud, D.S., Augustsson, K., Rimm, E.B., Stampfer, M.J., Willet, W.C., and Giovannucci, E. (2001). A prospective study on intake of animal products and risk of prostate cancer. Cancer Causes Control *12*, 557–567.

Pamplona, R., and Barja, G. (2006). Mitochondrial oxidative stress, aging and caloric restriction: the protein and methionine connection. Biochim. Biophys. Acta *1757*, 496–508.

Pan, A., Sun, Q., Bernstein, A.M., Schulze, M.B., Manson, J.E., Stampfer, M.J., Willett, W.C., and Hu, F.B. (2012). Red meat consumption and mortality: results from 2 prospective cohort studies. Arch. Intern. Med. *172*, 555–563.

Peng, W., Robertson, L., Gallinetti, J., Mejia, P., Vose, S., Charlip, A., Chu, T., and Mitchell, J.R. (2012). Surgical stress resistance induced by single amino acid deprivation requires Gcn2 in mice. Sci. Transl. Med. *4*, 18ra11.

Pollak, M.N., Schernhammer, E.S., and Hankinson, S.E. (2004). Insulin-like growth factors and neoplasia. Nat. Rev. Cancer *4*, 505–518.

Prentice, R.L., Mossavar-Rahmani, Y., Huang, Y., Van Horn, L., Beresford, S.A., Caan, B., Tinker, L., Schoeller, D., Bingham, S., Eaton, C.B., et al. (2011). Evaluation and comparison of food records, recalls, and frequencies for energy and protein assessment by using recovery biomarkers. Am. J. Epidemiol. *174*, 591–603.

Ross, M.H. (1961). Length of life and nutrition in the rat. J. Nutr. *75*, 197–210.

Sanz, A., Caro, P., Ayala, V., Portero-Otin, M., Pamplona, R., and Barja, G. (2006). Methionine restriction decreases mitochondrial oxygen radical generation and leak as well as oxidative damage to mitochondrial DNA and proteins. FASEB J. *20*, 1064–1073.

Saydah, S., Graubard, B., Ballard-Barbash, R., and Berrigan, D. (2007). Insulin-like growth factors and subsequent risk of mortality in the United States. Am. J. Epidemiol. *166*, 518–526.

Smith, W.J., Underwood, L.E., and Clemmons, D.R. (1995). Effects of caloric or protein restriction on insulin-like growth factor-I (IGF-I) and IGF-binding proteins in children and adults. J. Clin. Endocrinol. Metab. *80*, 443–449.

Stein, P.K., Soare, A., Meyer, T.E., Cangemi, R., Holloszy, J.O., and Fontana, L. (2012). Caloric restriction may reverse age-related autonomic decline in humans. Aging Cell *11*, 644–650.

Steuerman, R., Shevah, O., and Laron, Z. (2011). Congenital IGF1 deficiency tends to confer protection against post-natal development of malignancies. Eur. J. Endocrinol. *164*, 485–489.

Tatar, M., Kopelman, A., Epstein, D., Tu, M.P., Yin, C.M., and Garofalo, R.S. (2001). A mutant Drosophila insulin receptor homolog that extends life-span and impairs neuroendocrine function. Science *292*, 107–110.

Villareal, D.T., Apovian, C.M., Kushner, R.F., and Klein, S.; American Society for Nutrition; NAASO, The Obesity Society (2005). Obesity in older adults: technical review and position statement of the American Society for Nutrition and NAASO, The Obesity Society. Am. J. Clin. Nutr. *82*, 923–934.

Wallace, J.I., Schwartz, R.S., LaCroix, A.Z., Uhlmann, R.F., and Pearlman, R.A. (1995). Involuntary weight loss in older outpatients: incidence and clinical significance. J. Am. Geriatr. Soc. *43*, 329–337.

Wei, M., Fabrizio, P., Hu, J., Ge, H., Cheng, C., Li, L., and Longo, V.D. (2008). Life span extension by calorie restriction depends on Rim15 and transcription factors downstream of Ras/PKA, Tor, and Sch9. PLoS Genet. *4*, e13.

Wei, M., Fabrizio, P., Madia, F., Hu, J., Ge, H., Li, L.M., and Longo, V.D. (2009). Tor1/Sch9-regulated carbon source substitution is as effective as calorie restriction in life span extension. PLoS Genet. *5*, e1000467.

Willett, W.C. (2006). The Mediterranean diet: science and practice. Public Health Nutr. *9* (1A), 105–110.

Wolpin, B.M., Michaud, D.S., Giovannucci, E.L., Schernhammer, E.S., Stampfer, M.J., Manson, J.E., Cochrane, B.B., Rohan, T.E., Ma, J., Pollak, M.N., and Fuchs, C.S. (2007). Circulating insulin-like growth factor binding protein-1 and the risk of pancreatic cancer. Cancer Res. *67*, 7923–7928.

Woudstra, T., and Thomson, A.B. (2002). Nutrient absorption and intestinal adaptation with ageing. Best Pract. Res. Clin. Gastroenterol. *16*, 1–15.

Youngman, L.D. (1993). Protein restriction (PR) and caloric restriction (CR) compared: effects on DNA damage, carcinogenesis, and oxidative damage. Mutat. Res. *295*, 165–179.

Cell Metabolism
Article

The Ratio of Macronutrients, Not Caloric Intake, Dictates Cardiometabolic Health, Aging, and Longevity in Ad Libitum-Fed Mice

Samantha M. Solon-Biet,[1,2,3,4,13] Aisling C. McMahon,[1,2,3,13] J. William O. Ballard,[5] Kari Ruohonen,[6] Lindsay E. Wu,[7] Victoria C. Cogger,[1,2,3] Alessandra Warren,[1,2,3] Xin Huang,[1,2,3] Nicolas Pichaud,[5] Richard G. Melvin,[8] Rahul Gokarn,[2,3] Mamdouh Khalil,[3] Nigel Turner,[9] Gregory J. Cooney,[9] David A. Sinclair,[7,10] David Raubenheimer,[1,4,11,12] David G. Le Couteur,[1,2,3,*] and Stephen J. Simpson[1,4,*]

[1]Charles Perkins Centre, The University of Sydney, Sydney NSW 2006, Australia
[2]Centre for Education and Research on Aging, Concord Hospital, The University of Sydney, Sydney NSW 2139, Australia
[3]ANZAC Research Institute, Concord Hospital, The University of Sydney, Sydney NSW 2139, Australia
[4]School of Biological Sciences, The University of Sydney, NSW 2006, Australia
[5]School of Biotechnology and Biomolecular Sciences, University of New South Wales, Sydney NSW 2052, Australia
[6]EWOS Innovation, Dirdal 4335, Norway
[7]Laboratory for Aging Research, School of Medical Sciences, University of New South Wales, Sydney NSW 2052, Australia
[8]Institute of Biotechnology, University of Helsinki, Helsinki 00014, Finland
[9]Garvan Institute of Medical Research, University of New South Wales, Darlinghurst NSW 2010, Australia
[10]The Paul F. Glenn Laboratories for the Biological Mechanisms of Aging, Department of Genetics, Harvard Medical School, Boston, MA 02115, USA
[11]Institute of Natural Sciences, Massey University, Auckland 0632, New Zealand
[12]Faculty of Veterinary Science, The University of Sydney, Sydney NSW 2006, Australia
[13]These authors contributed equally to this work
*Correspondence: david.lecouteur@sydney.edu.au (D.G.L.C.), stephen.simpson@sydney.edu.au (S.J.S.)
http://dx.doi.org/10.1016/j.cmet.2014.02.009

SUMMARY

The fundamental questions of what represents a macronutritionally balanced diet and how this maintains health and longevity remain unanswered. Here, the Geometric Framework, a state-space nutritional modeling method, was used to measure interactive effects of dietary energy, protein, fat, and carbohydrate on food intake, cardiometabolic phenotype, and longevity in mice fed one of 25 diets ad libitum. Food intake was regulated primarily by protein and carbohydrate content. Longevity and health were optimized when protein was replaced with carbohydrate to limit compensatory feeding for protein and suppress protein intake. These consequences are associated with hepatic mammalian target of rapamycin (mTOR) activation and mitochondrial function and, in turn, related to circulating branched-chain amino acids and glucose. Calorie restriction achieved by high-protein diets or dietary dilution had no beneficial effects on lifespan. The results suggest that longevity can be extended in ad libitum-fed animals by manipulating the ratio of macronutrients to inhibit mTOR activation.

INTRODUCTION

Resolving the effects of dietary macronutrients on aging and health remains a fundamental challenge, with profound implications for human health. As in much of nutrition research, the focus has mainly concerned the effects of individual macronutrients, with proponents of fat, sugar, and protein each claiming primacy in the search for explanations for the global increase in rates of obesity and metabolic disease and dietary solutions for their prevention and treatment. There is, however, growing evidence from studies on a wide range of species that, rather than macronutrients acting singly, it is their interactive effects (i.e., their balance) that are more important for health and aging. In particular, it has emerged that the balance of protein to nonprotein energy in the diet is especially significant, influencing total energy intake, growth and development, body composition, reproduction, aging, gut microbial ecology, the susceptibility to obesity and metabolic disease, immune function, and resistance to infectious diseases (Blumfield et al., 2012; Gosby et al., 2011; Huang et al., 2013; Lee et al., 2008; Mayntz et al., 2009; Piper et al., 2011; Ponton et al., 2011; Simpson and Raubenheimer, 2009, 2012).

Defining what represents a balanced diet—and the consequences of not attaining such balance—is a high priority in nutrition research. Progress has been impeded, however, by the logistical challenges involved in designing dietary experiments able to disentangle the individual and interactive influences of multiple nutrients on the phenotype. The development of the Geometric Framework for nutrition (GF) now provides a platform for taming this complexity (Lee et al., 2008; Mayntz et al., 2005; Piper et al., 2011; Simpson and Raubenheimer, 2009, 2012). GF, a state-space modeling approach that explores how an animal responds to the problem of balancing multiple and changing nutrient needs in a multidimensional and variable nutritional environment, has been successful in solving and reconciling diverse and often conflicting conclusions about how nutrition influences

biology across taxa. The GF considers nutrition as an n-dimensional space in which the n components of any diet are represented by separate axes (in the case of macronutrients, there are three axes: protein, carbohydrate, and fat). Responses of individuals, such as lifespan, are phenotypic features that are superimposed on this n-dimensional nutritional space by plotting response surfaces (Lee et al., 2008; Piper et al., 2011; Simpson and Raubenheimer, 2009, 2012).

Here, we have used the GF to investigate how the balance and concentrations of macronutrients affect feeding, aging, and age-related cardiometabolic health in ad libitum-fed mice. We first consider how dietary macronutrients interact to determine chronic food and energy intakes in animals monitored over their lifetime and into old age. A central dogma of aging research is that caloric restriction (reduction of access to dietary energy to about 30%–50% of that consumed by ad libitum-fed controls, supplemented with micronutrients; Everitt et al., 2010) increases lifespan and delays aging, yet recent research has shown that the relationship between diet and aging is complex, particularly in ad libitum-fed animals, in which compensatory feeding regulates the relationship between dietary constituents and the actual dietary intake (Le Couteur et al., 2014; Simpson and Raubenheimer, 2007). Thus, we relate macronutrient intakes to longevity, in particular testing the extent to which lifespan in ad libitum-fed mice is determined by calorie intake per se or by the balance of protein to carbohydrate, as recently proposed from GF studies of insects (Fanson et al., 2009; Lee et al., 2008). These results are then related to known physiological mechanisms that link nutrition with aging biology. We focus on the mammalian target of rapamycin (mTOR) because it is activated by amino acids, thereby plausibly linking diet to a broad suite of cellular responses associated with aging (Kapahi et al., 2010). Moreover, inhibition of mTOR with rapamycin increases lifespan in mice fed a standard diet and represents evidence of pharmacological life extension in normal mammals (Harrison et al., 2009; Miller et al., 2011). We propose that the beneficial effects on aging generated by rapamycin might be replicated by titrating the intake of macronutrients, particularly protein. Finally, we establish the relationship between macronutrient and energy intake with key aspects of latelife cardiometabolic phenotype, which is an important determinant of lifespan and likely to contribute to many aspects of the aging process itself (Le Couteur and Lakatta, 2010).

The results provide an overarching schema for the relationship between diet balance, health, and aging. By simultaneously measuring key physiological correlates, we also link the nutritional phenotype to underlying mechanisms and place these mechanisms in a broader nutritional context than hitherto possible.

RESULTS

The data we present derive from 858 mice fed one of 25 diets differing systematically in protein, carbohydrate, and fat content and energy density. By their nature, these data are complex, and their graphical representation in 3D nutrient space is challenging, but can only be appreciated using this methodology. To assist understanding, the narrative of the main text is illustrated by 2D response surfaces, which are provided in figures and supplemental figures. These surfaces are interpreted statistically using General Additive Models (GAM). The complete statistical analyses are provided for each surface in the tables in the Supplemental Information.

Compensatory Feeding Occurred for Protein and Carbohydrate, but Less so for Fat

Mice were fed ad libitum over a lifetime on 1 of 25 diets differing in content of protein (5%–60%), fat (16%–75%), carbohydrate (16%–75%), and energy (8, 13, or 17 kJ/g of food) (Table S1). These dietary compositions were chosen according to the GF to sample a representative number of nutritional vectors (Figure S1 available online) and nutrient concentrations within protein-carbohydrate-fat diet space. One-third of the mice were culled at 15 months of age, and the remainder continued until they died naturally. This age was chosen for the cull because it represents late middle age, but before significant numbers of mice have died, which would introduce survivor bias into the results.

Food (Figures 1A and S2A) and energy intakes (Figures 1C and S2B) were plotted as response surfaces mapped onto diet composition space and interpreted statistically using GAM. Food intake was assessed meticulously, including measurements of discarded food with fecal matter removed, and values are similar to a previous study using this model (Huang et al., 2013). Values reported are per animal per day, averaged over the period of 6–15 months of age, during which time intakes were stable. As the concentrations of either protein or carbohydrate decreased in the diet, chronic food intake increased. This pattern of increasing food intake as nutrient concentrations fall in the food is consistent with compensatory feeding for these macronutrients controlled by nutrient-specific regulatory feedbacks (Sørensen et al., 2008). Regulatory feeding effects were most evident for dietary protein and less marked for dietary carbohydrate. In contrast, fat content in the diet was largely unregulated and thus had negligible influence on food intake (Figures 1A and 1B). Note that both protein and carbohydrate intakes decelerated as their proportions rose in the diet, whereas fat intake continued to increase as the proportion of dietary fat increased (Figure 1B, red lines show the values where half the maximal nutrient intake is reached). Food intake was reduced with high-protein-content diets once protein intake exceeded about 10 kJ/day, whereas carbohydrate intake decelerated once carbohydrate intake exceeded about 15 kJ/day. High-fat diets had minimal impact on food intake.

If nutrient-specific feedback mechanisms exist for fat (as they do, for example, in carnivores; Hewson-Hughes et al., 2011; Mayntz et al., 2009), they are clearly dominated by competing inputs from protein and carbohydrate. Consequently, total energy intake was highest on those diets with low protein and/or low carbohydrate content because compensatory overeating to achieve the protein or carbohydrate intake targets (sensu the GF; Simpson and Raubenheimer, 2012) was not counterbalanced by marked inhibitory effects of fat on total food intake. Leptin titers were positively associated with body fat (Figure 1D) and total macronutrient intake (Figure S2C), implying that leptin was not suppressing appetite.

At 6 and 15 months, mice ate similar amounts of protein regardless of the energy density of the diet, consistent with regulation to a protein intake target. However, at 24 months, which

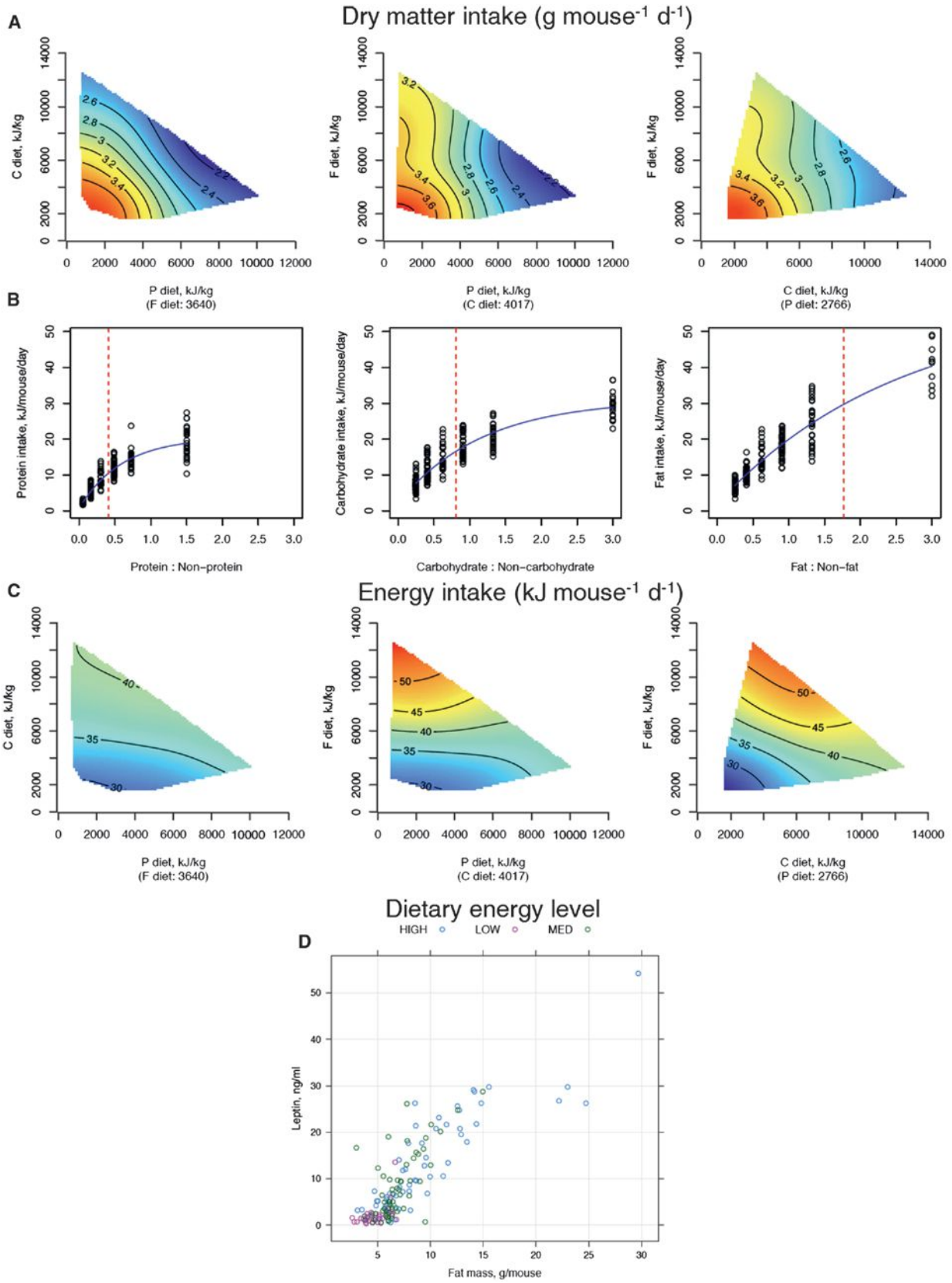

(legend on next page)

represents old age, mice ate similar amounts of food regardless of the energy density of their diets. This led to a reduction in the intake of energy and macronutrients in the old mice on the low-energy density diets and, conversely, increased intakes in old mice on high-energy density diets (Figure S2D).

The Balance of Dietary Macronutrients Influenced Longevity

The GF was used to establish the effects of macronutrient intakes on longevity. Median lifespan was greatest for animals whose intakes were low in protein and high in carbohydrate, but was not influenced by total calorie intake (Figure 2A). The results are consistent with recent reports in invertebrates showing that the ratio of protein to carbohydrate in the diet influences lifespan (Lee et al., 2008; Piper et al., 2011). The survival curves for the different ratios of protein to carbohydrate (Figure 2B) show that the longest median survival occurred in cohorts of mice on the lowest ratio diets, and there was a clear correlation between the ratio and lifespan. Median lifespan increased from about 95 to 125 weeks (approximately 30%; Table S2) as the protein-to-carbohydrate ratio decreased.

The presence of compensatory feeding for protein and carbohydrate, but less so for fat, shows that there is a complex interplay between dietary protein, carbohydrates, and total energy intake in ad libitum-fed animals, which may have competing consequences for lifespan and cellular regulatory pathways. Therefore, Cox regression analysis was performed to assess the independent effects of energy intake and protein-to-carbohydrate ratio on lifespan and to take into account individual animal survival data. Analyses were performed both for total macronutrient and energy intakes (Figures 2D and 2E) and for intakes corrected for lean body mass (Figures 2F and 2G). The proportional hazards assumption was tested and found to be valid for each analysis (data not shown). Overall, there was an increase in the hazard ratio for death as the protein to carbohydrate ratio increased, consistent with the univariate analysis (Figures 2D and 2F).

Reduction in calorie intake was achieved by diluting the food with nondigestible cellulose, which allows ad libitum feeding but restricts total energy intake when compensation for dilution by increasing food intake is incomplete. Mice fed experimental diets containing 50% nondigestible cellulose ate a greater bulk of food (3.6 ± 0.4 versus 2.5 ± 0.4 g/day) but ingested about 30% less total energy than mice provided with food containing higher energy content (29.9 ± 3.2 versus 42.1 ± 7.3 kJ/day). Therefore, these mice had a reduction in energy intake similar to those reported in nearly all other studies of calorie restriction in which access to food was restricted (Everitt et al., 2010). Except at the oldest ages, mice on the low-energy diets were able to achieve their protein target through increasing chronic food intake (protein intake: 9.6 ± 4.3 kJ/day with low-energy diets versus 9.6 ± 6.3 kJ/day with high-energy diets). When corrected for lean body mass, the hazard ratio for death was not influenced by calorie intake, except at the highest energy intakes, which were achieved only by low-protein, high-fat diets (Figure 2G). The results suggest that energy restriction achieved by dietary dilution in ad libitum-fed animals does not extend lifespan, probably because animals can reach their target protein intake. It should be noted that previous caloric restriction experiments that reduce total food availability and observe longevity extension are unable to conclusively determine whether this effect was due to restriction of total calories or one or more specific nutrients in the diet (such as protein); previous aging studies in which protein content of the diet was reduced in ad libitum-fed animals may not have increased lifespan because of compensatory feeding.

The Relationship between Diet and Longevity Was Associated with Hepatic mTOR Activation

To link these relationships to signaling pathways and mechanisms implicated in appetite, aging, and cardiometabolic health, we measured insulin, activation state of mTOR in the liver, circulating amino acids, and hepatic mitochondrial activity. Insulin and mTOR are strongly implicated in the relationship between diet and aging (Burnett et al., 2011; Fontana et al., 2010; Kapahi et al., 2010). Amino acids, particularly branched-chain amino acids (BCAA), are key signals for insulin release and mTOR activation (Chotechuang et al., 2009; Yang et al., 2010).

Among plasma free amino acids, BCAA levels correlated positively with chronic daily protein intake, with maximum levels occurring at the protein intake of approximately 10–20 kJ/mouse/day (Figures 3A and S3A). In strong contrast to BCAA, all other free amino acids correlated negatively with protein intake (Table 1 and Table S5). For BCAA, there was a sigmoidal relationship with the dietary protein:carbohydrate ratio, reaching a plateau at just below about 45 μg/ml when the protein:carbohydrate ratio was approximately 0.5–0.6 (Figure 3B). Insulin was influenced by both dietary protein and carbohydrate and was minimal when protein intake was lowest and highest when carbohydrate intake was between 15 and 25 kJ/day (Figure 3C).

The activation of mTOR (the ratio of phosphorylated mTOR to total mTOR) was influenced by protein intake, albeit the effect, although significant, was small (Figure 3D). However, mTOR activation was strongly influenced by circulating glucose and BCAAs, reflecting protein and carbohydrate intakes, and on this analysis mTOR activation increased 3-fold as the plasma ratio of BCAAs to glucose increased (Figure 3E).

Figure 1. The Effects of Dietary Macronutrients on Food Intake

(A) Response surfaces showing the relationship between dry matter (DM) intake versus macronutrient content of the diet. Surfaces were fitted using generalized additive models (GAMs) with thin-plate splines. Three 2D slices are given to show all three nutrient dimensions (protein, P; carbohydrate, C; fat, F). For each 2D slice, the third factor is at its median (shown below the x axis in parentheses). In all surfaces, red indicates the highest value, while blue indicates the lowest value, with the colors standardized across the three slices.

(B) Relationship between protein, carbohydrate, and fat intake versus the proportion of protein, carbohydrate, and fat in the diet relative to the other macronutrients, respectively. A decelerating curve indicates regulation for a given nutrient, with the asymptote reflecting the target intake for that nutrient.

(C) Response surfaces showing the relationship between total energy intake versus macronutrient content of the diet. Energy intake was highest on low P:high F and low C:high F diets, presumably because mice overate in an attempt to achieve their protein or carbohydrate targets, with less compensatory suppression of food intake by fat.

(D) Relationship between body fat and leptin levels, according to the three energy density diets. See also Figure S2 and Table S3.

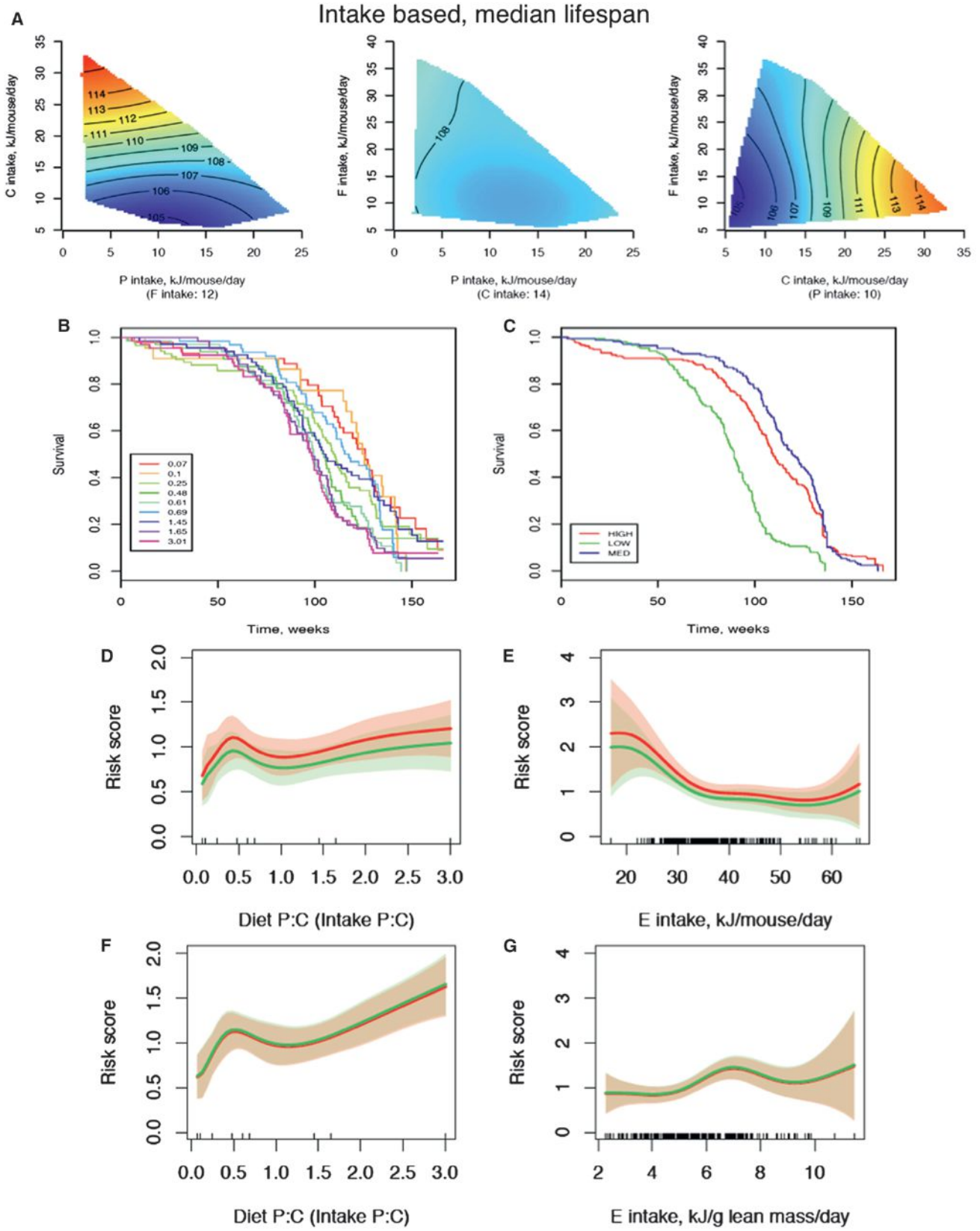

(legend on next page)

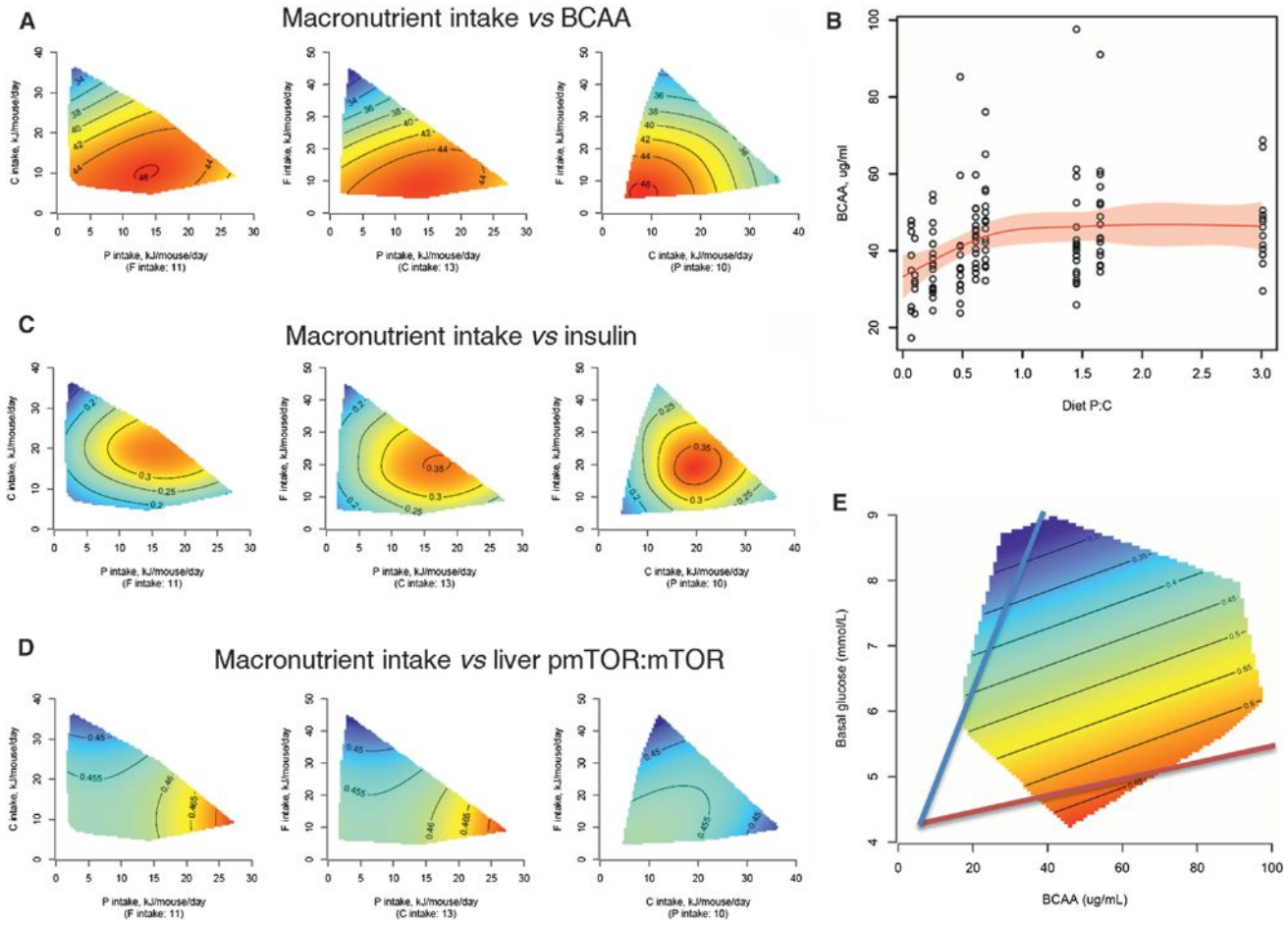

Figure 3. Mechanisms for the Relationship between Diet and Longevity

(A) Response surfaces showing the effect of macronutrient intake on the concentration of branched-chain amino acids (BCAAs) at 15 months (μg/ml). For each 2D slice, the third factor is at its median (shown below x axis in parenthesis).

(B) BCAAs in relation to dietary P:C ratio. Red curve is a fitted response by a GAM. Shadowed area shows 95% confidence interval of the fit.

(C) Response surfaces showing the effect of macronutrient intake on the concentration of insulin (ng/ml) at 15 months.

(D) Response surfaces showing the effect of macronutrient intake on mTOR activation (measured as the ratio of phosphorylated mTOR to total mTOR) in the liver at 15 months.

(E) Response surface showing the relationship between blood glucose, BCAA, and mTOR activation. The lowest activation state of mTOR is associated with a low ratio (blue line), and the highest activation state is associated with a high ratio (red line). See also Figure S3 and Table S5.

Changes in mitochondrial function and number are implicated in aging (Martin and Loeb, 2004). We used the Seahorse XF Extracellular Flux Analyzer (Horan et al., 2012) to study mitochondrial function in the liver because this is the main metabolic organ. Overall, the results indicate that a low protein intake in ad libitum-fed mice was associated with increased mitochondrial activity and elevated free radical production in the liver, which is similar to effects reported in caloric restriction studies (López-Lluch et al., 2006). There was a general pattern for dietary protein and protein intake to be positively associated with citrate

Figure 2. The Effects of Dietary Macronutrients and Energy Intake on Longevity

(A) Response surfaces showing the relationship between protein (P), carbohydrate (C), and fat (F) intake versus median lifespan (weeks). For each 2D slice, the third factor is at its median (shown below the x axis in parentheses). In all surfaces, red indicates the highest value, while blue indicates the lowest value, with the colors standardized across the three slices.

(B and C) Kaplan-Meier survival curves according to differing dietary protein:carbohydrate ratios (B) and dietary energy density (C).

(D) The relationship between the ratio of protein to carbohydrate in the diet and the risk of death. A Cox regression analysis was performed with gender and energy intake as covariates for males (red) and females (green). The bands show the 95% confidence intervals.

(E) The relationship between energy intake and the risk of death. A Cox regression analysis was performed with gender and the ratio of dietary protein to carbohydrate as covariates.

(F) As for (D), but based on protein:carbohydrate intakes corrected for lean body mass.

(G) As for (E), with energy intake corrected for lean body mass. See also Table S4.

Table 1. Correlation Coefficients for Relationships between Protein Intake and Circulating Amino Acid Levels

aa	Coefficient	aa	Coefficient	aa	Coefficient
alanine	−0.617	glutathione	−0.152	phenylalanine	−0.016
arginine	−0.553	glycine	−0.159	proline	−0.358
asparagine	−0.498	histidine	−0.217	serine	−0.627
aspartic acid	0.015	isoleucine*	0.176*	taurine	−0.189
citrulline	−0.584	leucine*	0.213*	threonine	−0.467
cysteine	−0.170	lysine	−0.461	tryptophan	−0.172
glutamic acid	−0.014	methionine	−0.193	tyrosine	−0.073
glutamine	−0.346	ornithine	−0.170	valine*	0.328*

Circulating BCAA levels correlated positively with daily protein intake. In contrast, all other free amino acids correlated negatively with protein intake. Asterisks indicate BCAAs.

synthase activity (which is a gold-standard marker of mitochondrial number; Larsen et al., 2012) (Figure S4) while negatively associated with state III and IVo mitochondrial respiration and hydrogen peroxide production, except when palmitoyl carnitine was used as a substrate (Figures 4A and 4B and Table S7). State III and IVo respiration rates were increased when fat intake was very high only when palmitoyl carnitine was used as a substrate (Figure 4B). This indicates that liver mitochondria only increased capacity for fat as a substrate when dietary fat was excessive.

The Balance of Macronutrients Influenced Latelife Cardiometabolic Phenotype

The aging phenotype was assessed at 15 months, when approximately one-third of the mice were culled (Figures 5, 6, and S5). Nutritional geometry showed that the balance of macronutrients influenced several important phenotypic characteristics, including body weight and composition, blood pressure, glucose tolerance, lipids, fatty liver, and bone mineral density.

Diets that were low in protein and high in carbohydrate (i.e., those that promoted longest life) were associated with lower blood pressure (Figures 5C and 5D), improved glucose tolerance (Figure 6A), higher levels of high-density lipoprotein (HDLc; Figure 6B), reduced levels of low-density lipoprotein (LDLc; Figure 6C), and lower triglycerides (Figure 6D). This is consistent with human data suggesting that long-term adherence to high-protein, low-carbohydrate diets is linked with increased cardiovascular disease (Floegel and Pischon, 2012; Lagiou et al., 2012) and indicates that the balance of protein to carbohydrate, rather than energy intake, may be the driver of a healthy cardiometabolic profile. However, diets with low protein:carbohydrate ratios were also associated with some characteristics usually considered to be associated with poorer health outcomes, such as increased body fat with reduced body lean (Figure 5B) and fatty liver (Figure S5). These paradoxical results are consistent with some human epidemiological studies that indicate that in old age there is a diminution, or even reversal, of the association between these risk factors and outcomes such as remaining life expectancy (Le Couteur and Simpson, 2011).

DISCUSSION

We have used the Geometric Framework to disentangle the interactive effects of dietary macronutrients on appetite, total energy intake, metabolic health, and longevity outcomes in ad libitum-fed mice. There were regulatory compensatory feeding responses to dietary protein and carbohydrate, but dietary fat had little influence on food intake. This does not necessarily indicate that fat exerted no negative feedback onto intake, but rather that any such feedback is dominated by competing feedbacks from protein and carbohydrate. In this regard, it is interesting to note that a primary feedback emanating from body fat depots, leptin, was not associated with lower energy intake, perhaps indicating development of resistance to leptin in high-fat-, low-protein-fed animals (Pelleymounter et al., 1995). The net result of the asymmetrical interactions between regulatory feedbacks generated by the macronutrients was passive intake of excess fat in response to the drive to ingest target levels of protein and carbohydrate.

When the protein:carbohydrate ratio was very low, mice did not achieve their protein intake target, and subsequently, there were lower circulating BCAAs. As the protein content of the diet increased, energy intake was suppressed, and BCAA levels were stabilized at a higher constant level. In marked contrast, plasma concentrations of all other amino acids fell as protein intake increased. The results support the thesis that BCAAs play a key role in protein appetite and regulation of food intake (Fromentin et al., 2012).

The balance of macronutrients, in particular the protein:carbohydrate ratio, had a marked effect on longevity and latelife health. As the protein:carbohydrate ratio increased, there were concomitant increases in hepatic mTOR activation, apparently associated with the combination of elevated circulating BCAAs and low glucose. Given the evidence that activation of mTOR is proaging (Burnett et al., 2011; Fontana et al., 2010; Kapahi et al., 2010), our results support this as a mechanism to explain the life-extending effects of a low-protein, high-carbohydrate diet. Indeed, the pattern of interactive effects of BCAAs and glucose—as a reflection of dietary protein and carbohydrate—on activation of mTOR (Figure 3E) are as we predicted previously from an understanding of nutritional geometry and the established role of mTOR in regulating the aging process (Simpson and Raubenheimer, 2009).

Both BCAAs and insulin activate mTOR, and both are required for activation of pathways downstream of mTOR (Chotechuang et al., 2009). Chronic exposure to high-protein, low-carbohydrate diets resulted in the lowest food intakes, but elevated both mTOR and insulin, with reduced lifespan. The data indicate

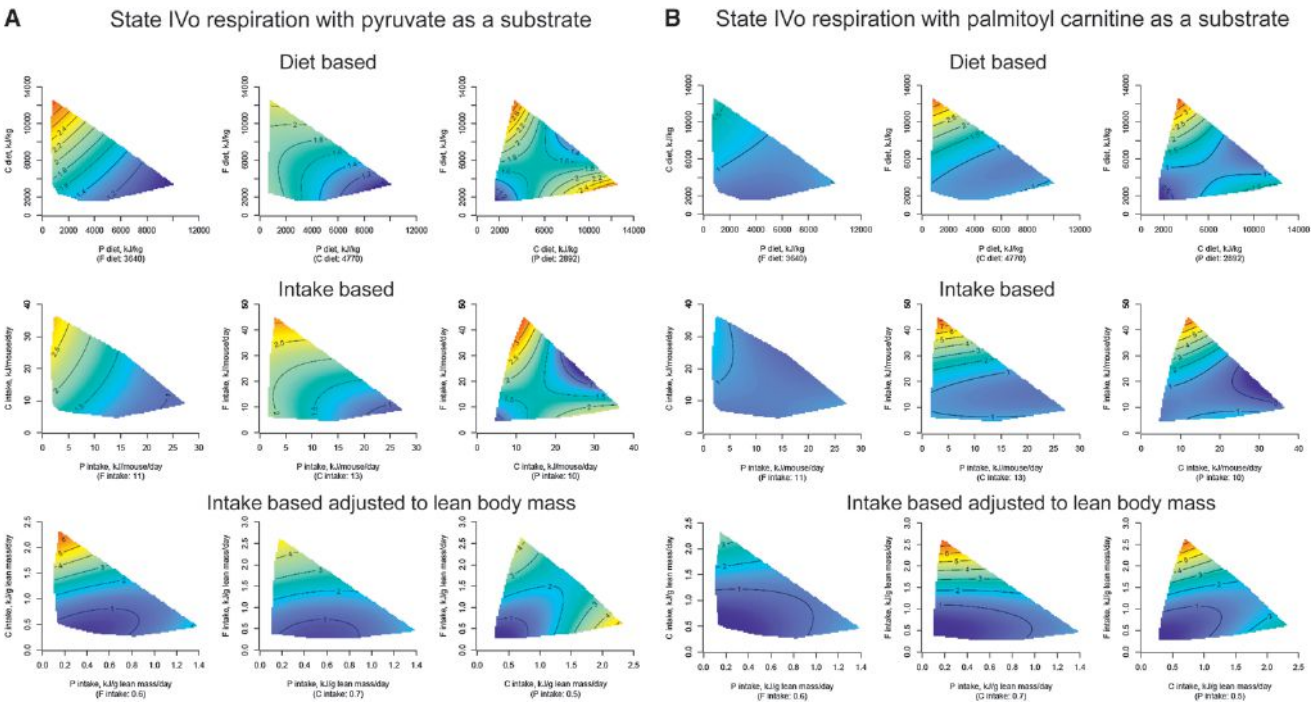

Figure 4. The Effects of Macronutrient Balance on Mitochondrial Function in the Liver

(A) Response surfaces showing the effect of dietary macronutrients on mitochondrial state IVo respiration with pyruvate as substrate (pmol O_2 consumed/min/U of citrate synthase) in the liver at 15 months. Surfaces are shown for diet-based data (top), intake-based data (middle), and intake-based data adjusted to lean body mass (bottom). The highest activity is indicated in red (low-protein diets), and the lowest is indicated in blue.

(B) Response surfaces showing the effect of dietary macronutrients on mitochondrial state IVo respiration with palmitoyl carnitine as substrate (pmol O_2 consumed/min/U of citrate synthase) in the liver at 15 months. Surfaces are shown for diet-based data (top), intake-based data (middle), and intake-based data adjusted to lean body mass (bottom). The highest activity is indicated in red (high-fat diets), and the lowest is indicated in blue. See also Figure S4 and Tables S6 and S7.

that a healthy diet is one that is titrated to generate low mTOR activation and low insulin levels, but must also take into account compensatory feeding, where animals over- or undereat in order to achieve their protein and carbohydrate targets. High-protein diets are recommended for older people to manage sarcopenia, and we noted a positive relationship between protein intake, body lean, and bone mineral density. On the other hand, epidemiological studies have shown that low-protein, high-carbohydrate diets are associated with improved health in humans (Floegel and Pischon, 2012; Lagiou et al., 2012), which is consistent with our overall conclusions.

Our results show that healthy aging is not achieved in mice fed high-protein diets and/or diluted diets to reduce calorie intake, but rather by low-protein diets (especially, we might predict, those low in BCAAs), where additional energy requirements are met by dietary carbohydrates rather than fats. A priority is to establish whether the same applies for humans, especially considering that high-protein diets are widely promoted for weight loss and health. An additional priority is to consider the makeup of lipids in the diet and the quality of carbohydrates. Given the profound effects of the balance of macronutrients on energy intake, health, and longevity, it is clear that dietary interventions aimed at influencing health or aging outcomes must be considered in the context of the underlying dietary landscape.

EXPERIMENTAL PROCEDURES

Animals and Husbandry

C57BL/6 male and female mice (3 weeks old; n = 858) (Animal Resources Centre, WA, Australia) were housed three per cage in standard approved cages (*Tecniplast*, Varese, Italy) in the Molecular Physiology Unit of the ANZAC Research Institute, which is a specific pathogen-free facility designed for housing transgenic mice. A custom-designed two-chamber Perspex insert, designed to collect food spillage (Sørensen et al. 2008), was placed beneath the food hopper of each cage to collect food waste for quantification. Mice were maintained at 24°C–26°C and 44%–46% humidity under a 12 hr light:12 hr dark photoperiod, with lights on at 0600. All protocols were approved by the Sydney Local Health District Animal Welfare Committee (Protocol No. 2009/003).

Experimental diet treatments were custom designed and manufactured in dry, pelleted form by Specialty Feeds (Table S1). The diet treatments addressed both nutritional quantity and quality. To manipulate diet quantity, indigestible cellulose was added to diet treatments, yielding 3 total energy (caloric) density regimes fixed at 8, 13, and 17 kJ/g (referred to as low, medium, and high energy, respectively).

Mice were provided ad libitum access throughout their lifetime to 1 of 25 diets varying in content of protein, carbohydrate, and fat. Food intake was measured weekly for 6 months, followed by monthly measurements thereafter, and corrected for spillage and water content. Mice were checked daily, and body weight measurements were recorded to correspond with food intake measurements. Animals losing more than 20% body weight were culled.

Glucose Tolerance

At 15 months of age, glucose tolerance tests (GTTs) were performed on 668 mice. Animals were fasted for 4 hr prior to testing. Basal glucose levels were

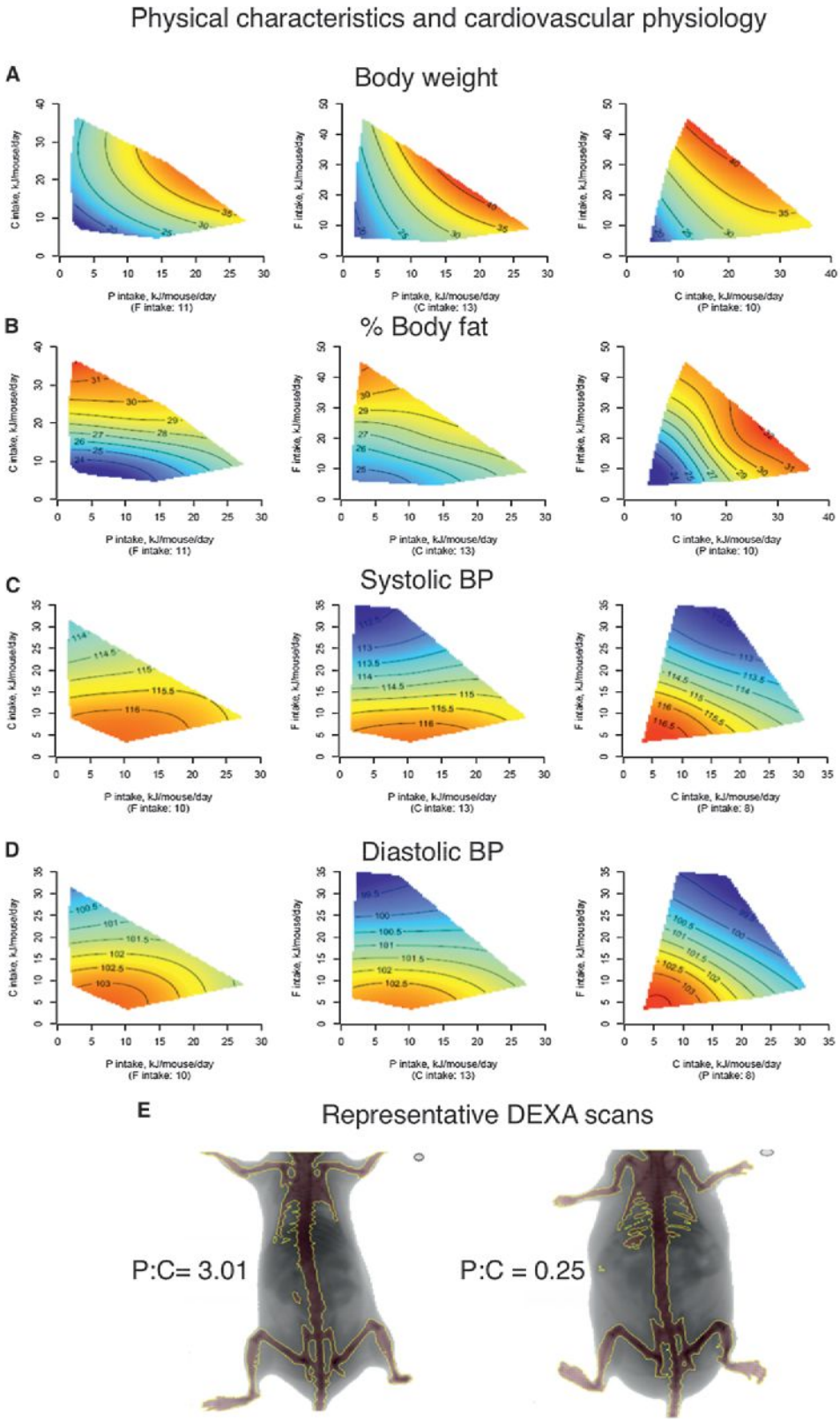

Figure 5. The Effects of Macronutrients on Latelife Physical Characteristics and Cardiovascular Physiology

(A–E) Response surfaces show body weight (g) (A), body fat (%) (B), systolic (C) and diastolic blood pressures (mmHg) (D), and representative DEXA scans (E) showing the effect of chronic high P:C and low P:C intakes at 15 months of age. See also Figure S5 and Table S8.

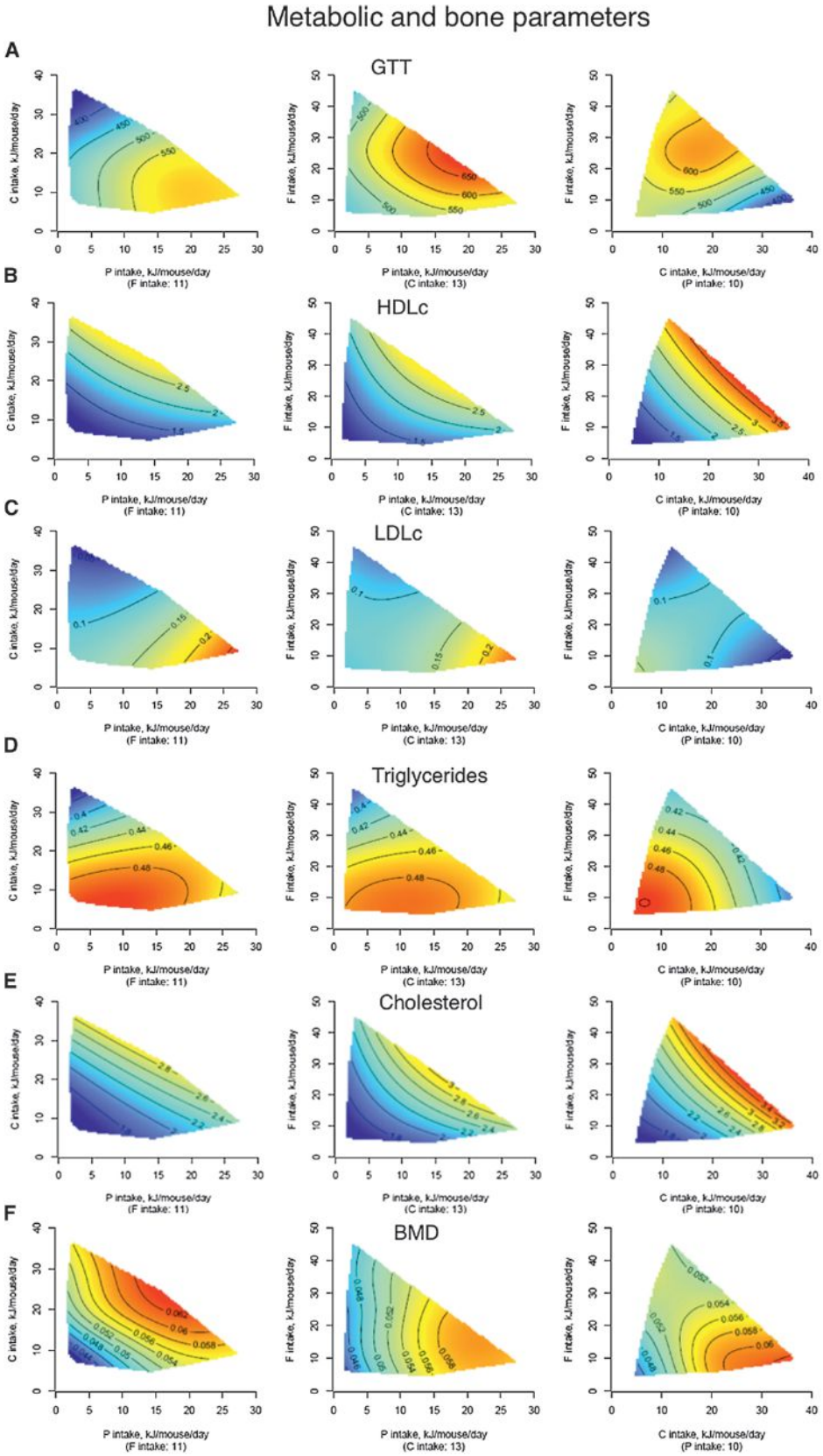

(legend on next page)

determined (Accu-Chek Performa). Glucose (1.5 g/kg) was then administered via intraperitoneal (i.p.) injection. Blood was sampled at 15, 30, 45, 60, and 90 min. The incremental area under the curve (AUC) was calculated using mean values per cage.

Blood Pressure

Blood pressure was measured indirectly in 240 conscious animals across all dietary groups with an automated multichannel tail-cuff system (MC4000; Hatteras Instruments) at 12 months. Animals were acclimatized to the system for 3 days prior to data collection.

At 15 months, one-third of the animals were culled, and tissues were harvested for further analyses. The mice were assigned a number (1–3) on arrival and housed 3 per cage. At 15 months of age, the number 2 animal from each cage was selected for culling, provided that animals 1 and 3 were still alive. If there were only two animals alive at this time point, no individual was culled (to prevent long-term single housing as much as possible).

Body Composition

Body composition was assessed in 180 mice across all diets by dual-energy X-ray absorptiometry (DEXA) using the GE PIXImus2 Series Densitometer (GE Medical Systems Ultrasound and BMD) under general anesthesia (i.p. ketamine:xylazine) immediately prior to culling.

Plasma Insulin and Leptin

Plasma insulin levels were measured using the Mouse Ultrasensitive Insulin ELISA Kit (ALPCO Diagnostics). Plasma leptin levels were quantified using the Mouse Leptin ELISA Kit (Millipore).

Plasma Amino Acids

Amino acids were analyzed at the Australian Proteome Analysis Facility, Macquarie University, using the Waters AccQ-Tag Ultra Chemistry Kit (Waters Corporation).

Liver Histology

Embedded liver tissue was sectioned at 4 μm and stained with hematoxylin and eosin and Sirius Red. Extent of steatosis was assessed and scored (0, +, ++, +++) by four independent observers blinded to tissue category.

Mitochondrial Function

Mitochondrial functions were assessed in liver tissue using the Seahorse XF Extracellular Flux Analyzer, which generates the key parameters of mitochondrial function using fresh isolated mitochondria from homogenized liver tissue: basal respiration, ATP production, proton leak, maximal respiration, glycolysis, and spare respiratory capacity (Horan et al., 2012). Different conditions were used to measure the mitochondrial oxygen consumption, e.g., by providing different combinations of substrates (pyruvate-malate, glutamate-malate, succinate-rotenone, palmitoyl carnitine-malate) to the electron transport system. State III was monitored after injection of ADP, and State IVo was monitored after injection of oligomycin. Respiratory control ratios (RCRs) were calculated as State III / State IVo. Mitochondrial amount as well as substrate, ADP, and inhibitor concentrations were optimized prior to experiments. Hydrogen peroxide production was measured with an Amplex Red Kit using the same substrates as for mitochondrial respiration. Hydrogen peroxide production and enzymatic activities (3-hydroxyacyl coenzyme A dehydrogenase, aspartate aminotransferase, and citrate synthase) were measured spectrophotometrically on the same mitochondrial isolations. Citrate synthase activity was used to normalize the results, which are therefore expressed as mitochondrial function per mitochondrion.

Blood Lipids and Biochemistry

Blood cholesterol, triglycerides, high-density lipoprotein cholesterol (HDLc), low-density lipoprotein cholesterol (LDLc), liver function tests (alanine transaminase ALT, aspartate aminotransferase AST, gamma-glutamyl transpeptidase GGT), and creatinine were performed at the Concord Hospital Pathology Department.

Liver mTOR and Phospho-mTOR

Frozen liver tissue samples were sectioned into 20 mg blocks and homogenized (QIAGEN TissueLyser LT) in 400 μl RIPA buffer containing Tris-HCl, NaCl, Triton X-100, Na-deoxycholate, SDS, and Roche protease inhibitor tablets (cOmplete, EDTA-free Protease Inhibitor Cocktail). Protein concentration was checked using a bicinchoninic acid (BCA) assay (Thermo Scientific Pierce BCA Protein Assay Kit), and a standard curve was developed with BSA controls. Samples were then diluted into a 2 mg/ml concentration in a 100 μl volume with Laemmli buffer and 50 mM TCEP BondBreaker, and 20 μg of protein were separated on 4%–15% gradient Mini-PROTEAN TGX gels. Gels were transferred onto nitrocellulose membranes at 25 V and 2.5 A for 10 min on a Trans-Blot Turbo Transfer System. Membranes were blocked for 1 hr in 5% skim milk in Tris-buffered saline (TBS). Membranes were washed 3 times for 10 min in wash buffer (TBS 0.1% Tween 20) and incubated overnight in primary antibody solution (5% BSA, TBS 0.1% Tween 20). Membranes were washed 3 times as before and incubated for 1 hr in secondary antibody solution (5% skim milk in TBS 0.1% Tween, 0.01% SDS). Membranes were washed three times as before, rinsed in water, and analyzed on a LI-COR Odyssey System. Densitometry was performed using LI-COR software, and results were analyzed using Prism (GraphPad). Antibodies used were total mTOR (4517 L27D4; Cell Signaling Technology), phospho-Ser2448 mTOR (5536 D9C2; Cell Signaling Technology), and α-tubulin (T6199, clone DM1A; Sigma).

Statistical Modeling and Analysis

Intake Transformations

Macronutrient, energy, and dry matter intake data were analyzed both per mouse with no body size adjustment and by adjusting the intakes to lean body mass. Body fat was determined from 1 mouse of each of 174 cages out of 250 cages at 15 months. These body fat values were used to calculate the lean mass from the cage average body weight. For any missing data, lean mass was estimated from the total body weight by using the average body fat percentage of their specific diet based on the data from the 174 cages. This imputation was used for the phenotypic data, average feed intake data, individual survival data, and blood pressure data. For the median lifespan data, the diet averages of the body fat were used to calculate the lean mass from the average body weight.

Response Surfaces

GAMs with thin-plate splines were used to model the responses either over the diet macronutrient composition or over mice macronutrient intake spaces. GAMs were fitted with the help of the mgcv package of the R language (R Core Team, 2012, v.2.15.13) (Wood, 2006). The mgcv package is based on Wood (2003). An extra penalty was used in the fits to allow a specific term to end up with zero estimated degrees of freedom and thus be excluded from the final model. The macronutrient effects were broken down to main effects and interactions. The responses included dry matter, energy and macronutrient intake, median lifespan, several phenotypic measurements, and mitochondrial function.

Survival Analysis

Survival curves for different dietary energy levels and protein:carbohydrate (P:C) ratios were visualized by Kaplan-Meier estimator using the survival package of the R language. This package is based on Therneau and Grambsch (2000). The same package was used to fit the Cox proportional hazard model to actual lifespans in relation to diet protein:carbohydrate ratio and energy

Figure 6. The Effects of Macronutrients on Latelife Metabolic and Bone Parameters

(A–F) Response surfaces show glucose tolerance (incremental area under curve, AUC) (A), HDLc (mmol/l) (B), LDLc (mmol/l) (C), triglycerides (mmol/l) (D), cholesterol (mmol/l) (E), and bone mineral density (g/cm^2) (F) at 15 months of age. Low-protein diets were associated with improved glucose tolerance, increased HDLc, and reduced LDLc and cholesterol, all beneficial to the cardiometabolic profile. As expected, triglyceride levels were largely driven by carbohydrate intake. Bone mineral density was adversely affected by both low-protein and low-carbohydrate intakes, being maximal when the combination of protein and carbohydrate intake was high. See also Table S9.

intake. The effects of diet protein:carbohydrate ratio and energy intake were modeled with the help of penalized splines (psplines) as described in the survival package documentation. The proportional hazard assumption was diagnosed by plotting (Therneau and Grambsch, 2000).

Liver Steatosis

Steatosis was assessed as a score ranging from 0 to 3. The scores were modeled with an ordinal regression (proportional odds). The effects of diet composition and macronutrient intakes were modeled with the help of additive splines using the VGAM package of the R language that is based on Yee (1996).

Various Other Methods

Multilevel (mixed-effects) models were used to investigate whether mouse age affected intakes on different dietary energy densities by adding cage as a random effect. A multilevel model was required since the data are repeated measures of the same cages over time. The models were fitted with the help of the lme4 package of R (Bates et al., 2012). The macronutrient intake in relation to diet composition (appetite regulation) was analyzed by fitting an asymptotic regression model with nonlinear least squares. The relationship between some phenotypic responses and diet protein:carbohydrate ratio and energy intake were modeled with single predictor GAMs with the mgcv package of R. Similar GAMs were used to model the protein intake in relation to diet protein:carbohydrate ratio at different ages of the mice. For the GAMs the 95% confidence intervals were approximated as the mean ± 2 standard errors of the predictions. For the mixed-effects and general linear models, the 95% confidence intervals were solved by a posterior simulation with 1,500 random draws from the model as described by Gelman and Hill (2007).

SUPPLEMENTAL INFORMATION

Supplemental Information includes Supplemental Experimental Procedures, five figures, and nine tables and can be found with this article online at http://dx.doi.org/10.1016/j.cmet.2014.02.009.

ACKNOWLEDGMENTS

Funding was obtained from the Australian National Health and Medical Research Council (NHMRC project grant 571328), the Ageing and Alzheimers Research Fund of Concord RG Hospital, and the Sydney Medical School Foundation. Additionally, S.J.S. was supported by an Australian Research Council Laureate Fellowship; D.R. was part funded by Gravida, the National Research Centre for Growth and Development, New Zealand; and L.E.W. was supported by an early career fellowship from the Cancer Institute NSW (CINSW), Australia. We acknowledge the assistance of the Departments of Biochemistry and Anatomical Pathology, Concord RG Hospital. We thank Leon McQuade for amino acid analyses and Andrew Holmes, Arthur Conigrave, and Patrick Bertolino for their contribution to other aspects of the study protocol. We are extremely grateful to John Speakman and Linda Partridge for their detailed review of earlier versions of the manuscript. There are no conflicts of interest to declare.

Received: December 2, 2013
Revised: January 14, 2014
Accepted: February 11, 2014
Published: March 4, 2014

REFERENCES

Bates, D., Maechler, M., and Bolker, B. (2012). lme4: Linear mixed-effects models using S4 classes. R package version 0.999999-0, http://cran.r-project.org/web/packages/lme4/index.html.

Blumfield, M.L., Hure, A.J., MacDonald-Wicks, L.K., Smith, R., Simpson, S.J., Giles, W.B., Raubenheimer, D., and Collins, C.E. (2012). Dietary balance during pregnancy is associated with fetal adiposity and fat distribution. Am. J. Clin. Nutr. *96*, 1032–1041.

Burnett, C., Valentini, S., Cabreiro, F., Goss, M., Somogyvári, M., Piper, M.D., Hoddinott, M., Sutphin, G.L., Leko, V., McElwee, J.J., et al. (2011). Absence of effects of Sir2 overexpression on lifespan in C. elegans and Drosophila. Nature *477*, 482–485.

Chotechuang, N., Azzout-Marniche, D., Bos, C., Chaumontet, C., Gausserès, N., Steiler, T., Gaudichon, C., and Tomé, D. (2009). mTOR, AMPK, and GCN2 coordinate the adaptation of hepatic energy metabolic pathways in response to protein intake in the rat. Am. J. Physiol. Endocrinol. Metab. *297*, E1313–E1323.

Everitt, A.V., Rattan, S.I., Le Couteur, D.G., and de Cabo, R., eds. (2010). Calorie Restriction, Aging and Longevity (New York: Springer Press).

Fanson, B.G., Weldon, C.W., Pérez-Staples, D., Simpson, S.J., and Taylor, P.W. (2009). Nutrients, not caloric restriction, extend lifespan in Queensland fruit flies (Bactrocera tryoni). Aging Cell *8*, 514–523.

Floegel, A., and Pischon, T. (2012). Low carbohydrate-high protein diets. BMJ *344*, e3801.

Fontana, L., Partridge, L., and Longo, V.D. (2010). Extending healthy life span—from yeast to humans. Science *328*, 321–326.

Fromentin, G., Darcel, N., Chaumontet, C., Marsset-Baglieri, A., Nadkarni, N., and Tomé, D. (2012). Peripheral and central mechanisms involved in the control of food intake by dietary amino acids and proteins. Nutr. Res. Rev. *25*, 29–39.

Gelman, A., and Hill, J. (2007). Data analysis using regression and multilevel/hierarchical models. (Cambridge: Cambridge University Press).

Gosby, A.K., Conigrave, A.D., Lau, N.S., Iglesias, M.A., Hall, R.M., Jebb, S.A., Brand-Miller, J., Caterson, I.D., Raubenheimer, D., and Simpson, S.J. (2011). Testing protein leverage in lean humans: a randomised controlled experimental study. PLoS ONE *6*, e25929.

Harrison, D.E., Strong, R., Sharp, Z.D., Nelson, J.F., Astle, C.M., Flurkey, K., Nadon, N.L., Wilkinson, J.E., Frenkel, K., Carter, C.S., et al. (2009). Rapamycin fed late in life extends lifespan in genetically heterogeneous mice. Nature *460*, 392–395.

Hewson-Hughes, A.K., Hewson-Hughes, V.L., Miller, A.T., Hall, S.R., Simpson, S.J., and Raubenheimer, D. (2011). Geometric analysis of macronutrient selection in the adult domestic cat, Felis catus. J. Exp. Biol. *214*, 1039–1051.

Horan, M.P., Pichaud, N., and Ballard, J.W.O. (2012). Review: quantifying mitochondrial dysfunction in complex diseases of aging. J. Gerontol. A Biol. Sci. Med. Sci. *67*, 1022–1035.

Huang, X., Hancock, D.P., Gosby, A.K., McMahon, A.C., Solon, S.M., Le Couteur, D.G., Conigrave, A.D., Raubenheimer, D., and Simpson, S.J. (2013). Effects of dietary protein to carbohydrate balance on energy intake, fat storage, and heat production in mice. Obesity (Silver Spring) *21*, 85–92.

Kapahi, P., Chen, D., Rogers, A.N., Katewa, S.D., Li, P.W., Thomas, E.L., and Kockel, L. (2010). With TOR, less is more: a key role for the conserved nutrient-sensing TOR pathway in aging. Cell Metab. *11*, 453–465.

Lagiou, P., Sandin, S., Lof, M., Trichopoulos, D., Adami, H.O., and Weiderpass, E. (2012). Low carbohydrate-high protein diet and incidence of cardiovascular diseases in Swedish women: prospective cohort study. BMJ *344*, e4026.

Larsen, S., Nielsen, J., Hansen, C.N., Nielsen, L.B., Wibrand, F., Stride, N., Schroder, H.D., Boushel, R., Helge, J.W., Dela, F., and Hey-Mogensen, M. (2012). Biomarkers of mitochondrial content in skeletal muscle of healthy young human subjects. J. Physiol. *590*, 3349–3360.

Le Couteur, D.G., and Lakatta, E.G. (2010). A vascular theory of aging. J. Gerontol. A Biol. Sci. Med. Sci. *65*, 1025–1027.

Le Couteur, D.G., and Simpson, S.J. (2011). Adaptive senectitude: the prolongevity effects of aging. J. Gerontol. A Biol. Sci. Med. Sci. *66*, 179–182.

Le Couteur, D.G., Wilder, S.M., de Cabo, R., and Simpson, S.J. (2014). The evolution of research on ageing and nutrition. J. Gerontol. A Biol. Sci. Med. Sci. *69*, 1–2.

Lee, K.P., Simpson, S.J., Clissold, F.J., Brooks, R., Ballard, J.W., Taylor, P.W., Soran, N., and Raubenheimer, D. (2008). Lifespan and reproduction in Drosophila: New insights from nutritional geometry. Proc. Natl. Acad. Sci. USA *105*, 2498–2503.

López-Lluch, G., Hunt, N., Jones, B., Zhu, M., Jamieson, H., Hilmer, S., Cascajo, M.V., Allard, J., Ingram, D.K., Navas, P., and de Cabo, R. (2006).

Calorie restriction induces mitochondrial biogenesis and bioenergetic efficiency. Proc. Natl. Acad. Sci. USA *103*, 1768–1773.

Martin, G.M., and Loeb, L.A. (2004). Ageing: mice and mitochondria. Nature *429*, 357–359.

Mayntz, D., Raubenheimer, D., Salomon, M., Toft, S., and Simpson, S.J. (2005). Nutrient-specific foraging in invertebrate predators. Science *307*, 111–113.

Mayntz, D., Nielsen, V.H., Sørensen, A., Toft, S., Raubenheimer, D., Hejlesen, C., and Simpson, S.J. (2009). Balancing of protein and lipid intake by a mammalian carnivore, the mink (Mustela vison). Animal Behaviour *77*, 349–355.

Miller, R.A., Harrison, D.E., Astle, C.M., Baur, J.A., Boyd, A.R., de Cabo, R., Fernandez, E., Flurkey, K., Javors, M.A., Nelson, J.F., et al. (2011). Rapamycin, but not resveratrol or simvastatin, extends life span of genetically heterogeneous mice. J. Gerontol. A Biol. Sci. Med. Sci. *66*, 191–201.

Pelleymounter, M.A., Cullen, M.J., Baker, M.B., Hecht, R., Winters, D., Boone, T., and Collins, F. (1995). Effects of the obese gene product on body weight regulation in ob/ob mice. Science *269*, 540–543.

Piper, M.D., Partridge, L., Raubenheimer, D., and Simpson, S.J. (2011). Dietary restriction and aging: a unifying perspective. Cell Metab. *14*, 154–160.

Ponton, F., Wilson, K., Cotter, S.C., Raubenheimer, D., and Simpson, S.J. (2011). Nutritional immunology: a multi-dimensional approach. PLoS Pathog. *7*, e1002223.

Simpson, S.J., and Raubenheimer, D. (2007). Caloric restriction and aging revisited: the need for a geometric analysis of the nutritional bases of aging. J. Gerontol. A Biol. Sci. Med. Sci. *62*, 707–713.

Simpson, S.J., and Raubenheimer, D. (2009). Macronutrient balance and lifespan. Aging (Albany, N.Y. Online) *1*, 875–880.

Simpson, S.J., and Raubenheimer, D. (2012). The nature of nutrition. A unifying framework form animal adaption to human obesity. (Princeton: Princeton University Press).

Sørensen, A., Mayntz, D., Raubenheimer, D., and Simpson, S.J. (2008). Protein-leverage in mice: the geometry of macronutrient balancing and consequences for fat deposition. Obesity (Silver Spring) *16*, 566–571.

Therneau, T., and Grambsch, P.M. (2000). Modeling survival data: extending the Cox model. (New York: Springer).

Wood, S.N. (2003). Thin-plate regression splines. Journal of the Royal Statistical Society: Series B (Statistical Methodology) *65*, 95–114.

Wood, S. (2006). Generalized additive models: an introduction with R. (Boca Raton: Chapman and Hall/CRC).

Yang, J., Chi, Y., Burkhardt, B.R., Guan, Y., and Wolf, B.A. (2010). Leucine metabolism in regulation of insulin secretion from pancreatic beta cells. Nutr. Rev. *68*, 270–279.

Yee, T. (1996). Vector generalized additive models. Journal of the Royal Statistical Society: Series B (Statistical Methodology) *58*, 481–493.

Cell Metabolism
Article

A Switch from White to Brown Fat Increases Energy Expenditure in Cancer-Associated Cachexia

Michele Petruzzelli,[1] Martina Schweiger,[2] Renate Schreiber,[2] Ramon Campos-Olivas,[3] Maria Tsoli,[4] John Allen,[5] Michael Swarbrick,[5] Stefan Rose-John,[6] Mercedes Rincon,[7] Graham Robertson,[5] Rudolf Zechner,[2] and Erwin F. Wagner[1,*]

[1]BBVA Foundation-CNIO Cancer Cell Biology Programme, Spanish National Cancer Research Centre (CNIO), C/ Melchor Fernández Almagro 3, 28029 Madrid, Spain
[2]Institute of Molecular Biosciences, University of Graz, Humboldtstrasse 50, 8010 Graz, Austria
[3]Spectroscopy and Nuclear Magnetic Resonance Unit, Spanish National Cancer Research Centre (CNIO), C/ Melchor Fernández Almagro 3, 28029 Madrid, Spain
[4]Children's Cancer Institute Australia for Medical Research, UNSW Lowy Cancer Research Centre Building, C25 Kensington Campus UNSW, Sydney, NSW 2052, Australia
[5]Garvan Institute of Medical Research, 384 Victoria Street, Darlinghurst, NSW 2010, Australia
[6]Institute of Biochemistry, Christian-Albrechts University, Olshausenstr. 40, 24118 Kiel, Germany
[7]Division of Immunobiology, Department of Medicine, University of Vermont, 89 Beaumont Avenue / D305 Given Building, Burlington, VT 05405, USA
*Correspondence: ewagner@cnio.es
http://dx.doi.org/10.1016/j.cmet.2014.06.011

SUMMARY

Cancer-associated cachexia (CAC) is a wasting syndrome characterized by systemic inflammation, body weight loss, atrophy of white adipose tissue (WAT) and skeletal muscle. Limited therapeutic options are available and the underlying mechanisms are poorly defined. Here we show that a phenotypic switch from WAT to brown fat, a phenomenon termed WAT browning, takes place in the initial stages of CAC, before skeletal muscle atrophy. WAT browning is associated with increased expression of uncoupling protein 1 (UCP1), which uncouples mitochondrial respiration toward thermogenesis instead of ATP synthesis, leading to increased lipid mobilization and energy expenditure in cachectic mice. Chronic inflammation and the cytokine interleukin-6 increase UCP1 expression in WAT, and treatments that reduce inflammation or β-adrenergic blockade reduce WAT browning and ameliorate the severity of cachexia. Importantly, UCP1 staining is observed in WAT from CAC patients. Thus, inhibition of WAT browning represents a promising approach to ameliorate cachexia in cancer patients.

INTRODUCTION

Cancer-associated cachexia (CAC) is a paraneoplastic syndrome characterized by systemic inflammation, body weight loss, atrophy of adipose tissue, and skeletal muscle wasting. CAC is observed in a majority of cancer patients with advanced disease (Fearon et al., 2012; Tisdale, 2002). In addition to cancer patients, cachexia is typically seen at the end stage of various other morbidities, including infectious diseases, such as AIDS and tuberculosis, or chronic conditions, such as congestive heart failure, chronic obstructive lung disease, and multiple sclerosis (Tisdale, 2009). No effective treatment is currently available for cachexia, which is responsible for approximately 20% of total deaths in cancer patients (Fearon et al., 2013). Therefore, new therapeutic targets for cachexia prevention and treatment are urgently needed.

Metabolic dysfunction and increased metabolic rate have been proposed as causative for CAC (Blum et al., 2011), but the underlying mechanisms are at present poorly characterized (Tisdale, 2009). Activation of thermogenesis in the interscapular brown adipose tissue (BAT) has been observed in a syngeneic mouse tumor transplant model and suggested to contribute to the hypermetabolic state of cachexia (Tsoli et al., 2012). White adipose tissue (WAT) and BAT usually perform opposite physiological functions, with WAT responsible for energy accumulation in intracellular lipid droplets and BAT responsible for its dissipation as heat (Cannon and Nedergaard, 2004). Interscapular BAT is not the only thermogenic organ in mice and humans. Brown adipocytes can also be induced within WAT depots, a phenomenon termed WAT browning (Wu et al., 2013; Young et al., 1984). Brown adipocytes induced in WAT, also known as "beige" or "brite" cells (Harms and Seale, 2013), are derived from a precursor population distinct from both mature white and brown adipocytes (Wang et al., 2013). Several mechanisms have been proposed for WAT browning (Villarroya and Vidal-Puig, 2013), including prolonged cold exposure (Loncar et al., 1986), adrenergic activation (Cao et al., 2011), the myokine Irisin (Boström et al., 2012), and the prostaglandin synthesis enzyme cyclooxygenase (COX) 2 (Vegiopoulos et al., 2010). WAT browning is responsible for a significant increase in total energy expenditure (Shabalina et al., 2013), and stimulation of browning has therapeutic potential to promote body fat reduction (Yoneshiro et al., 2013).

WAT atrophy represents one of the hallmarks of cachexia and is caused by β-adrenergic activation and/or inflammatory cytokine-induced lipolysis (Das et al., 2011; Fearon et al., 2012). Notably, β-adrenergic stimulation is also responsible for WAT

browning during cold acclimation (Cao et al., 2011). Furthermore, several activators of interscapular BAT also promote WAT browning (Wu et al., 2013). Since the β-adrenergic pathway is active during cachexia, and increased thermogenesis in BAT has been observed in cachectic mice (Tsoli et al., 2012), we set out to investigate whether WAT browning occurs and to analyze its impact on CAC pathophysiology. WAT browning was observed in different model systems, indicating that it is a consistent feature of cachexia. WAT browning during CAC contributed to the systemic increase in energy expenditure and promoted the wasting syndrome. Decreasing WAT browning by silencing tumor production of interleukin-6 (IL-6) or pharmacological approaches employing an anti-IL-6 monoclonal antibody, a β3-adrenergic receptor antagonist, or the nonsteroidal anti-inflammatory drug sulindac ameliorated the severity of cachexia. Importantly, browning of adipose tissue was observed in samples from cancer cachexia patients, thus underlining the translational value of our findings.

RESULTS

Browning of Subcutaneous WAT Is a Consistent Finding in Mouse Models of CAC

A systematic morphological analysis of WAT depots in different mouse models of CAC led to the identification of a robust phenotypic switch from white to brown fat in subcutaneous WAT of cachectic mice. Genetically engineered mouse models (GEMMs) of lung and pancreatic cancer, Kras-lung cancer GEMM (Puyol et al., 2010), and Kras-pancreatic cancer GEMM (Hingorani et al., 2005), respectively, at the age of 6–8 months displayed a loss of more than 15% of total body weight, when compared to littermate controls (Figure 1A). At necropsy, GEMMs of cancer exhibited massive fat atrophy, as evidenced by complete loss of gonadal WAT (Figure 1B). Histological examination of subcutaneous inguinal and axillary WAT, also termed anterior subcutaneous WAT (Waldén et al., 2012), revealed the presence of abundant islets composed of small adipocytes with big nuclei, multilocular cytoplasm, and positive staining for the uncoupling protein-1 (UCP1) (Figures 1C and 1D). WAT browning was also evident in a third GEMM of CAC; K5-SOS mice with skin tumors (Sibilia et al., 2000) displayed increased UCP1 staining in subcutaneous WAT as well as in the residual gonadal WAT (Figure S1A, available online). Next, we investigated WAT morphology and UCP1 protein in a chemical model of liver carcinogenesis; 19 months after injection of the carcinogen diethylnitrosamine (DEN), 50% of mice became cachectic (Figure S1B) and exhibited morphological evidence of subcutaneous WAT browning (Figure 1E).

WAT browning was also observed in murine syngeneic graft models. At 2 weeks after injection of B16 melanoma cells or Lewis lung carcinoma (LLC) cells, mice lost 25% of gonadal WAT mass, while total body weight was reduced only in the graft model with B16 cells (Figures S1C and S1D). Although the severity of cachexia in the syngeneic graft models was milder compared to cachexia observed in the tumor GEMMs, subcutaneous WAT from mice in both graft models displayed evidence of WAT browning, as shown by increased UCP1 staining and decreased lipid droplet size (Figures 1F, 1G, S1E, and S1F). Lastly, WAT morphology was investigated in a xenogeneic graft model of human cancer. Two tumor samples, Panc34 and Panc42, were obtained from distinct pancreatic cancer patients and implanted subcutaneously in immunocompromised SCID mice with a defective lymphocyte response. At 3 months after implantation, mice from both groups grew xenograft tumors of similar size, lost more than 15% of total body weight, and displayed evidence of browning of subcutaneous WAT (Figures S1G–S1I). These data obtained in very diverse experimental models of cancer show that WAT browning represents a consistent finding in CAC.

WAT Browning Is an Early Event in the Pathophysiology of CAC

To investigate the kinetics of WAT browning and to determine whether it contributes to the wasting process in CAC, we focused on the K5-SOS mouse model of skin tumors, in which the temporal development of cachexia is rapid and reproducible. At 5 weeks of age, K5-SOS mice did not show evidence of loss of total body weight or skeletal muscle mass, but they exhibited increased spleen weight and a 50% reduction in gonadal WAT mass (precachectic mice) (Figures 2A and 2B). However, unequivocal signs of cachexia were evident in K5-SOS mice at 7 weeks of age, with significant total body weight loss (Figure 2A), anemia (Figures S2A and S2B), nearly complete atrophy of gonadal WAT, and a 50% reduction in skeletal muscle mass (Figures 2B and S2C–S2E). At the molecular level, changes described in skeletal muscle of cachectic mice (Zhou et al., 2010), such as increased nuclear staining of phospho-SMAD2, increased expression of the cell-cycle inhibitor *p21*, the proapoptotic gene *Bax*, and the proinflammatory cytokine interleukin-6 (*IL-6*), were observed in skeletal muscle of K5-SOS mice (Figures S2F and S2G). Also, increased activation of interscapular BAT was observed in cachectic mice (Figure S2H).

Remarkably, WAT browning was already detectable in precachectic mice and increased as cachexia developed (Figures 2C and 2D). *Ucp1* mRNA was upregulated in both inguinal and axillary WAT from cachectic K5-SOS mice, along with established molecular markers of browning, such as *Pgc1α*, *Pparγ*, *Cidea*, and *Prdm16* (Figures 2E and 2F). Browning of subcutaneous WAT in cachectic mice was associated with increased mitochondrial content and oxygen consumption (Figures 2G and 2H). Similarly, total levels of mitochondrial protein NDUFS1 were increased in subcutaneous WAT of cachectic mice (Figures S2I and S2J). Analysis of established expression signatures for beige-selective and brown-selective genes (Wu et al., 2012) showed a consistent increase of brown-selective markers in subcutaneous WAT of cachectic mice (Figures S3A and S3B). Furthermore, the percentage of proliferating cells was doubled in subcutaneous WAT of cachectic mice, when compared to controls (Figure S3C). Recent studies have shown that newly induced beige/brite adipocytes, induced in WAT by cold exposure or adrenergic β3-agonist treatment, arise by recruitment and de novo differentiation of progenitor cells (Wang et al., 2013). To better characterize the identity of proliferating cells in WAT of cachectic mice, we performed costaining experiments with established markers of adipocyte progenitors (Lee et al., 2012; Tang et al., 2011) and identified proliferating PDGFRα-positive cells, but not PDGFRβ or PPARγ cells (Figure S3D). These data show that WAT browning represents an early event

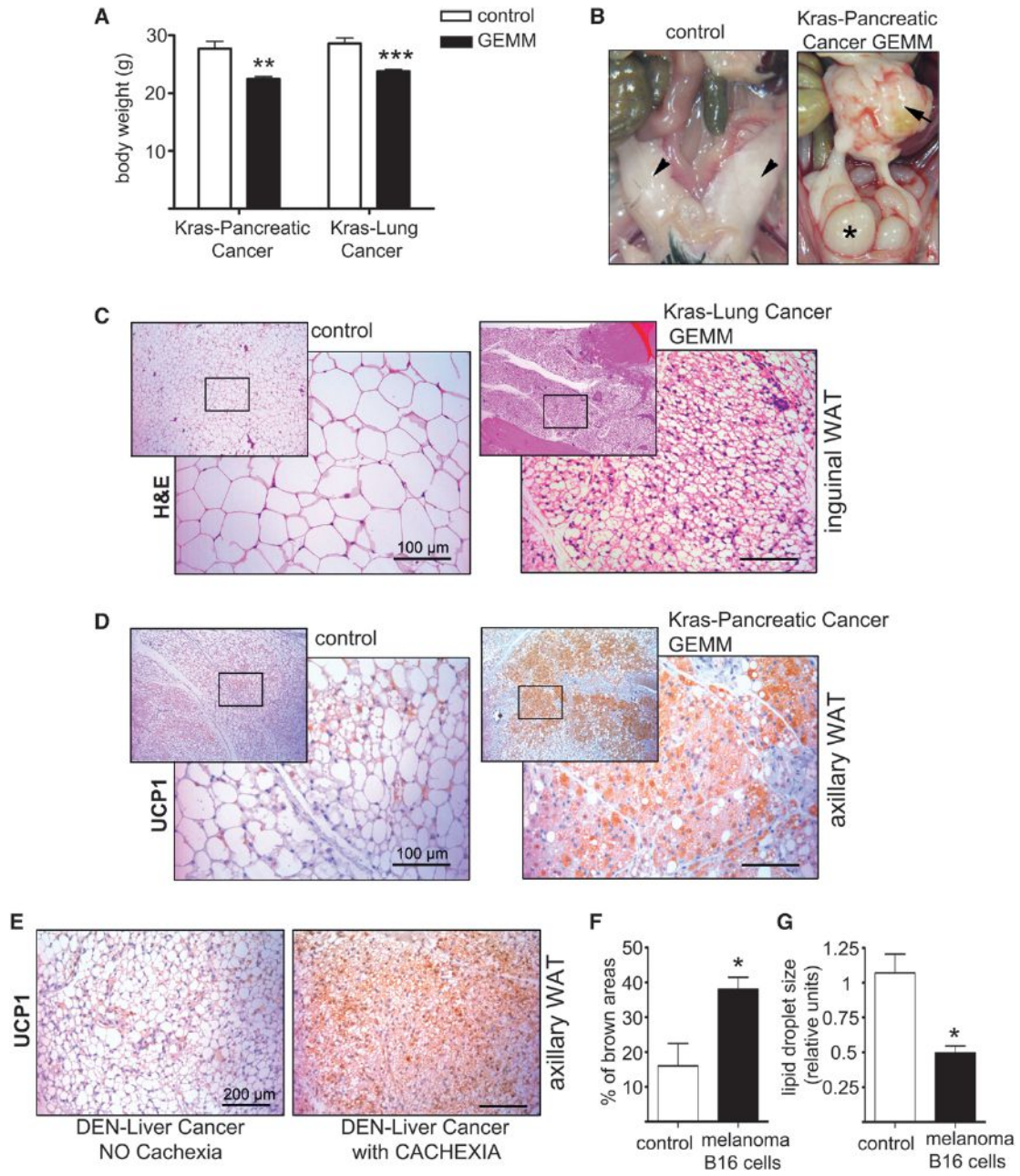

Figure 1. Browning of WAT Is a Consistent Finding in Mouse Models of CAC

(A) Total body weight in Kras-pancreatic cancer GEMM, Kras-lung cancer GEMM, and corresponding littermate controls (6–8 months old, n ≥ 6 per genotype).

(B) Representative macroscopic pictures of control mice and Kras-pancreatic cancer GEMM at autopsy. The arrowheads point to normal gonadal WAT in control mice. In the GEMM of pancreatic cancer (arrow), gonadal WAT is almost completely absent, and the gonads are visible (asterisk).

(C and D) Representative images of hematoxylin and eosin (H&E) (C) and UCP1 immunohistochemical (IHC) (D) staining of subcutaneous WAT in mice from (A).

(E) Representative images of UCP1 IHC staining of axillary WAT in mice in the DEN-induced model of liver tumors (16–18 months old, n = 3 per condition).

(F and G) Quantification of brown area extension (F) and lipid droplet size (G) in axillary WAT from mice in the graft model with melanoma B16 cells (12 weeks old, n ≥ 6 per condition).

Data are presented as mean ± SEM (*p < 0.05).

in the pathophysiology of cachexia, preceding skeletal muscle wasting. Moreover, WAT browning is associated with increased energy consumption in subcutaneous WAT and is characterized by activation of brown-selective genes and proliferation of PDGFRα progenitor cells.

Increased Systemic Energy Expenditure in Cachectic K5-SOS Mice

To determine the impact of WAT browning on systemic metabolism, we studied metabolic parameters in tumor-bearing mice. Precachectic K5-SOS mice (5 weeks old) were placed in

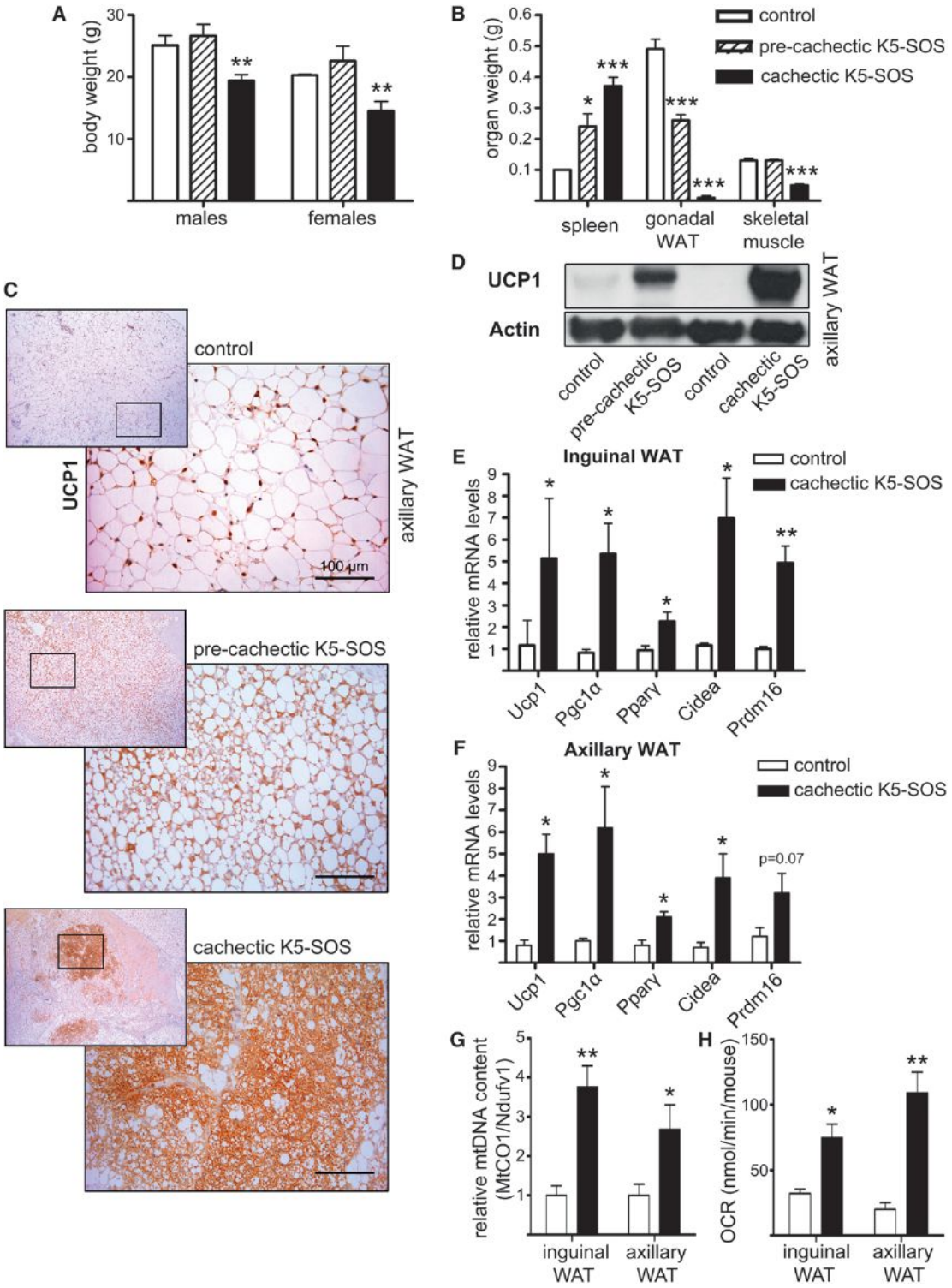

Figure 2. Browning of WAT Is an Early Event in the Pathophysiology of CAC

(A and B) Changes in total body (A) and organ (B) weight in 5-week-old (precachectic) and 7-week-old (cachectic) K5-SOS mice and littermate controls.

(C and D) Representative images of UCP1 IHC staining (C) and western blot analysis (D) of axillary WAT.

(E and F) Gene expression analysis of browning markers in inguinal (E) and axillary (F) WAT.

(G and H) Analysis of mitochondrial DNA content (G) and oxygen consumption rate (OCR) (H) in isolated inguinal and axillary WAT.

For all panels, n ≥ 8 per genotype and per group. Data are presented as mean ± SEM (*p < 0.05; **p < 0.01; ***p < 0.001).

metabolic cages and examined for 2 weeks. Energy expenditure (EE) progressively increased in K5-SOS mice over this time in both diurnal and nocturnal periods and reached significantly increased values during the last 3 days, when mice were overtly cachectic (Figures 3A and 3B). Respiratory exchange ratios (RERs) were reduced in K5-SOS mice, highlighting the importance of lipids as the primary fuel source in cachectic mice (Figures 3C and 3D). Food intake was increased in cachectic mice (Figure 3E), yet feeding a high-fat diet did not prevent loss of total body weight or tissue atrophy (Figures S4A and S4B). Notably, energy expenditure was increased in cachectic mice despite reduced locomotor activity (Figure 3F).

Increased glucose recycling via lactate, a metabolic pathway termed the Cori cycle, has been described in cachectic cancer patients and suggested to play a causal role in the increased energy expenditure (Holroyde et al., 1984; Tisdale, 2009). To analyze a possible contribution of the Cori cycle to the cachectic phenotype observed in K5-SOS mice, the levels of substrates for gluconeogenesis were measured by NMR in plasma and tissue extracts from liver and skeletal muscle. Although significantly increased levels of alanine (plasma and liver) and pyruvate (liver) were detected in cachectic mice, which may suggest enhanced Cori cycle activity, these increases were not accompanied by a corresponding increase in lactate levels, which remained unchanged and of much higher magnitude (Figures S4C–S4E). Furthermore, expression levels of key enzymes, transporters, and transcription factors involved in lactate metabolism (Summermatter et al., 2013) were similar in liver and skeletal muscle from K5-SOS and control mice (Figures S4F and S4G), indicating that the Cori cycle is not significantly active in this cachectic model.

Atrophy of gonadal WAT in K5-SOS mice was associated with increased triglyceride hydrolase activity due to increased activity of adipose triglyceride lipase (ATGL) and hormone-sensitive lipase (HSL), as confirmed by the reduction in fatty acid and glycerol release from gonadal WAT explants after addition of the respective lipase inhibitor (Figures 3G and 3H). Interestingly, while inhibition of ATGL and HSL led to a reduction greater than 85% in fatty acid and glycerol release from gonadal WAT of control mice (86% and 97% reduction, respectively), the fold reduction after lipase inhibitors was considerably less for K5-SOS mice (60% and 67% reduction, respectively), indicating that higher doses of inhibitors are required to counteract lipolysis during cachexia. Alternatively, other yet-unidentified lipases may become active and contribute to triacylglycerol hydrolysis and WAT loss in cachexia. Increased lipolysis was also evident in inguinal and axillary WAT (Figure 3I) due to pronounced overexpression of adipose ATGL, HSL, and phospho-HSL (Figure 3J). The increase in lipid mobilization and energy expenditure despite decreased locomotor activity suggests that WAT browning, together with enhanced thermogenesis in interscapular BAT, contributes to excessive substrate oxidation and wasting in CAC.

Role of Inflammation in the Pathophysiology of WAT Browning in Cachexia

Although it is established that WAT browning enhances thermogenesis (Cousin et al., 1992), rectal temperature was reduced in 7-week-old cachectic K5-SOS mice housed at standard temperatures (23°C) (Figure S5A). To evaluate whether WAT browning represents a defense mechanism against lower body temperature (Wu et al., 2013), mice were kept at thermoneutrality (30°C) starting at 4 weeks of age. Housing mice at thermoneutrality for 1 month did not affect the loss of WAT and skeletal muscle mass and did not rescue the reduction in body temperature or the WAT browning phenotype (Figures S5B–S5E). These data show that WAT browning in cachectic mice is independent of environmental thermal stimuli.

Searching for a common cause of WAT browning in all analyzed models of CAC, we reasoned that chronic inflammation would be a good candidate, since it is a hallmark of both clinical (Blum et al., 2011) and experimental CAC (Fearon et al., 2012). In order to define the potential role of inflammation in the pathogenesis of the WAT browning phenotype, we examined inflammation-induced signaling pathways in WAT of mice with the K5-SOS, Kras-pancreatic cancer GEMM, and colon carcinoma C26 syngeneic tumors (Tsoli et al., 2012). In all three models, STAT3 was activated, and phosphorylation of the MAPK p38 was increased in WAT of K5-SOS and C26 mice (Figures S6A–S6C). Increased expression of *Socs3*, downstream of STAT3, and *Cox1*, indicative of enhanced prostaglandin signaling, was observed (Figures S6D and S6E). Furthermore, systemic chronic inflammation was documented by leukocytosis with increased neutrophil/lymphocyte ratio (Figures S6F and S6G) and fibrosis of subcutaneous WAT and liver (Figures S6H–S6K). Notably, cachectic mice displayed increased IL-6 levels in blood (Figure S6L).

IL-6 is a proinflammatory cytokine with a major role in cachexia pathophysiology (Fearon et al., 2012). To further delineate the role of IL-6 in promoting WAT browning, we employed C26 carcinoma cells, which are IL-6 proficient, as well as a C26 tumor variant that lacks IL-6. Although the syngeneic tumor from IL-6-proficient C26 cells was smaller compared to the tumor from IL-6-deficient C26 cells (Figure 4A), only mice injected with IL-6-proficient C26 cells rapidly lost body weight and became cachectic (Figures 4B and 4C). Likewise, UCP1 protein content was high only in subcutaneous WAT of mice implanted with IL-6-proficient C26 tumors (Figure 4D). To confirm the role of IL-6 in causing cachexia in the C26 colon cancer model, we blocked IL-6 expression in IL-6-proficient C26 cells by stable incorporation of an shRNA targeting IL-6. Preventing IL-6 release by C26 tumors completely rescued the cachectic phenotype (Figures 4E and 4F). Notably, silencing IL-6 in C26 tumors also blocked the increased UCP1 protein expression in subcutaneous adipose tissue (Figure 4G). In addition, the increased mitochondrial respiratory function observed in axillary WAT from mice implanted with IL-6-proficient C26 cells was partially normalized after IL-6 silencing (Figure 4H).

To further address the role of IL-6 in WAT browning, an anti-IL-6 blocking antibody was used. Anti-IL-6 treatment was started in K5-SOS mice at 5 weeks of age, when a severe reduction in total fat mass was documented by dual-energy X-ray absorptiometry (DXA) analysis (Figure S6M). Treatment for 2 weeks with anti-IL-6 monoclonal antibody prevented the further reduction of total body fat and reduced UCP1 protein levels in subcutaneous WAT (Figures 4I and 4J). Despite the beneficial effect on WAT atrophy, total body loss was not affected by anti-IL-6 treatment (Figure S6N). The partial effect could be due to the inability of

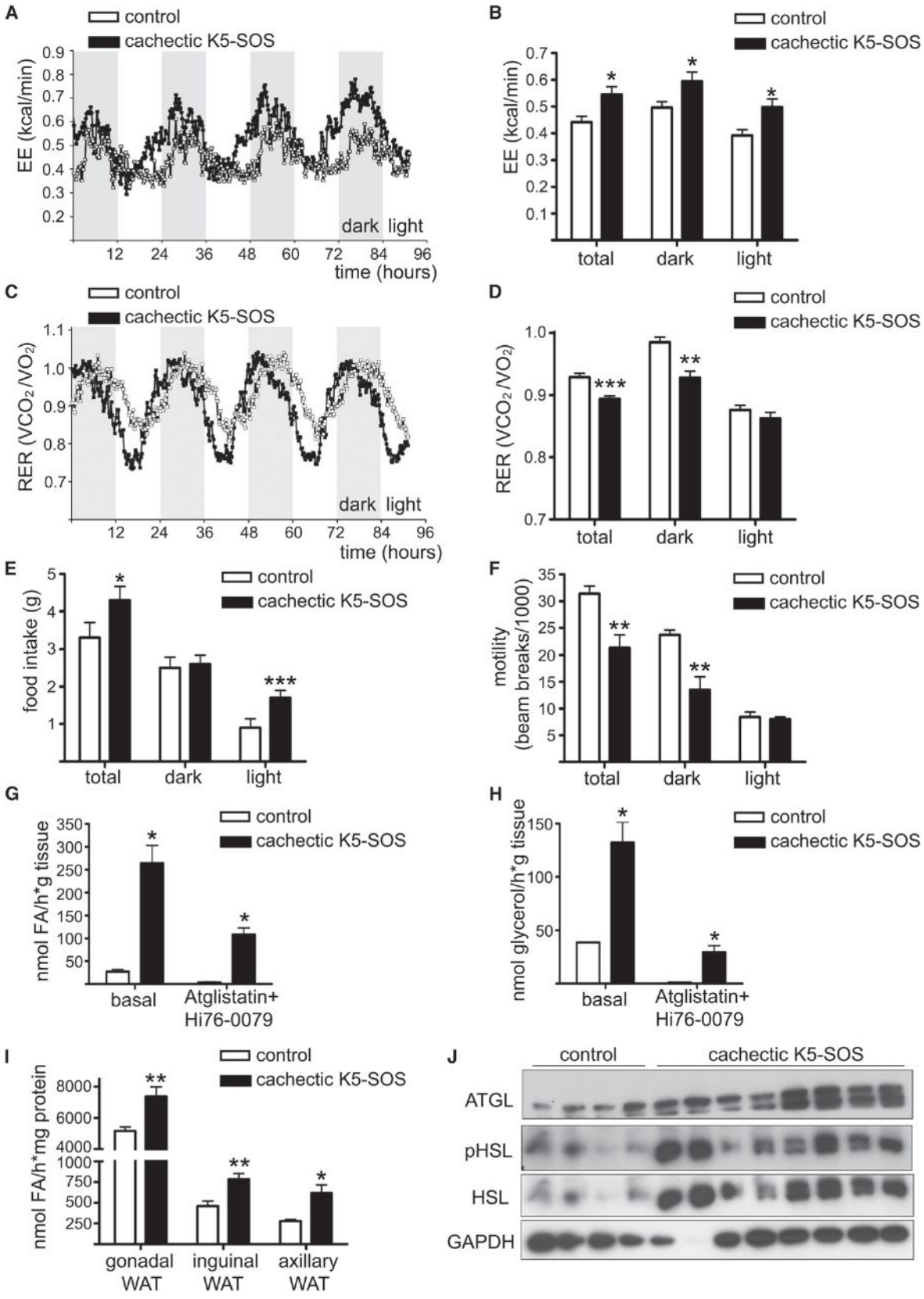

(legend on next page)

the antibody to fully neutralize IL-6. To complement these experiments, the severity of cachexia was investigated in IL-6 receptor knockout (IL-6-R-KO) mice. At 2 weeks after implantation of B16 melanomas, WAT atrophy was significantly reduced in mutant mice, although the protection against total body weight loss was small and did not reach statistical significance (Figures 4K and 4L). Importantly, UCP1 protein levels in subcutaneous WAT from IL-6-R-KO mice implanted with B16 melanoma cells were drastically reduced when compared to control mice (Figure 4M). Combined with the functional evidence for reversal of browning in the IL-6 knockdown C26 tumor model, these data establish that IL-6 signaling plays an important role in the WAT browning phenotype observed in mouse models of cachexia.

Role of β-Adrenergic Activation in the Pathogenesis of WAT Browning in Cachectic Mice

It has recently been reported that IL-6 determines alternative activation of macrophages (Mauer et al., 2014). Interestingly, alternatively activated macrophages sustain adaptive thermogenesis in BAT through enhanced recruitment of β-adrenergic fibers (Nguyen et al., 2011). Macrophage infiltration was evident in subcutaneous WAT of mice in the syngeneic graft model with IL-6-proficient C26 cells, as well as in other models of cachexia, including K5-SOS mice and mice in the xenogeneic transplant model with human pancreatic cancer (Figure S7A and data not shown). Gene expression analysis of axillary WAT in K5-SOS mice showed increased levels of markers of the alternatively activated M2 macrophages (*IL4* and *Arg1*), while levels of the M1 marker *TNFα* were unchanged (Figure S7B). Positive immunohistochemical staining for the rate-limiting enzyme of catecholamine synthesis, tyrosine hydroxylase (TH), confirmed β-adrenergic activation in WAT of cachectic mice (Figure S7C).

To determine the role of adrenergic innervation in the induction of the thermogenic program in cachectic mice, we tested whether bilateral surgical denervation of BAT would affect the increased UCP1 protein levels observed in this tissue in K5-SOS mice. At 1 week after surgery, BAT from denervated control mice appeared pale, displayed adipocytes of bigger dimensions with less vacuolization of the cytoplasm, and showed a drastic reduction in UCP1 protein levels (Figures 5A–5D). Interestingly, in K5-SOS mice, although BAT denervation was also effective in decreasing UCP1 levels, residual protein levels were higher than those in denervated control mice (Figures 5A–5D). These data suggest that the presence of an intact adrenergic innervation is essential for the complete induction of the thermogenic program in BAT of cachectic mice. However, even in the absence of innervation, adrenergic-independent mechanisms still determine a partial increase of UCP1 protein levels.

We next tested in vitro whether IL-6 was able to directly increase *Ucp1* levels in adipocytes. We used 3T3-L1 pre-white adipocytes retrovirally transduced with Cebp/β (Ortega-Molina et al., 2012), as a model of pre-brown adipocytes, as well as primary adipocytes from inguinal WAT. Treatment with the cyclic AMP inducer Forskolin increased *Ucp1* expression levels by 8-fold and 30-fold in the cell line and in primary adipocytes, respectively (Figures S7D and S7E). Although less robust, a statistically significant increase in *Ucp1* mRNA levels was observed after treatment of both cell models with recombinant murine IL-6 (Figures S7D and S7E), thus providing evidence for a small but distinct effect of the cytokine upon *Ucp1* expression in adipocytes.

These data show that chronic inflammation together with β-adrenergic activation functionally cooperate in the pathogenesis of increased adipose tissue thermogenesis in cachexia.

β3-Adrenergic Receptor Blockade and Anti-Inflammatory Treatment Ameliorate Cachexia

Adrenergic control of thermogenesis in adipose tissue is mediated mainly by β3-adrenergic receptors (Cao et al., 2011). To investigate the potential to prevent cachexia, treatment with the selective β3-adrenergic receptor (β3-AR) antagonist was started in mice after weaning, at 3 weeks of age, when no sign of cachexia was apparent in K5-SOS mice. Treating mice for 4 weeks with the selective β3-AR antagonist ameliorated cachexia and decreased UCP1 levels in subcutaneous WAT (Figures 6A–6C). While inhibition of β3-AR did not significantly reduce *Ucp1* mRNA expression levels in subcutaneous WAT of control mice, the treatment was effective in reducing *Ucp1* expression in K5-SOS mice (Figure 6C). Similarly, multilocular areas were reduced in subcutaneous WAT of K5-SOS mice treated with the selective β3-AR antagonist, when compared to vehicle-treated cachectic mice (Figure 6D).

The increased chronic inflammation observed in cachectic mice prompted us to treat K5-SOS mice with the nonselective COX1/2 inhibitor, nonsteroidal anti-inflammatory drug sulindac. Similarly to the experimental design with the β3-AR antagonist, the preventive potential of sulindac was tested starting the treatment at 3 weeks of age. Treating K5-SOS mice for 4 weeks with sulindac was very effective in ameliorating the severity of cachexia, along with a reduction of browning in subcutaneous WAT (Figures 6E–6H). Similarly to what was observed with the

Figure 3. Increased Systemic Energy Expenditure and Lipid Mobilization in Cachectic Mice

Precachectic K5-SOS mice and littermate controls (5 weeks old) were housed individually in metabolic cages and recorded during 2 weeks. Results of the last 3 days of measurement are shown, a time point at which K5-SOS mice were overtly cachectic.

(A) Energy expenditure (EE) at each time point.

(B) Average EE over the last 3 days

(C) Respiratory exchange ratio (RER) at each time point.

(D) Average RER over the last 3 days.

(E) Food intake.

(F) Overall motility.

(G and H) Fatty acid (FA) (G) and glycerol (H) release from gonadal WAT under basal conditions and after treatment with ATGL inhibitor (Atglistatin) plus HSL inhibitor (Hi76-0079).

(I) In vitro triglyceride hydrolase activity of lysates from gonadal, inguinal, and axillary WAT.

(J) Western blot analysis of ATGL, phospho-HSL, and HSL protein levels in axillary WAT.

For all panels, $n \geq 6$ per genotype. Data are presented as mean ± SEM (*$p < 0.05$; **$p < 0.01$; ***$p < 0.001$).

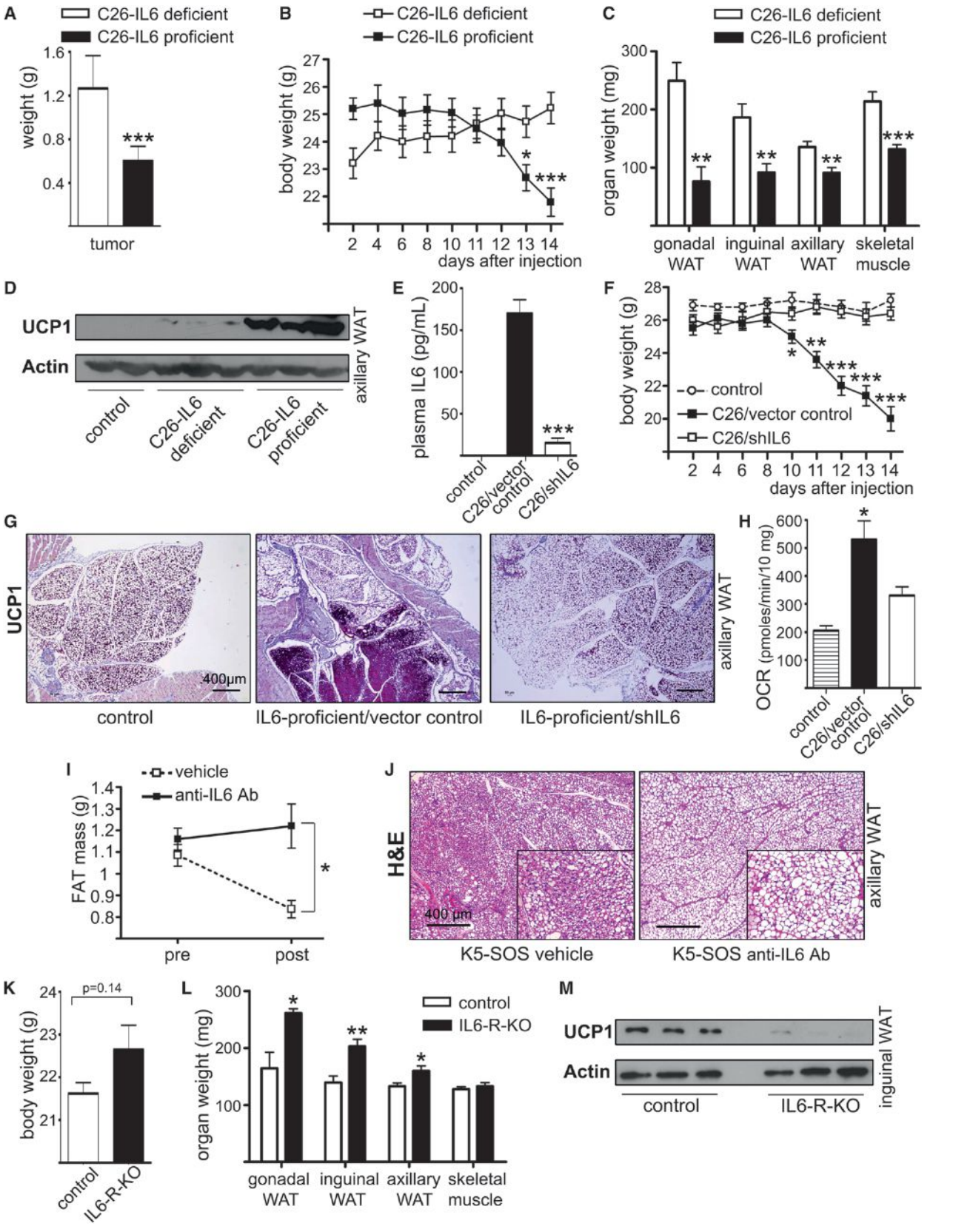

(legend on next page)

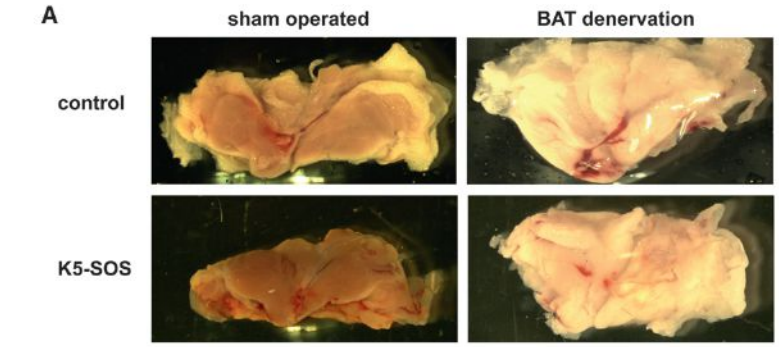

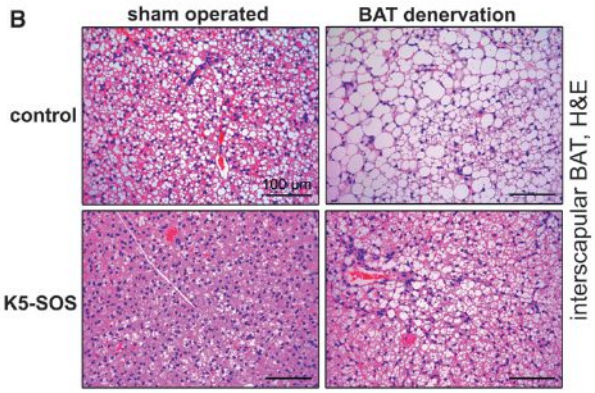

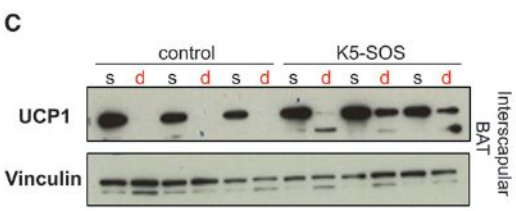

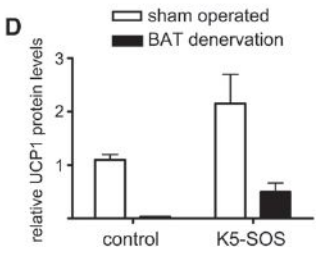

Figure 5. Reduced UCP1 Protein Levels in Interscapular BAT after BAT Denervation in Cachectic Mice

(A) Representative macroscopic pictures of BAT from 5-week-old K5-SOS mice and littermate controls, 1 week after bilateral BAT denervation surgery or sham operation.

(B) Representative images of H&E staining of BAT.

(C and D) Western blot analysis of UCP1 protein levels (C) and corresponding quantification (s, sham operated; d, BAT denervation) (D).

Data are presented as mean ± SEM; n = 3 per genotype and per condition.

β3-AR antagonist, sulindac treatment only reduced *Ucp1* mRNA expression levels in cachectic mice (Figure 6G). Notably, a reduction in UCP1 protein levels in WAT of sulindac-treated mice was already detected after 1 week of treatment (Figures S7F and S7G), a time point when amelioration of cachexia was not yet seen, thus showing that the reduction of WAT browning is an early effect of sulindac treatment.

These experiments show that preventive treatments are effective in ameliorating the severity of cancer cachexia and that nonsteroidal anti-inflammatory drugs are more potent than β3-AR blockade.

UCP1 Expression in Adipose Tissue from Cancer Cachexia Patients

Next, we explored the translational value of our findings and obtained eight samples of adipose tissue from cachectic cancer patients (Figure 7A). Despite the different anatomical location of the various adipose samples and regardless of the site of origin of the primary tumor, adipose tissue from cachectic patients exhibited morphologic features of atrophy: individual fat cells were reduced in size, had lost much of their cytoplasm, and showed a rounded or epithelioid appearance (Sternberg, 2006) (Figure 7B). In contrast, intestinal adipose tissue from patients with colon cancer, but no cachexia, appeared normal, with big adipocytes and small nuclei and being rich in lipids (Figure 7B). Importantly, a positive UCP1

Figure 4. Role of Inflammation and IL-6 in the Pathophysiology of WAT Browning in Cachexia

(A) Tumor weight in mice in the graft model with C26 colon cancer cells proficient or deficient for IL-6 (12 weeks old, n = 7 per condition).

(B and C) Changes in body (B) and organ (C) weight of mice in (A).

(D) Western blot analysis of UCP1 protein levels in axillary WAT of mice in (A).

(E) Plasma IL-6 levels in mice in the graft model with C26/IL-6 proficient cells with stable incorporation of shIL-6 or control vector (12 weeks old, n = 6 per condition).

(F) Measurement of body weight of mice in (E).

(G) Representative images of UCP1 IHC staining of axillary WAT of mice in (E).

(H) Analysis of oxygen consumption rate in isolated axillary WAT of mice in (E).

(I) Measurement of total WAT mass by DXA scan in K5-SOS mice before and after treatment with rat anti-mouse IL-6 monoclonal antibody or vehicle (pre: 5 weeks old; post: 7 weeks old; n = 5 per condition and per time point).

(J) Representative images of H&E staining of axillary WAT of mice in (I).

(K and L) Changes in total body (K) and organ (L) weight in IL-6-receptor KO mice and littermate controls, in the graft model with melanoma B16 cells (10 weeks old, n = 6 per genotype).

(M) Western blot analysis of UCP1 protein levels in axillary WAT of mice in (K).

Data are presented as mean ± SEM (*p < 0.05; **p < 0.01; ***p < 0.001).

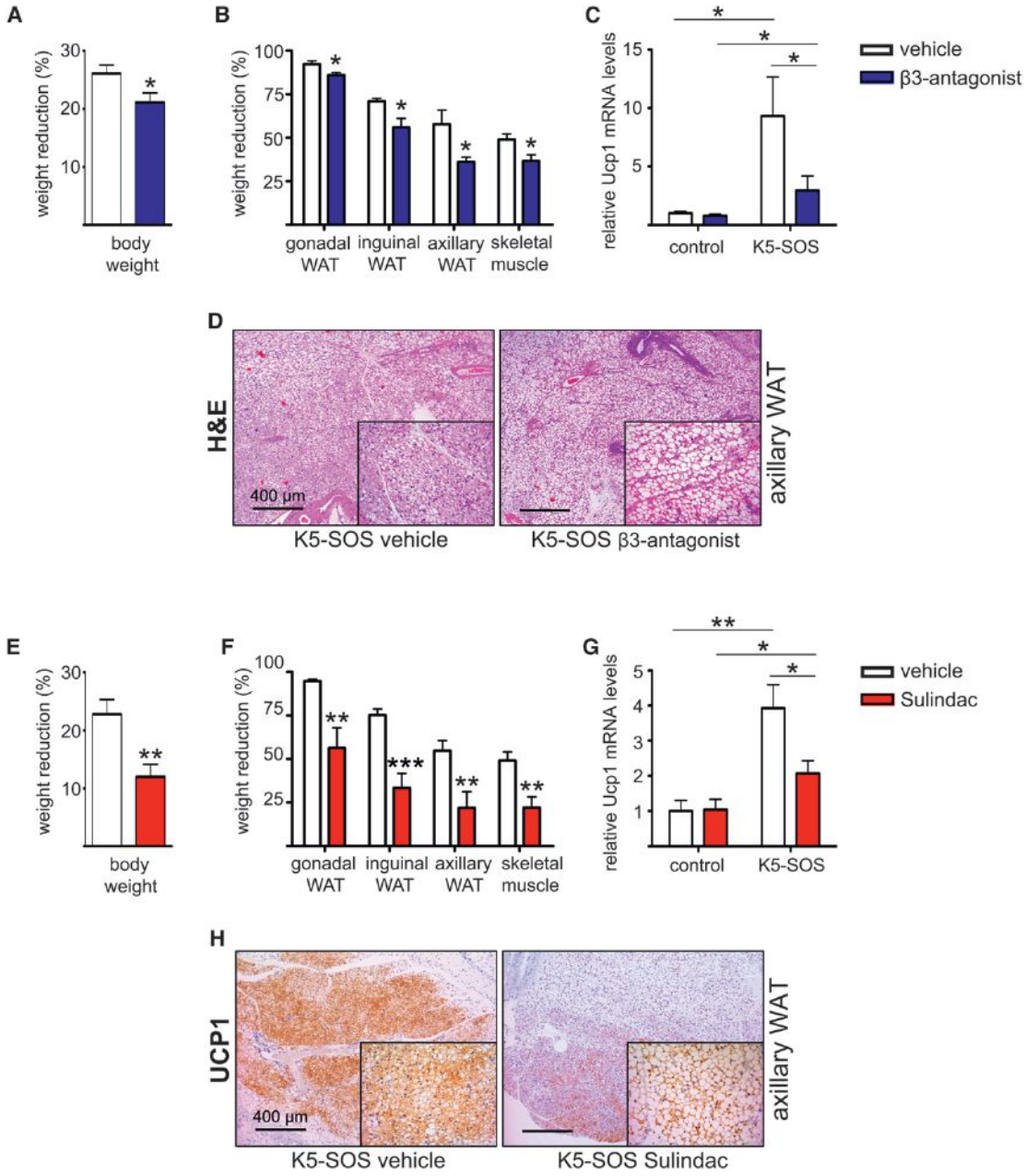

Figure 6. Amelioration of Cachexia by β3-Adrenergic Receptor Antagonism or Anti-Inflammatory Treatment

(A and B) Changes in total body weight (A) and organ weight (B) in K5-SOS mice treated with β3-AR antagonist or vehicle (7 weeks old, n ≥ 5 per genotype and per condition).

(C) Analysis of *Ucp1* gene expression levels in inguinal WAT in K5-SOS mice and littermate controls treated with β3-AR antagonist or vehicle.

(D) Representative images of H&E staining of axillary WAT in K5-SOS mice treated with β3-AR antagonist or vehicle.

(E and F) Changes in total body (E) and organ (F) weight in K5-SOS mice treated with sulindac or vehicle (7 weeks old, n ≥ 5 per genotype and per condition).

(G) Analysis of *Ucp1* gene expression levels in inguinal WAT in K5-SOS mice and littermate controls treated with sulindac or vehicle.

(H) Representative images of UCP1 IHC staining of axillary WAT in K5-SOS mice treated with sulindac or vehicle.

Data are presented as mean ± SEM (*$p < 0.05$; **$p < 0.01$; ***$p < 0.001$).

immunohistochemical staining was documented in seven out of eight samples analyzed (Figures 7A, 7C, and 7D). UCP1 staining was not evident in the only one adipose tissue sample from the pericardium observed, which may reflect differences in predisposition toward activation of the thermogenic program in adipose depots from anatomically distinct locations. Importantly, UCP1 staining was observed in samples from intestinal adipose tissue as well as fat surrounding the liver, kidney, and pancreas (Figure 7A). In contrast, 0/20 samples of intestinal adipose tissue from colon cancer patients without cachexia stained positive for

UCP1 (Figure 7C). These findings suggest that a common biological process may underlie adipocyte atrophy and UCP1 expression in cancer cachexia patients.

DISCUSSION

Cachexia is a lethal syndrome and a frequent complication in patients suffering from malignancy or chronic cardiac, pulmonary, neurological, and infectious diseases. Originally conceived as a state of ''autocannibalism,'' in which the organism depletes its resources to provide nourishment to the tumor, cachexia is now described as an inflammatory and neuroendocrine response (Fearon et al., 2012). The severity of cachexia is commonly unrelated to tumor size or stage, with small tumors often responsible for severe wasting, as in the case of pancreatic and lung cancer (Tisdale, 2009). A combination of reduced food intake and abnormal metabolism characterizes the pathophysiology of cachexia and determines the negative energy and protein balance (Fearon et al., 2013). Unfortunately, improving nutritional intake has limited therapeutic potential, and available treatment options have no effect on the impaired metabolism (Fearon et al., 2013). Therefore, the prognosis of cachexia is currently very poor.

Here, we show that WAT browning represents an early and systemic event in cachexia pathophysiology and contributes to the increased energy expenditure and lipid mobilization. Increased energy expenditure was associated with activation of a thermogenic program in adipocytes characterized by increased mitochondrial content and uncoupling activity. The thermogenic activity was increased in interscapular BAT as well as in subcutaneous WAT depots. Interestingly, in subcutaneous WAT from cachectic mice there was a preferential increase in expression levels of brown-selective over beige-selective genes. This finding may seem unexpected, given the reported increased expression of beige-selective genes in subcutaneous WAT, when compared to interscapular BAT (Wu et al., 2012). However, these gene signatures were established in cell lines and validated in mice kept at ambient temperature, when the thermogenic program is not active in subcutaneous adipose depots. In fact, after activation of the thermogenic program, both inguinal and axillary WAT from cachectic mice displayed a gene expression profile that more closely resembled that of interscapular BAT. These data suggest that gene expression markers may be indicative of the activation state of the adipose tissue rather than its anatomical origin.

Activation of the thermogenic program in subcutaneous WAT occurs as a response to lower temperatures (Cousin et al., 1992). Although rectal temperature was decreased in cachectic mice, this occurred at a later clinical stage, when the cachectic phenotype was fully apparent. Several mechanisms account for hypothermia in terminal cachectic mice, including decreased insulating capacity due to loss of total WAT mass and decreased heat production due to reduced locomotor activity. Hypothermia in terminal mice may suggest that WAT browning is a compensatory mechanism. In contrast, WAT browning took place early in the progression of cachexia, preceding body weight loss, muscle atrophy, and hypothermia. Remarkably, different from cold-induced thermogenesis (Champigny and Ricquier, 1990), increasing the ambient temperature to thermoneutrality (30°C) did not suppress WAT browning in cachectic mice.

The role of UCP1 in metabolism goes beyond thermoregulation, as exemplified by diet- and β-adrenergic-induced thermogenesis, which are both active at thermoneutrality (Feldmann et al., 2009). To date, WAT browning has been described as a beneficial event, promoting weight loss and improving insulin sensitivity in metabolic diseases (Boström et al., 2012; Feldmann et al., 2009). However, here we show that WAT browning is deleterious in the context of cancer, contributing to energy dissipation and progression toward cachexia.

The pathophysiology of CAC is multifactorial, with many different mediators cooperating at different stages of the disease and in different cancer types (Fearon et al., 2012). We show that systemic inflammation plays a critical role in the pathogenesis of WAT browning. It is well known that inflammatory cytokines are pyrogenic and change the thermoneutrality set-point in the hypothalamus (Gordon, 2012). Experiments with IL-6 knockout mice have shown that IL-6 is required for maximal induction of UCP1 protein in subcutaneous fat depots in response to cold exposure (Knudsen et al., 2014). Circulating levels of IL-6 were increased in cachectic mice, and activation of IL-6 signaling was documented in adipose depots by phosphorylation of Stat3. The role of IL-6 was critical in the syngeneic graft model with C26 cancer cells, where genetic blockade of IL-6 production within the tumor prevented WAT browning and cachexia. Moreover, WAT browning was reduced in IL-6-R-KO mice implanted with B16 melanoma cells. Despite these facts, it cannot be excluded that other mediators in addition to IL-6 could stimulate WAT browning in cachectic mice. In this regard, the protection observed in IL-6-R-KO mice implanted with B16 melanoma cells was only partial, thus confirming that different mechanisms other than IL-6 signaling contribute to cachexia.

The mechanism by which IL-6 induces WAT browning in cachectic mice may involve alternative activation of macrophages (Mauer et al., 2014) and recruitment of β-adrenergic fibers (Nguyen et al., 2011). Indeed, surgical ablation experiments showed that the presence of an intact adrenergic innervation was essential for the complete induction of the thermogenic program in BAT of cachectic mice. Although it was not possible to perform surgical denervation of the subcutaneous WAT, results of β3-AR blockade support a role for sympathetic innervations in the pathogenesis of WAT browning in cachexia. In addition, in vitro experiments showed a direct effect of IL-6 on *Ucp1* expression in isolated adipocytes. Even if the effect was mild, chronically increased circulating IL-6 levels may induce thermogenesis in adipose tissue, either alone or in combination with other cytokines.

Circulating levels of IL-6 in patients with cancer correlate with weight loss and reduced survival (Moses et al., 2009; Scott et al., 1996). Blocking IL-6 in patients with CAC has been shown to ameliorate several symptoms and signs of cachexia, like fatigue, anorexia, and anemia, although it is ineffective upon loss of lean mass (Bayliss et al., 2011). Results with monoclonal anti-IL-6 antibody in the K5-SOS mouse model recapitulate the partial benefit observed in clinical trials and support the concept that treatment of cachexia in cancer patients must start early (Fearon et al., 2013). Due to the severity of commonly reported side effects associated with anti-IL-6 therapy (Berti et al., 2013), it

A

sample	Primary cancer	Location of adipose tissue	UCP1
1	Kaposi's sarcoma	Intestinal Fat	+
2	Melanoma	Intestinal Fat	+
3	Cholangiocarcinoma	Perihepatic Fat	+
4	Colon Adenocarcinoma	Pericardial Fat	-
5	Pancreatic Neuroendocrine Cancer	Intestinal Fat	+
6	Pleomorphic Carcinoma Lung	Unspecified Origin	+
7	Lung Adenocarcinoma	Perirenal Fat	+
8	Lung Adenocarcinoma	Peripancreatic Fat	+

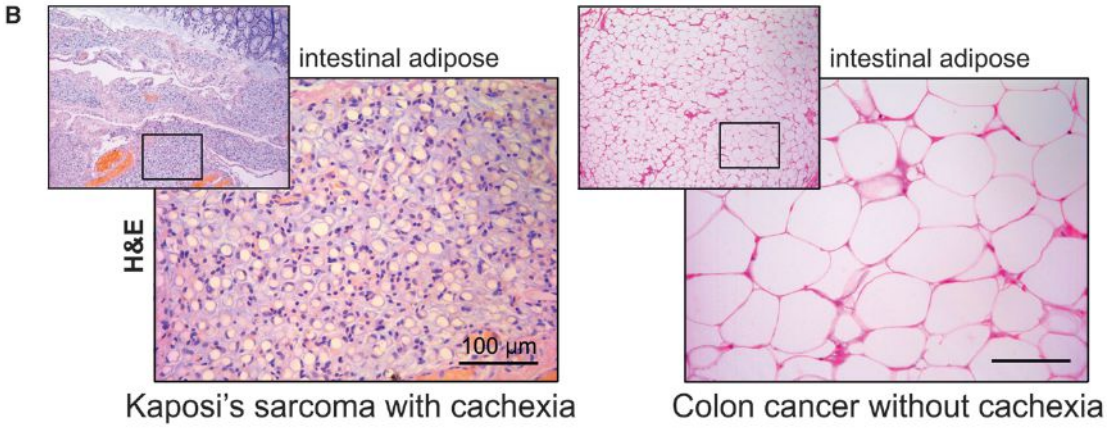

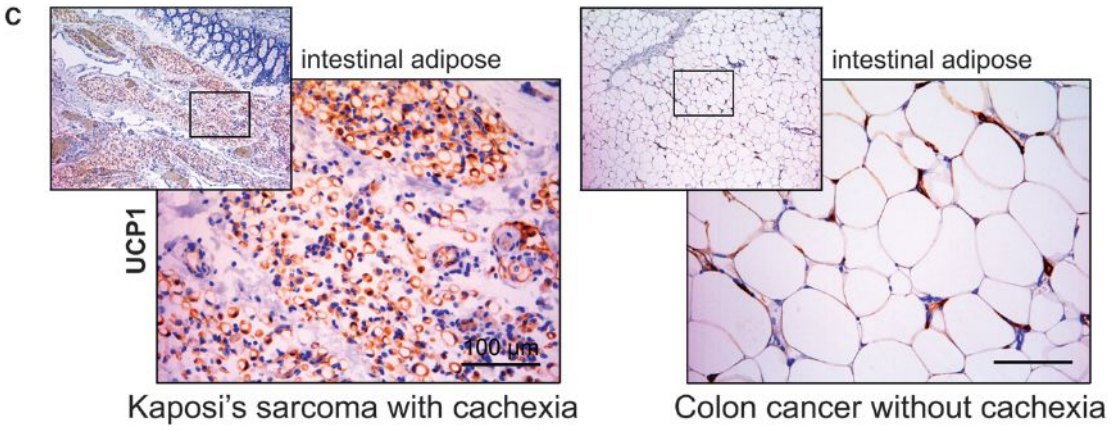

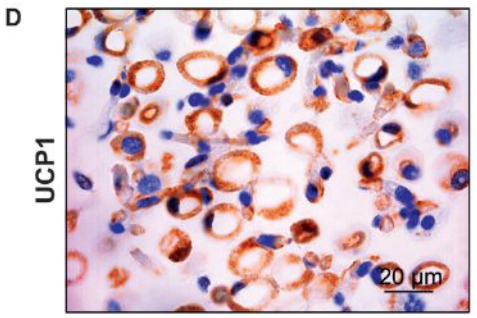

(legend on next page)

may prove difficult to prevent cachexia by IL-6 inhibition in early-stage cancer patients. Alternative preventive strategies may involve the use of β3-AR antagonists or, especially, nonsteroidal anti-inflammatory drugs, which were effective in experimental models. While both β3-AR blockade and sulindac treatment significantly reduced WAT browning in cachectic mice, other mechanisms could contribute to the therapeutic effect. Anti-inflammatory treatment has been shown to reduce the acute phase response and attenuate tumor progression in both preclinical models and patients with metastatic tumors (Lundholm et al., 1994). β3-AR blockade may protect against cachexia by means of decreased lipolysis (Tisdale, 2009), although β-adrenergic activation is only one of several pathways to account for increased lipolysis in CAC (Agustsson et al., 2007), and the presence of uniformly increased adrenergic activity in humans with CAC remains to be documented (Klein and Wolfe, 1990).

The induction of brown adipocytes in WAT depots of humans (Cypess et al., 2009; van Marken Lichtenbelt et al., 2009; Virtanen et al., 2009) has been shown recently to significantly affect overall energy balance (Yoneshiro et al., 2013). Human brown fat is composed of adipocytes similar to both classical interscapular brown adipocytes (Cypess et al., 2013; Jespersen et al., 2013; Lidell et al., 2013) and mouse white adipocytes converted into brown (Sharp et al., 2012; Wu et al., 2012). Moreover, a recent imaging study showed increased metabolic activity of BAT in PET-CTs of cancer patients (Huang et al., 2011). We have shown a switch from white to brown adipocytes in WAT of mice with CAC. WAT browning, together with enhanced thermogenesis in interscapular BAT, contributed to increased systemic energy expenditure. Also, preventing WAT browning by means of β3-AR antagonists or nonsteroidal anti-inflammatory drugs ameliorated the wasting process. The observation of increased UCP1 staining in adipose tissue from cachectic cancer patients indicates that adipocyte atrophy may be associated with increased thermogenic activity in human cancer cachexia. These data suggest that inhibition of WAT browning represents a promising approach to ameliorate the severity of cachexia in cancer patients.

EXPERIMENTAL PROCEDURES

Mice and Treatments

Mouse strains employed in this study have been previously described: Kras-pancreatic cancer GEMM (Hingorani et al., 2005), Kras-lung cancer GEMM (Puyol et al., 2010), K5-SOS mice (Sibilia et al., 2000), and IL-6-R-KO mice (McFarland-Mancini et al., 2010). All studies were performed with littermates of the same genetic background as controls. For the hepatic carcinogen model, 15-day-old mice on a mixed C57BL/6/129 background were injected intraperitoneally (i.p.) with 25 mg/kg DEN (Sigma-Aldrich). LLC cells (4×10^6) or B16 melanoma cells (2×10^6) were injected subcutaneously at dorsum just below the neck in C57Bl/6 mice. C26 cells (1×10^6) were injected subcutaneously into the right flank of Balb/C × DBA1 hybrids. Mice used for injection of tumor cells as well as control animals were 10–12 weeks of age. Xenograft experiments were conducted in accordance with institutional guidelines of the CNIO (Protocol PA34/2012). Chow (D8604, Harlan) and 45% high-fat diet (D12451, Research Diets) were used in this study. For the thermoneutrality experiment, mice were introduced in the 30°C environment 1 week after weaning (4 weeks old) and housed with four mice per cage. Mice were acclimatized for 1 week prior to monitoring. Rat anti-mouse IL-6 monoclonal antibody (clone: MP5-20F3) was administered i.p. (five doses of 200 μg each, once each 3 days). The β3-AR antagonist SR59230A (Sigma-Aldrich; 3 mg/kg body weight per day) was administered through osmotic minipumps (Alzet). Sulindac (Sigma-Aldrich) was administered in drinking water (180 mg/l). Full methods are described in the Supplemental Experimental Procedures.

Human Tumor Samples

After patients' informed consent had been obtained, excess tissues from resected pancreatic carcinomas were xenografted at Hospital de Madrid - Centro Integral Oncologico Clara Campal (FHM.06.10 "Establishment of bank for tumors and healthy tissue in patients with cancer") under the indicated Institutional Review Board approved protocols.

qRT-PCR/Immunoblot Analysis

Quantitative RT-PCR reactions were performed using GoTaq RT-qPCR Master Mix (Promega) and Eppendorf fluorescence thermocyclers (Eppendorf). The 2-ΔΔCT method was used to quantify amplified fragments. Expression levels were normalized using two housekeeping genes (Actin and Gapdh). Primer sequences will be provided on request. Immunoblot analysis was performed using standard protocols and the following antibodies: mouse monoclonal anti-Actin (Sigma-Aldrich, A4700), rabbit polyclonal anti-ATGL (Cell Signaling Technology, #2138), rabbit monoclonal anti-GAPDH (Cell Signaling Technology, #2118), rabbit polyclonal anti-HSL (Cell Signaling Technology, #4107), rabbit monoclonal anti-NDUFS1 (Abcam, ab157221), rabbit polyclonal anti-p38α MAP-Kinase (Cell Signaling Technology, #9218), rabbit polyclonal anti-Phospho-HSL (Cell Signaling Technology, #4126), rabbit polyclonal anti-Phospho-p38α MAP-Kinase (Thr180/182; Cell Signaling Technology, #9211), rabbit polyclonal anti-Phospho-STAT3 (Tyr705; Cell Signaling Technology, #9131), rabbit polyclonal anti-STAT3 (Cell Signaling Technology, #9132), rabbit polyclonal anti-UCP1 (Abcam, ab10983), mouse monoclonal anti-Vinculin (Sigma-Aldrich, V9131).

Oxygen Consumption Rate

Oxygen consumption rates (OCRs) in homogenized adipose tissue depots were analyzed by high-resolution respirometry (Oxygraph 2k, Oroboros Instruments) using glycerol-3-phosphate as substrate. Electron transfer via complex I in the respiratory chain was blocked by the addition of rotenone.

Indirect Calorimetric Studies

To measure O_2 consumption, CO_2 production, food intake, and spontaneous motility, mice were housed in metabolic cages (LabMaster, TSE Systems GmbH). Animals were familiarized to single housing for at least 3 days prior to monitoring.

IL-6 Knockdown in C26 Tumors

IL-6 expression in C26 cells was knocked down with lentiviral constructs from the MISSION shRNA Library (Sigma-Aldrich). Transduced cells were selected with puromycin, single-cell clones were derived, and the clones were tested by qPCR and ELISA for reduced IL-6 expression after in vitro IL-1β stimulation. The C26 tumors with the stably integrated IL-6 shRNA construct or vector control were implanted into mice as outlined above.

Dual Energy X-Ray Absorptiometry Analysis

Whole-body fat mass density was measured by a PIXImus2 scanner according to the manufacturer's protocol (Lunar Corporation).

Surgical Denervation

Mice (4 weeks old) underwent bilateral surgical denervation of the interscapular BAT under isoflurane anesthesia. A transverse incision was made just

Figure 7. UCP1 Expression in Atrophic WAT from Cancer Cachexia Patients

(A) Origin of the primary tumor, anatomical location of the WAT, and UCP1 IHC status in the human cancer cachexia samples analyzed.
(B and C) Representative images of H&E (B) and UCP1 IHC (C) staining of intestinal WAT from cancer patients with or without cachexia.
(D) Magnification of UCP1 IHC staining in intestinal WAT from the cachectic patient in (C).

anterior to the BAT, and the organ was exposed. After carefully moving the BAT outward from the surrounding muscle and white adipose tissue, the sympathetic chains innervating the organ were exposed. Denervation was performed by isolation and resection with scissors of the five branches of the left and right intercostal nerve bundles, without disrupting the blood circulation. In sham-operated mice, the sympathetic chains innervating BAT were exposed but not resected. Mice were sacrificed 1 week after surgery.

Human Cancer Cachexia Slides

Paraffin sections of adipose tissue from cancer patients were obtained at tumor biopsy or at necropsy. The samples were provided by the CNIO Tumor Bank, CNIO, Madrid, and The Biobank of Hospital Clínic - IDIBAPS, Barcelona, in accordance with the ethical guidelines of the Helsinki Declaration.

Statistical Analysis

Results are presented as mean ± SEM. p value was calculated using Student's t test.

SUPPLEMENTAL INFORMATION

Supplemental Information includes Supplemental Experimental Procedures and seven figures and can be found with this article online at http://dx.doi.org/10.1016/j.cmet.2014.06.011.

AUTHOR CONTRIBUTIONS

M.P. conceived the hypothesis, designed and performed experiments, and wrote the manuscript. M. Schweiger performed lipolysis, metabolic chambers, and thermoneutrality experiments and helped edit the manuscript. R.S. performed western blot analysis and mitochondrial DNA and OCR measurements. R.C.-O. performed NMR experiments and helped edit the manuscript. M.T. performed analysis in the C26 transplant model. J.A. performed IL-6 shRNA knockdown. M. Swarbrick performed IHC and mitochondrial tests. S.R.-J. provided the anti-IL-6 antibody. M.R. provided IL-6-R-KO mice and helped edit the manuscript. G.R. and R.Z. designed experiments and helped edit the manuscript. E.F.W. secured funding, supervised the project, and wrote the manuscript.

ACKNOWLEDGMENTS

We thank the members of the Wagner lab for help and critical reading; S. Leceta, G. Luque, and G. Medrano for help with mouse procedures; and N. Djouder, M.A. Fawal, C. Heeschen, M. López, and M. Serrano for support and advice. We also thank C. Ambrogio, S. García, and M. Barbacid for Cancer GEMMs, E. Lopez-Guadamillas for 3T3-L1/Cebp/β cells, R.W. Hamacher for carcinogen-treated mice, M. Hidalgo for xenograft samples, the CNIO Tumor Bank and IDIBAPS Biobank, Barcelona for human samples, and M. Morente for expert pathological analysis. S.R.-J. was supported by the Deutsche Forschungsgemeinschaft, Germany (SFB654, project C5). G.R. was funded by Paul Ainsworth and the Dawkins family donations to the Garvan Foundation. The R.Z. laboratory is supported by the Fondation Leducq (12CVD04), an ERC-Advanced grant (LIPOCHEX Nr. 340896), the Z136 Wittgenstein Award, and the F30 SFB LIPOTOX from the Austrian Science Fund. The E.F.W. laboratory is supported by the Banco Bilbao Vizcaya Argentaria Foundation (F-BBVA), a grant from the Spanish Ministry of Economy (BFU2012-40230), and an ERC-Advanced grant (ERC-FCK/2008/37). M.P. was funded in part by a Caja-Navarra fellowship and the Union for International Cancer Control.

Received: December 18, 2013
Revised: April 28, 2014
Accepted: June 4, 2014
Published: July 17, 2014

REFERENCES

Agustsson, T., Rydén, M., Hoffstedt, J., van Harmelen, V., Dicker, A., Laurencikiene, J., Isaksson, B., Permert, J., and Arner, P. (2007). Mechanism of increased lipolysis in cancer cachexia. Cancer Res. *67*, 5531–5537.

Bayliss, T.J., Smith, J.T., Schuster, M., Dragnev, K.H., and Rigas, J.R. (2011). A humanized anti-iL-6 antibody (ALD518) in non-small cell lung cancer. Expert Opin. Biol. Ther. *11*, 1663–1668.

Berti, A., Boccalatte, F., Sabbadini, M.G., and Dagna, L. (2013). Assessment of tocilizumab in the treatment of cancer cachexia. J. Clin. Oncol. *31*, 2970.

Blum, D., Omlin, A., Baracos, V.E., Solheim, T.S., Tan, B.H., Stone, P., Kaasa, S., Fearon, K., and Strasser, F.; European Palliative Care Research Collaborative (2011). Cancer cachexia: a systematic literature review of items and domains associated with involuntary weight loss in cancer. Crit. Rev. Oncol. Hematol. *80*, 114–144.

Boström, P., Wu, J., Jedrychowski, M.P., Korde, A., Ye, L., Lo, J.C., Rasbach, K.A., Boström, E.A., Choi, J.H., Long, J.Z., et al. (2012). A PGC1-α-dependent myokine that drives brown-fat-like development of white fat and thermogenesis. Nature *481*, 463–468.

Cannon, B., and Nedergaard, J. (2004). Brown adipose tissue: function and physiological significance. Physiol. Rev. *84*, 277–359.

Cao, L., Choi, E.Y., Liu, X., Martin, A., Wang, C., Xu, X., and During, M.J. (2011). White to brown fat phenotypic switch induced by genetic and environmental activation of a hypothalamic-adipocyte axis. Cell Metab. *14*, 324–338.

Champigny, O., and Ricquier, D. (1990). Effects of fasting and refeeding on the level of uncoupling protein mRNA in rat brown adipose tissue: evidence for diet-induced and cold-induced responses. J. Nutr. *120*, 1730–1736.

Cousin, B., Cinti, S., Morroni, M., Raimbault, S., Ricquier, D., Pénicaud, L., and Casteilla, L. (1992). Occurrence of brown adipocytes in rat white adipose tissue: molecular and morphological characterization. J. Cell Sci. *103*, 931–942.

Cypess, A.M., Lehman, S., Williams, G., Tal, I., Rodman, D., Goldfine, A.B., Kuo, F.C., Palmer, E.L., Tseng, Y.H., Doria, A., et al. (2009). Identification and importance of brown adipose tissue in adult humans. N. Engl. J. Med. *360*, 1509–1517.

Cypess, A.M., White, A.P., Vernochet, C., Schulz, T.J., Xue, R., Sass, C.A., Huang, T.L., Roberts-Toler, C., Weiner, L.S., Sze, C., et al. (2013). Anatomical localization, gene expression profiling and functional characterization of adult human neck brown fat. Nat. Med. *19*, 635–639.

Das, S.K., Eder, S., Schauer, S., Diwoky, C., Temmel, H., Guertl, B., Gorkiewicz, G., Tamilarasan, K.P., Kumari, P., Trauner, M., et al. (2011). Adipose triglyceride lipase contributes to cancer-associated cachexia. Science *333*, 233–238.

Fearon, K.C., Glass, D.J., and Guttridge, D.C. (2012). Cancer cachexia: mediators, signaling, and metabolic pathways. Cell Metab. *16*, 153–166.

Fearon, K., Arends, J., and Baracos, V. (2013). Understanding the mechanisms and treatment options in cancer cachexia. Nat Rev Clin Oncol *10*, 90–99.

Feldmann, H.M., Golozoubova, V., Cannon, B., and Nedergaard, J. (2009). UCP1 ablation induces obesity and abolishes diet-induced thermogenesis in mice exempt from thermal stress by living at thermoneutrality. Cell Metab. *9*, 203–209.

Gordon, C.J. (2012). Thermal physiology of laboratory mice: Defining thermoneutrality. J. Therm. Biol. *37*, 654–685.

Harms, M., and Seale, P. (2013). Brown and beige fat: development, function and therapeutic potential. Nat. Med. *19*, 1252–1263.

Hingorani, S.R., Wang, L., Multani, A.S., Combs, C., Deramaudt, T.B., Hruban, R.H., Rustgi, A.K., Chang, S., and Tuveson, D.A. (2005). Trp53R172H and KrasG12D cooperate to promote chromosomal instability and widely metastatic pancreatic ductal adenocarcinoma in mice. Cancer Cell *7*, 469–483.

Holroyde, C.P., Skutches, C.L., Boden, G., and Reichard, G.A. (1984). Glucose metabolism in cachectic patients with colorectal cancer. Cancer Res. *44*, 5910–5913.

Huang, Y.C., Chen, T.B., Hsu, C.C., Li, S.H., Wang, P.W., Lee, B.F., Kuo, C.Y., and Chiu, N.T. (2011). The relationship between brown adipose tissue activity and neoplastic status: an (18)F-FDG PET/CT study in the tropics. Lipids Health Dis. *10*, 238.

Jespersen, N.Z., Larsen, T.J., Peijs, L., Daugaard, S., Homøe, P., Loft, A., de Jong, J., Mathur, N., Cannon, B., Nedergaard, J., et al. (2013). A classical brown adipose tissue mRNA signature partly overlaps with brite in the supraclavicular region of adult humans. Cell Metab. *17*, 798–805.

Klein, S., and Wolfe, R.R. (1990). Whole-body lipolysis and triglyceride-fatty acid cycling in cachectic patients with esophageal cancer. J. Clin. Invest. *86*, 1403–1408.

Knudsen, J.G., Murholm, M., Carey, A.L., Biensø, R.S., Basse, A.L., Allen, T.L., Hidalgo, J., Kingwell, B.A., Febbraio, M.A., Hansen, J.B., and Pilegaard, H. (2014). Role of IL-6 in exercise training- and cold-induced UCP1 expression in subcutaneous white adipose tissue. PLoS ONE *9*, e84910.

Lee, Y.H., Petkova, A.P., Mottillo, E.P., and Granneman, J.G. (2012). In vivo identification of bipotential adipocyte progenitors recruited by β3-adrenoceptor activation and high-fat feeding. Cell Metab. *15*, 480–491.

Lidell, M.E., Betz, M.J., Dahlqvist Leinhard, O., Heglind, M., Elander, L., Slawik, M., Mussack, T., Nilsson, D., Romu, T., Nuutila, P., et al. (2013). Evidence for two types of brown adipose tissue in humans. Nat. Med. *19*, 631–634.

Loncar, D., Bedrica, L., Mayer, J., Cannon, B., Nedergaard, J., Afzelius, B.A., and Svajger, A. (1986). The effect of intermittent cold treatment on the adipose tissue of the cat. Apparent transformation from white to brown adipose tissue. J. Ultrastruct. Mol. Struct. Res. *97*, 119–129.

Lundholm, K., Gelin, J., Hyltander, A., Lönnroth, C., Sandström, R., Svaninger, G., Körner, U., Gülich, M., Kärrefors, I., Norli, B., et al. (1994). Anti-inflammatory treatment may prolong survival in undernourished patients with metastatic solid tumors. Cancer Res. *54*, 5602–5606.

Mauer, J., Chaurasia, B., Goldau, J., Vogt, M.C., Ruud, J., Nguyen, K.D., Theurich, S., Hausen, A.C., Schmitz, J., Brönneke, H.S., et al. (2014). Signaling by IL-6 promotes alternative activation of macrophages to limit endotoxemia and obesity-associated resistance to insulin. Nat. Immunol. *15*, 423–430.

McFarland-Mancini, M.M., Funk, H.M., Paluch, A.M., Zhou, M., Giridhar, P.V., Mercer, C.A., Kozma, S.C., and Drew, A.F. (2010). Differences in wound healing in mice with deficiency of IL-6 versus IL-6 receptor. J. Immunol. *184*, 7219–7228.

Moses, A.G., Maingay, J., Sangster, K., Fearon, K.C., and Ross, J.A. (2009). Pro-inflammatory cytokine release by peripheral blood mononuclear cells from patients with advanced pancreatic cancer: relationship to acute phase response and survival. Oncol. Rep. *21*, 1091–1095.

Nguyen, K.D., Qiu, Y., Cui, X., Goh, Y.P., Mwangi, J., David, T., Mukundan, L., Brombacher, F., Locksley, R.M., and Chawla, A. (2011). Alternatively activated macrophages produce catecholamines to sustain adaptive thermogenesis. Nature *480*, 104–108.

Ortega-Molina, A., Efeyan, A., Lopez-Guadamillas, E., Muñoz-Martin, M., Gómez-López, G., Cañamero, M., Mulero, F., Pastor, J., Martinez, S., Romanos, E., et al. (2012). Pten positively regulates brown adipose function, energy expenditure, and longevity. Cell Metab. *15*, 382–394.

Puyol, M., Martín, A., Dubus, P., Mulero, F., Pizcueta, P., Khan, G., Guerra, C., Santamaría, D., and Barbacid, M. (2010). A synthetic lethal interaction between K-Ras oncogenes and Cdk4 unveils a therapeutic strategy for non-small cell lung carcinoma. Cancer Cell *18*, 63–73.

Scott, H.R., McMillan, D.C., Crilly, A., McArdle, C.S., and Milroy, R. (1996). The relationship between weight loss and interleukin 6 in non-small-cell lung cancer. Br. J. Cancer *73*, 1560–1562.

Shabalina, I.G., Petrovic, N., de Jong, J.M., Kalinovich, A.V., Cannon, B., and Nedergaard, J. (2013). UCP1 in brite/beige adipose tissue mitochondria is functionally thermogenic. Cell Rep *5*, 1196–1203.

Sharp, L.Z., Shinoda, K., Ohno, H., Scheel, D.W., Tomoda, E., Ruiz, L., Hu, H., Wang, L., Pavlova, Z., Gilsanz, V., and Kajimura, S. (2012). Human BAT possesses molecular signatures that resemble beige/brite cells. PLoS ONE *7*, e49452.

Sibilia, M., Fleischmann, A., Behrens, A., Stingl, L., Carroll, J., Watt, F.M., Schlessinger, J., and Wagner, E.F. (2000). The EGF receptor provides an essential survival signal for SOS-dependent skin tumor development. Cell *102*, 211–220.

Sternberg, S.S. (2006). Histology for Pathologists. (Philadelphia: Lippincott Williams & Wilkins).

Summermatter, S., Santos, G., Pérez-Schindler, J., and Handschin, C. (2013). Skeletal muscle PGC-1α controls whole-body lactate homeostasis through estrogen-related receptor α-dependent activation of LDH B and repression of LDH A. Proc. Natl. Acad. Sci. USA *110*, 8738–8743.

Tang, W., Zeve, D., Seo, J., Jo, A.Y., and Graff, J.M. (2011). Thiazolidinediones regulate adipose lineage dynamics. Cell Metab. *14*, 116–122.

Tisdale, M.J. (2002). Cachexia in cancer patients. Nat. Rev. Cancer *2*, 862–871.

Tisdale, M.J. (2009). Mechanisms of cancer cachexia. Physiol. Rev. *89*, 381–410.

Tsoli, M., Moore, M., Burg, D., Painter, A., Taylor, R., Lockie, S.H., Turner, N., Warren, A., Cooney, G., Oldfield, B., et al. (2012). Activation of thermogenesis in brown adipose tissue and dysregulated lipid metabolism associated with cancer cachexia in mice. Cancer Res. *72*, 4372–4382.

van Marken Lichtenbelt, W.D., Vanhommerig, J.W., Smulders, N.M., Drossaerts, J.M., Kemerink, G.J., Bouvy, N.D., Schrauwen, P., and Teule, G.J. (2009). Cold-activated brown adipose tissue in healthy men. N. Engl. J. Med. *360*, 1500–1508.

Vegiopoulos, A., Müller-Decker, K., Strzoda, D., Schmitt, I., Chichelnitskiy, E., Ostertag, A., Berriel Diaz, M., Rozman, J., Hrabe de Angelis, M., Nüsing, R.M., et al. (2010). Cyclooxygenase-2 controls energy homeostasis in mice by de novo recruitment of brown adipocytes. Science *328*, 1158–1161.

Villarroya, F., and Vidal-Puig, A. (2013). Beyond the sympathetic tone: the new brown fat activators. Cell Metab. *17*, 638–643.

Virtanen, K.A., Lidell, M.E., Orava, J., Heglind, M., Westergren, R., Niemi, T., Taittonen, M., Laine, J., Savisto, N.J., Enerbäck, S., and Nuutila, P. (2009). Functional brown adipose tissue in healthy adults. N. Engl. J. Med. *360*, 1518–1525.

Waldén, T.B., Hansen, I.R., Timmons, J.A., Cannon, B., and Nedergaard, J. (2012). Recruited vs. nonrecruited molecular signatures of brown, "brite," and white adipose tissues. Am. J. Physiol. Endocrinol. Metab. *302*, E19–E31.

Wang, Q.A., Tao, C., Gupta, R.K., and Scherer, P.E. (2013). Tracking adipogenesis during white adipose tissue development, expansion and regeneration. Nat. Med. *19*, 1338–1344.

Wu, J., Boström, P., Sparks, L.M., Ye, L., Choi, J.H., Giang, A.H., Khandekar, M., Virtanen, K.A., Nuutila, P., Schaart, G., et al. (2012). Beige adipocytes are a distinct type of thermogenic fat cell in mouse and human. Cell *150*, 366–376.

Wu, J., Cohen, P., and Spiegelman, B.M. (2013). Adaptive thermogenesis in adipocytes: is beige the new brown? Genes Dev. *27*, 234–250.

Yoneshiro, T., Aita, S., Matsushita, M., Kayahara, T., Kameya, T., Kawai, Y., Iwanaga, T., and Saito, M. (2013). Recruited brown adipose tissue as an antiobesity agent in humans. J. Clin. Invest. *123*, 3404–3408.

Young, P., Arch, J.R., and Ashwell, M. (1984). Brown adipose tissue in the parametrial fat pad of the mouse. FEBS Lett. *167*, 10–14.

Zhou, X., Wang, J.L., Lu, J., Song, Y., Kwak, K.S., Jiao, Q., Rosenfeld, R., Chen, Q., Boone, T., Simonet, W.S., et al. (2010). Reversal of cancer cachexia and muscle wasting by ActRIIB antagonism leads to prolonged survival. Cell *142*, 531–543.

Cell Metabolism
Article

β-Aminoisobutyric Acid Induces Browning of White Fat and Hepatic β-Oxidation and Is Inversely Correlated with Cardiometabolic Risk Factors

Lee D. Roberts,[1] Pontus Boström,[2,3] John F. O'Sullivan,[1] Robert T. Schinzel,[1,4,5,6] Gregory D. Lewis,[1,7,8] Andre Dejam,[1] Youn-Kyoung Lee,[1,4,5] Melinda J. Palma,[1] Sondra Calhoun,[2] Anastasia Georgiadi,[3] Ming-Huei Chen,[9,10,11] Vasan S. Ramachandran,[9,12] Martin G. Larson,[9,13] Claude Bouchard,[14] Tuomo Rankinen,[14] Amanda L. Souza,[8] Clary B. Clish,[8] Thomas J. Wang,[1,7,15] Jennifer L. Estall,[16] Alexander A. Soukas,[17] Chad A. Cowan,[1,4,5,7] Bruce M. Spiegelman,[2] and Robert E. Gerszten[1,7,8,*]

[1]Cardiovascular Research Center, Massachusetts General Hospital, Harvard Medical School, Boston, MA 02114, USA
[2]Dana-Farber Cancer Institute and Harvard Medical School, 3 Blackfan Circle, CLS Building, Floor 11, Boston, MA 02115, USA
[3]Institutionen för Cell–Och Molekylärbiologi (CMB), Karolinska Institutet, von Eulers väg 3, 171 77 Stockholm, Sweden
[4]Department of Stem Cell and Regenerative Biology, Harvard University, Cambridge, MA 02138, USA
[5]Center for Regenerative Medicine, Massachusetts General Hospital, Boston, MA 02114, USA
[6]Institut für Biologie–Mikrobiologie, Fachbereich Biologie, Chemie, Pharmazie, Freie Universität Berlin, Königin-Luise-Strasse 12-16,14195 Berlin, Germany
[7]Cardiology Division, Massachusetts General Hospital, Harvard Medical School, Boston, MA 02114, USA
[8]Broad Institute of MIT and Harvard, Cambridge, MA 02142, USA
[9]Framingham Heart Study of the National Heart, Lung, and Blood Institute and Boston University School of Medicine, Framingham, MA 01702, USA
[10]Department of Neurology, Boston University School of Medicine, Boston, MA 02118, USA
[11]Department of Biostatistics, Boston University School of Public Health, Boston, MA 02118, USA
[12]Cardiology Section, Boston Medical Center, Boston University School of Medicine, Boston, MA 02118, USA
[13]Department of Mathematics and Statistics, Boston University, Boston, MA 02215, USA
[14]Pennington Biomedical Research Center, Baton Rouge, LA 70808, USA
[15]Cardiology Division, Vanderbilt University, Nashville, TN 37232, USA
[16]Institut de Recherches Cliniques de Montreal, Montreal, QC H2W 1R7, Canada
[17]Center for Human Genetic Research, Massachusetts General Hospital, Harvard Medical School, Boston, MA 02114, USA
*Correspondence: rgerszten@partners.org
http://dx.doi.org/10.1016/j.cmet.2013.12.003

SUMMARY

The transcriptional coactivator peroxisome proliferator-activated receptor-gamma coactivator-1α (PGC-1α) regulates metabolic genes in skeletal muscle and contributes to the response of muscle to exercise. Muscle PGC-1α transgenic expression and exercise both increase the expression of thermogenic genes within white adipose. How the PGC-1α-mediated response to exercise in muscle conveys signals to other tissues remains incompletely defined. We employed a metabolomic approach to examine metabolites secreted from myocytes with forced expression of PGC-1α, and identified β-aminoisobutyric acid (BAIBA) as a small molecule myokine. BAIBA increases the expression of brown adipocyte-specific genes in white adipocytes and β-oxidation in hepatocytes both in vitro and in vivo through a PPARα-mediated mechanism, induces a brown adipose-like phenotype in human pluripotent stem cells, and improves glucose homeostasis in mice. In humans, plasma BAIBA concentrations are increased with exercise and inversely associated with metabolic risk factors. BAIBA may thus contribute to exercise-induced protection from metabolic diseases.

INTRODUCTION

Exercise is an effective intervention for both the prevention and the treatment of obesity and type 2 diabetes (Knowler et al., 2002). Recent studies suggest that skeletal muscle integrates many of the signals contributing to the salutary effects of exercise (Bassel-Duby and Olson, 2006). The transcriptional coactivator peroxisome proliferator-activated receptor-gamma coactivator-1α (PGC-1α) controls an extensive set of metabolic programs within skeletal muscle and in part regulates the adaptive response of muscle to exercise (Handschin and Spiegelman, 2006; Olesen et al., 2010). PGC-1α regulates these metabolic programs by binding to nuclear receptors and other transcription factors to form active transcriptional complexes (Puigserver et al., 1999). Exercise enhances the expression of PGC-1α, which results in increased mitochondrial biogenesis and fatty acid β-oxidation, greater glucose transport, and an induction of muscular fiber type switching toward a more oxidative phenotype (Lin et al., 2002; Michael et al., 2001; Wu et al., 1999).

Transgenic mice with muscle-specific PGC-1α expression show an enhanced ability to perform endurance exercise and have an increased peak oxygen uptake (Calvo et al., 2008).

These transgenic mice also demonstrate increased expression of brown adipocyte-specific genes within white adipose tissue (WAT) and an increased adipose respiratory phenotype (Boström et al., 2012), suggesting that skeletal muscle signals to other tissues to alter their function. In addition, exercise increases mitochondrial number and brown adipocyte-specific gene expression in white adipose depots and ameliorates glucose intolerance induced by a high-fat diet (Sutherland et al., 2009; Xu et al., 2011). Exercise also enhances the brown proliferative adipocyte progenitor cell population and brown fat adipogenesis (Xu et al., 2011). Cells expressing brown-adipocyte specific genes have been reported as being interspersed within the WAT of rodents and humans (so-called beige cells) (Ishibashi and Seale, 2010; Petrovic et al., 2010) and demonstrate antidiabetic and antiobesity effects in rodent models (Kopecky et al., 1995; Melnyk et al., 1997; Seale et al., 2007). Uncoupling protein-1 (UCP-1) and cell death-inducing DFFA-like effector a (CIDEA) are among the brown adipocyte-specific genes increased in expression in WAT by exercise and by muscle-specific PGC-1α expression (Cao et al., 2011). UCP-1 uncouples the mitochondrial electron transport chain from ATP synthesis, an activity that is key to the thermogenic role of brown adipose tissue (BAT) (Enerbäck et al., 1997). Likewise, CIDEA is a mitochondrial brown adipocyte-specific gene with a role in the regulation of the thermogenic process.

Gene expression arrays and a bioinformatics approach recently highlighted irisin as a novel secreted protein by which PGC-1α-dependent signals from muscle drive functional changes in other tissues (Boström et al., 2012). There is strong motivation to investigate whether additional mechanisms triggered by PGC-1α expression in muscle might confer hormone-like signals to modulate fat metabolism or contribute to the benefits of exercise, especially with regard to small molecules. Here we applied a liquid chromatography-mass spectrometry (LC-MS) metabolic profiling technique to identify small molecules secreted from myocytes with forced expression of PGC-1α. We then tested the effects of candidate small molecules on WAT in vitro and in vivo and examined metabolites in the context of cardiometabolic risk factors and exercise in humans.

RESULTS

β-Aminoisobutyric Acid Is Regulated by PGC-1α and Increases Expression of Brown Adipocyte-Specific Genes

Serum-free media taken from muscle cells with forced expression of PGC1-α increases mRNA levels of several brown adipocyte-specific genes when transferred to primary adipocytes (Boström et al., 2012). To identify candidate small molecules that might be contributing to this phenomenon, we applied LC-MS metabolic profiling to this media and compared the findings to media from GFP-expressing control cells. As expected, glucose levels were significantly decreased in the supernatants of the PGC-1α-overexpressing cells (−15.3%, p = 0.025) (Michael et al., 2001). Four metabolites, β-aminoisobutyric acid (BAIBA), γ-aminobutyric acid (GABA), cytosine, and 2′-deoxycytidine, were significantly enriched in the media of the PGC-1α-overexpressing myocytes (BAIBA, 2.7-fold increase, p = 0.01; GABA, 1.9-fold increase, p = 0.004; cytosine, 3.9-fold increase, p = 0.02; 2′-deoxycytidine, 3.4-fold increase, p = 0.02) (Figure 1A).

We assessed the ability of these candidate molecules to increase the expression of brown adipocyte-specific genes using the primary stromal vascular fraction isolated from subcutaneous (inguinal) WAT of mice during 6 days of the differentiation process to mature adipocytes. BAIBA treatment enhanced UCP-1 and CIDEA mRNA by 5.3-fold and 2.25-fold, respectively, as assessed by quantitative PCR (Figure 1B). GABA, cytosine, and 2′-deoxycytidine treatment did not induce concordant upregulation of brown adipocyte-specific genes, so we focused subsequent analyses on BAIBA. BAIBA concentrations in the low micromolar range significantly increased UCP-1 in the primary adipocytes in a dose-dependent manner (Figure 1C). By contrast, BAIBA did not significantly alter the expression of the canonical white adipocyte gene adiponectin (ADIPOQ), which is also expressed to a similar extent in the beige cell population (Wu et al., 2012). To strengthen the link between BAIBA secretion and PGC1-α expression, we analyzed the concentration of BAIBA in the media of muscle cells in response to increased expression of PGC1-α using an adenoviral vector. Increased levels of PGC-1α lead to an increase in the concentration of BAIBA in the media (Figure S1 available online).

Exposure of Human-Induced Pluripotent Stem Cells to BAIBA during Differentiation to Mature White Adipocytes Induces a Brown Adipocyte-like Phenotype

Since BAIBA induced expression of brown adipocyte-specific genes in primary adipocytes differentiated from the stromal vascular fraction, we investigated whether BAIBA would induce a browning response in human pluripotent stem cells during their differentiation to mature white adipocytes (Figure S2). BJ fibroblasts reprogrammed with modified RNA (BJ RiPS) human induced pluripotent stem cells (IPSCs) were differentiated into mesenchymal progenitor cells as previously reported (Ahfeldt et al., 2012). Lentiviral-mediated expression of PPARG2 or both PPARG2 and CCAAT/enhancer-binding protein β (CEBPB) in these human pluripotent stem cell-derived mesenchymal progenitor cells was used to program their differentiation into either white or brown mature adipocytes, respectively (Enerbäck et al., 1997; Kajimura et al., 2009; Wright et al., 2000). Administration of BAIBA to IPSCs differentiated into mature white adipocytes conferred a dose-dependent increase in the expression of brown-adipocyte specific genes, including UCP-1, CIDEA, and PRDM16. Expression of ELOVL3, a critical enzyme for lipid accumulation and metabolic activity in brown adipocytes, was also slightly increased (Figure 2A). BAIBA did not significantly alter the expression of the canonical white adipocyte gene adiponectin (ADIPOQ) (Figure S3A). The effect of BAIBA on the expression of brown adipocyte-specific genes was reproduced in white adipocytes derived from other human pluripotent cell lines (Figure S3B). By contrast, mesenchymal progenitor cells differentiated into mature brown adipocytes in the presence of BAIBA did not exhibit an increase in the classical browning response genes, suggesting BAIBA does not initiate the thermogenic response in BAT in vitro (Figure S3C). One prior publication found that BAIBA does not affect UCP-1expression in intrascapular BAT in vivo (Begriche et al., 2008), which might relate to known differences between the development of beige cells and

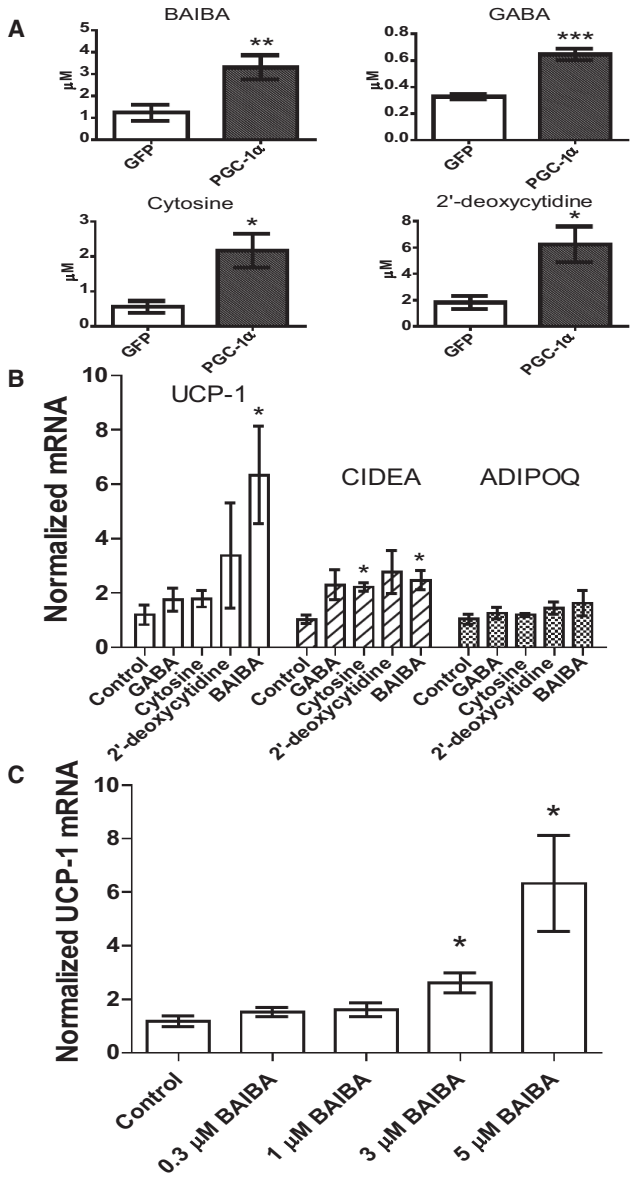

Figure 1. Metabolites Accumulate in the Media of Myocytes as a Result of Forced PGC-1α Expression and Stimulate Expression of Brown Adipocyte-Specific Genes in Adipocytes

(A) Media from myocytes transduced with an adenoviral vector expressing either PGC-1α (n = 6) or GFP (n = 6) was analyzed using an LC-MS-based metabolite profiling method.

(B) BAIBA (5 μM) induces expression of brown adipocyte-specific genes in primary adipocytes. Additional metabolites tested at physiologically relevant doses included GABA (3 μM), cytosine (1 μM), and 2-deoxycytidine (15 μM). BAIBA significantly increased the expression of the brown adipocyte-specific genes UCP-1 and CIDEA. The expression of adiponectin (ADIPOQ) was unchanged. Cumulative data from a total of five independent observations are shown.

(C) BAIBA concentrations in the low micromolar range significantly and dose-dependently increased the expression of the brown adipocyte-specific gene UCP-1.

*p ≤ 0.05, **p ≤ 0.01, ***p ≤ 0.001. Data are represented as mean ± SEM. See also Figure S1.

activation of classical brown fat (Frontini and Cinti, 2010; Wu et al., 2012).

To establish whether the observed transcriptional changes conferred functional effects, we assessed the uptake of [3H]-2-deoxy-D-glucose in the PPARG2-programmed cells. We observed a striking increase in the basal and insulin-stimulated glucose uptake in the presence of BAIBA (Figure 2B). Furthermore, the basal oxygen consumption rate (OCR) was found to be higher in the programmed white adipocytes treated with BAIBA, as assessed by an extracellular flux analyzer. Oligomycin was then used to inhibit the ATP synthase. The OCR of white adipocytes treated with BAIBA remained higher than the untreated white adipocytes, consistent with increased uncoupling. The addition of the electron transport chain decoupler carbonyl cyanide m-chlorophenylhydrazone (CCCP) allowed the measurement of the maximal respiratory capacity. Programmed white adipocytes treated with BAIBA showed significantly higher respiratory capacity compared to the untreated programmed white adipocytes (Figures 2C and 2D). In addition, bright-field images and BODIPY fluorescent staining demonstrate that PPARG2-programmed cells contain the single large, well-defined lipid droplet characteristic of mature white adipocytes; this morphology was maintained when the cells were treated with BAIBA (Figure 2E). Fluorescent immunostaining revealed a higher degree of UCP-1 staining in the PPARG2 programmed white adipocytes treated with BAIBA when compared to untreated cells. Together, these data indicate that BAIBA activates a browning gene program and increases the mitochondrial activity of human IPSCs differentiated into white adipocytes.

BAIBA Induces Increased Expression of Brown/Beige Adipocyte-Specific Genes In Vivo

To examine whether BAIBA could dose-dependently induce the expression of brown adipocyte-specific genes in WAT in vivo, mice were treated with 100 mg/kg/day or 170 mg/kg/day of BAIBA in drinking water for 14 days based on preliminary dose escalation studies. BAIBA treatment led to a 2.7-fold (100 mg/kg/day) and 12.2-fold (170 mg/kg/day) increased plasma concentration of the metabolite by 14 days (100 mg/kg/day BAIBA; 2 ± 0.03 μM, p = 0.009, 170 mg/kg/day BAIBA; 8.9 ± 0.5 μM, p < 0.0001) (Figure 3A). Expression analysis of inguinal WAT using qPCR revealed significant increases in brown adipocyte-specific genes UCP-1 (100 mg/kg/day BAIBA; 8.8-fold increase, p = 0.03, 170 mg/kg/day BAIBA; 12.1-fold increase, p = 0.02) and CIDEA (100 mg/kg/day BAIBA; 3.4-fold increase, p = 0.03, 170 mg/kg/day BAIBA; 5.24-fold increase, p = 0.005), recapitulating the in vitro findings (Figure 3B). Expression of PGC-1α and cytochrome *c* were also increased following BAIBA treatment (PGC-1α, 100 mg/kg/day BAIBA; 1.3-fold increase, p = 0.09, 170 mg/kg/day BAIBA; 2.6-fold increase, p = 0.02; cytochrome *c*, 100 mg/kg/day BAIBA; 1.64-fold increase, p = 0.03, 170 mg/kg/day BAIBA; 5.8-fold increase, p = 0.04).

BAIBA Levels Are Increased in the Plasma of Muscle PGC-1α-Expressing and Exercising Mice

Since BAIBA was elevated in the media of cultured myocytes by forced expression of PGC-1α, we tested whether plasma concentrations of this metabolite were increased in mice with muscle-specific transgenic expression of PGC-1α (MCK-PGC1α) and

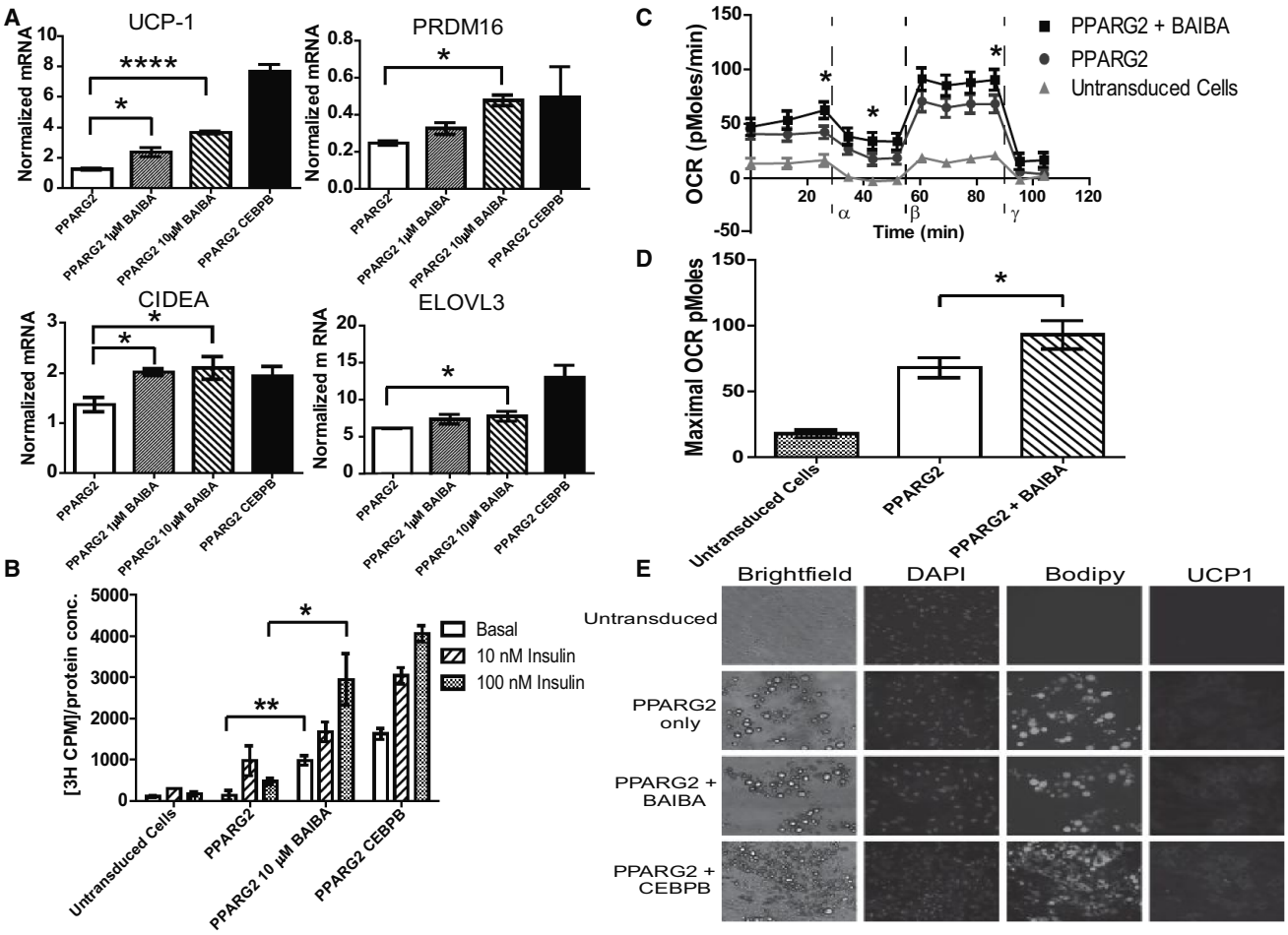

Figure 2. BAIBA Treatment of BJ RiPS Human iPSCs Induces Brown Adipocyte-Specific Gene Expression and Function

(A) BAIBA significantly and dose-dependently increased the expression of brown-adipocyte-specific genes in human IPSC-derived mature adipocytes.

(B) BAIBA increased both basal and insulin-stimulated glucose uptake in human IPSC-derived adipocytes, assessed by [3H]-2-deoxy-D-glucose transport (data from three independent observations).

(C) The oxygen consumption rate (OCR) of human IPSC-derived white adipocytes with and without BAIBA treatment; untransduced cells differentiated with adipogenic media (green line), PPARG2-programmed cells (blue line), and PPARG2-programmed cells treated with BAIBA (black line). The OCR was measured over time with the addition of oligomycin (α), carbonyl cyanide *m*-chlorophenyl hydrazone (CCCP) (β), and antimycin (γ).

(D) BAIBA significantly increased the maximal OCR of PPARG2-transduced adipocytes (data are from n = 10 independent observations).

(E) Images of untransduced cells, PPARG2-programmed white adipocytes, PPARG2-programmed white adipocytes treated with BAIBA, and PPARG2-CEBPB-programmed brown adipocytes. Shown from left to right: bright-field images illustrating the morphology of the cells; 4′,6-diamidino-2-phenylindole (DAPI) fluorescent nuclear staining (blue), fluorescent staining with the neutral lipid dye BODIPY (green), and fluorescent images of immunostaining with antibodies against the marker protein UCP-1 (red) (100× magnification). *$p \leq 0.05$, **$p \leq 0.01$, ***$p \leq 0.001$, ****$p < 0.0001$. Data are represented as mean ± SEM. See also Figures S2 and S3.

with chronic exercise in wild-type animals. The MCK-PGC1α transgenic mouse has 10-fold increased expression of PGC-1α in gastrocnemius (Viscomi et al., 2011; Wu et al., 2011). Plasma concentrations of BAIBA were significantly increased 11-fold to 6.5 ± 2.5 μM, $p = 0.03$, as a result of PGC-1α muscle forced expression in vivo (Figure 3C). By contrast, the absence of PGC-1α decreases the plasma concentration of BAIBA as compared to wild-type controls (0.77-fold decrease, $p = 0.046$) (Figure 3D).

In exercise-trained wild-type mice subjected to 3 weeks of free wheel running, UCP-1 expression in the subcutaneous inguinal WAT was significantly increased by 25-fold compared to sedentary controls (Boström et al., 2012). LC-MS analysis of metabolites extracted from the gastrocnemius and quadriceps of exercise trained mice demonstrated a 5.2- ± 0.09-fold, $p < 0.0001$ and 2.2- ± 0.5-fold, $p < 0.0001$, increase in BAIBA concentrations, respectively. Analysis of plasma from the exercise trained mice confirmed a highly significant increase in the plasma concentration of BAIBA (19% increase to 2.6 ± 0.05 μM, $p = 0.001$) as compared to sedentary controls (Figure 3E).

BAIBA Decreases Weight Gain and Improves Glucose Tolerance in Mice

Since browning of WAT improves glucose homeostasis and reduces weight gain (Boström et al., 2012), we examined the functional effect of BAIBA on weight gain and glucose tolerance in vivo. Six-week-old mice were either treated with BAIBA

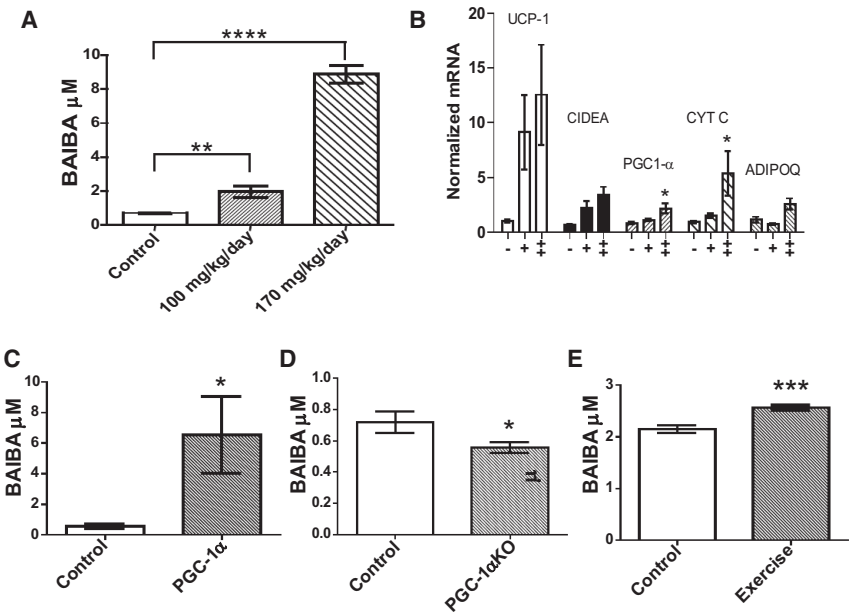

Figure 3. BAIBA Induces Expression of Brown Adipocyte-Specific Genes in WAT In Vivo, and Muscle-Specific PGC-1α Expression and Exercise Significantly Increase Plasma BAIBA Levels

(A) The plasma concentration of BAIBA in mice given 100 mg/kg/day (n = 5) or 170 mg/kg/day (n = 5) of the metabolite in their drinking water significantly increased over 14 days as compared to age-matched control mice (n = 5).

(B) Expression of brown adipocyte-specific genes in inguinal WAT from control mice (–) (n = 5), mice treated with 100 mg/kg/day BAIBA for 14 days (+) (n = 5), or mice treated with 170 mg/kg/day BAIBA for 14 days (++) (n = 5).

(C) Plasma BAIBA from muscle-specific PGC-1α transgenic mice (n = 5) was analyzed using LC-MS and compared to age-matched control mice (n = 5).

(D) Plasma BAIBA from PGC-1α knockout mice (n = 9) was analyzed using LC-MS and compared to age-matched control mice (n = 8).

(E) Mice were subjected to a 3 week free wheel running exercise regimen (n = 6) or housed as sedentary controls (n = 6), and plasma BAIBA levels were assessed by LC-MS. *$p \leq 0.05$, **$p \leq 0.01$, ***$p \leq 0.001$, ****$p < 0.0001$. Data are represented as mean ± SEM.

(100 mg/kg/day) or remained untreated (control mice). Their weights were monitored weekly. Weight was slightly decreased in the mice by the end of BAIBA treatment (ANOVA, p = 0.01) (Figure 4A). Analysis of body composition using MRI demonstrated BAIBA treatment significantly decreased body fat in the mice (body fat, control = 13.1% ± 1.25%; BAIBA = 9% ± 0.92%, p = 0.02) (Figure 4B). Consistent with the effects on thermogenic and β-oxidation gene expression and body weights, analysis with metabolic cages indicated that oxygen consumption (VO2) and whole-body energy expenditure were increased in the BAIBA-treated mice (VO2, two-way ANOVA, $p \leq 0.0001$, energy expenditure, two-way ANOVA, $p \leq 0.0001$) (Figures 4C and 4D) without any significant difference in activity (control = 8,758 ± 417.5 beam breaks per day, BAIBA = 9,504 ± 1,043 beam breaks per day, p = 0.52) (Figure 4E) or food intake (control = 3.79 ± 0.4 g per day, BAIBA = 4.1 ± 0.2 g per day, p = 0.5) (Figure 4F). The mice were also challenged with an intraperitoneal glucose tolerance test (IPGTT) (Figure 4G). BAIBA was found to significantly improve the glucose tolerance in the mice as determined by the area under the curve of the IPGTT (−15.9%, $p \leq 0.05$) (Figure 4H).

PPARα Mediates BAIBA-Induced Effects on Adipose Tissue In Vitro and In Vivo

We next examined how BAIBA may be driving the increase in thermogenic gene expression. In a focused interrogation of potential downstream mediators, we observed that BAIBA significantly increases the expression of PPARα in white adipocytes both in vitro (2.4-fold increase, Figure 5A) and in the inguinal white fat depot in vivo (2.2-fold increase, Figure 5B). PPARα is a key transcription factor known to stimulate the expression of UCP-1 (Boström et al., 2012; Komatsu et al., 2010). We were interested to find that the selective PPARα antagonist GW6471 significantly abrogated the BAIBA-stimulated increase in thermogenic gene expression in primary adipocytes (Figure 5C). The functional interaction between the BAIBA and GW6471 treatments on thermogenic gene expression was confirmed using two-way ANOVA ($p < 0.005$). To further define the contribution of PPARα to the browning response of primary white adipocytes in vitro, we isolated the stromal vascular fraction from the subcutaneous WAT of PPARα null mice and differentiated the cells into mature adipocytes in the presence or absence of BAIBA. Analysis of the thermogenic gene expression in these cells using qPCR demonstrated a loss of the BAIBA-induced browning effect in the setting of PPARα deficiency (Figure 5D), consistent with the findings seen with the biochemical inhibitor.

The role of PPARα in the BAIBA-induced increase in thermogenic gene expression in WAT in vivo was also examined using PPARα null mice. PPARα null mice were treated with 100 mg/kg/day BAIBA in drinking water for 14 days. qPCR analysis of subcutaneous (inguinal) WAT demonstrated that BAIBA failed to increase expression of thermogenic genes, including UCP-1, CIDEA, PGC-1α, and cytochrome *c*, in the PPARα null mice (Figure 5E). Therefore, these results indicate that BAIBA increases expression of the browning gene program through a specific PPARα-dependent mechanism.

BAIBA Increases Hepatic β-Oxidation through PPARα

BAIBA may also function to induce additional tissue-specific salutary effects. Exercise has been shown to increase liver β-oxidation (Oh et al., 2006; Rabøl et al., 2011; Rector et al., 2011). Therefore we investigated whether BAIBA would directly induce β-oxidation gene expression in hepatocytes in vitro. Hepatocytes were incubated with 5 μM BAIBA for 6 days. BAIBA significantly increased the expression of PPARα (5.4-fold, $p < 0.0001$), carnitine palmitoyltransferase 1 (CPT1) (2.2-fold, $p < 0.0001$), the very-long-chain acyl-CoA dehydrogenase (ACADvl) (1.3-fold, p = 0.03), the medium-chain acyl-CoA dehydrogenase

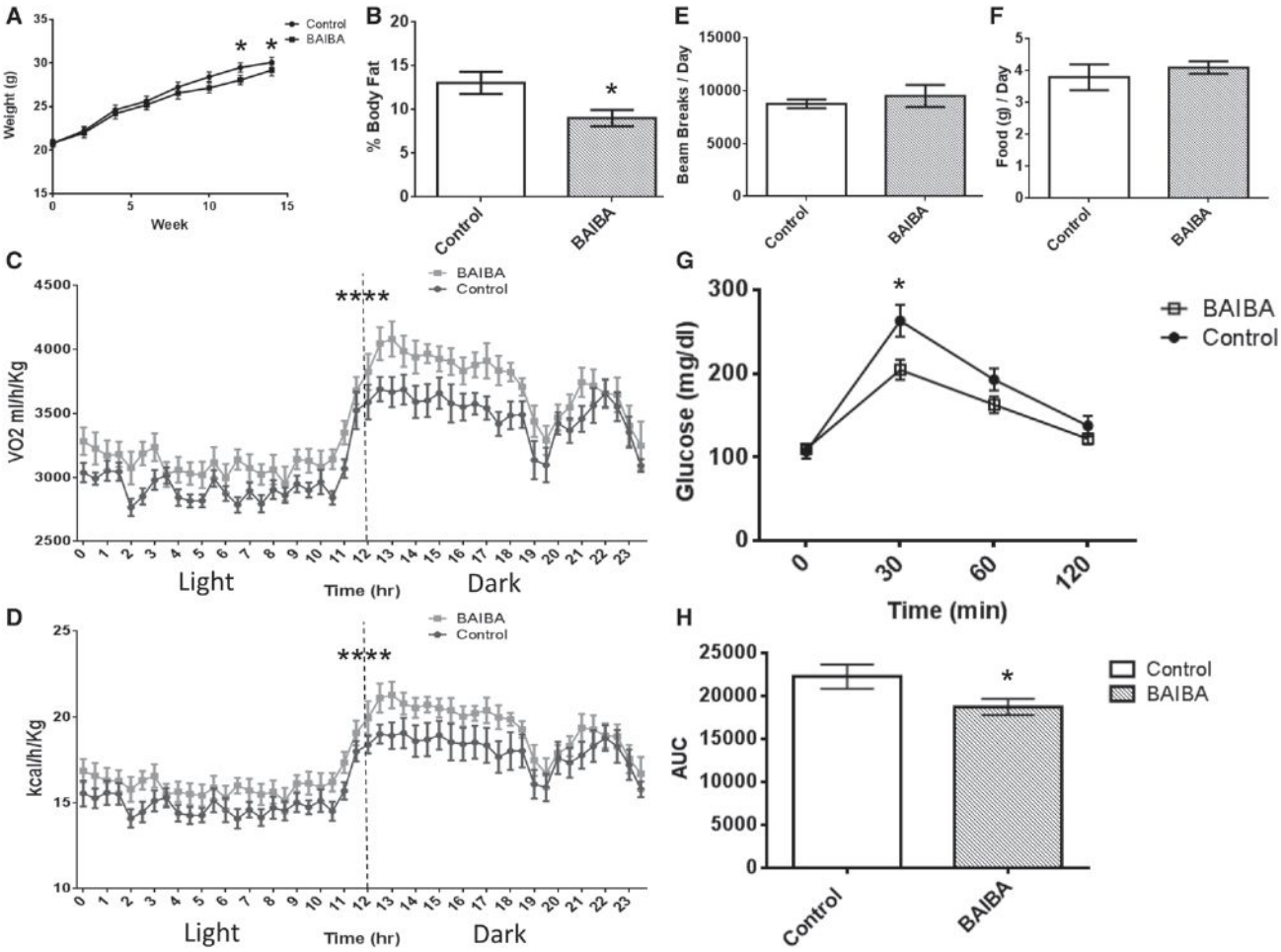

Figure 4. BAIBA Decreases Weight Gain and Improves Glucose Tolerance in Mice

(A) The weights of mice given 100 mg/kg/day BAIBA (n = 8) in their drinking water compared to untreated controls (n = 8).

(B) The percentage body fat of 100 mg/kg/day BAIBA treated mice (n = 8) compared to untreated controls (n = 8).

(C) Diurnal oxygen consumption of control mice (n = 8) and BAIBA (100 mg/kg/day)-treated mice (n = 8).

(D) Diurnal energy expenditure of control mice (n = 8) and BAIBA (100 mg/kg/day)-treated mice (n = 8).

(E) Activity of control mice (n = 8) and mice treated with BAIBA 100 mg/kg/day.

(F) Food consumption of control mice and mice treated with BAIBA 100 mg/kg/day.

(G) Mice treated with BAIBA 100 mg/kg/day for 14 weeks showed significantly improved glucose tolerance as determined by an IPGTT.

(H) The area under the curve of an IPGTT comparing BAIBA-treated mice to untreated controls (control, n = 8; BAIBA, n = 8). *$p < 0.05$. Data are represented as mean ± SEM.

(ACADm) (1.2-fold, $p = 0.005$), and acyl-CoA oxidase 1 (ACOX1) (1.2-fold $p = 0.004$) (Figure 6A). The interaction between BAIBA and β-oxidation gene expression was also determined to be significant by two-way ANOVA ($p < 0.0001$).

As BAIBA increased the expression of β-oxidation genes in vitro, we investigated whether BAIBA would induce hepatic β-oxidation gene expression in vivo. The expression of key genes involved in fatty acid β-oxidation was measured in the liver of mice treated with 100 mg/kg/day BAIBA for 14 days using qPCR. As in vitro, BAIBA significantly increased the expression of PPARα (1.73-fold $p = 0.03$), CPT1 (2.5-fold $p = 0.0005$), ACADvl (1.3-fold $p = 0.04$), ACADm (1.2-fold $p < 0.05$), and ACOX1 (1.4-fold, $p = 0.03$) (Figure 6B). The functional interaction between BAIBA and β-oxidation gene expression was confirmed using two-way ANOVA ($p < 0.0001$).

To establish whether the observed transcriptional changes conferred functional effects, we measured the respiratory rate of hepatocytes treated with BAIBA for 6 days at a range of concentrations. The addition of the electron transport chain uncoupler carbonyl cyanide-4-(trifluoromethoxy)phenylhydrazone (FCCP) allowed the measurement of the maximal respiratory capacity. BAIBA treatment significantly and dose dependently increased the maximal oxygen consumption rate (OCR) of the hepatocytes (ANOVA, $p = 0.03$) (Figure 6C). Together these data demonstrate that BAIBA induces a transcriptional change in hepatocytes leading to a more oxidative phenotype.

We then examined whether BAIBA is driving the increase in hepatic fatty acid β-oxidation through a conserved PPARα mechanism, as was observed with brown-adipocyte gene

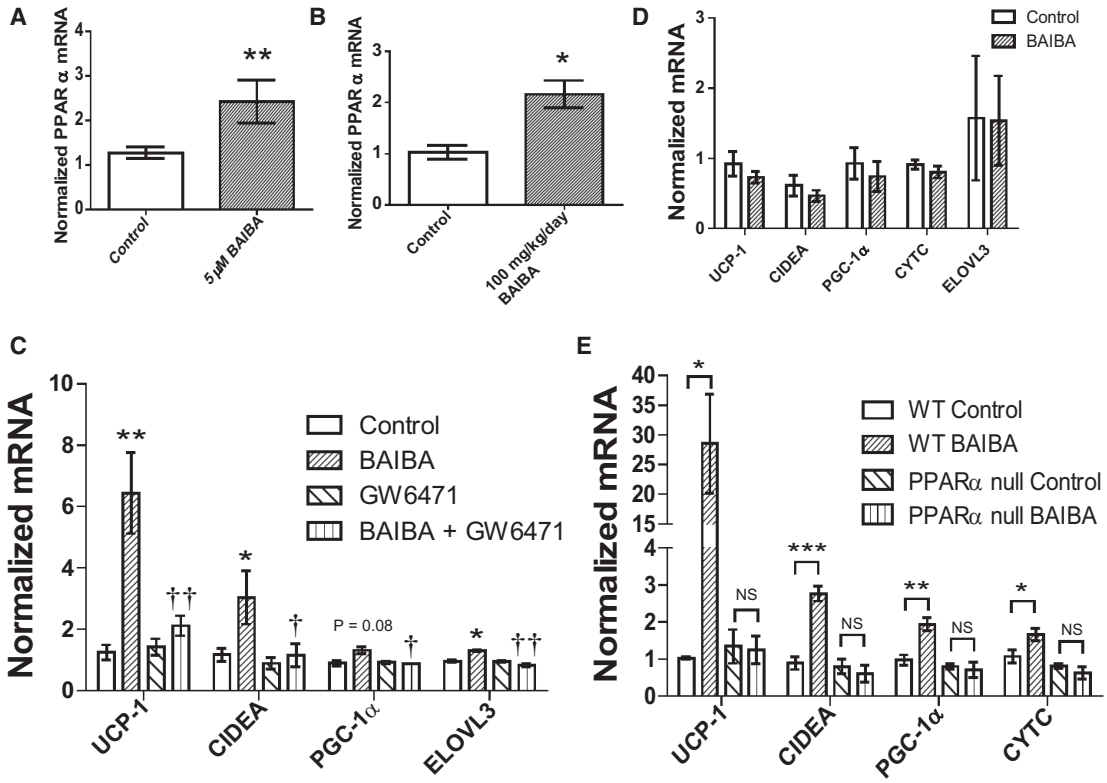

Figure 5. PPARα Functions Downstream of BAIBA

(A) BAIBA (5 μM) induces expression of PPARα in primary adipocytes over 6 days (six independent observations).

(B) Expression of PPARα in inguinal WAT from control mice (n = 5) and mice treated with 100 mg/kg/day BAIBA for 14 days (n = 5).

(C) Primary adipocytes treated with BAIBA (5 μM) and/or GW6471 for 6 days. $^{\dagger}p < 0.05$, $^{\dagger\dagger}p < 0.01$ compared to BAIBA treatment.

(D) BAIBA (5 μM) failed to induce expression of brown adipocyte-specific genes in primary adipocytes isolated from the inguinal WAT of PPARα null mice (six independent observations).

(E) Expression of brown adipocyte-specific genes in inguinal WAT from wild-type (WT) control mice (n = 5), WT mice treated with 100 mg/kg/day BAIBA for 14 days (n = 5), PPARα null control mice (n = 5), and PPARα null mice treated with 100 mg/kg/day BAIBA for 14 days (n = 5). $^{*}p < 0.05$, $^{**}p \leq 0.01$ compared to control. Data are represented as mean ± SEM. See also Figure S4.

expression in white adipocytes. We show that BAIBA significantly increases the expression of PPARα both in vitro and in vivo. PPARα is known to regulate hepatic free fatty acid transport, uptake, and catabolism via β-oxidation (Berger and Moller, 2002; Gulick et al., 1994). The BAIBA-induced increase in expression of the fatty acid β-oxidation genes, CPT1, ACADvl, ACADm, and ACOX1 was abolished by the selective PPARα antagonist, GW6471 (Figure 6D). The functional interaction between the BAIBA and GW6471 treatments on β-oxidation gene expression was confirmed using two-way ANOVA ($p < 0.0001$).

The role of PPARα in the BAIBA-induced increase in hepatic fatty acid β-oxidation gene expression in in vivo was also examined using PPARα null mice. PPARα null mice were treated with 100 mg/kg/day BAIBA in drinking water for 14 days. Expression analysis of liver using qPCR demonstrated that BAIBA failed to increase expression of β-oxidation genes, including CPT1, ACADvl, ACADm, and ACOX1, in the PPARα null mice (Figure 6E). Together, these results indicate that BAIBA increases hepatic fatty acid oxidation gene expression through a PPARα-dependent mechanism.

BAIBA Plasma Concentrations Are Inversely Correlated with Cardiometabolic Risk Factors in Humans and Are Increased during Exercise Training

We examined the association of plasma BAIBA levels with metabolic traits in a large human cohort study. In 2,067 random subjects enrolled in the longitudinal, community-based Framingham Heart Study (FHS), BAIBA levels were inversely correlated with fasting glucose ($p = 0.0003$), insulin ($p < 0.0001$), the Homeostatic Model Assessment-Insulin Resistance (HOMA-IR) ($p < 0.0001$), triglycerides ($p < 0.0001$), and total cholesterol ($p < 0.0001$) in age- and sex-adjusted analyses. In addition, there was a trend toward an inverse association with BMI ($p = 0.08$).

We also assessed BAIBA concentrations in humans before and after an exercise training intervention. As part of the HERITAGE Family Study, sedentary subjects were recruited for a 20 week program of supervised exercise training as described in the Experimental Procedures. Metabolomic profiling was performed on plasma from 80 subjects before and after the exercise training intervention. Following the 20 week exercise program, the average VO_2 max of the subjects had increased by more than 20%. The plasma BAIBA concentration increased by 17%

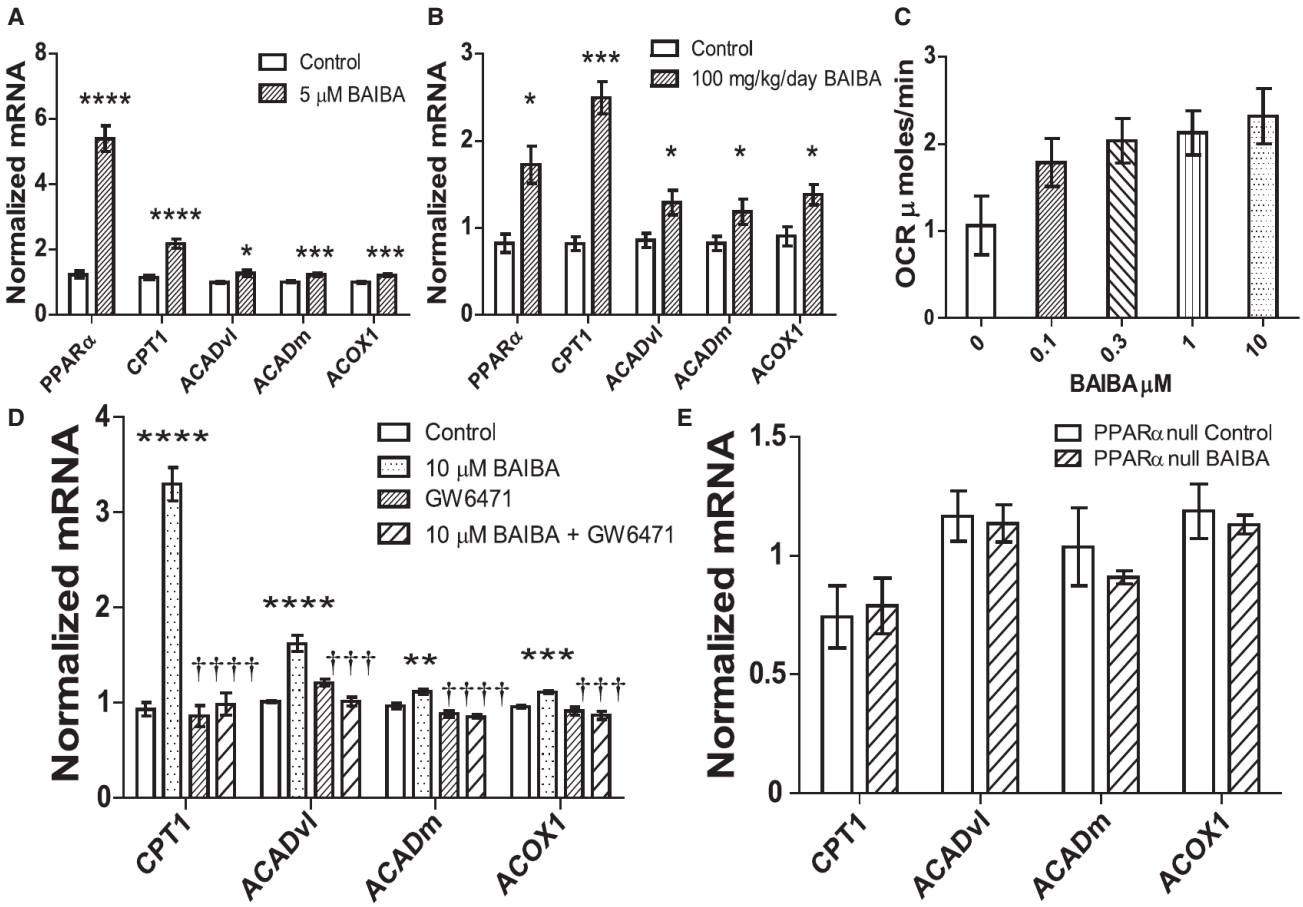

Figure 6. BAIBA Increases Hepatic β-Oxidation through PPARα

(A) BAIBA (5 μM) induces expression of fatty acid β-oxidation genes in hepatocytes treated for 6 days (control = 6; BAIBA, 5 μM = 6).

(B) BAIBA dose-dependently induces expression of hepatic fatty acid β-oxidation genes in vivo. Expression of fatty acid β-oxidation genes in the liver of control mice (n = 5) and mice treated with 100 mg/kg/day BAIBA for 14 days (n = 5).

(C) BAIBA dose-dependently increases the maximal oxygen consumption rate of hepatocytes.

(D) qPCR of key β-oxidation genes in hepatocytes treated with BAIBA and/or PPARα antagonist GW6471 for 6 days (data from five independent observations). $^{\dagger\dagger\dagger}p \leq 0.001$, $^{\dagger\dagger\dagger\dagger}p < 0.0001$ compared to BAIBA treatment.

(E) Expression of β-oxidation genes in liver from PPARα null control mice (n = 5) and PPARα null mice treated with 100 mg/kg/day BAIBA for 14 days (n = 5). $^{*}p < 0.05$, $^{**}p \leq 0.01$, $^{***}p \leq 0.001$, $^{****}p < 0.0001$ compared to control. All data are represented as mean ± SEM.

(±5% SEM, p = 0.03), a very consistent percentage increase compared with the murine exercise data.

Integration of Human Genetic and Transcriptional Data Highlights a Role for PGC-1α in BAIBA Generation

The availability of BAIBA levels and genome-wide genotyping in 1,000 FHS participants allowed us to identify genes responsible for modulating metabolite levels in humans in an unbiased manner. These analyses highlighted putative enzymes involved in BAIBA generation (Table 1). AGXT2 encodes the enzyme alanine-glyoxylate aminotransferase 2, which catalyzes the transamination between BAIBA and pyruvate. Strong association was noted (p = 1.38E-45) between the top SNP at the locus, rs37370, and BAIBA concentrations in FHS. AGXT2 has previously been associated with the urine concentration of BAIBA in humans (Suhre et al., 2011). Other significant associations involved ACADS (rs476676, p = 2.63E-05) and ACADSB (rs11248396, p = 0.0008), which encode enzymes catalyzing the reaction forming methacryl-CoA from isobutryl-CoA upstream of BAIBA. The analyses also highlighted HADHA (rs10165599, p = 0.0008), which encodes the enzyme hydroxyacyl-CoA dehydrogenase responsible for the catalysis of the reaction forming β-hydroxyisobutyryl-CoA from methacryl-CoA in the biogenesis of BAIBA. In addition to variants in the biosynthetic pathway, SNPs were also identified in genes for two solute carriers, SLC6A13 (rs2289957, p = 2.1E-10) and SLC6A6 (rs11128708, p = 3.17E-05), which encode the GABA transporter GAT2 and the taurine transporter TauT, respectively, which may also function as BAIBA transporters (Bröer, 2008; Liu et al., 1999).

To then examine potential mechanisms by which PGC-1α expression might increase levels of BAIBA, we performed transcriptional analysis on PGC-1α-overexpressing myocytes. There was striking overlap between BAIBA pathway participants

Table 1. Integration of Human Genetic and Transcriptional Data Highlights a Role for PGC-1α in BAIBA Generation

	Myocyte PGC-1α Expression		FHS GWAS
Gene	Fold Change	p Value	p Value
AGXT2	1.4	<0.01	1.38×10^{-45}
ACADS	2	<0.05	2.63×10^{-5}
HADHA	2.9	<0.05	8.00×10^{-4}
SLC6A6	2.5	<0.05	3.17×10^{-5}
HIBADH	2.5	<0.05	–
HADH	2.5	<0.05	–
HADH2	1.9	<0.05	–
SLC6A13	–	–	2.10×10^{-10}
ACADSB	–	–	8.00×10^{-4}

Shown are the transcriptional changes in genes associated with the BAIBA biosynthesis pathway in primary myocytes expressing PGC-1α as assessed by expression arrays (left panel). Right panel includes genes in the BAIBA biosynthesis pathway and the significance of their relationship to BAIBA plasma concentrations in the Framingham Heart Study. See also Figure S5.

highlighted by GWAS and those increased by forced PGC-1α expression. AGXT2 was found to be increased by PGC-1α overexpression in myocytes (fold change = 1.4, $p < 0.01$), as was the expression of ACADS (fold change = 2.0, $p < 0.05$) and HADHA (fold change = 2.9, $p < 0.05$). The expression of the TauT transporter, SLC6A6, was also increased by PGC-1α expression (fold change = 2.5, $p < 0.05$).

In addition, forced PGC-1α expression in muscle in turn increased expression of DLD, HIBADH, HADH, and HADH2, genes encoding the enzymes dihydrolipoamide dehydrogense, 3-hydroxyisobutyrate dehydrogenase, L-3-hydroxyacyl-coenzyme A dehydrogenase, and hydroxyacyl-coenzyme A dehydrogenase, type II, respectively (DLD fold change = 2.78, $p < 0.05$; HIBADH fold change = 2.5, $p < 0.05$; HADH fold change = 2.5, $p < 0.05$; HADH2 fold change = 1.9, $p < 0.05$). These enzymes catalyze the formation of isobutryl-CoA from valine as part of the branched-chain alpha-keto acid dehydrogenase complex, and methylmalonate semialdehyde from β-hydroxyisobutyric acid in the pathway producing BAIBA. Thus, PGC-1α increases the expression of genes encoding the metabolic enzymes required for production and transport of BAIBA in myocytes, a number of which are genetic determinants of BAIBA plasma concentrations in humans (Figure S5).

DISCUSSION

Transgenic mice expressing PGC-1α in their skeletal muscle display an improved capability for exercise (Calvo et al., 2008). Muscle-specific PGC-1α expression in mice also increases the expression of brown adipocyte-specific genes and changes the characteristics of WAT to a more brown-like phenotype (Boström et al., 2012). These cells have been termed beige cells (Ishibashi and Seale, 2010; Petrovic et al., 2010). A similar effect has been identified in the WAT of mice undergoing exercise programs (Boström et al., 2012; Sutherland et al., 2009; Xu et al., 2011). The identification of the PGC-1α-dependent polypeptide hormone irisin, which is secreted into circulation from muscle and triggers the browning response of WAT, establishes one mechanism by which signals from muscle during exercise can mediate energy metabolism in other tissues (Boström et al., 2012). However, this recent discovery does not exclude a potential role for other mediators, especially small molecules.

BAIBA was identified in a screen of small molecules generated by myocytes expressing PGC-1α in vitro and was subsequently found to be increased in the plasma of both chronically exercised and muscle-specific PGC-1α transgenic mice. Intramuscular levels of BAIBA were also strikingly increased by exercise, though elevation of BAIBA in other tissues is also possible. BAIBA increases the expression of brown adipocyte-specific genes both in vitro and in vivo through a PPARα-mediated mechanism. BAIBA also functions to increase hepatic fatty acid β-oxidation through PPARα. Treating mice with BAIBA improves glucose tolerance. We were interested to find that BAIBA treatment during differentiation of white adipocytes from BJ RiPS IPSCs also induces a brown adipocyte-like phenotype with concordant functional effects on basal and insulin-stimulated glucose uptake and oxygen consumption. In humans, BAIBA plasma concentrations are increased by regular exercise and are significantly inversely correlated with multiple cardiometabolic risk factors. Finally, by integrating human genetic data and in vitro transcriptional findings, we highlight a cassette of BAIBA biosynthetic enzymes that are under PGC-1α transcriptional control in muscle. We note that while the browning effect appears to be operative in our studies, our findings do not exclude the possibility that macroscopic brown adipose depots in mice increase energy expenditure and contribute to the observed effects.

BAIBA is a nonprotein β-amino acid that can be generated by catabolism of the branched-chain amino acid valine. Our expression studies would seem to highlight a role for PGC-1α expression in muscle with the production of BAIBA from valine. Fasting plasma concentrations of valine are correlated with obesity and serum insulin (Felig et al., 1969; Newgard et al., 2009), and we recently identified valine plasma concentration as a predictor of future development of diabetes (Wang et al., 2011). Skeletal muscle is a major site of branched-chain amino acid utilization, and during exercise catabolism of the branched-chain amino acids is elevated (Harper et al., 1984; Shimomura et al., 2006). Furthermore, the expression of genes in the valine degradation pathway was found to be increased in the skeletal muscle of physically active members of twin pairs compared to their inactive cotwins (Leskinen et al., 2010). Several enzymes of the valine degradation pathway are shared with that of β-oxidation of fatty acids (ACADSB, ACADS, ACADM, HADHA, and HADH), a number of which we found to be transcriptionally controlled by PGC-1α in myocytes. It would seem evolutionarily advantageous to integrate the production of a metabolite myokine signal with the β-oxidation pathway, the primary source of energy for muscle during endurance exercise. Thus, our findings suggest a possible connection between valine utilization in skeletal muscle during exercise and beneficial effects on peripheral WAT.

Independently, BAIBA treatment has been found to reduce weight gain in partially leptin-deficient (*ob*/+) mice (Begriche et al., 2008). Glucose tolerance was improved in the *ob*/+ mice treated with BAIBA, consistent with the diminished weight

gain. Prior work suggests that BAIBA may enhance fatty acid oxidation and reduces de novo lipogenesis in the liver (Begriche et al., 2008; Maisonneuve et al., 2004; Note et al., 2003). Interestingly, the effect of BAIBA on hepatic lipid metabolism mirrors the action of exercise, which has also been shown to increase liver fatty acid oxidation and decrease hepatic lipogenesis through PPARα (Oh et al., 2006; Rabøl et al., 2011; Rector et al., 2011). The effects of BAIBA on browning of white adipose depots were not evaluated in any prior studies. Our studies demonstrate the PPARα-dependent mechanism of BAIBA's salutary effects on liver β-oxidation and extend the prior literature by identifying its link to PGC-1α, browning of WAT, and relationship to chronic exercise. Future work may also uncover beneficial effects of BAIBA on other tissues. Our work also highlights BAIBA as a potential disease marker in human populations.

While we demonstrate that BAIBA increases expression of PPARα, and that BAIBA-induced browning of WAT requires this nuclear receptor, as yet the direct mechanism of action upstream of PPARα is unknown. PPARα null mice remain resistant to cold, can activate cold-induced thermogenesis, and express equivalent levels of UCP-1 in intrascapular brown adipose tissue compared to wild-type controls (Kersten et al., 1999). Moreover, as PPARα null mice do not have reduced UCP-1 expression in WAT compared to controls following cold exposure (Xue et al., 2005), absence of PPARα does not blunt the general browning effect. Therefore, our results indicate that BAIBA increases browning gene expression through a specific PPARα-dependent mechanism. BAIBA may function to activate a cell surface receptor since structurally similar metabolites, including butyrate and isobutyrate, activate short chain carboxylic acid receptors in white adipocytes (Brown et al., 2003). Ascertaining the cell signaling pathways by which BAIBA leads to increased PPARα expression will be a focus of future studies.

In summary, we identify BAIBA as a small molecule myokine representing the first in its class of nonadrenergic activators of the thermogenic program in WAT (Whittle and Vidal-Puig, 2012). The identification of BAIBA as a PGC-1α-mediated and exercise-triggered signal has significant implications not only for our understanding of exercise and its protective role against the development of metabolic diseases, but also for potential therapeutics for type 2 diabetes and the metabolic syndrome.

EXPERIMENTAL PROCEDURES

Myocyte Culture

Primary satellite cells (myoblasts) were isolated and differentiated into myotubes as previously described (Boström et al., 2012; Megeney et al., 1996). At day 2 of differentiation, myocytes were transduced with an adenovirus expressing either PGC-1α or GFP as previously described (St-Pierre et al., 2003). At 24 hr posttransduction, cells were washed with PBS and freestyle media (GIBCO/Invitrogen). Freestyle media was added to GFP and PGC-1α-expressing myocytes, and cells were incubated for 24 hr. Media was collected and cleared with centrifugation (1,000 g, 4°C for 5 min × 3). The supernatant was then snap frozen in aliquots.

Culture and Differentiation of the Mouse Primary Adipocytes Isolated from Inguinal White Adipose Stromal Vascular Fraction

Primary white adipose stromal vascular cells were fractionated as previously described (Soukas et al., 2001). Stromal vascular cells were then cultured and induced to differentiate into adipocytes according to published methods (Boström et al., 2012; Seale et al., 2011). During the 6 day differentiation process, cells were cultured with saline (control); GABA 3 μM; cytosine 1 μM; 2′-deoxycytidine 15 μM; and BAIBA 0.3, 1, 3, and 5 μM.

Maintenance of Pluripotent Cells, Generation of Mesenchymal Progenitor Cells, and Adipocyte Differentiation

Human induced pluripotent stem cells were maintained and differentiated into mature brown and white adipocytes as previously described (Ahfeldt et al., 2012; Schinzel et al., 2011). Differentiation was carried out either in the absence of BAIBA, in the case of controls, and with two concentrations of BAIBA at 1 μM or 10 μM in the differentiation media. Adipogenic differentiation medium was supplemented for 16 days with doxycyline 700 ng/ml, and afterward cells were maintained in culture in the absence of doxycycline until day 21.

Production of Lentivirus and Transduction

Lentivirus production and transduction of cells with Lenti-PPARG2 or Lenti-CEBPB were performed as previously described (Ahfeldt et al., 2012).

Glucose Uptake Assay

Glucose uptake was measured by incubating IPSC-derived adipocytes with 2-deoxy-D-[3H] glucose 0.5 μCi/ml (Perkin-Elmer) as described previously (Ahfeldt et al., 2012).

Measurement of Adipocyte OCR

Cells were plated in gelatin-coated XF24-well cell culture microplates (Seahorse Bioscience) and differentiated into adipocytes. Oxygen consumption and mitochondrial function were measured by XF24 Extracellular Flux Analyzer (Seahorse Biosciences) as described previously (Ahfeldt et al., 2012).

Hepatocyte Culture

H4IIE hepatocytes (ATCC) were seeded at 200,000 cells per well in a 24-well collagen I-coated plate. The cells were incubated in MEM media (ATCC supplemented with 10% FBS (Sigma) and penicillin/streptomycin) with 5 μM BAIBA (n = 6), 1 μM GW6471 PPARα antagonist (n = 6), and 1 μM GW6471 and 5 μM BAIBA (n = 6) for 6 days.

Hepatocyte Respirometry

H4IIE hepatocytes were plated at 40,000 cells per well and grown for 6 days in Oxoplates OP96F (PreSens) with MEM + 10% FBS media (Sigma Aldrich). Serum-free MEM media (100 μl) containing BAIBA in a range of concentrations (0–10 μM) (n = 6 per dose) was added into the wells of an OxoPlate. The media was exchanged every 2 days with the addition of fresh compounds. After 6 days each well was then overlaid with 250 μl of mineral oil after the addition of 5 μM of final concentration of carbonyl cyanide 4-(trifluoromethoxy)phenylhydrazone (FCCP). Wells containing oxygen-free water (cal 0) and air-saturated water (cal 100) served as standards. Oxygen-free water was prepared by dissolving 1 g of sodium sulfite in 100 ml of water. Air-saturated water was prepared by shaking 100 ml of water vigorously for 2 min. The oxygen concentration in each well was measured immediately and at 15 min and 30 min after mineral oil addition. Fluorescence of each well was measured in dual kinetic mode (Multiskan Ascent CF, Thermo Lab- Systems). Filter pair 1 (544/650 nm) detects fluorescence of the indicator dye. The second filter pair (544/590 nm) measures fluorescence of the reference dye. Oxygen tension was calculated according to the Stern-Volmer equation and transformed into nanomoles of oxygen. The difference between baseline, 15 min, and 30 min oxygen tension was used to calculate the oxygen consumption per min per well.

Animal Experimentation

Muscle-specific PGC-1α transgenic mice were generated and maintained as previously described (Boström et al., 2012; Lin et al., 2002). For the exercise experiments, 12-week-old B6 mice were used (Jackson Laboratory, Bar Harbor, ME). Endurance exercise was carried out using free wheel running for 3 weeks (n = 6) (Rasbach et al., 2010). Controls were age matched sedentary littermates (n = 6). For the short-term BAIBA treatment cohort, 6-week-old C57BL6/J mice (Jackson Laboratory, Bar Harbor, ME) were weight matched and assigned to groups for treatment. Mice were treated with either 100 mg/kg/day or 170 mg/kg/day BAIBA in their drinking water for 2 weeks

and fed a standard chow diet ad libitum (Prolab RMH 3000-5P75, Labdiet). 129S4/SvJae-*Ppara*^{tm1Gonz}/J mice (Jackson Laboratory) were weight matched and assigned to groups for treatment. Mice were treated with 100 mg/kg/day BAIBA in their drinking water for 2 weeks and fed a standard chow diet ad libitum. For the long-term BAIBA treatment cohort, 6-week-old C57BL6/J mice (Jackson Laboratory, Bar Harbor, ME) were weight matched and assigned to groups for treatment (n = 11 per group). Mice were treated with 100 mg/kg/day BAIBA in their drinking water for 14 weeks and fed a standard chow diet ad libitum (Prolab RMH 3000-5P75, Labdiet).

Study mice were fasted and sacked, and plasma was collected via left ventricular puncture at completion of the study (week 16). Inguinal WAT and liver were rapidly dissected, snap frozen in liquid nitrogen, and stored at −80°C until mRNA extraction. All mice were housed in a controlled temperature, lighting, and humidity environment.

All animal experiments were approved by the Subcommittee on Research Animal Care at Massachusetts General Hospital.

Indirect Calorimetry

All experiments were performed with 6-week-old mice treated with either BAIBA (100 mg/kg/day) or water for 14 weeks (n = 8 mice per group). A PhenoMaster system (TSE Systems, Calo-(D)/Feed/BW-XZ, 16 mice) was used to monitor oxygen consumption, carbon dioxide production, food intake, daily body mass, and locomotory activity. The PhenoMaster system was calibrated before each experiment. Animals were subjected to a 7-day acclimation period in a training cage without monitoring to habituate to the environment of the metabolic cages. Animals were maintained in normal cedar bedding at 22°C throughout the monitoring period. Twice hourly measurements for each animal were obtained for oxygen and carbon dioxide with ad libitum access to food and water (or water plus BAIBA) on a controlled 12 hr light/dark cycle. Cages contained one mass sensor to monitor food intake and a second sensor attached to a glass housing to measure body mass. Oxygen consumption is expressed normalized to body mass.

Intraperitoneal Glucose Tolerance Test

Mice (n = 11 per group) were fasted for 6 hr with free access to water prior to the IPGTT, conducted as previously described (Wang et al., 2013).

Gene Expression Analysis

Total RNA from human cell lines, mouse inguinal WAT stromal vascular fraction derived primary adipocytes, hepatocytes, and mouse WAT and liver was extracted with Trizol (Invitrogen) and purified via the RNeasy mini kit (QIAGEN) according to the manufacturer's instructions. The RNA yield was determined using the NanoDrop ND-1000 spectrophotometer (NanoDrop Technologies). RNA was normalized and converted to cDNA using the Superscript First-Strand Kit (Invitrogen). Quantitative RT-PCR was performed using a Realplex Mastercycler (Eppendorf) with the Quantifast-SYBR Green PCR mix (QIAGEN). All data were normalized to 18SrRNA or HPRT and quantitative measures obtained using the Δ-Δ-CT method.

Framingham Heart Study

Analyses were performed in 2,067 individuals in the Offspring Cohort who were free of diabetes and cardiovascular disease and had measurement of BAIBA concentrations in fasting plasma samples (Wang et al., 2011). Genotyping was performed on the Affymetrix GeneChip Human Mapping 500K Array SetR and 50K Human Gene Focused PanelR with parameters and data analysis as previously described (Rhee et al., 2013). The human study protocols were approved by the Institutional Review Boards of Boston University Medical Center and Massachusetts General Hospital, and all participants provided written informed consent.

HERITAGE Clinical Exercise Study

The HERITAGE Family Study is a clinical trial that enrolled 557 individuals of various ages (16–65 years) to determine the effects of 20 weeks of highly controlled endurance training on physiologic measures and risk factors for cardiometabolic disease. Only individuals who were previously sedentary, free of pre-existing disease, and not taking any medications that would affect any of the outcome variables were entered into the study (Bouchard et al., 1995). Endurance training was conducted (3 days/week for a total of 60 exercise sessions) on cycle ergometers that were computer controlled to maintain the participants' heart rates at fixed percentages of their aerobic capacity (*V*O2max). The training program started at 55% of *V*O2max for 30 min/session and gradually increased to 75% of *V*O2max for 50 min/session, where it was maintained during the last 6 weeks of training. Peripheral plasma samples were collected from 80 HERITAGE participants before and after the 20 week endurance training program. Of the participants in this study, 50% were male. The mean age was 34 years, and the mean BMI was 26. Baseline V02 max was 2,577 ml 0_2/min, which increased to 3,007 ml 0_2/min after training.

Metabolic Profiling

Metabolic profiling of amino acids, biogenic amines, and other polar plasma metabolites were analyzed by LC-MS as previously described (Roberts et al., 2012; Wang et al., 2011). Metabolite concentrations were determined using the standard addition method.

Statistical Analyses

For metabolite analyses in FHS, log transformation of BAIBA concentrations was applied to approximate a normal distribution. Partial correlation coefficients were estimated between BAIBA and the following metabolic variables, after adjustment for age and sex: body mass index (BMI), fasting glucose, fasting insulin, total cholesterol, triglycerides, homeostasis model assessment of insulin resistance (HOMA-IR), and the homeostasis model assessment of β cell function (HOMA-B), calculated as previously described (Wang et al., 2011).

For FHS GWAS analyses, a linear mixed effects model that accounts for familial relatedness with an additive genetic model with one degree of freedom was used (Chen and Yang, 2010).

For animal studies, all results, unless otherwise stated, are expressed as means, and error bars depict SEM. A two-tailed Student's t test or ANOVA was used to determine p value.

SUPPLEMENTAL INFORMATION

Supplemental Information includes five figures and supplemental text and can be found with this article at http://dx.doi.org/10.1016/j.cmet.2013.12.003.

ACKNOWLEDGMENTS

This work was supported by NIH R01 DK081572, NIH R01 HL098280, the Leducq Foundation, and the American Heart Association (R.E.G.) and by NIH DK 31405 (B.M.S.). The Framingham Heart Study is supported by NIH/NHLBI N01-HC-25195. L.D.R. is supported by a Leducq Foundation Career Development Award. P.B. is supported by the Wenner-Gren Foundation and the Swedish Heart and Lung Foundation. The HERITAGE Family Study is supported by NIH-RO1-HL045670. C.B. is supported by the John W. Barton Sr. Chair in Genetics and Nutrition.

Received: September 10, 2012
Revised: October 9, 2013
Accepted: December 10, 2013
Published: January 7, 2014

REFERENCES

Ahfeldt, T., Schinzel, R.T., Lee, Y.K., Hendrickson, D., Kaplan, A., Lum, D.H., Camahort, R., Xia, F., Shay, J., Rhee, E.P., et al. (2012). Programming human pluripotent stem cells into white and brown adipocytes. Nat. Cell Biol. *14*, 209–219.

Bassel-Duby, R., and Olson, E.N. (2006). Signaling pathways in skeletal muscle remodeling. Annu. Rev. Biochem. *75*, 19–37.

Begriche, K., Massart, J., Abbey-Toby, A., Igoudjil, A., Lettéron, P., and Fromenty, B. (2008). Beta-aminoisobutyric acid prevents diet-induced obesity in mice with partial leptin deficiency. Obesity (Silver Spring) *16*, 2053–2067.

Berger, J., and Moller, D.E. (2002). The mechanisms of action of PPARs. Annu. Rev. Med. *53*, 409–435.

Boström, P., Wu, J., Jedrychowski, M.P., Korde, A., Ye, L., Lo, J.C., Rasbach, K.A., Boström, E.A., Choi, J.H., Long, J.Z., et al. (2012). A PGC1-α-dependent

myokine that drives brown-fat-like development of white fat and thermogenesis. Nature *481*, 463–468.

Bouchard, C., Leon, A.S., Rao, D.C., Skinner, J.S., Wilmore, J.H., and Gagnon, J. (1995). The HERITAGE family study. Aims, design, and measurement protocol. Med. Sci. Sports Exerc. *27*, 721–729.

Bröer, S. (2008). Amino acid transport across mammalian intestinal and renal epithelia. Physiol. Rev. *88*, 249–286.

Brown, A.J., Goldsworthy, S.M., Barnes, A.A., Eilert, M.M., Tcheang, L., Daniels, D., Muir, A.I., Wigglesworth, M.J., Kinghorn, I., Fraser, N.J., et al. (2003). The Orphan G protein-coupled receptors GPR41 and GPR43 are activated by propionate and other short chain carboxylic acids. J. Biol. Chem. *278*, 11312–11319.

Calvo, J.A., Daniels, T.G., Wang, X., Paul, A., Lin, J., Spiegelman, B.M., Stevenson, S.C., and Rangwala, S.M. (2008). Muscle-specific expression of PPARgamma coactivator-1alpha improves exercise performance and increases peak oxygen uptake. J. Appl. Physiol. *104*, 1304–1312.

Cao, L., Choi, E.Y., Liu, X., Martin, A., Wang, C., Xu, X., and During, M.J. (2011). White to brown fat phenotypic switch induced by genetic and environmental activation of a hypothalamic-adipocyte axis. Cell Metab. *14*, 324–338.

Chen, M.H., and Yang, Q. (2010). GWAF: an R package for genome-wide association analyses with family data. Bioinformatics *26*, 580–581.

Enerbäck, S., Jacobsson, A., Simpson, E.M., Guerra, C., Yamashita, H., Harper, M.E., and Kozak, L.P. (1997). Mice lacking mitochondrial uncoupling protein are cold-sensitive but not obese. Nature *387*, 90–94.

Felig, P., Marliss, E., and Cahill, G.F., Jr. (1969). Plasma amino acid levels and insulin secretion in obesity. N. Engl. J. Med. *281*, 811–816.

Frontini, A., and Cinti, S. (2010). Distribution and development of brown adipocytes in the murine and human adipose organ. Cell Metab. *11*, 253–256.

Gulick, T., Cresci, S., Caira, T., Moore, D.D., and Kelly, D.P. (1994). The peroxisome proliferator-activated receptor regulates mitochondrial fatty acid oxidative enzyme gene expression. Proc. Natl. Acad. Sci. USA *91*, 11012–11016.

Handschin, C., and Spiegelman, B.M. (2006). Peroxisome proliferator-activated receptor gamma coactivator 1 coactivators, energy homeostasis, and metabolism. Endocr. Rev. *27*, 728–735.

Harper, A.E., Miller, R.H., and Block, K.P. (1984). Branched-chain amino acid metabolism. Annu. Rev. Nutr. *4*, 409–454.

Ishibashi, J., and Seale, P. (2010). Medicine. Beige can be slimming. Science *328*, 1113–1114.

Kajimura, S., Seale, P., Kubota, K., Lunsford, E., Frangioni, J.V., Gygi, S.P., and Spiegelman, B.M. (2009). Initiation of myoblast to brown fat switch by a PRDM16-C/EBP-beta transcriptional complex. Nature *460*, 1154–1158.

Kersten, S., Seydoux, J., Peters, J.M., Gonzalez, F.J., Desvergne, B., and Wahli, W. (1999). Peroxisome proliferator-activated receptor alpha mediates the adaptive response to fasting. J. Clin. Invest. *103*, 1489–1498.

Knowler, W.C., Barrett-Connor, E., Fowler, S.E., Hamman, R.F., Lachin, J.M., Walker, E.A., and Nathan, D.M.; Diabetes Prevention Program Research Group (2002). Reduction in the incidence of type 2 diabetes with lifestyle intervention or metformin. N. Engl. J. Med. *346*, 393–403.

Komatsu, M., Tong, Y., Li, Y., Nakajima, T., Li, G., Hu, R., Sugiyama, E., Kamijo, Y., Tanaka, N., Hara, A., and Aoyama, T. (2010). Multiple roles of PPARalpha in brown adipose tissue under constitutive and cold conditions. Genes Cells *15*, 91–100.

Kopecky, J., Clarke, G., Enerbäck, S., Spiegelman, B., and Kozak, L.P. (1995). Expression of the mitochondrial uncoupling protein gene from the aP2 gene promoter prevents genetic obesity. J. Clin. Invest. *96*, 2914–2923.

Leskinen, T., Rinnankoski-Tuikka, R., Rintala, M., Seppänen-Laakso, T., Pöllänen, E., Alen, M., Sipilä, S., Kaprio, J., Kovanen, V., Rahkila, P., et al. (2010). Differences in muscle and adipose tissue gene expression and cardio-metabolic risk factors in the members of physical activity discordant twin pairs. PLoS ONE *5*, 5, http://dx.doi.org/10.1371/journal.pone.0012609.

Lin, J., Wu, H., Tarr, P.T., Zhang, C.Y., Wu, Z., Boss, O., Michael, L.F., Puigserver, P., Isotani, E., Olson, E.N., et al. (2002). Transcriptional co-activator PGC-1 alpha drives the formation of slow-twitch muscle fibres. Nature *418*, 797–801.

Liu, M., Russell, R.L., Beigelman, L., Handschumacher, R.E., and Pizzorno, G. (1999). beta-alanine and alpha-fluoro-beta-alanine concentrative transport in rat hepatocytes is mediated by GABA transporter GAT-2. Am. J. Physiol. *276*, G206–G210.

Maisonneuve, C., Igoudjil, A., Begriche, K., Lettéron, P., Guimont, M.C., Bastin, J., Laigneau, J.P., Pessayre, D., and Fromenty, B. (2004). Effects of zidovudine, stavudine and beta-aminoisobutyric acid on lipid homeostasis in mice: possible role in human fat wasting. Antivir. Ther. (Lond.) *9*, 801–810.

Megeney, L.A., Kablar, B., Garrett, K., Anderson, J.E., and Rudnicki, M.A. (1996). MyoD is required for myogenic stem cell function in adult skeletal muscle. Genes Dev. *10*, 1173–1183.

Melnyk, A., Harper, M.E., and Himms-Hagen, J. (1997). Raising at thermoneutrality prevents obesity and hyperphagia in BAT-ablated transgenic mice. Am. J. Physiol. *272*, R1088–R1093.

Michael, L.F., Wu, Z.D., Cheatham, R.B., Puigserver, P., Adelmant, G., Lehman, J.J., Kelly, D.P., and Spiegelman, B.M. (2001). Restoration of insulin-sensitive glucose transporter (GLUT4) gene expression in muscle cells by the transcriptional coactivator PGC-1. Proc. Natl. Acad. Sci. USA *98*, 3820–3825.

Newgard, C.B., An, J., Bain, J.R., Muehlbauer, M.J., Stevens, R.D., Lien, L.F., Haqq, A.M., Shah, S.H., Arlotto, M., Slentz, C.A., et al. (2009). A branched-chain amino acid-related metabolic signature that differentiates obese and lean humans and contributes to insulin resistance. Cell Metab. *9*, 311–326.

Note, R., Maisonneuve, C., Lettéron, P., Peytavin, G., Djouadi, F., Igoudjil, A., Guimont, M.C., Biour, M., Pessayre, D., and Fromenty, B. (2003). Mitochondrial and metabolic effects of nucleoside reverse transcriptase inhibitors (NRTIs) in mice receiving one of five single- and three dual-NRTI treatments. Antimicrob. Agents Chemother. *47*, 3384–3392.

Oh, K.S., Kim, M., Lee, J., Kim, M.J., Nam, Y.S., Ham, J.E., Shin, S.S., Lee, C.M., and Yoon, M. (2006). Liver PPARalpha and UCP2 are involved in the regulation of obesity and lipid metabolism by swim training in genetically obese db/db mice. Biochem. Biophys. Res. Commun. *345*, 1232–1239.

Olesen, J., Kiilerich, K., and Pilegaard, H. (2010). PGC-1alpha-mediated adaptations in skeletal muscle. Pflugers Arch. *460*, 153–162.

Petrovic, N., Walden, T.B., Shabalina, I.G., Timmons, J.A., Cannon, B., and Nedergaard, J. (2010). Chronic peroxisome proliferator-activated receptor gamma (PPARgamma) activation of epididymally derived white adipocyte cultures reveals a population of thermogenically competent, UCP1-containing adipocytes molecularly distinct from classic brown adipocytes. J. Biol. Chem. *285*, 7153–7164.

Puigserver, P., Adelmant, G., Wu, Z.D., Fan, M., Xu, J.M., O'Malley, B., and Spiegelman, B.M. (1999). Activation of PPARgamma coactivator-1 through transcription factor docking. Science *286*, 1368–1371.

Rabøl, R., Petersen, K.F., Dufour, S., Flannery, C., and Shulman, G.I. (2011). Reversal of muscle insulin resistance with exercise reduces postprandial hepatic de novo lipogenesis in insulin resistant individuals. Proc. Natl. Acad. Sci. USA *108*, 13705–13709.

Rasbach, K.A., Gupta, R.K., Ruas, J.L., Wu, J., Naseri, E., Estall, J.L., and Spiegelman, B.M. (2010). PGC-1alpha regulates a HIF2alpha-dependent switch in skeletal muscle fiber types. Proc. Natl. Acad. Sci. USA *107*, 21866–21871.

Rector, R.S., Uptergrove, G.M., Morris, E.M., Borengasser, S.J., Laughlin, M.H., Booth, F.W., Thyfault, J.P., and Ibdah, J.A. (2011). Daily exercise vs. caloric restriction for prevention of nonalcoholic fatty liver disease in the OLETF rat model. Am. J. Physiol. Gastrointest. Liver Physiol. *300*, G874–G883.

Rhee, E.P., Ho, J.E., Chen, M.H., Shen, D., Cheng, S., Larson, M.G., Ghorbani, A., Shi, X., Helenius, I.T., O'Donnell, C.J., et al. (2013). A genome-wide association study of the human metabolome in a community-based cohort. Cell Metab. *18*, 130–143.

Roberts, L.D., Souza, A.L., Gerszten, R.E., and Clish, C.B. (2012). Targeted metabolomics. Curr. Protoc. Mol. Biol. *Chapter 30*, Unit 30 32 31–24.

Schinzel, R.T., Ahfeldt, T., Lau, F.H., Lee, Y.K., Cowley, A., Shen, T., Peters, D., Lum, D.H., and Cowan, C.A. (2011). Efficient culturing and genetic

manipulation of human pluripotent stem cells. PLoS ONE *6*, e27495, http://dx.doi.org/10.1371/journal.pone.0027495.

Seale, P., Kajimura, S., Yang, W., Chin, S., Rohas, L.M., Uldry, M., Tavernier, G., Langin, D., and Spiegelman, B.M. (2007). Transcriptional control of brown fat determination by PRDM16. Cell Metab. *6*, 38–54.

Seale, P., Conroe, H.M., Estall, J., Kajimura, S., Frontini, A., Ishibashi, J., Cohen, P., Cinti, S., and Spiegelman, B.M. (2011). Prdm16 determines the thermogenic program of subcutaneous white adipose tissue in mice. J. Clin. Invest. *121*, 96–105.

Shimomura, Y., Honda, T., Shiraki, M., Murakami, T., Sato, J., Kobayashi, H., Mawatari, K., Obayashi, M., and Harris, R.A. (2006). Branched-chain amino acid catabolism in exercise and liver disease. J. Nutr. Suppl. *136*, 250S–253S.

Soukas, A., Socci, N.D., Saatkamp, B.D., Novelli, S., and Friedman, J.M. (2001). Distinct transcriptional profiles of adipogenesis in vivo and in vitro. J. Biol. Chem. *276*, 34167–34174.

St-Pierre, J., Lin, J., Krauss, S., Tarr, P.T., Yang, R., Newgard, C.B., and Spiegelman, B.M. (2003). Bioenergetic analysis of peroxisome proliferator-activated receptor gamma coactivators 1alpha and 1beta (PGC-1alpha and PGC-1beta) in muscle cells. J. Biol. Chem. *278*, 26597–26603.

Suhre, K., Wallaschofski, H., Raffler, J., Friedrich, N., Haring, R., Michael, K., Wasner, C., Krebs, A., Kronenberg, F., Chang, D., et al. (2011). A genome-wide association study of metabolic traits in human urine. Nat. Genet. *43*, 565–569.

Sutherland, L.N., Bomhof, M.R., Capozzi, L.C., Basaraba, S.A.U., and Wright, D.C. (2009). Exercise and adrenaline increase PGC-1alpha mRNA expression in rat adipose tissue. J. Physiol. *587*, 1607–1617.

Viscomi, C., Bottani, E., Civiletto, G., Cerutti, R., Moggio, M., Fagiolari, G., Schon, E.A., Lamperti, C., and Zeviani, M. (2011). In vivo correction of COX deficiency by activation of the AMPK/PGC-1α axis. Cell Metab. *14*, 80–90.

Wang, T.J., Larson, M.G., Vasan, R.S., Cheng, S., Rhee, E.P., McCabe, E., Lewis, G.D., Fox, C.S., Jacques, P.F., Fernandez, C., et al. (2011). Metabolite profiles and the risk of developing diabetes. Nat. Med. *17*, 448–453.

Wang, T.J., Ngo, D., Psychogios, N., Dejam, A., Larson, M.G., Vasan, R.S., Ghorbani, A., O'Sullivan, J., Cheng, S., Rhee, E.P., et al. (2013). 2-aminoadipic acid is a biomarker for diabetes risk. J. Clin. Invest. *123*, 4309–4317.

Whittle, A.J., and Vidal-Puig, A. (2012). NPs—heart hormones that regulate brown fat? J. Clin. Invest. *122*, 804–807.

Wright, H.M., Clish, C.B., Mikami, T., Hauser, S., Yanagi, K., Hiramatsu, R., Serhan, C.N., and Spiegelman, B.M. (2000). A synthetic antagonist for the peroxisome proliferator-activated receptor gamma inhibits adipocyte differentiation. J. Biol. Chem. *275*, 1873–1877.

Wu, Z.D., Puigserver, P., Andersson, U., Zhang, C.Y., Adelmant, G., Mootha, V., Troy, A., Cinti, S., Lowell, B., Scarpulla, R.C., and Spiegelman, B.M. (1999). Mechanisms controlling mitochondrial biogenesis and respiration through the thermogenic coactivator PGC-1. Cell *98*, 115–124.

Wu, J., Ruas, J.L., Estall, J.L., Rasbach, K.A., Choi, J.H., Ye, L., Boström, P., Tyra, H.M., Crawford, R.W., Campbell, K.P., et al. (2011). The unfolded protein response mediates adaptation to exercise in skeletal muscle through a PGC-1α/ATF6α complex. Cell Metab. *13*, 160–169.

Wu, J., Boström, P., Sparks, L.M., Ye, L., Choi, J.H., Giang, A.H., Khandekar, M., Virtanen, K.A., Nuutila, P., Schaart, G., et al. (2012). Beige adipocytes are a distinct type of thermogenic fat cell in mouse and human. Cell *150*, 366–376.

Xu, X.H., Ying, Z.K., Cai, M., Xu, Z.B., Li, Y.J., Jiang, S.Y., Tzan, K., Wang, A.X., Parthasarathy, S., He, G.L., et al. (2011). Exercise ameliorates high-fat diet-induced metabolic and vascular dysfunction, and increases adipocyte progenitor cell population in brown adipose tissue. Am. J. Physiol. Regul. Integr. Comp. Physiol. *300*, R1115–R1125.

Xue, B., Coulter, A., Rim, J.S., Koza, R.A., and Kozak, L.P. (2005). Transcriptional synergy and the regulation of Ucp1 during brown adipocyte induction in white fat depots. Mol. Cell. Biol. *25*, 8311–8322.

Cell Metabolism
Article

Adipocyte Inflammation Is Essential for Healthy Adipose Tissue Expansion and Remodeling

Ingrid Wernstedt Asterholm,[1,4] Caroline Tao,[1] Thomas S. Morley,[1] Qiong A. Wang,[1] Fernando Delgado-Lopez,[3] Zhao V. Wang,[1] and Philipp E. Scherer[1,2,*]
[1]Department of Internal Medicine, Touchstone Diabetes Center
[2]Department of Cell Biology
UT Southwestern Medical Center, 5323 Harry Hines Boulevard, Dallas, TX 75390-8549, USA
[3]Facultad de Medicina, Universidad Catolica del Maule, Avenida San Miguel 3605, Talca, Chile
[4]Present address: Institute of Neuroscience and Physiology, Sahlgrenska Academy at the University of Gothenburg, Box 432, 405 30 Gothenburg, Sweden
*Correspondence: philipp.scherer@utsouthwestern.edu
http://dx.doi.org/10.1016/j.cmet.2014.05.005

SUMMARY

Chronic inflammation constitutes an important link between obesity and its pathophysiological sequelae. In contrast to the belief that inflammatory signals exert a fundamentally negative impact on metabolism, we show that proinflammatory signaling in the adipocyte is in fact required for proper adipose tissue remodeling and expansion. Three mouse models with an adipose tissue-specific reduction in proinflammatory potential were generated that display a reduced capacity for adipogenesis in vivo, while the differentiation potential is unaltered in vitro. Upon high-fat-diet exposure, the expansion of visceral adipose tissue is prominently affected. This is associated with decreased intestinal barrier function, increased hepatic steatosis, and metabolic dysfunction. An impaired local proinflammatory response in the adipocyte leads to increased ectopic lipid accumulation, glucose intolerance, and systemic inflammation. Adipose tissue inflammation is therefore an adaptive response that enables safe storage of excess nutrients and contributes to a visceral depot barrier that effectively filters gut-derived endotoxin.

INTRODUCTION

Adipose tissue expansion in response to excess caloric intake is an important systemic response to avoid the lipotoxic side effects exerted by excess lipid and fatty acid (FA) deposition in cells other than adipocytes. The basic mechanisms, leading to a gradual and "healthy" expansion of fat pads, are starting to be elucidated. Healthy expansion is associated with appropriate angiogenesis and vascular and extracellular matrix (ECM) remodeling.

Increased adiposity is more often than not associated with an increased risk for a number of chronic diseases, including diabetes, cardiovascular disease, and some types of cancers (Park et al., 2011). The underlying mechanisms for the link between obesity and these diseases are not fully understood but are likely to involve a state of chronic systemic low-grade inflammation.

The causality between local adipose tissue inflammation, systemic inflammation, and metabolic dysfunction has, however, not been studied. Therefore, we developed three distinct but complementary mouse models to investigate the role of adipose tissue inflammation in high-fat-diet (HFD)-induced metabolic disturbances. By design, two models express the anti-inflammatory factors in adipose tissue constitutively, while one model is inducible.

Analysis of these three mouse models reveals that the inability to mount an appropriate local proinflammatory response at the level of the adipocyte reduces adipose tissue expansion under normal physiological as well as under HFD-fed conditions. This inability to expand adipose tissue is associated with ectopic lipid deposition and a deteriorated metabolic profile. Furthermore, we demonstrate that mesenteric adipose tissue (MWAT, a visceral fat depot) plays an important role for proper intestinal barrier function. An ineffective response of MWAT to proinflammatory stimuli with respect to its expansion is associated with a "leaky gut," colitis, and metabolic dysfunction. Thus, these mouse models demonstrate that a local inflammatory response derived from the adipocyte is an adaptive response and an important preemptive factor for ensuing obesity-associated systemic inflammation.

RESULTS

We have recently developed a mouse model (the "adipochaser mouse") in which we can permanently activate β-galactosidase expression in all preexisting adipocytes by a short bout of doxycycline treatment. Removal of doxycycline enables the detection of newly differentiated adipocytes that are negative for the blue X-Gal-LacZ staining (Wang et al., 2013). Repeated local LPS injections into adipose tissue stimulate adipogenesis without affecting overall weight gain (Sadler et al., 2005). Exploiting our adipochaser mouse, we are able to confirm the findings by Sadler and colleagues. New adipocyte formation was evident in the LPS-injected inguinal WAT (IWAT) depot, but not in the control depot (Figure 1A and data not shown). These observations suggest that the induction of acute inflammation in the

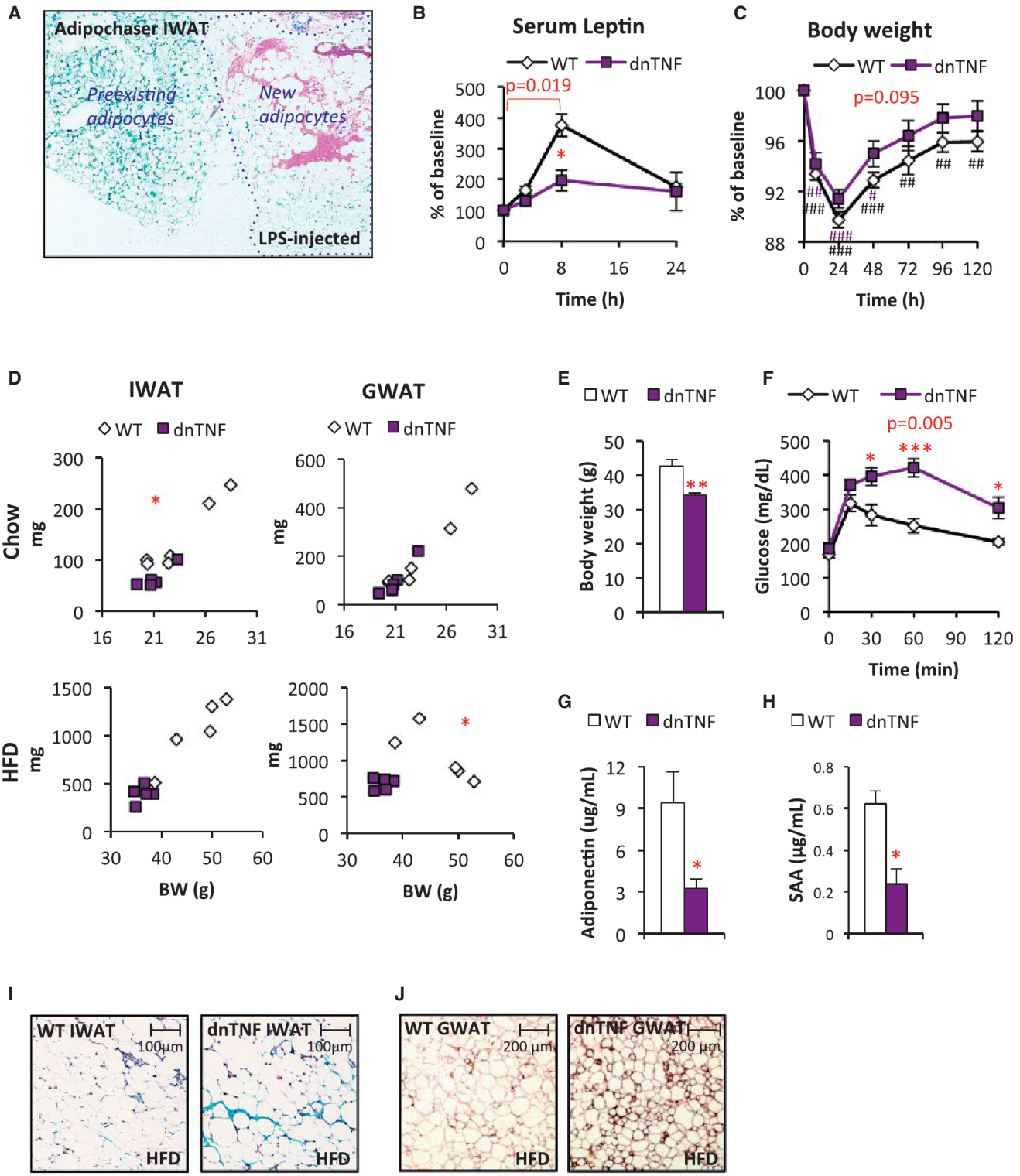

Figure 1. Reduced Fat Mass and Glucose Tolerance in dnTNF tg Mice

(A) X-Gal-LacZ stained LPS-injected Adipochaser IWAT (blue, preexisting adipocytes; white, new adipocytes).

(B and C) Leptin and body weight change after i.p. injection with 0.3 mg/kg LPS in dnTNF tg and wild-type female mice.

(D) IWAT and GWAT weight in relation to body weight in chow (top) and HFD-fed (bottom) male dnTNF tg and wild-type controls.

(E–H) Body weight, glucose tolerance test, serum adiponectin, and SAA levels in male dnTNF tg and littermate controls after 11 weeks of HFD feeding.

(I) Representative Trichrome stain of IWAT in male dnTNF tg and littermate controls after 11 weeks of HFD feeding.

(legend continued on next page)

context of intact adipose tissue stimulates adipogenesis in vivo. We therefore hypothesized that acute inflammation within adipose tissue may play an essential role for adipose tissue expansion, remodeling, and overall homeostasis by stimulating ECM degradation and angiogenesis. To study the role of inflammation in adipose tissue, we developed a mouse model expressing a dominant-negative version of the potent proinflammatory cytokine TNF-α (dnTNF) (Steed et al., 2003) under the control of the ap2 promoter ("dnTNF tg"). This is a version of TNF-α that effectively heterotrimerizes with wild-type TNF-α subunits, but the presence of a mutant subunit engages the TNF receptors nonproductively. aP2 promoter-driven constructs are predominantly transcribed in adipocytes, but expression has been reported in macrophages and other tissues, such as the heart and the brain, though at much lower levels. Our dnTNF tg mice express the transgene specifically in adipose tissue, but also to a minor extent in isolated peritoneal macrophages (see Figure S1A available online). The low level of dnTNF expression in macrophages does not affect the inflammatory state of thioglycollate-activated peritoneal macrophages, since a number of cytokines and M1/2 markers (e.g., TNF-α, IL-1β, TGF-β, Arg1, and CD11c) remained unaltered compared to macrophages isolated from littermate controls (Figure S1B).

As expected, unchallenged chow-fed dnTNF tg do not display significant differences with respect to genes involved in inflammation or macrophage polarization, e.g., TNF-α, F4/80, CD11c, NOS2, CD206, and CD301 in adipose tissue (data not shown). However, the dnTNF tg mice display a reduced NFκB activation in adipose tissue (as judged by reduced IκBα phosphorylation) in response to an intraperitoneal injection with TNF-α (Figure S1C). Furthermore, LPS induces a highly specific response on adipocytes in adipose tissue, leading to an acute increase in serum leptin levels. In the presence of dnTNF, this LPS-mediated increase in serum leptin levels is significantly blunted (Figure 1B). This indicates that an autocrine TNF-α loop is part of the LPS-mediated effects on leptin release. Despite the increase in serum SAA and α1acid-glycoprotein (Figure S1D and data not shown), the body weight recovery is slightly faster in the dnTNF tg mice (Figure 1C). Combined, these results confirm that the dnTNF transgene is indeed functional, and that it exerts its effects primarily at the level of adipose tissue, while leaving the inflammatory response in other tissues, such as the liver, fully intact.

Reduced Body Weight, Fat Mass and Glucose Tolerance in HFD-Fed dnTNF tg Mice

In young chow-fed mice, the body weights trend to be lower in the dnTNF mice. The IWAT weight is reduced, while the gonadal WAT (GWAT) weight is similar between genotypes (Figure 1D). This pattern changes upon HFD feeding. The degree of HFD-induced obesity is reduced in the dnTNF mice (Figure 1E). This is particularly apparent in GWAT, which is much more prominently affected than the IWAT depot in HFD-fed mice (Figure 1D). In absolute terms, both GWAT and IWAT are of reduced size in HFD-fed dnTNF tg mice compared to littermates. The reduced IWAT weight is, however, proportional to the lower body weight in the dnTNF mice. Brown adipose tissue (BAT) and MWAT are, however, of similar sizes in dnTNF and littermate controls, regardless of diet (data not shown). Similar results were seen when the dnTNF transgene was bred into the genetically obese *ob/ob* background, indicating that there are leptin-independent mechanisms responsible for the reduced body and GWAT mass weight in dnTNF mice (Figure S1E).

We went on to test whether the reduced body weight translates into the expected improvements in metabolic parameters. To our surprise, HFD-fed dnTNF tg mice are severely glucose intolerant and have lower adiponectin levels, despite lower levels of circulating SAA compared to littermate controls (Figures 1F–1H).

These observations suggest that adipose tissue TNF-α signaling is relevant for adipose tissue remodeling and expansion. Consistent with this hypothesis, we found increased amounts of ECM deposits in IWAT of HFD-fed dnTNF mice compared to littermate controls (Figure 1I). This result is consistent with a need for TNF-α for successful ECM remodeling in the context of wound healing (Heo et al., 2011; Saika et al., 2006). The HFD-induced adipocyte hypertrophy in IWAT is similar between genotypes (relative adipocyte sizes 1.00 ± 0.3 and 0.94 ± 0.1 for, respectively, wild-type and dnTNF tg IWAT; $p = 0.84$), despite about 60% reduced IWAT depot weight in the dnTNF tg mice (Figure 1D), suggesting that inhibition of TNF-α-signaling either causes a reduced capacity for adipogenesis in vivo or may simply be secondary to the increased fibrosis. Disruption of this fibrotic state, such as in the context of HFD-exposed mice lacking collagen VI (Khan et al., 2009), reduces adipocyte apoptosis. In contrast, enhanced fibrosis increases the rate of adipocyte death (Halberg et al., 2009). In line with fibrosis-induced adipocyte death, prolonged HFD-feeding (22 weeks) leads to an increased presence of crown-like structures (CLSs) in the GWAT of dnTNF tg mice. This is apparent when examining infiltrating macrophages (as judged by Mac2 staining) surrounding dead adipocytes (as judged by perilipin-negative staining) (Figure 1J). We did not, however, detect a difference in adipocyte death rates in IWAT, and no difference was observed in GWAT at earlier stages of HFD feeding (data not shown). Thus, a reduction in adipogenesis is more likely to explain the enlarged adipocytes in IWAT and the reduced GWAT size in HFD-fed dnTNF tg mice.

Essential Role for Acute Inflammation for Adipose Tissue Functionality

Given the many studies showing the negative impact of TNF-α on insulin sensitivity as well as on adipocyte differentiation (Engelman et al., 2000; Gustafson and Smith, 2006; Hotamisligil et al., 1993), the metabolic and adipose tissue dysfunction seen in the dnTNF tg mice is rather surprising at first sight. However, our observations do not contradict a model in which *chronic* inflammation is an important contributor toward the metabolic syndrome. Rather, though, "immunologic fitness" as we have previously defined it (Asterholm et al., 2012), seems to be an

(J) Representative perilipin (red) and mac2 (brown) immunostain in GWAT after 22 weeks of HFD feeding in male dnTNF tg and littermate control. Error bars represent SEM; $p < 0.05$ according to Student's t test was considered significant and is indicated by */#; **/##$p < 0.01$; ***/###$p < 0.001$ (*difference in between genotype, #difference from initial weight). p values in red indicate difference between groups during the indicated time course according to repeated-measurement ANOVA.

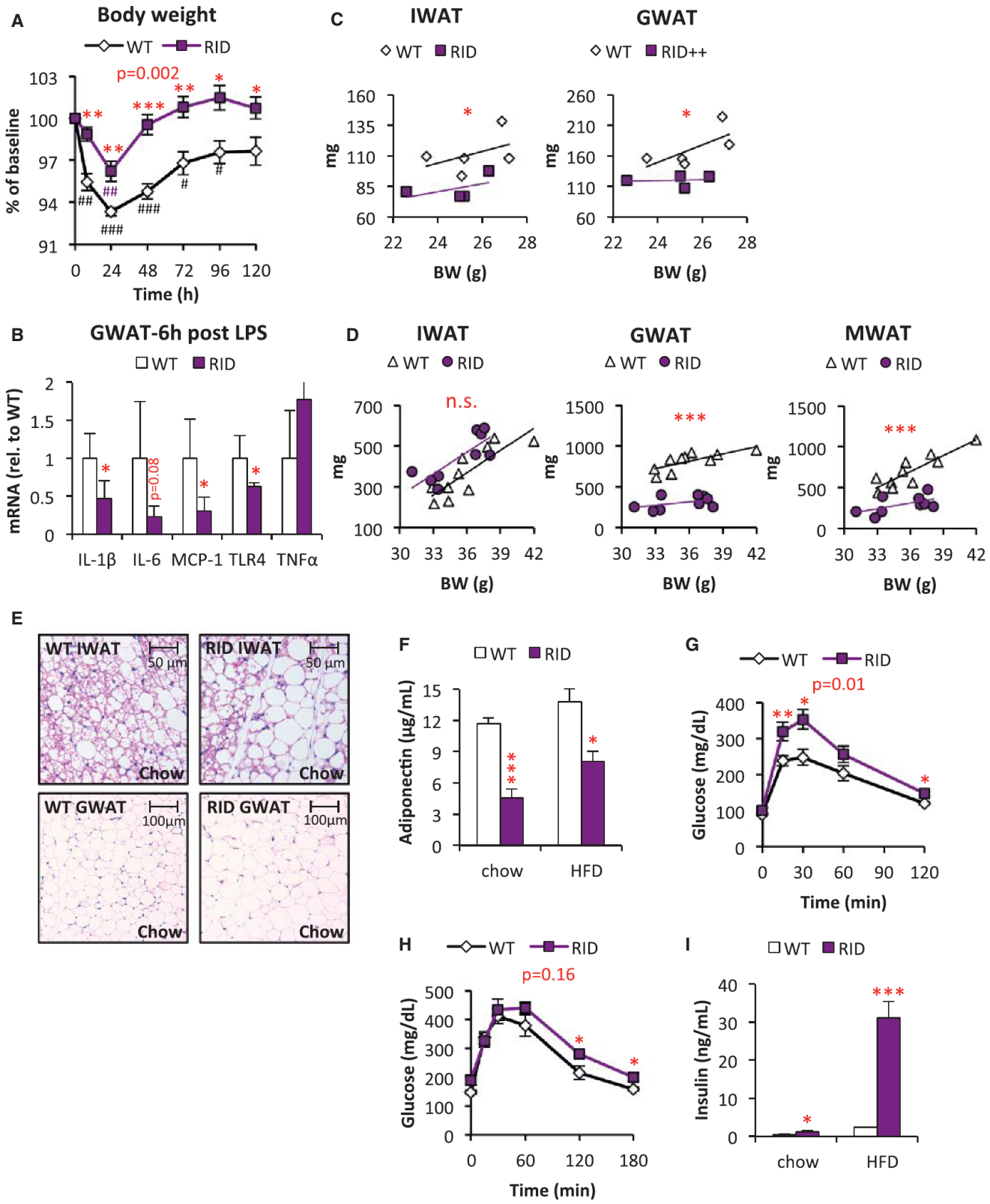

Figure 2. Reduced Fat Mass and Reduced Glucose Tolerance in RID tg Mice

(A) LPS (0.3 mg/kg)-induced body weight change in male RID tg and wild-type controls.

(B) Gene expression in GWAT harvested from male RID tg and wild-type controls 6 hr after LPS injection.

(legend continued on next page)

important component for tissue homeostasis in general and for adipose tissue in particular. To further explore this concept of "physiological adipose tissue inflammation," we wanted to test an additional model to strengthen the general validity of our initial findings in these dnTNF tg mice. To do so, we generated a more potent adipose-specific anti-inflammatory model. This second mouse model takes advantage of RIDα/β (RID), an adenoviral protein complex that suppresses the local host immune response by potently inhibiting a number of proinflammatory signaling pathways (e.g., TLR4-, TNF-α- and IL-1β-mediated signaling) (Lichtenstein et al., 2004; Delgado-Lopez and Horwitz, 2006). Similar to the dnTNF tg mice, we put the expression of RID under the control of the aP2 promoter (RID tg). Just as for the dnTNF tg mouse model, we detected a high transgene expression in adipocytes with low level expression also seen in macrophages, but not in other tissues (Figure S2A). Upon isolating fresh peritoneal thioglycollate-stimulated macrophages from wild-type and RID mice, we did not detect any difference in macrophage function, suggesting that the trace levels of expression do not amount to an effective suppression of inflammation in macrophages (Figure S2B). Consistent with a potent action within the adipocyte, the RID tg mice display a significantly blunted response to LPS in adipose tissue, associated with a reduced response to LPS-induced body weight loss as well (Figures 2A and 2B). Moreover, and also similar to the dnTNF tg mice, fat pad weights of the RID tg mice are reduced. The more effective anti-inflammatory effects in the RID tg lead to a significant reduction in both IWAT and GWAT depot sizes, even in young chow-fed mice (Figure 2C). HFD feeding causes an even more dramatic difference with respect to the visceral GWAT and MWAT depots, while the subcutaneous IWAT depot no longer differs in size from the wild-type controls under these conditions (Figure 2D). BAT weights are similar between genotypes, with or without HFD challenge (data not shown). Despite the reduced overall amounts of white adipose tissue, the RID tg mice do not display altered overall body weight (Figure S2C).

Body composition, as assessed by NMR, confirmed a slightly reduced fat mass in both the dnTNF and the RID tg mice compared to wild-type controls, and as little as 2 days of HFD feeding enhances this difference between genotypes (Figures S2D and S2E). Lean body mass was however unaltered in both mouse models (Figures S2D and S2E). We also investigated whether these transgenic mice display an altered energy balance, but neither food intake nor oxygen consumption differed from their respective controls (data not shown). Thus, the reduced body weight in the dnTNF must be caused by an alteration in energy balance that is too small to be detected with available methods. In contrast, the respiratory quotient (RQ = VO_2/VCO_2) was significantly altered. HFD-fed dnTNF tg mice display a lower RQ in the dark phase, and the RID tg mice display a lower dark phase-RQ on both chow and HFD. This reduction in RQ in both dnTNF and RID tg mice compared to their controls indicates a heavier reliance on FA oxidation for their energy need (Figures S2F and S2G). Typically, healthy mice burn carbohydrates during the dark phase. At this time of day, they have the highest food intake and hence the highest insulin levels. Thus, a lower RQ during the dark phase, reflective of reduced carbohydrate use, is an indication of systemic insulin resistance and metabolic inflexibility in both transgenic strains.

The inhibition of adipogenesis (as gauged by the estimated number of adipocytes) is even more pronounced in the RID tg mice (Figure 2E). Chow-fed RID tg mice display 17% ± 2% larger adipocytes in IWAT ($p < 0.05$) and a trend toward larger adipocytes in GWAT (27% ± 11% larger, $p = 0.14$) despite the fact that these depots are 25% (IWAT) and 30% (GWAT) smaller than in wild-type controls (Figure 2C). The circulating SAA levels are, to our surprise, higher in chow-fed RID tg mice, but this difference disappears on HFD; i.e., the HFD-induced increase in SAA is more pronounced in wild-type mice (Figure S2H). Similar to the dnTNF tg mice, the RID tg adipose phenotype is associated with both reduced adiponectin levels and glucose intolerance (Figures 2F and 2G). In fact, RID tg mice have a substantial degree of glucose intolerance with mild hyperinsulinemia already under unchallenged, chow-fed conditions at a young age. It could very well be that the lower adiponectin levels contribute to this impaired insulin sensitivity. HFD feeding aggravates the metabolic phenotype further, and the RID tg mice continue to display reduced glucose tolerance despite severe hyperinsulinemia relative to the wild-type controls (Figures 2H and 2I). Upon closer analysis of the adipose tissue, we found elevated levels of collagen in HFD-fed RID tg IWAT. Interestingly, in these experiments, we noticed that HFD induces a rapid and dramatic reduction of septa in IWAT. These septa are easily detectable with a Picrosirius red stain, while somewhat less apparent with Trichrome stain, and correspond to collagen streaks that compartmentalize adipose tissue "units" in young wild-type mice (Figures 3A and S3A). There is no description in the literature of either the developmental origin or the relevance of these functional "miniunits" in adipose tissue. The reduction in septa can be quantified by total collagen measurements. HFD-fed wild-type, but not RID tg, mice have a reduced total amount of collagen per milligram adipose tissue compared to the levels in chow-fed controls (Figure 3B). Thus, adipose tissue fibrosis in obesity may, at least in some cases, be the consequence of reduced ECM degradation, rather than an increase in ECM production. We should also note that total collagen content measurements of adipose tissue do not necessarily reflect states of pathological fibrosis, since healthy chow-fed mice have higher

(C) IWAT and GWAT in relation to body weight in chow-fed male RID tg and wild-type mice.
(D) IWAT, GWAT, and MWAT in relation to body weight in 15-week HFD-fed male RID tg and wild-type mice.
(E) Representative H&E stain of IWAT and GWAT in male RID tg and wild-type mice on chow.
(F) Adiponectin levels in male RID tg and wild-type mice on chow and after 12 weeks of HFD.
(G and H) Glucose tolerance in (G) chow-fed and (H) 12-week HFD-fed male RID tg and wild-type mice.
(I) Serum-insulin levels in 3 hr fasted male RID tg and wild-type mice. One-way ANOVA analysis shows that both diet ($F = 8.1$, $p = 0.013$) and genotype ($F = 12.3$, $p = 0.004$) contribute significantly to collagen levels. Error bars represent SEM; $p < 0.05$ according to Student's t test was considered significant and is indicated by */#; **/##$p < 0.01$; ***/###$p < 0.001$ (*difference in between genotype, #difference from initial weight). p values in red indicate difference between groups during time courses according to repeated-measurement ANOVA.

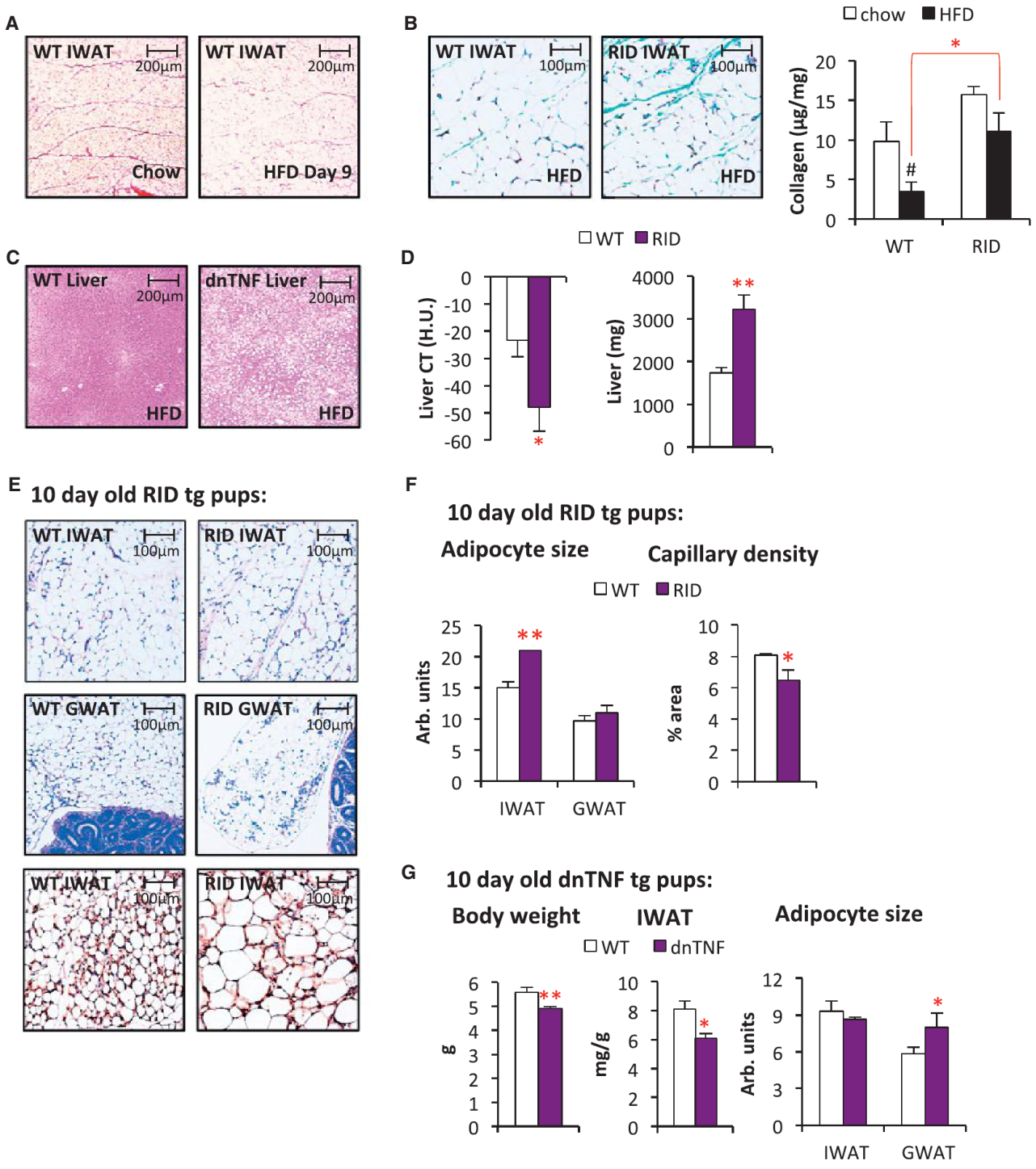

Figure 3. Increased HFD-Induced Steatosis and Delayed Adipose Tissue Development in dnTNF and RID tg Mice

(A) Representative Picrosirius red stain of IWAT from 8-week-old C57B6 males on chow and after 9 days with HFD.

(B) Representative Trichrome stain and collagen levels in IWAT of HFD-fed male RID tg and wild-type mice.

(C) Representative H&E stain of liver sections from 11-week HFD-fed male dnTNF tg and littermate control.

(D) Liver fat quantified by CT and liver weight in 11-week HFD-fed male RID tg and wild-type controls.

(E and F) Representative H&E stain of IWAT and GWAT sections and endomucin immune stain of IWAT (bottom panels) and (with quantification shown in F) from 10-day-old male RID tg and wild-type pups.

(G) Body weight, IWAT weight, and adipocyte sizes in 10-day-old dnTNF tg and littermate controls. Error bars represent SEM; $p < 0.05$ according to Student's t test was considered significant and is indicated by */#; **$p < 0.01$; ***$p < 0.001$ (*significantly different from WT, #significantly different from untreated controls of same genotype).

levels of collagen in IWAT than metabolically challenged obese mice. Instead, these data suggest that, beyond biochemical measurements, a histological examination also has to be performed to accurately assess whether a pathological condition prevails (e.g., the collagen deposits show up as irregular streaks or in association with CLSs) or whether the collagen deposits are in the form of well-organized septa, as seen in the lean animals.

Reduced HFD-Induced Adipose Tissue Expansion in dnTNF and RID tg Mice Is Associated with Hepatic Steatosis

These initial observations support the hypothesis that the ability to mount a proinflammatory response is intimately coupled to adipose tissue expansion, proper remodeling, and the resolution of inflammation. We therefore wanted to determine whether the reduced storage capacity in adipose tissue leads to increased ectopic lipid deposition. Indeed, both the dnTNF and the RID tg mice display an increased degree of HFD-induced hepatic steatosis (Figures 3C and 3D). Given the blunted HFD-induced weight gain in the dnTNF tg mice and the higher anti-inflammatory potency of the RID transgene, it is not surprising that the effects on the liver are more severe in the RID tg mice. In addition to the increased amounts of liver fat, RID tg mice also display a high level of hepatomegaly during HFD-fed conditions (Figure 3D). Thus, the increased ectopic lipid deposition in dnTNF and RID tg mice can, at least in part, explain the more severe degree of HFD-induced metabolic dysfunction compared to controls in these mouse models.

Adipocyte Inflammation Is Important for Early Postnatal Adipogenesis

The observations so far argue that the reduced adipose tissue mass in the dnTNF and the RID tg mice is the consequence of a decreased adipogenesis rate, partially offset by a more pronounced hypertrophy of existing adipocytes. Moreover, the reduced overall fat mass cannot solely be the consequence of an altered energy balance, since only the dnTNF, but not the RID transgenic, mice display lower body weights; and adipose depot sizes in both the dnTNF and the RID tg mice are disproportionately reduced beyond what is expected from the body weight differentials to wild-type mice. We were therefore prompted to further explore the phenomenon of reduced adipose expansion and remodeling in these anti-inflammatory models. First, we explored whether adipogenesis is already negatively affected during postnatal development. Immediately at birth, wild-type mice rapidly expand their IWAT depots. IWAT pads grow substantially within 1–2 weeks, while the visceral adipose depots remain almost undetectable at this young age. We measured the differences in adipose tissue size in 10-day-old pups. Indeed, the RID tg pups display fewer, but larger, adipocytes in developing IWAT, while body weights are unaltered compared to wild-type controls (Figures 3E and 3F and data not shown). This difference is associated with a decrease in vascular density as judged by IHC stains of endomucin of IWAT (Figures 3E and 3F). The dnTNF mice display a similar, albeit less dramatic, phenotype. The 10-day-old dnTNF tg pups have a slightly reduced total body weight, though the IWAT weight is reduced both in relation to body weight and in absolute terms compared to littermate controls (Figure 3G). The dnTNF adipocytes in GWAT are larger, while the adipocytes in IWAT are of similar size compared to wild-type adipocytes on postnatal day 10 (Figure 3G). Even the dnTNF tg mice have therefore a reduced number of adipocytes, since the adipose depots are overall smaller. There is no evidence of dead adipocytes in either GWAT or IWAT in any of the genotypes (Figure S3B for RID tg; data not shown for dnTNF tg).

A concern in this context is that both RID tg and dnTNF could lead to inhibition of adipogenesis due to cytotoxic effects or due to unspecific interference with the differentiation program. To investigate this possibility, we isolated stromal vascular cells from IWAT of wild-type, dnTNF, and RID tg mice; propagated them in culture; and then subjected the cells to an in vitro differentiation protocol and assessed the degree of differentiation by several different criteria (Figures S3C–S3E). All three cell preparations differentiated to the same extent as judged by appearance of lipid droplets in bright field microscopy (Figure S3C), oil red O staining (Figure S3D), and immunoblotting for the adipocyte marker adiponectin (Figure S3E). Thus, the reduced adipogenic potential in the transgenic mice is truly a function of the reduced ability of these cells to respond to external proinflammatory stimuli in the context of an intact adipose tissue depot, rather than a cell-autonomous differentiation defect due to transgene expression.

The first few postnatal days are associated with an increased exposure to many new antigens due to microbial colonization of the gut, concomitant with a sudden intake of large quantities of milk. A large intake of lipids has been shown to acutely cause inflammatory responses in various tissues, including adipose tissue (Asterholm et al., 2012; Magne et al., 2010). We hypothesize that the likely increase in the systemic levels of bacterial toxins further elevates the lipid-induced proinflammatory response, and facilitates angiogenesis that in turn is permissive for adipogenesis (Figure S4A). Hence, we suggest that gut bacteria play a major role in proper storage of excess nutrients during this early postnatal stage. To test this hypothesis, we exposed wild-type and RID transgenic mice for 5 weeks prior to mating to a chow diet supplemented with antibiotics that effectively deplete the commensal microflora (Rakoff-Nahoum et al., 2004). The antibiotics were removed from the food between E0 and E16 and were reintroduced again at day E17 to avoid potentially harmful effects of these drugs on fetal development. There was no effect on the offspring's body weight, neither by antibiotics nor by genotype, and all pups survived and appeared healthy regardless of treatment group. We found that antibiotic-treated wild-type offspring display reduced amounts of adipose tissue at 10 days of age compared to the untreated control mice. The RID tg pups display a reduced amount of adipose tissue relative to wild-type mice, regardless of whether they were on antibiotics or not (Figure 4A). Thus, the presence or absence of bacterially derived toxins in the RID tg pups has no effect on adipose tissue growth, supporting the notion that a local inflammatory response is an important component of normal adipose tissue expansion. Furthermore, the male breeders used in this study were sacrificed after 5 weeks of treatment, and their MWAT was collected for histological analysis. We found that antibiotic-treated wild-type mice have a reduced capillary density in their MWAT compared to controls (Figure 4B). This observation provides additional support for the idea

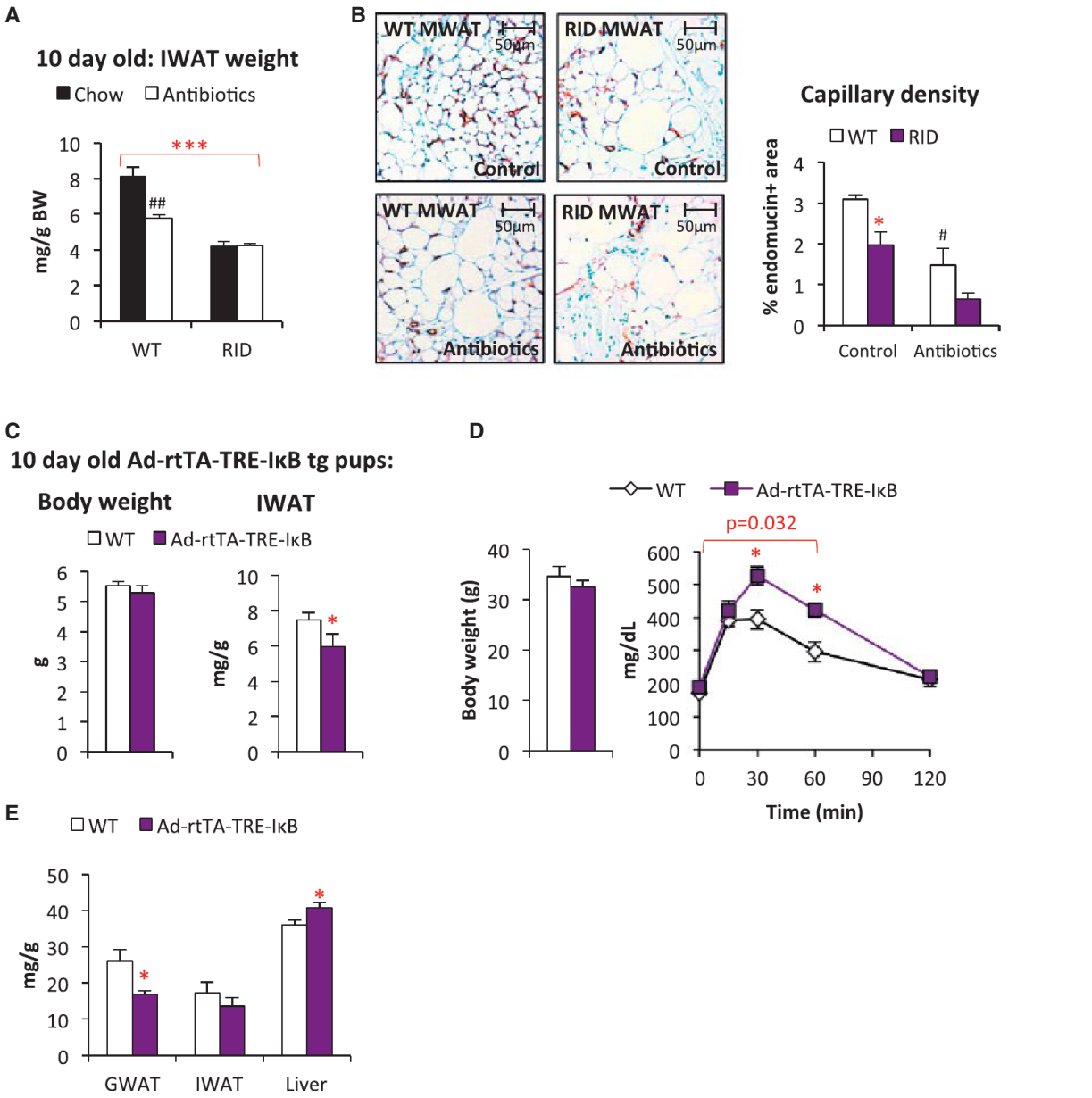

Figure 4. Ablation of Gut Microbiota Affects Capillary Density, and Ad-rtTA-TRE-IκB tg Mice Display Reduced Adipogenesis and Glucose Tolerance

(A) Effect of antibiotics treatment on IWAT weight in 10-day-old RID tg and wild-type pups. One-way ANOVA analysis shows that both treatment ($F = 5.3$, $p = 0.026$) and genotype ($F = 29.4$, $p < 0.001$) contribute significantly to the IWAT weight.

(B) Effect of antibiotics treatment on capillary density in MWAT as judged by endomucin immune stain in male RID tg and wild-type mice. One-way ANOVA analysis shows that both treatment ($F = 35.1$, $p = 0.002$) and genotype ($F = 14.8$, $p = 0.012$) contribute significantly to capillary density in MWAT.

(C) Body weight and IWAT weight in doxycycline-treated 10-day-old Ad-rtTA-TRE-IκB tg and littermate controls.

(D) Body weight and glucose tolerance in 8-week HFD-fed male Ad-rtTA-TRE-IκB tg and littermate controls.

(E) Dissected tissue weight in 8-week HFD-fed Ad-rtTA-TRE-IκB tg and littermate controls. Error bars represent SEM; $p < 0.05$ according to Student's t test was considered significant and is indicated by */#; **/##$p < 0.01$; ***$p < 0.001$ (*significantly different from WT, #significantly different from untreated controls of same genotype). p value in red indicates difference between groups during the indicated time course according to repeated-measurement ANOVA).

that bacterially induced inflammation leads to increased angiogenesis, at least locally in MWAT (Figure S4B). RID tg mice had a reduced capillary density, even in the absence of antibiotic treatment (Figure 4B). Furthermore, the average MWAT adipocyte size is 20% ± 5% ($p < 0.05$) larger, while the MWAT depot weight is 73% ± 7% reduced, indicating a dramatic reduction in the number of MWAT adipocytes in RID tg mice compared to wild-type controls. Antibiotic treatment did not have an impact on adipocyte size, but tended to reduce the capillary density even further in the RID tg MWAT, suggesting that additional cells

beyond adipocytes play a role in the response to microbial toxins in adult MWAT (Figure 4B).

Reduced Adipogenesis and HFD-Induced Glucose Intolerance in an Inducible Adipocyte-Specific Anti-Inflammatory Model

Since the effects seen in adipose tissue expansion and metabolic health were quite striking in the RID tg and dnTNF mice, we wanted to test whether we could see a similar phenomenon in an adipocyte-specific inducible model. To that end, we generated a mouse that expresses a mutated human IκBα(S32G-S36A) version under the control of a tet-responsive element (TRE-IκB tg). IκBα(S32G-S36A) is an effective inhibitor of the NFκB pathway. This TRE-IκB tg model was crossed with transgenic mice expressing the "tet-on" transcription factor rtTA under the control of the highly adipocyte-specific adiponectin promoter (Ad-rtTA tg) (Wang et al., 2010). Upon exposing Ad-rtTA-TRE-IκB tg mice to doxycycline, IκBα(S32G-S36A) mRNA gets selectively induced in adipocytes, whereas no expression is observed in other tissues, such as the liver (Figure S4C). When we analyzed the impact of the expression of this anti-inflammatory protein during late gestation and the first 10 days of the postnatal period by exposing both wild-type and transgenic dams to doxycycline, the pups expressing IκBα(S32G-S36A) displayed a reduced IWAT weight, while no effect on body weight was observed (Figure 4C). The adipocyte sizes were, however, similar between genotypes (data not shown), arguing for lower total number of inguinal adipocytes in 10-day-old Ad-rtTA-TRE-IκB tg pups. Similar to the other models, there was no evidence of any dead adipocytes, as judged by perilipin stain (data not shown).

We investigated the metabolic phenotype of Ad-rtTA-TRE-IκB tg mice. We found no difference between genotypes in either body weight or glucose tolerance on doxycycline-supplemented chow (data not shown). Challenging the mice with HFD for 8 weeks, however, revealed a significant difference between genotypes. Ad-rtTA-TRE-IκB tg mice were more glucose intolerant than littermate controls, despite comparable body weights (Figure 4D). Similar to the dnTNF and the RID tg mice, the GWAT weight was reduced, while the liver weights were increased in the HFD-fed Ad-rtTA-TRE-IκB tg mice (Figure 4E). In contrast, there was no difference in IWAT, MWAT, and BAT weights (Figure 4E; data not shown). To assess whether the Ad-rtTA-TRE-IκB tg mice are more susceptible to develop HFD-induced hepatic steatosis, livers were harvested from a second cohort of mice after 1, 6, and 10 weeks on doxycycline-supplemented HFD. We found a strong trend toward increased HFD-induced hepatic steatosis in relation to body weight (Figure S4D). These findings confirm, in a third independent system, that the inability to mount a proinflammatory response in adipose tissue impairs adipose tissue expansion associated with metabolic dysfunction.

Impaired β_3-Adrenergic Receptor Agonist-Induced Adipose Tissue Remodeling in RID tg Mice

The adipose tissue response to chronic β_3-adrenergic receptor (AR) agonist involves a transient acute bout of inflammation and, over time, triggers "browning" of the IWAT as defined by an increased number of multilocular cells expressing uncoupling protein (UCP)-1 (Granneman et al., 2005; Mottillo et al., 2010). There is also evidence for increased adipogenesis in GWAT in response to chronic β_3-AR-agonist treatment (Lee et al., 2012; Wang et al., 2013). We aimed to investigate whether adipose tissue "beiging" depends on a proinflammatory response. We examined one of our models, the RID tg mice and exposed them and their wild-type controls to daily β_3-AR-agonist and bromodeoxyuridine (BrdU) injections for 10 days. Rather dramatic differences were apparent with respect to the response to this chronic β_3-AR-agonist treatment. Wild-type adipose tissues displayed a much "browner" color than the RID tg adipose tissue (Figure 5A), and IWAT contained a large number of multilocular adipocytes, while RID IWAT only displays a modest response in this respect (Figure 5B). In line with these observations, the resulting UCP-1 mRNA levels are also reduced in both IWAT and GWAT in the RID tg mice (Figure S5A). Furthermore, very few BrdU-positive adipocytes were found in GWAT after chronic β_3-AR-agonist in RID tg mice, while several positive cells are found in the wild-type GWAT (Figure 5C). We measured β_3-AR mRNA expression as well as the acute lipolytic response to β_3-AR-agonist treatment and found no difference in β_3-AR expression (Figure S5A). The β_3-AR-agonist-induced serum FFA increase is just marginally affected in the RID mice (Figure S5B). This eliminates receptor abundance and activity as a trivial explanation for these findings. Along the same rationale, receptor abundance and signaling are therefore unlikely to explain the differences in β_3-AR agonist-induced "beiging" between genotypes. We have previously reported that inducible adipocyte-specific expression of VEGF-A leads to a "browning" of adipose tissue, similar to the effects reported for chronic β_3-AR agonist treatment (Sun et al., 2012). Therefore, we speculated that the lack of β_3-AR agonist induced-"beiging" in the RID tg mice may relate to a reduced ability to induce proangiogenic mediators. Indeed, upon examining the gene expression response in IWAT within 3 hr of a single dose of β_3-AR agonist, we find a blunted induction of several proinflammatory cytokines in the RID tg mice (Figure 5D). Furthermore, the mRNA expression levels of classical proangiogenic mediators, such as VEGF-A, angiopoetin-1, and angiopoetin-2 (Angpt1 and Angpt2) are also reduced in the β_3-AR agonist-treated RID tg mice (Figure 5D). Notably, we did not detect an acute β_3-AR agonist-mediated *induction* of these proangiogenic mediators in the wild-type mice. Rather, the difference between genotypes relates mainly to a *downregulation* of these particular genes in response to β_3-AR agonist in the RID tg mice. Thus, in the context of acute β_3-AR agonist stimulation, it seems that a potent inflammatory response is necessary to maintain the expression of VEGF-A, Angpt1, and Angpt2 in IWAT. A comparable gene expression pattern was also seen in GWAT, albeit the individual variation is larger than in IWAT (Figure S5C).

The Reduced MWAT Expansion in the RID tg Mice Is Associated with a "Leaky Gut"

The RID tg mice have a more severe metabolic phenotype than the dnTNF tg and the Ad-rtTA-TRE-IκB tg mice. It caught our attention that the dnTNF tg and the Ad-rtTA-TRE-IκB tg mice display a normal HFD-induced MWAT expansion and mesenteric adipocyte size (data not shown). In contrast, MWAT expansion is dramatically reduced in the RID tg mice (Figure 2D). This indicates

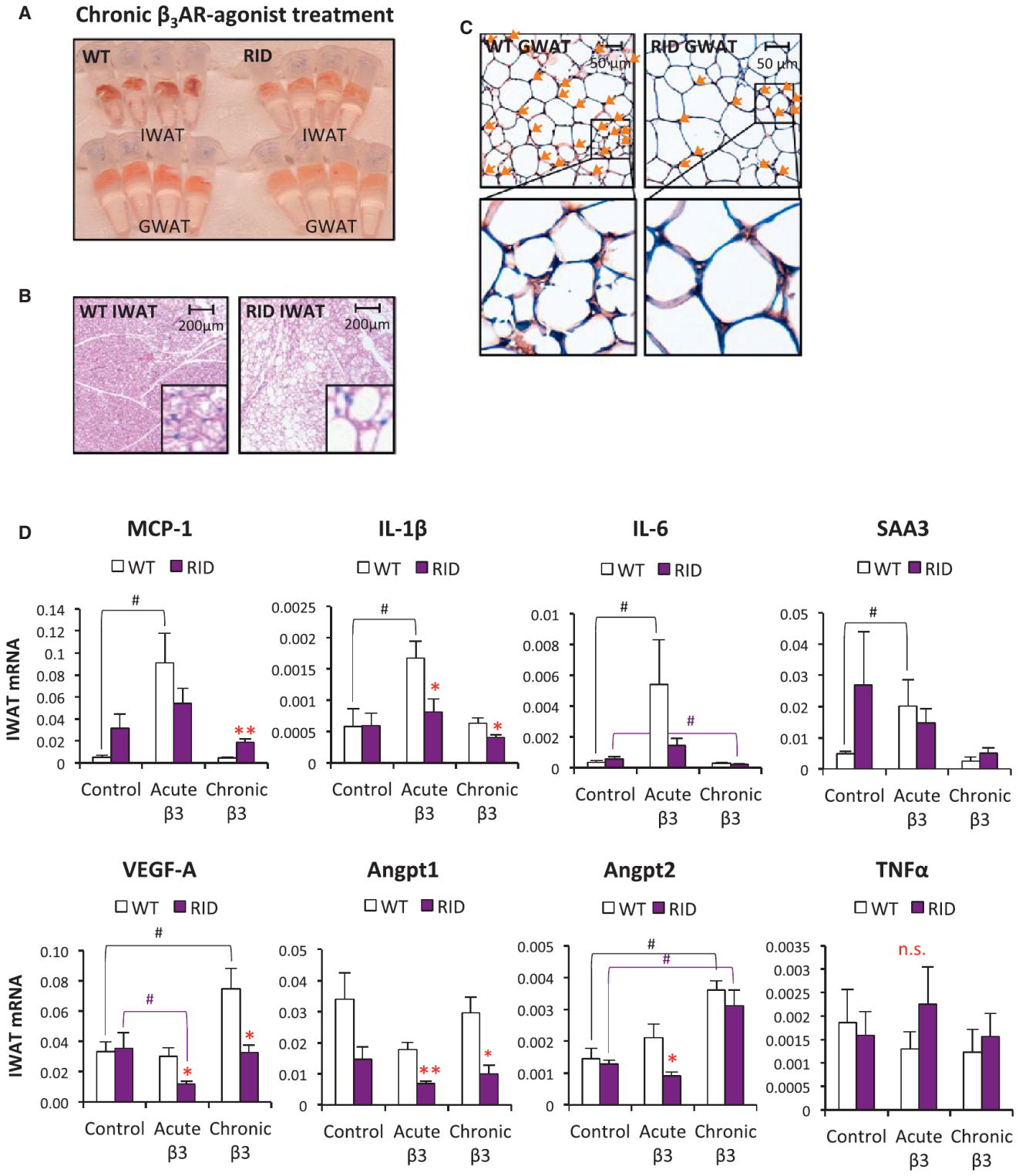

Figure 5. Reduced β_3AR-Agonist-Induced Browning of White Adipose Tissue in RID tg Mice

(A) Photo of IWAT and GWAT harvested from male RID tg and wild-type mice after chronic β_3-AR-agonist treatment (10 days with daily i.p injection with 1 mg/kg in PBS).

(B) Representative H&E stain of IWAT from male RID tg and wild-type mice after chronic β_3-AR-agonist treatment.

(C) Representative BrdU immunostain of GWAT harvested after chronic β_3-AR-agonist treatment (coadministered with 10 mg/kg BrdU) in male RID tg and wild-type mice. Orange arrows point toward BrdU-positive nuclei.

(legend continued on next page)

that inhibition of inflammatory signaling in our mouse models is compensated for by an increase in other inflammatory signaling pathways in the mesenteric area. These compensatory mechanisms are, however, not present or effective in GWAT or IWAT. Moreover, the glucose intolerance seen in young unchallenged RID tg mice cannot be explained by hepatic steatosis, since comparably low levels of hepatic lipids are seen between chow-fed wild-type and RID tg mice, at least while the body weights are <30 g (Figure 6A). We noted, however, that SAA levels are increased and both the liver size and the average size of the individual hepatocytes are enlarged in the chow-fed RID tg mice, even in the absence of steatosis (Figures S2H, 6B, and 6C). Furthermore, the spleens of the RID tg mice are also enlarged (Figure 6D). Taken together, these observations argue for a state of elevated hepatic stress and increased systemic immune activation in the RID tg mice. A likely explanation for these phenomena is an increased exposure to bacterial toxins that are leaking out from the gut. In line with this hypothesis, we found elevated levels of anti-LPS IgGs and increased intestinal permeability as judged by the circulating levels of FITC-dextran after an oral load in young RID tg mice (6–8 weeks old with a body weight of $\leq$20 g) on a chow diet (Figures 6E and 6F). Treatment with 2% dextran sulfate sodium (DSS) through drinking water, which damages the colonic epithelium, increases permeability and causes colitis, leads to a further elevation of anti-LPS IgGs levels and serves as a positive control for the plasma anti-LPS IgG assay (Figure 6E). The colons of the DSS-treated RID tg mice display increased pathological changes, such as an increased degree of colon hyperplasia, more severe crypt disruption and leukocyte infiltration, and further increased spleen size compared to the DSS-treated wild-type mice (Figures 6G and 6H). Furthermore, the DSS-treated RID tg mice have increased expression of CD14, TLR4, TNF-α, MCP-1, MIP-1α, F4/80, and MPO mRNA in colon, which supports the histological findings and indicates that there is a higher degree of inflammation, with enhanced recruitment/infiltration of macrophages and neutrophils, compared to the DSS-treated wild-type mice (Figure 7A). It should also be noted that even the non-DSS-treated RID tg mice display mild colon hyperplasia and elevated colon expression of CD14 and SAA3 mRNA (Figures 6G and 7A).

Despite the lack of an effect on body weight, DSS treatment does, however, impair glucose tolerance in regular wild-type mice (Figure S6A). This suggests that impaired intestinal barrier function alone (even in the absence of HFD) can have a negative impact on systemic metabolic regulation. This also suggests that at least some of the RID tg phenotype may be improved if exposure to bacterial toxins is limited. We put this hypothesis to the test and found that indeed, a 5-week antibiotics treatment normalizes spleen size and insulin levels in the transgenic mice (Figures 7B and 7C). To a large extent, the expression of the liver acute phase reactants SAA1 and SAA2 is also lowered to levels seen in the untreated wild-type mice (Figure 7D). These data suggest that RID tg mice suffer from impaired intestinal barrier function, leading to "leaky gut" and colitis. This also provides an explanation for their hepatomegaly, spleen enlargement, and glucose intolerance, even in the absence of an exogenous inflammatory challenge.

In contrast to the RID tg mice, the dnTNF tg and the Ad-rtTA-TRE-IκB tg mice, with their associated normal MWAT expansion, do not display hepatomegaly, enlarged spleen, or colon hyperplasia (data not shown). This leads us to conclude that MWAT inflammation and its subsequent expansion is an adaptive response that plays a significant role in sustaining proper intestinal barrier function and healthy symbiosis between the commensal microflora and the host.

The intestinal barrier is, however, not only preventing bacterial toxins from leaking out, but it also contributes to a healthy symbiosis with colonizing bacteria. An impaired intestinal barrier and/or chronic inflammation may lead to unfavorable shifts in microbial composition. This is based on the observation that gut flora can be transferred from mouse to mouse and affect the pathogenesis of obesity and hepatic steatosis (Garrett et al., 2010; Henao-Mejia et al., 2012). As expected, we found a difference in bacterial composition as judged by qPCR analysis of eight different bacterial strains of DNA isolated from cecal content from wild-type and RID tg mice housed in different cages. Cecal levels of *Lactobacillus murinus*, *Mucispirillum Schaedleri*, and *Eubacterium Plexicaudatum* were increased, and there was a trend for reduced levels of *Firmicutes sp.* In contrast, the levels of *Lactobacillus sp.*, *Clostridium sp.*, and *B. Distasonis-Porphyromonas* were similar between RID tg and wild-type mice (Figure S6B). Differences in bacterial composition are not necessarily a reflection of a direct negative effect of the RID tg transgene on intestinal barrier function but can also be secondary to metabolic disturbances and also differ between litters and cages. Importantly, the metabolic dysfunction in RID tg is apparent regardless of whether the mice under comparison are littermates or not. Furthermore, there is no difference in either HFD-induced body weight gain, glucose tolerance, insulin levels, or hepatic steatosis in wild-type mice cohoused either with unrelated wild-type mice or with RID tg (data not shown). Thus, the potential negative effect of an altered bacterial composition in the RID tg mice is not potent enough to have an impact on metabolic health in the context of a normal immune defense in wild-type mice. We can also conclude that the wild-type gut flora does not offer a significant protective effect on the metabolic phenotype in the RID tg mice.

DISCUSSION

The data presented here argue that a reduced ability to sense and respond to proinflammatory stimuli at the level of the adipocyte decreases the capacity for healthy adipose tissue expansion and remodeling. This inability results in increased HFD-induced hepatic steatosis and metabolic dysfunction. Interestingly, while the ability to sense proinflammatory cues that trigger expansion is of importance for all fat pads, a

(D) Gene expression analyses of IWAT 3 hr (acute) after β_3-AR-agonist injection and after chronic treatment (IWAT harvested 24 hr after last injection) in male RID tg and wild-type mice. Error bars represent SEM; $p < 0.05$ according to Student's t test was considered significant and is indicated by */#; **/##$p < 0.01$ (*significantly different from WT, #significantly different from untreated controls of same genotype). Additional one-way ANOVA analyses have been performed for Figure 4D (Table S3).

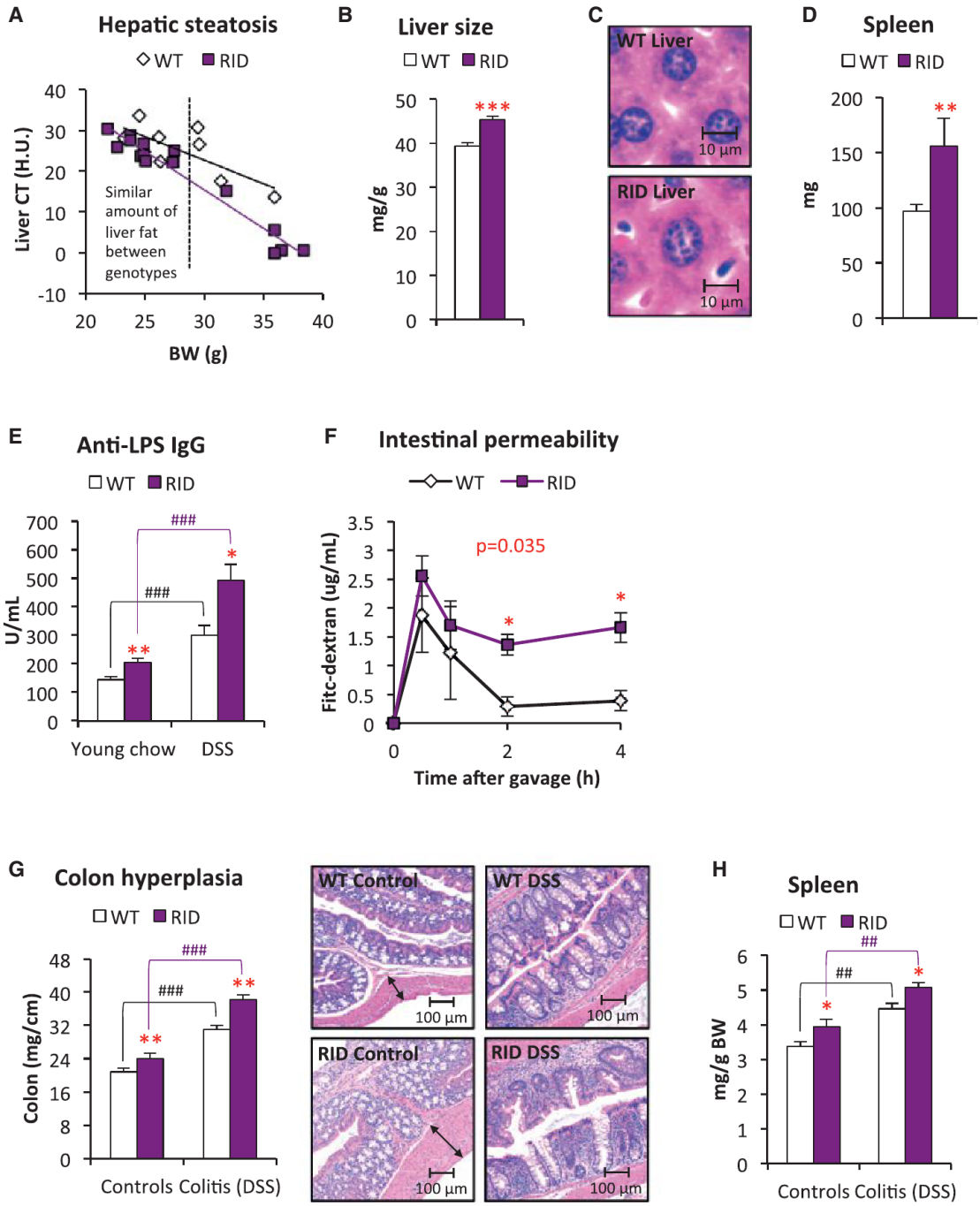

Figure 6. Leaky Gut and Colitis Associated with Signs of Systemic Inflammation in RID tg Mice

(A) Liver fat quantified by CT in chow-fed male RID tg and wild-type mice.

(B and C) (B) Liver weight and (C) representative H&E stain of liver sections to show hepatocyte size in chow-fed male RID tg and wild-type mice with a body weight < 30 g.

(D) Spleen size in chow-fed RIDs chow-fed male RID tg and wild-type mice.

(E) Serum levels of anti-LPS IgG in young chow-fed versus DSS-treated male RID tg and wild-type mice. One-way ANOVA analysis shows that both treatment ($F = 78.8$, $p < 0.001$) and genotype ($F = 26.4$, $p < 0.001$) contribute significantly to anti-LPS IgG levels.

(F) Serum levels of FITC-dextran after an oral load in young chow-fed female RID tg and wild-type mice.

(G and H) (G) Colon weight/length ratios, representative H&E images of colon, and (H) spleen weight in untreated, and in response to DSS-treated, male RID tg and wild-type mice. One-way ANOVA analysis shows that both treatment ($F = 153.6/47.3$, $p < 0.001/< 0.001$) and genotype ($F = 27.4/13.9$, $p < 0.001/0.05$) contribute significantly to both colon thickness and spleen size. Error bars represent SEM; $p < 0.05$ according to Student's t test was considered significant and is indicated by */#; **/##$p < 0.01$; ***/###$p < 0.001$ (*significantly different from WT, #significantly different from untreated controls of same genotype). p value in red indicates differences between groups during time course according to repeated-measurement ANOVA.

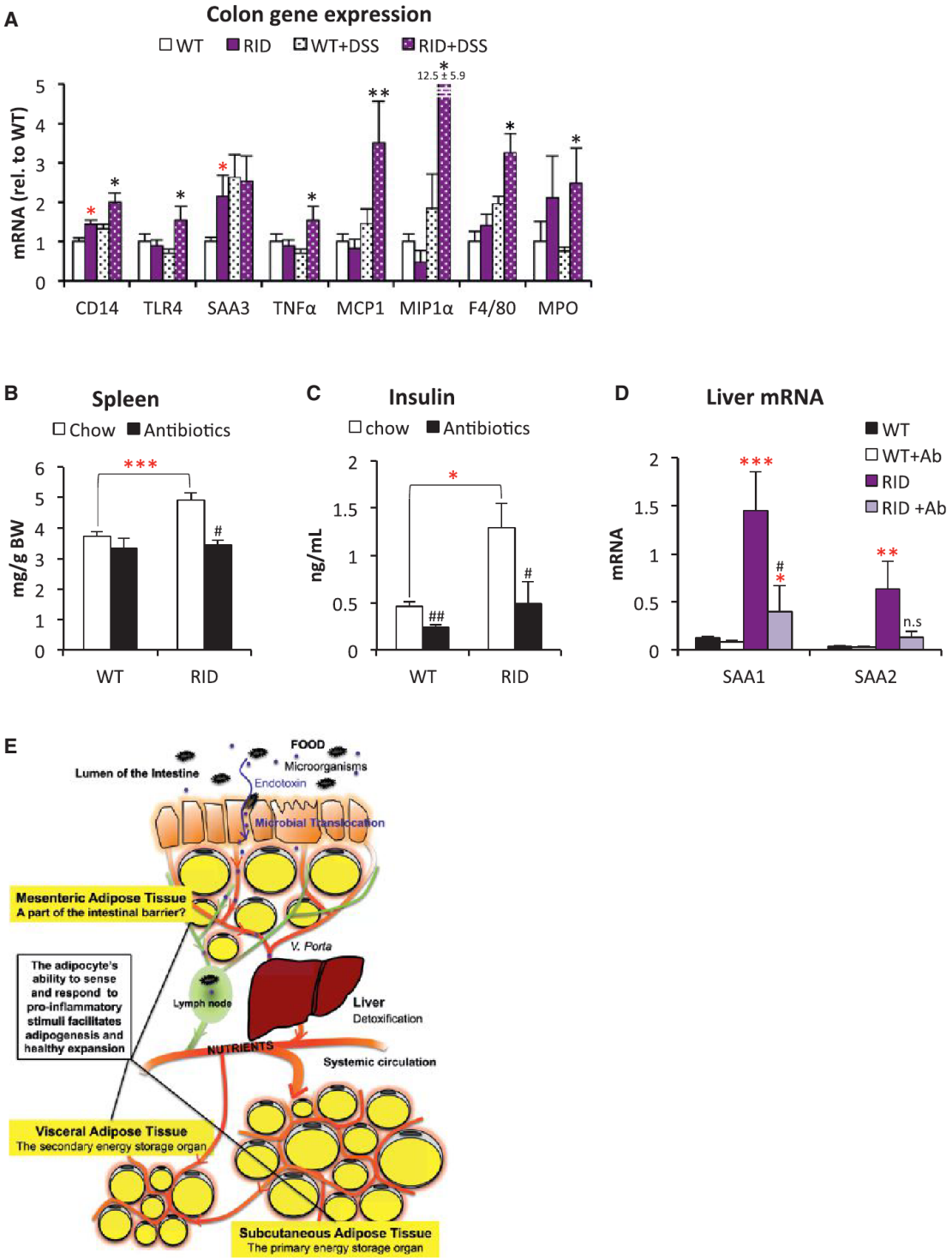

Figure 7. Antibiotics Treatment Improves the RID tg Mouse Phenotype

(A) Gene expression analysis of proximal colon in untreated, and in response to three bouts of DSS treatments, in male RID tg and wild-type mice.

(B–D) (B) Spleen, (C) fasting serum-insulin, and (D) SAA1 and SAA2 mRNA levels in liver in control or antibiotic-treated male RID tg and wild-type mice. One-way ANOVA analysis shows that both treatment ($F = 15.8/8.7/12.1/5.8$, $p = 0.001/0.003/0.004/0.03$) and genotype ($F = 19.3/17.1/23.6/31.8$, $p < 0.001/0.001/ < 0.001/ < 0.001$) contribute significantly to spleen size, insulin levels, liver SAA1, and liver SAA2 levels.

(E) Summary and proposed model: Acute inflammation is essential for healthy adipose tissue expansion and proper remodeling. Inability of adipose tissue to accurately sense and respond to inflammatory stimuli leads to reduced adipose tissue expansion and an increased risk for microbial translocation. Error bars represent SEM; $p < 0.05$ according to Student's t test was considered significant and is indicated by */#; **/##$p < 0.01$; ***$p < 0.001$ (*significantly different from WT, #significantly different from untreated controls of same genotype).

deficiency in this regard has particularly profound consequences for the functionality of the visceral MWAT depot. We observe that the lack of MWAT expansion is associated with increased intestinal permeability and colitis, resulting in chronic systemic inflammation and metabolic dysfunction, even in the absence of HFD.

The Underlying Mechanism for Inflammation-Induced Adipose Tissue Expansion

Adipose tissue expands either through hypertrophy of existing adipocytes or adipogenesis, i.e., differentiation of new adipocytes from adipogenic precursor cells. All models studied here establish a reduced number of adipocytes in most depots examined. Chronic HFD feeding leads to a more pronounced GWAT depot weight difference, while the IWAT depot weight differences between tg and wild-type mice are reduced. Nevertheless, both GWAT and IWAT depots are at all times populated by fewer adipocytes in the transgenic mice than in the wild-type mice, reflecting a reduced rate of adipogenesis. Thus, the ability to mount an acute inflammatory response is playing a more important role in facilitating adipogenesis than in adipocyte hypertrophy.

The concept of inflammation-driven adipogenesis may seem contradictory at first, since proinflammatory cytokines, such as TNF-α, are lipolytic and block adipocyte differentiation in vitro (Gustafson and Smith, 2006). The situation in vitro is, however, substantially different from the situation in vivo, since there is neither a need for angiogenesis nor ECM remodeling under in vitro conditions. In fact, several older studies support a role of local inflammation in increased adipogenesis. For instance, Sadler and colleagues show that low-dose LPS leads to adipocyte hyperplasia at the site of administration (Sadler et al., 2005), and there is a selective increase in the amount of MWAT in Crohn's disease as well as in experimentally induced colitis (Gambero et al., 2007; Sheehan et al., 1992). Moreover, a very recent study on proliferation and differentiation of PDGFRα$^+$ adipocyte progenitors in vivo demonstrates that different adipogenic conditions are associated with an upregulation of different sets of inflammatory and macrophage-associated genes in white adipose tissue (Lee et al., 2013).

It is likely that several distinct mechanisms contribute toward the inflammation-driven adipogenic response, with several interconnected processes triggering adipose tissue growth. Here, we found that HFD feeding acutely (within days) leads to a reduction of the total levels of collagen in IWAT in wild-type mice, but not to the same extent in the dnTNF and the RID tg mice. Thus, healthy adipose tissue expansion is associated with a net loss of adipose tissue collagen, while dysfunctional adipose tissue in more advanced obesity displays an increased number of ECM deposits, along with chronic inflammation and hypoxia. The inability to effectively degrade ECM limits the capacity for healthy adipose tissue expansion. RID tg adipose tissue also has a reduced capillary density. In line with this finding, the capillary density of wild-type MWAT gets reduced by ablation of gut microbiota. These data demonstrate that proinflammatory responses in adipose tissue are essential for both proper ECM remodeling and angiogenesis, two processes known to facilitate adipogenesis in vivo, and therefore are likely mediators of the inflammation-induced adipose tissue expansion phenomenon (Cao, 2007; Cristancho and Lazar, 2011).

Chronic systemic inflammation interferes with optimal metabolic fitness. However, in light of our findings in three independent adipocyte anti-inflammatory models (summarized in Table S1), the view of adipose inflammation as a driving force for systemic inflammation and metabolic dysfunction is an oversimplification. Rather, we postulate that a potent acute inflammatory response is essential for adipose tissue protection, remodeling, and expansion (Figure 7E). This facilitates the return to a healthy equilibrium with metabolic homeostasis that subsequently allows the inflammation to reach resolution as opposed to becoming chronic.

EXPERIMENTAL PROCEDURES

Animals

Adipochaser mice were described in Wang et al. (2013). aP2-dnTNF, aP2-RID, and TRE-IκBα(S32G-S36A) transgenic mice were used in a pure C57B6/J (dnTNF and TRE-IκB) or on a FVB background (RID). Mice were maintained on a 12 hr dark/light cycle and housed in groups of four to five with unlimited access to water, chow (number 5058, Lab-Diet) or HFD (number D12492, Research Diets Inc.) as indicated for the individual experiments. In all experiments, littermate controls were used unless specifically stated otherwise. The Institutional Animal Care and Use Committee of the University of Texas Southwestern Medical Center, Dallas, has approved all animal experiments.

LPS-Induced Adipogenesis

Adipochaser mice were fed doxycycline-supplemented chow (600 mg/kg) for 1 week and were thereafter switched to regular chow 3 days prior the experiment. The right IWAT depot of adipochaser mice was injected twice a week for 2 weeks with 20 μg lipopolysaccharide (LPS, Sigma, USA) in 50 μl PBS, while the left IWAT depot remained untreated. Five weeks later, tissues were harvested for X-Gal-LacZ staining (performed as previously described [Wang et al., 2013]).

LPS and TNFα Response In Vivo

The mice received one intraperitoneal injection with 0.3 mg/kg LPS in PBS or 0.5 μg/mouse TNFα (recombinant mouse TNFα, Biolegend, USA) in PBS supplemented with 1% BSA. Blood was collected from the tail at indicated time points.

Oral Glucose Tolerance Test

The mice were fasted for 3 hr during the light phase, and blood samples were drawn from the tail vein before and 15, 30, 60, and 120 min after an intragastric load with 2.5 g/kg glucose in PBS.

Adipose Tissue Collagen Levels Measurements

Pieces of IWAT (~50 mg) were snap frozen in N_2 (l) until analysis. The total collagen content was measured, using a commercial kit (QuickZyme Biosciences, Netherlands).

Hepatic Steatosis Measurements

Quantification of hepatic steatosis was performed by computerized tomography (CT) or standard biochemical tissue triglyceride analysis. The CT analysis was performed as previously described (Asterholm and Scherer, 2010). In brief, mice were anesthetized with Isoflurane, and a CT scan was performed at a resolution of 93 μm using the short scan mode (180°) on an eXplore Locus in vivo MicroCT Scanner from GE Healthcare. Liver lipid content was estimated by obtaining the average CT value in multiple regions well within the liver, as validated in Asterholm and Scherer (2010).

Intestinal Permeability Assay In Vivo

The mice were fasted for 5 hr; thereafter they were given an oral load with 0.6 mg/g FITC-labeled dextran (average mole weight 4000, Sigma). Blood samples were collected at indicated time points and the serum was diluted two times in PBS and loaded together with known standards diluted

in 50/50 PBS/control serum on a 96-well plate and analyzed (485 nm_{ex}, 535 nm_{em}) on a POLARstar Optima Analyzer.

Statistical Analysis

Data are in generally expressed as mean ± SEM. The Student's t test and one- or two-way ANOVA (repeated measurement) were used for comparisons between groups; log transformation was performed as necessary to obtain normal distribution. SPSS software (version 21) was used for these statistical calculations; *$p < 0.05$ was considered significant; **$p < 0.01$; ***$p < 0.001$.

SUPPLEMENTAL INFORMATION

Supplemental information includes Supplemental Experimental Procedures, six figures, and three tables and can be found with this article online at http://dx.doi.org/10.1016/j.cmet.2014.05.005.

AUTHOR CONTRIBUTIONS

I.W.A. designed the study, carried out the research, interpreted the results, and wrote the manuscript. C.T., T.S.M., Q.A.W., F.D.-L., and Z.V.W. assisted in study design, performed research, and reviewed the manuscript. P.E.S. designed the study, analyzed the data, reviewed and revised the manuscript, and is responsible for the integrity of this work. All authors approved the final version of the manuscript.

ACKNOWLEDGMENTS

We would like to thank Dr. David E. Szymkowski from Xencor Inc. for providing the cDNA constructs encoding dnTNFα and for his guidance on the experimental design. We thank Dr. Bob Hammer and the Transgenic Core Facility at UTSW for the generation of the transgenic lines, Dr. Lora Hooper for advice on the antibiotics experiments, John Shelton and the Histology Core for assistance with histology, and the UTSW Metabolic Core Unit for help in phenotyping. Supported by the National Institutes of Health (grants R01-DK55758, R01- DK099110, and P01DK088761 to P.E.S.). I.W.A. is supported by the Throne-Holst Foundation, the Swedish Research Council (2006-3931 and 2012-1601), VINNOVA (2011-01336), and NovoNordisk Excellence Project Award. Z.V.W. is supported by a postdoctoral fellowship from the American Heart Association (10POST4320009), Q.A.W. is supported by a postdoctoral fellowship from the American Diabetes Association (7-11-MN-47), and T.S.M. is supported by NIH Training Grant T32-GM083831.

Received: February 11, 2014
Revised: April 9, 2014
Accepted: April 28, 2014
Published: June 12, 2014

REFERENCES

Asterholm, I.W., and Scherer, P.E. (2010). Enhanced metabolic flexibility associated with elevated adiponectin levels. Am. J. Pathol. *176*, 1364–1376.

Asterholm, I.W., McDonald, J., Blanchard, P.G., Sinha, M., Xiao, Q., Mistry, J., Rutkowski, J.M., Deshaies, Y., Brekken, R.A., and Scherer, P.E. (2012). Lack of "immunological fitness" during fasting in metabolically challenged animals. J. Lipid Res. *53*, 1254–1267.

Cao, Y. (2007). Angiogenesis modulates adipogenesis and obesity. J. Clin. Invest. *117*, 2362–2368.

Cristancho, A.G., and Lazar, M.A. (2011). Forming functional fat: a growing understanding of adipocyte differentiation. Nat. Rev. Mol. Cell Biol. *12*, 722–734.

Delgado-Lopez, F., and Horwitz, M.S. (2006). Adenovirus RIDalphabeta complex inhibits lipopolysaccharide signaling without altering TLR4 cell surface expression. J Virol *80*, 6378–6386.

Engelman, J.A., Berg, A.H., Lewis, R.Y., Lisanti, M.P., and Scherer, P.E. (2000). Tumor necrosis factor alpha-mediated insulin resistance, but not dedifferentiation, is abrogated by MEK1/2 inhibitors in 3T3-L1 adipocytes. Mol. Endocrinol. *14*, 1557–1569.

Gambero, A., Marostica, M., Abdalla Saad, M.J., and Pedrazzoli, J., Jr. (2007). Mesenteric adipose tissue alterations resulting from experimental reactivated colitis. Inflamm. Bowel Dis. *13*, 1357–1364.

Garrett, W.S., Gordon, J.I., and Glimcher, L.H. (2010). Homeostasis and inflammation in the intestine. Cell *140*, 859–870.

Granneman, J.G., Li, P., Zhu, Z., and Lu, Y. (2005). Metabolic and cellular plasticity in white adipose tissue I: effects of beta3-adrenergic receptor activation. Am. J. Physiol. Endocrinol. Metab. *289*, E608–E616.

Gustafson, B., and Smith, U. (2006). Cytokines promote Wnt signaling and inflammation and impair the normal differentiation and lipid accumulation in 3T3-L1 preadipocytes. J. Biol. Chem. *281*, 9507–9516.

Halberg, N., Khan, T., Trujillo, M.E., Wernstedt-Asterholm, I., Attie, A.D., Sherwani, S., Wang, Z.V., Landskroner-Eiger, S., Dineen, S., Magalang, U.J., et al. (2009). Hypoxia-inducible factor 1alpha induces fibrosis and insulin resistance in white adipose tissue. Mol. Cell. Biol. *29*, 4467–4483.

Henao-Mejia, J., Elinav, E., Jin, C., Hao, L., Mehal, W.Z., Strowig, T., Thaiss, C.A., Kau, A.L., Eisenbarth, S.C., Jurczak, M.J., et al. (2012). Inflammasome-mediated dysbiosis regulates progression of NAFLD and obesity. Nature *482*, 179–185.

Heo, S.C., Jeon, E.S., Lee, I.H., Kim, H.S., Kim, M.B., and Kim, J.H. (2011). Tumor necrosis factor-alpha-activated human adipose tissue-derived mesenchymal stem cells accelerate cutaneous wound healing through paracrine mechanisms. J. Invest. Dermatol. *131*, 1559–1567.

Hotamisligil, G.S., Shargill, N.S., and Spiegelman, B.M. (1993). Adipose expression of tumor necrosis factor-alpha: direct role in obesity-linked insulin resistance. Science *259*, 87–91.

Khan, T., Muise, E.S., Iyengar, P., Wang, Z.V., Chandalia, M., Abate, N., Zhang, B.B., Bonaldo, P., Chua, S., and Scherer, P.E. (2009). Metabolic dysregulation and adipose tissue fibrosis: role of collagen VI. Mol. Cell. Biol. *29*, 1575–1591.

Lee, Y.H., Petkova, A.P., Mottillo, E.P., and Granneman, J.G. (2012). In vivo identification of bipotential adipocyte progenitors recruited by beta3-adrenoceptor activation and high-fat feeding. Cell Metab. *15*, 480–491.

Lee, Y.H., Petkova, A.P., and Granneman, J.G. (2013). Identification of an adipogenic niche for adipose tissue remodeling and restoration. Cell Metab. *18*, 355–367.

Lichtenstein, D.L., Toth, K., Doronin, K., Tollefson, A.E., and Wold, W.S. (2004). Functions and mechanisms of action of the adenovirus E3 proteins. Int. Rev. Immunol. *23*, 75–111.

Magne, J., Mariotti, F., Fischer, R., Mathe, V., Tome, D., and Huneau, J.F. (2010). Early postprandial low-grade inflammation after high-fat meal in healthy rats: possible involvement of visceral adipose tissue. J. Nutr. Biochem. *21*, 550–555.

Mottillo, E.P., Shen, X.J., and Granneman, J.G. (2010). beta3-adrenergic receptor induction of adipocyte inflammation requires lipolytic activation of stress kinases p38 and JNK. Biochim. Biophys. Acta *1801*, 1048–1055.

Park, J., Euhus, D.M., and Scherer, P.E. (2011). Paracrine and endocrine effects of adipose tissue on cancer development and progression. Endocr. Rev. *32*, 550–570.

Rakoff-Nahoum, S., Paglino, J., Eslami-Varzaneh, F., Edberg, S., and Medzhitov, R. (2004). Recognition of commensal microflora by toll-like receptors is required for intestinal homeostasis. Cell *118*, 229–241.

Sadler, D., Mattacks, C.A., and Pond, C.M. (2005). Changes in adipocytes and dendritic cells in lymph node containing adipose depots during and after many weeks of mild inflammation. J. Anat. *207*, 769–781.

Saika, S., Ikeda, K., Yamanaka, O., Flanders, K.C., Okada, Y., Miyamoto, T., Kitano, A., Ooshima, A., Nakajima, Y., Ohnishi, Y., et al. (2006). Loss of tumor necrosis factor alpha potentiates transforming growth factor beta-mediated pathogenic tissue response during wound healing. Am. J. Pathol. *168*, 1848–1860.

Sheehan, A.L., Warren, B.F., Gear, M.W., and Shepherd, N.A. (1992). Fat-wrapping in Crohn's disease: pathological basis and relevance to surgical practice. Br. J. Surg. *79*, 955–958.

Steed, P.M., Tansey, M.G., Zalevsky, J., Zhukovsky, E.A., Desjarlais, J.R., Szymkowski, D.E., Abbott, C., Carmichael, D., Chan, C., Cherry, L., et al. (2003). Inactivation of TNF signaling by rationally designed dominant-negative TNF variants. Science *301*, 1895–1898.

Sun, K., Wernstedt Asterholm, I., Kusminski, C.M., Bueno, A.C., Wang, Z.V., Pollard, J.W., Brekken, R.A., and Scherer, P.E. (2012). Dichotomous effects of VEGF-A on adipose tissue dysfunction. Proc. Natl. Acad. Sci. USA *109*, 5874–5879.

Wang, Z.V., Deng, Y., Wang, Q.A., Sun, K., and Scherer, P.E. (2010). Identification and characterization of a promoter cassette conferring adipocyte-specific gene expression. Endocrinology *151*, 2933–2939.

Wang, Q.A., Tao, C., Gupta, R.K., and Scherer, P.E. (2013). Tracking adipogenesis during white adipose tissue development, expansion and regeneration. Nat. Med. *19*, 1338–1344.

Cell Metabolism
Article

Partial and Transient Reduction of Glycolysis by PFKFB3 Blockade Reduces Pathological Angiogenesis

Sandra Schoors,[1,2,8] Katrien De Bock,[1,2,8] Anna Rita Cantelmo,[1,2,8] Maria Georgiadou,[1,2,8] Bart Ghesquière,[1,2] Sandra Cauwenberghs,[1,2] Anna Kuchnio,[1,2] Brian W. Wong,[1,2] Annelies Quaegebeur,[1,2] Jermaine Goveia,[1,2] Francesco Bifari,[1,2] Xingwu Wang,[1,2] Raquel Blanco,[3] Bieke Tembuyser,[1,2] Ivo Cornelissen,[1,2] Ann Bouché,[1,2] Stefan Vinckier,[1,2] Santiago Diaz-Moralli,[4] Holger Gerhardt,[3,5,6] Sucheta Telang,[7] Marta Cascante,[4] Jason Chesney,[7] Mieke Dewerchin,[1,2,9] and Peter Carmeliet[1,2,9,*]

[1]Laboratory of Angiogenesis and Neurovascular link, Vesalius Research Center, Department of Oncology, University of Leuven, Leuven 3000, Belgium
[2]Laboratory of Angiogenesis and Neurovascular link, Vesalius Research Center, VIB, Leuven 3000, Belgium
[3]Vascular Biology Laboratory, London Research Institute, Cancer Research UK, London WC2A 3LY, UK
[4]Department of Biochemistry and Molecular Biology and IBUB, Universitat de Barcelona, Barcelona 08007, Spain
[5]Vascular Patterning Laboratory, Vesalius Research Center, University of Leuven, Leuven 3000, Belgium
[6]Vascular Patterning Laboratory, Vesalius Research Center, VIB, Leuven 3000, Belgium
[7]James Graham Brown Cancer Center, University of Louisville, Louisville, KY 40202, USA
[8]These authors contributed equally to this work and are co-first authors
[9]These authors contributed equally to this work and are co-last authors
*Correspondence: peter.carmeliet@vib-kuleuven.be
http://dx.doi.org/10.1016/j.cmet.2013.11.008

SUMMARY

Strategies targeting pathological angiogenesis have focused primarily on blocking vascular endothelial growth factor (VEGF), but resistance and insufficient efficacy limit their success, mandating alternative antiangiogenic strategies. We recently provided genetic evidence that the glycolytic activator phosphofructokinase-2/fructose-2,6-bisphosphatase 3 (PFKFB3) promotes vessel formation but did not explore the antiangiogenic therapeutic potential of PFKFB3 blockade. Here, we show that blockade of PFKFB3 by the small molecule 3-(3-pyridinyl)-1-(4-pyridinyl)-2-propen-1-one (3PO) reduced vessel sprouting in endothelial cell (EC) spheroids, zebrafish embryos, and the postnatal mouse retina by inhibiting EC proliferation and migration. 3PO also suppressed vascular hyperbranching induced by inhibition of Notch or VEGF receptor 1 (VEGFR1) and amplified the antiangiogenic effect of VEGF blockade. Although 3PO reduced glycolysis only partially and transiently in vivo, this sufficed to decrease pathological neovascularization in ocular and inflammatory models. These insights may offer therapeutic antiangiogenic opportunities.

INTRODUCTION

Angiogenesis stimulates the progression of numerous disorders. Hence, targeting this process by blocking angiogenic signals such as vascular endothelial growth factor (VEGF) has become a clinically attractive strategy (Singh and Ferrara, 2012). However, insufficient efficacy and resistance limit its success (Ebos and Kerbel, 2011; Potente et al., 2011). Although combination treatment with multiple agents blocking distinct angiogenic signals might offer benefit, a concern remains that angiogenesis relapses through compensation by other angiogenic factors. We therefore explored a fundamentally different antiangiogenic strategy.

Targeting endothelial cell (EC) metabolism for antiangiogenesis has received little attention (De Bock et al., 2013a; Harjes et al., 2012). Since angiogenic signaling pathways converge onto metabolism, and ECs rely on glycolysis for generating most (85%) of their ATP (De Bock et al., 2013b), we hypothesized that targeting glycolysis might provide an alternative therapeutic opportunity for reducing pathological neovascularization. However, given that previous antiglycolytic, anticancer therapies were not always successful (Granchi and Minutolo, 2012; Raez et al., 2013), it was unknown if antiglycolytic strategies could inhibit pathological angiogenesis.

We focused on phosphofructokinase-2/fructose-2,6-bisphosphatase-3 (PFKFB3), since silencing in vitro or inactivation in vivo of this glycolytic activator reduced glycolysis and impaired vessel sprouting (De Bock et al., 2013b). This enzyme is an activator of a key glycolytic enzyme, 6-phosphofructo-1-kinase (PFK-1), which converts fructose-6-phosphate (F6P) to fructose-1,6-bisphosphate ($F1,6P_2$). PFKFB isoenzymes synthesize fructose-2,6-bisphosphate ($F2,6P_2$), an allosteric activator of PFK-1 and potent stimulator of glycolysis (Van Schaftingen et al., 1982). Of all PFKFB isoenzymes, PFKFB3 has a much (700-fold) higher kinase than bisphosphatase activity and promotes production of $F2,6P_2$ and glycolysis (Yalcin et al., 2009). PFKFB3 is also the most abundant isoenzyme in ECs (De Bock et al., 2013b). Here, we characterized the antiangiogenic therapeutic potential of a PFKFB3 inhibitor.

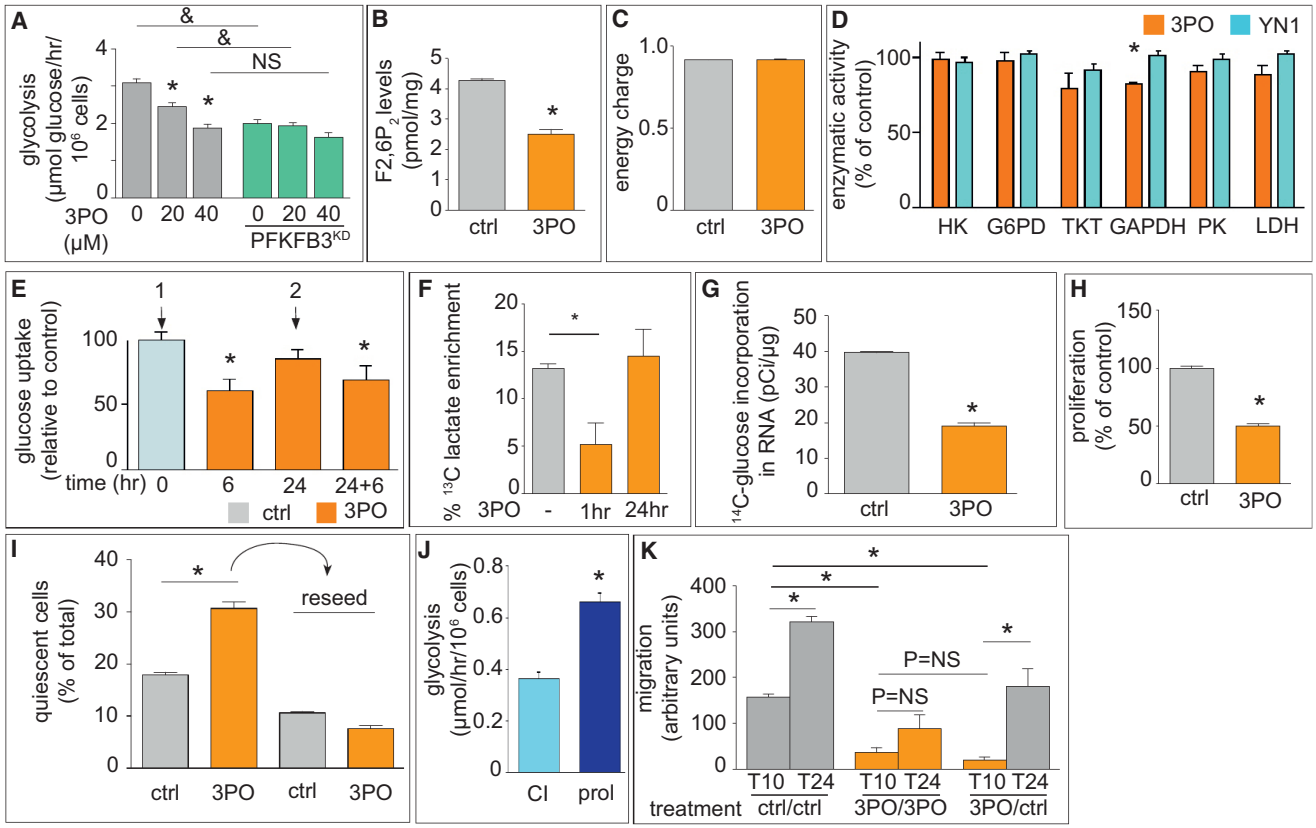

Figure 1. 3PO Inhibits Glycolysis in ECs

(A) Glycolytic flux in control or PFKFB3-silenced ECs, showing that 3PO reduced glycolysis in control cells but was ineffective in further reducing glycolysis in PFKFB3-silenced cells (mean ± SEM; n = 3; *p < 0.05 versus vehicle; &p < 0.05 versus control).

(B) Quantification of fructose-2,6-bisphosphate ($F2,6P_2$) content, showing reduced $F2,6P_2$ levels after PFKFB3 inhibition by 3PO (mean ± SEM; n = 3; *p < 0.05).

(C) PFKFB3 blockade by 3PO did not affect the energy charge ([ATP] + ½[ADP]) / ([ATP] + [ADP] + [AMP]) (mean ± SEM; n = 3; p = not significant [NS]) at 24 hr.

(D) Enzymatic activity of glycolytic enzymes measured in extracts of ECs, treated with a concentration of 3PO or YN1 that effectively inhibited glycolysis, showing that these PFKFB3 blockers failed to affect their enzymatic activity (mean ± SEM; n = 3; *p < 0.05). HK, hexokinase; G6PD, glucose 6-phosphate dehydrogenase; TKT, transketolase; GAPDH, glyceraldehyde 3-phosphate dehydrogenase; PK, pyruvate kinase; LDH, lactate dehydrogenase.

(E) Glucose uptake in vivo, showing that a first injection of 3PO (vertical arrow 1) lowered 2-[1-^{14}C]-DG uptake in the diaphragm modestly and transiently during the first 6 hr, but not after 24 hr. A second administration of 3PO after 24 hr (vertical arrow 2) reduced glucose uptake again to the same level as the first administration (mean ± SEM; n = 3; *p < 0.05).

(F) GC-MS analysis of ^{13}C enrichment in lactate, showing that lactate production from [U-^{13}C]-glucose in the blood was transiently reduced upon 3PO treatment after 1 hr, but not any longer after 24 hr (mean ± SEM; n = 4 for ctrl and n = 5 for 3PO; *p < 0.05 versus vehicle at the same time point).

(G) [6-^{14}C]glucose incorporation assay, showing that 3PO reduced the synthesis of RNA in EC monolayers (mean ± SEM; n = 3; *p < 0.01).

(H) [^{3}H]thymidine incorporation assay, showing that 3PO reduced proliferation of EC monolayers (mean ± SEM; n = 3; *p < 0.01).

(I) FACS quantification of 5-ethynyl-2′-deoxyuridine (EdU^{-}) ECs, showing that 3PO treatment increased the fraction of quiescent ECs. Upon reseeding in the absence of 3PO, ECs reinitiate proliferation (mean ± SEM; n = 3; *p < 0.05).

(J) Glycolytic flux is lower in quiescent ECs (81% ± 3% synchronized in G_0/G_1 by contact inhibition [CI]) than in proliferating (prol) ECs (35% ± 1% in G_0 upon replating) (mean ± SEM; n = 3; *p < 0.05).

(K) Quantification of MitoC-treated EC migration in scratch wound assays over time (10 and 24 hr), showing reduced migration upon PFKFB3 blockade (3PO). When 3PO was removed from the medium 10 hr after the initiation of the treatment, ECs resumed migration (mean ± SEM; n = 3; *p < 0.05). See also Figure S1.

RESULTS

PFKFB3 Blockers Reduce Glycolysis in EC Monolayers In Vitro

To explore if pharmacological blockade of the kinase activity of PFKFB3 reduced glycolysis in human umbilical venous endothelial cells (HUVECs, abbreviated as ECs) and affected vessel sprouting, we used the small molecule compound 3-(3-pyridinyl)-1-(4-pyridinyl)-2-propen-1-one (3PO) (Chesney et al., 1999; Clem et al., 2008). Key findings were confirmed by using 7,8-dihydroxy-3-(4-hydroxyphenyl)-chromen-4-one (YN1), another PFKFB3 blocker (Seo et al., 2011). 3PO and YN1 dose dependently reduced glycolysis in ECs, but by no more than 35%–40% (Figure 1A; Figure S1A available online). 3PO evoked comparable effects in arterial ECs (Figure S1B). PFKFB3 blockade thus reduced glycolysis incompletely, i.e., less than the nonmetabolizable glucose analog 2-deoxy-D-glucose (2DG), which reduced glycolysis by ~80% (Figure S1C). 3PO

also lowered F2,6P_2 levels by 41% (Figure 1B). 3PO, however, did not lower the energy charge (Figure 1C) and, unlike 2DG, did not increase oxygen consumption (Figure S1D).

3PO and YN1 did not inhibit the enzymatic activity of a panel of glycolytic enzymes when analyzing EC lysates (Figure 1D) or purified enzymes (Figures S1E–S1I). When measuring glycolytic flux by using D-[5-^{3}H]-glucose, 3PO did not further reduce glycolysis in ECs in which PFKFB3 was silenced to nearly undetectable protein levels (Figure 1A). YN1 reduced glycolysis in PFKFB3-silenced cells slightly more (Figure S1A), in agreement with its partial effect on PFKFB4 (Seo et al., 2011).

PFKFB3 Blockade Reduces Glycolysis Partially and Transiently In Vivo

We also determined the effect of 3PO on glycolysis in vivo in mice by measuring 2-[1-^{14}C]-deoxy-D-glucose (2-[1-^{14}C]-DG) uptake as an indirect parameter of glycolysis. 3PO lowered 2-[1-^{14}C]-DG uptake by 38% and 41% in the diaphragm and heart, but only transiently during 6 hr (Figure 1E). However, a second administration of 3PO 24 hr later comparably reduced 2-[1-^{14}C]-DG uptake (Figure 1E). Intravenous injection of [U-^{13}C]-glucose and analysis of ^{13}C-lactate enrichment in the blood by gas chromatography-mass spectrometry (GC-MS) confirmed the transient reduction in glycolysis upon 3PO injection (Figure 1F).

PFKFB3 Blockers Reduce EC Proliferation and Migration In Vitro

In EC monolayers, 3PO reduced [6-^{14}C]-glucose incorporation in RNA, a process involving the nonoxidative branch of the pentose phosphate pathway (non-oxPPP) that generates pentoses for nucleotide synthesis (Figure 1G). 3PO also decreased EC proliferation (Figure 1H), in agreement with PFKFB3 silencing data (De Bock et al., 2013b). Instead, 3PO increased the fraction of quiescent ECs (Figure 1I). This effect was reversible, as removal of 3PO restored the fraction of cycling cells (Figure 1I). In accordance, glycolysis was 40% lower in contact-inhibited quiescent ECs than in cycling ECs (Figure 1J). To study EC migration in the absence of confounding effects of proliferation, we treated ECs with mitomycin C (MitoC) to inhibit proliferation. 3PO reduced MitoC-treated EC migration in a scratch wound and modified Boyden chamber assay, and the effects were reversible upon washout of 3PO (Figure 1K; Figure S1J). Similar data were obtained for YN1 (Figures S1K and S1L).

PFKFB3 Blockers Impair Vessel Sprouting In Vitro

To study the effect of PFKFB3 blockers on vessel sprouting, we used EC spheroids. Similar to that in vivo, a tip cell with filopodia-like protrusions takes the lead, while proliferating stalk cells elongate the sprout. PFKFB3 was essential for vessel outgrowth, as both 3PO and YN1 shortened sprout length and decreased sprout numbers (Figures 2A–2D; Figures S2A, S2B, S2D, and S2E), similar to the effect induced by PFKFB3 silencing (De Bock et al., 2013b). 2DG also reduced vessel sprouting (Figures S2C–S2E), but unlike 3PO-treated spheroids that retained a healthy morphology, 2DG-treated spheroids disintegrated and eventually died, as revealed by TO-PRO 3 staining (Figures S2F–S2H), indicating that near-complete inhibition of glycolysis causes cellular demise and death. Counting of Hoechst 33342-stained nuclei revealed that 3PO reduced EC numbers in vascular sprouts (Figures 2E–2G). 3PO also decreased the incorporation of bromodeoxyuridine (BrdU) in spheroid sprout ECs (Figure 2H), indicating that blockade of PFKFB3 impairs sprouting at least partially via reducing EC proliferation. 3PO also impaired EC migration, as it reduced sprouting after MitoC treatment (Figures 2I and 2J). Furthermore, 3PO impeded capillary tube formation (Figures S2I and S2J).

PFKFB3 increases glycolysis but decreases the oxidative pentose phosphate pathway (oxPPP) flux (Herrero-Mendez et al., 2009). This pathway with its rate-limiting enzyme glucose-6-phosphate dehydrogenase (G6PD) generates NADPH, used to reduce oxidized glutathione for antioxidant defense. Notably, 3PO increased the oxPPP flux (Figure 2K) and, consistent with previous reports that the oxPPP promotes angiogenesis (De Bock et al., 2013a; Leopold et al., 2003), blocking the oxPPP by 6-aminonicotinamide (6AN) decreased vessel sprouting (Figures 2L and 2M). However, this increase did not explain the impaired vessel sprouting phenotype by 3PO, since blocking the oxPPP by 6AN did not abrogate the antisprouting activity of 3PO (Figures 2L and 2M). Furthermore, addition of sodium pyruvate at a concentration that increases oxygen consumption (De Bock et al., 2013b) did not rescue the impaired vessel sprouting in 3PO-treated spheroids (Figures S2K and S2L), indicating that diminishing glycolysis by 3PO did not reduce vessel sprouting by diminishing entry of glycolytic intermediates into the tricarboxylic acid (TCA) cycle for oxidative glucose metabolism.

PFKFB3 Blockade Does Not Alter the Expression of Tip- or Stalk-Enriched Genes

We analyzed if PFKFB3 impeded tip or stalk cell formation by reducing the expression of VEGF receptor 2 (VEGFR2) and Dll4, known to influence tip versus stalk cell formation, respectively (Geudens and Gerhardt, 2011; Potente et al., 2011). However, RT-PCR analysis revealed that 3PO did not alter the expression of tip or stalk cell-enriched genes (Figure 2N). Indeed, 3PO did not affect transcript levels of Dll4 or of the Notch1 target genes HES1, HEY1, and HEY2. Expression of VEGFR2 was also not affected by 3PO at the mRNA or protein level (Figure 2N; Figure S2M). Since 2DG interferes with glycosylation by affecting the hexosamine biosynthetic pathway, a side pathway of glycolysis, we examined if 3PO had similar effects. However, VEGFR2 was detected as a fully glycosylated 230 kDa form in 3PO-treated ECs (Figure S2M), suggesting that glycosylation was not impaired. Fluorescence-activated cell sorting (FACS) analysis also failed to reveal a difference in VEGFR2 levels on the cell surface (Figure S2N). Overall, consistent with PFKFB3 loss-of-function studies in ECs (De Bock et al., 2013b), the impaired vessel sprouting by 3PO was not attributable to a change in the expression of tip versus stalk cell signature.

PFKFB3 Blockers Impair Vessel Sprouting in Zebrafish

To explore the functional in vivo relevance of PFKFB3 inhibition, we used *fli1:EGFP^{y1}* zebrafish embryos expressing GFP in ECs and focused on intersomitic vessels (ISVs), which branch off from the dorsal aorta in a ventral-to-dorsal direction and establish the dorsal longitudinal anastomosing vessel (DLAV). We analyzed only viable embryos without developmental defects

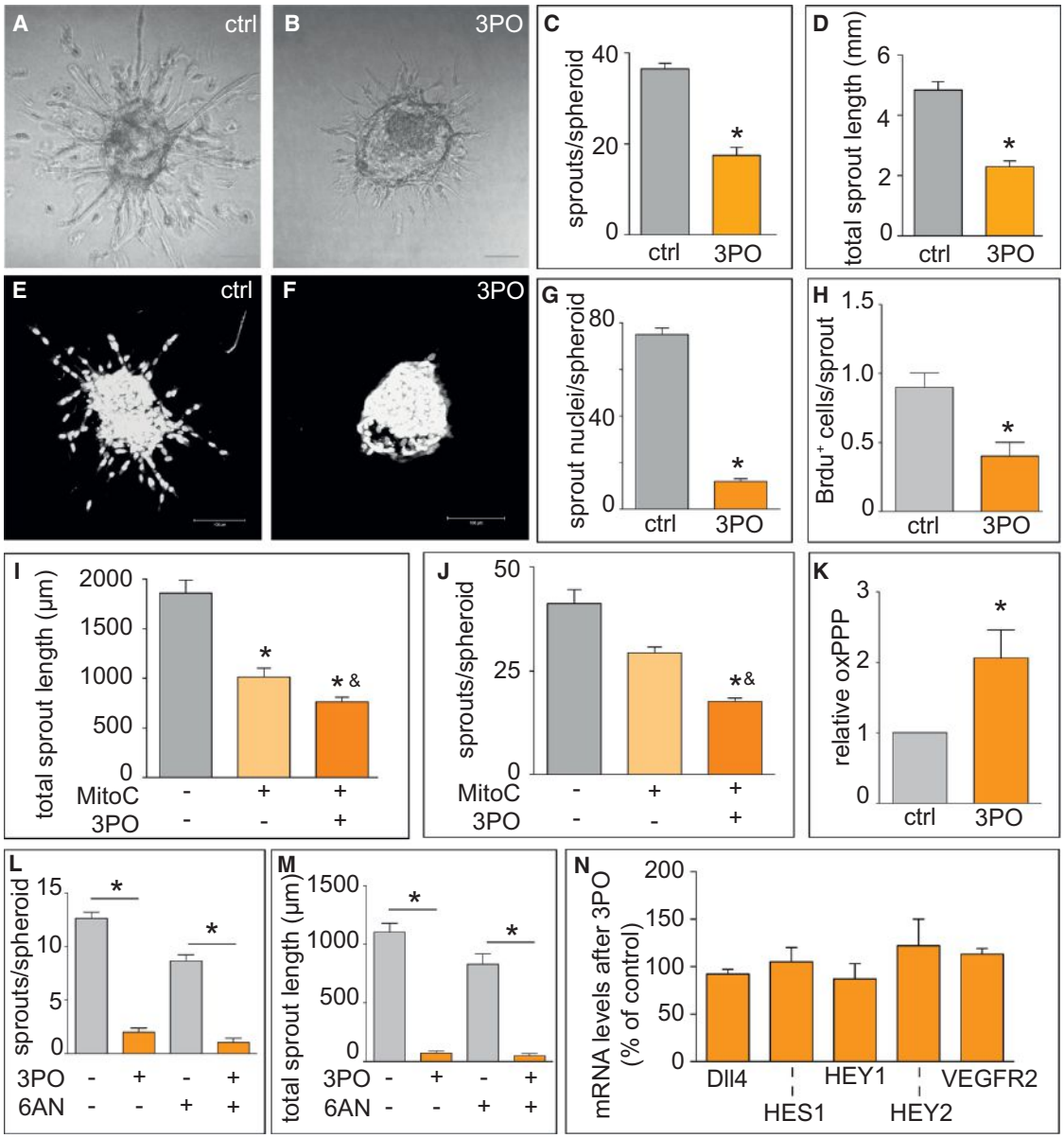

Figure 2. Pharmacological Blockade of PFKFB3 by 3PO Impairs Sprouting In Vitro

(A and B) Representative bright-field micrographs of control (A) and 3PO-treated (B) EC spheroids, showing reduced vascular sprouting in spheroids in the presence of the PFKFB3 inhibitor 3PO (B). Scale bars: 50 μm.

(C and D) Morphometric quantification of EC spheroid sprouting, revealing that blockade of PFKFB3 by 3PO reduced the number of sprouts per spheroid (C) and total sprout length (D) (mean ± SEM; n = 30; *p < 0.01).

(E and F) Representative fluorescence photographs of Hoechst 33342-stained EC spheroids (E), showing a reduced number of EC nuclei in the sprouts of 3PO treated spheroids (F).

(G) Quantification of Hoechst 33342-stained ECs, showing that 3PO treatment reduces the number of nuclei per sprout (mean ± SEM; n = 30 spheroids; *p < 0.001).

(H) Quantification of $BrdU^+$ ECs in spheroid sprouts, showing reduced proliferation upon PFKFB3 blockade by 3PO (mean ± SEM; n = 23 spheroids; *p < 0.005).

(I and J) Morphometric quantification of EC spheroid sprouting, revealing that blockade of PFKFB3 by 3PO reduced the total sprout length (I) and number of sprouts per spheroid (J) even after MitoC-induced mitotic arrest (mean ± SEM; n = 30; *p < 0.05 versus ctrl and $^{\&}$p < 0.05 versus MitoC).

(K) Quantification of oxPPP, showing increased flux upon 3PO treatment (mean ± SEM; n = 4; *p < 0.04).

(L and M) Morphometric quantification of vessel sprouting from EC spheroids upon 6AN treatment, showing that blockade of the oxPPP affects neither the 3PO-induced reduction of the number of sprouts per spheroids (L) nor the total sprout length (M) (mean ± SEM; n = 20; *p < 0.0001).

(N) mRNA expression analysis of DLL4, HES1, HEY1, HEY2, and VEGFR2, showing unaltered expression after PFKFB3 blockade (mean ± SEM; n = 3; p = NS). See also Figure S2.

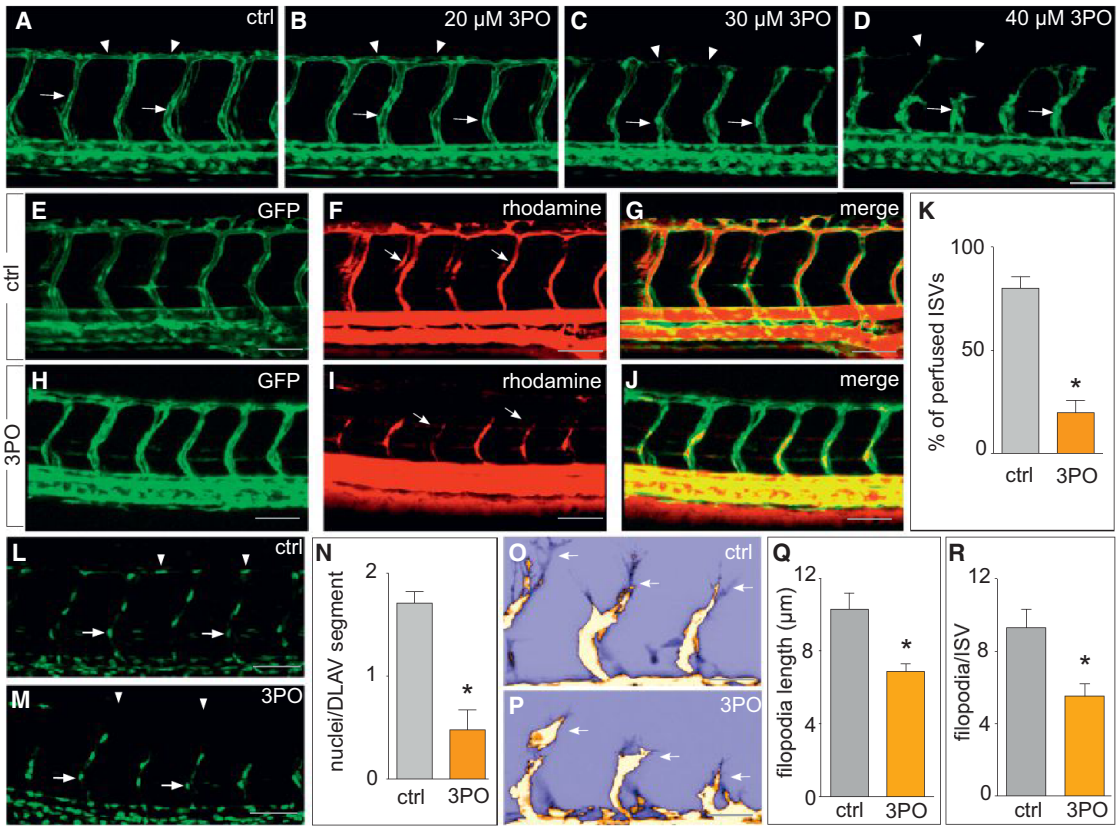

Figure 3. Pharmacological Blockade of PFKFB3 Impairs Vascular Development in Zebrafish Embryos

(A–D) Confocal images of GFP$^+$ vessels in 35 hpf *fli1:EGFP^{y1}* embryos treated with DMSO (ctrl) (A), 3PO (20 μM) (B), 3PO (30 μM) (C), or 3PO (40 μM) (D) from 20 hpf onward, showing impaired outgrowth of ISVs (arrows) and defective formation of the DLAV (arrowheads). Scale bars: 50 μm.

(E–J) Confocal images of 48 hpf *fli1:EGFP^{y1}* embryos after intracardiac angiography with rhodamine-labeled dextran, showing that compared to control embryos, 3PO treatment (40 μM; from 20 hpf onward) reduced ISV perfusion. Control, GFP signal (E); control, rhodamine-dextran signal (F); control, merge (G); 3PO treated, GFP signal (H); 3PO treated, rhodamine-dextran signal (I); 3PO treated, merge (J).

(K) Quantification of perfused ISVs in *Tg(kdrl:EGFP;gata1:DsRed)* zebrafish (mean ± SEM; n = 3 for control and n = 4 for 3PO; *p < 0.001).

(L–N) Confocal images of GFP$^+$ vessels in 35 hpf *fli1:nEGFP^{y7}* zebrafish embryos treated with DMSO (ctrl) (L) or 3PO (40 μM) (M) from 20 hpf onward, showing that 3PO reduced EC numbers in the ISVs (arrows) and in the DLAV (arrowheads), and quantification (N) (mean ± SEM; n = 8 for control and 6 for 3PO; *p < 0.0001).

(O and P) Pseudocolor lookup table (LUT) high-magnification confocal images of GFP$^+$ ISVs in 35 hpf *fli1:EGFP^{y1}* zebrafish embryos showing that compared to controls (O), embryos treated with 3PO (45 μM) have fewer and shorter filopodia (P).

(Q and R) Quantification of the filopodia length (Q) and number (R) (filopodia length: n = 30 for ctrl and n = 20 for 3PO; *p < 0.0001; filopodia number per ISV: n = 4; *p < 0.005). See also Figure S3 and Movie S1.

and with an intact circulation (Figure S3A–S3D). When treating embryos with 3PO from 20 hr postfertilization (hpf) onward, just prior to the onset of ISV sprouting, 3PO dose dependently impaired ISV sprouting (Figures 3A–3D). At 40 μM, only <5% of the embryos formed ISVs, but these vessels had perfusion defects (see below). Time-lapse video imaging of 3PO-treated embryos showed that the ISVs failed to grow out normally and established only an incomplete DLAV (Movie S1). At the highest concentration of 3PO (40 μM), a fraction of ISVs stalled midway, exhibiting blunt ends without side branches or anastomoses, and failed to form a DLAV (Figure 3D). Withdrawal of 3PO reinitiated branching, showing that 3PO did not cause irreversible EC demise (Figures S3E–S3G). Similar results were obtained for YN1 (Figures S3H–S3J). Angiography after intracardiac injection of rhodamine-labeled dextran showed that 3PO reduced the number of perfused ISVs (Figures 3E–3J). Analysis of *Tg(kdrl:EGFP;GATA1:DsRed)* zebrafish, in which vessels are GFP$^+$ and erythrocytes are DsRED$^+$, confirmed these findings (Figure 3K).

Counting of EC nuclei in *fli1:nEGFP^{y7}* zebrafish embryos, expressing GFP in endothelial nuclei, showed that 3PO decreased EC numbers in the DLAV (Figures 3L–3N). In addition, time-lapse video imaging revealed that 3PO altered the leading edge of the vascular front, where tip cells reside. In contrast to the rapidly advancing and dynamically exploring vascular front in control embryos, tip cells in 3PO-treated embryos were less dynamic and exploratory and moved more slowly, almost creeping forward (Movie S1). In control embryos, tip cells were polarized in a rear-to-front direction, often projecting at the leading edge two to three ''foot-like'' cytosolic protrusions (2–3 μm wide) from where multiple, rapidly moving, and highly motile long filopodia extended (Figures 3O–3R). By contrast, in 3PO-treated embryos, tip cells projected shorter, thinner, and more blunt-ended ''foot-like''

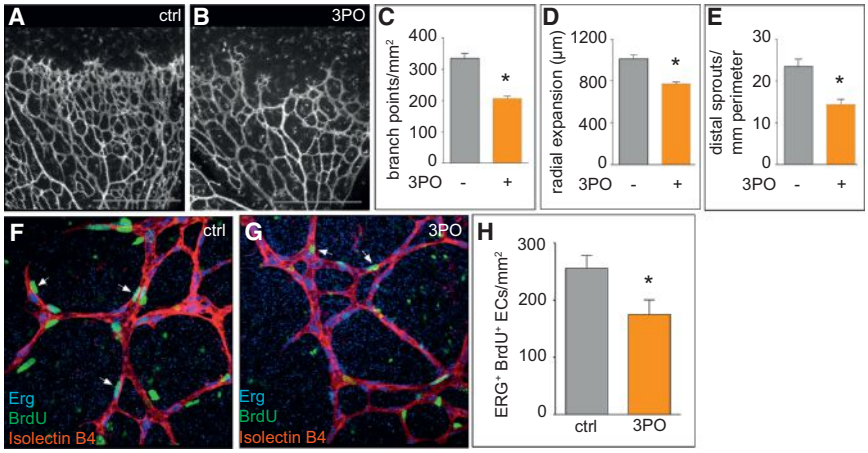

Figure 4. Pharmacological PFKFB3 Blockade Impairs Vascular Development in Mice

(A and B) Confocal images of isolectin-B4-stained (gray) retinal vessels of postnatal day 5 (P5) pups at high magnification, showing, as compared to DMSO-treated mice (A), reduced vascular branching in 3PO-treated mice (50 mg/kg) (B). Scale bars: 50 μm.

(C–E) Quantification of the effect of 3PO treatment on the number of branch points (C), radial expansion (D), and the number of distal sprouts with filopodia (E) in the retinal vasculature of 3PO-treated mice (mean ± SEM; n = 3 for ctrl and n = 5 for 3PO; *p < 0.001).

(F and G) Triple staining for Erg (blue), isolectin B4 (red), and BrdU (green) at the vascular front of the retinal plexus of control (F) and 3PO-treated (G) mice confirmed that EC proliferation was reduced in 3PO-treated mice (G) (mean ± SEM; n = 3; p < 0.05). Arrows: proliferating ECs.

(H) Quantification of $BrdU^+$ Erg^+ cells/mm^2 retinal area, revealing lower proliferation of retinal ECs after 3PO treatment (mean ± SEM; n = 3; *p < 0.05). Scale bars: 50 μm. See also Figure S4.

cytosolic protrusions and extended fewer and shorter filopodia (Figures 3O–3R).

PFKFB3 Blockers Impair Vessel Sprouting in the Mouse Retina

We also studied the effects of PFKFB3 blockade on vascular sprouting in the postnatal retina, a widely used mouse model to characterize tip and stalk cell phenotypes. Treatment of pups with 3PO at postnatal days 1–4 (P1–P4) reduced the number of branch points (Figures 4A–4C), the radial expansion of the vascular plexus (Figure 4D), and the number of distal sprouts with filopodia (Figure 4E). YN1 also reduced vessel branching in the retina (Figures S4A–S4D). Staining of retinal flat mounts for isolectin B4, BrdU, and Erg (an EC-specific nuclear transcription factor) revealed that fewer Erg^+ $BrdU^+$ ECs were present in the vascular plexus in 3PO-treated mice, suggesting that EC proliferation was impaired (Figures 4F–4H). Confirming the gene expression data in EC monolayers, 3PO did not affect the expression of the tip cell-enriched marker *Pdgfb* in retinal tip cells (Figures S4E and S4F).

Blocking PFKFB3 Inhibits Vascular Hyperbranching

We then explored if PFKFB3 blockade counteracted vascular hyperbranching. VEGFR1 (Flt1) is an inhibitor of vascular branching and, consistent with previous findings (Krueger et al., 2011), *flt1* knockdown ($flt1^{KD}$) caused ISV hyperbranching (Figures 5A and 5B). 3PO normalized ISV hyperbranching in a large fraction of $flt1^{KD}$ embryos and reduced the severity of vascular overgrowth (Figures 5C and 5D). While 64% of control-treated $flt1^{KD}$ embryos exhibited signs of severe ISV hyperbranching in at least 4 out of 10 ISVs per embryo, only 20% of 3PO-treated $flt1^{KD}$ embryos showed this phenotype, and up to 29% of them formed completely normal ISVs. 3PO also reduced ISV side branches in $flt1^{KD}$ embryos (side branches per ISV: 100% ± 10% for $flt1^{KD}$ controls versus 54% ± 10% for 3PO-treated $flt1^{KD}$; n = 3 experiments, each with >8 embryos per condition; $p < 0.01$ by univariate test). We also analyzed ISV perfusion. In control embryos, intracardiac angiography with rhodamine-labeled dextran showed that PFKFB3 blockade impaired vessel lumen formation and perfusion (see above). In contrast, ISVs in Flt1-silenced ($flt1^{KD}$) embryos had an enlarged lumen, but PFKFB3 blockade largely normalized ISV lumen size in $flt1^{KD}$ embryos (Figures S5A–S5F) without impairing vessel perfusion (Figure S5G).

We also induced vascular hyperbranching by blocking Dll4/Notch signaling (Hellström et al., 2007). In EC spheroids, N-(N-(3,5-Difluorophenacetyl)-L-alanyl)-S-phenylglycine t-butyl ester (DAPT) increased the number and length of the vessel sprouts, but this hypersprouting was abrogated by 3PO (Figures S5H–S5K). 3PO also rescued vascular hyperbranching in zebrafish embryos upon silencing of Dll4 (Figures S5L–S5O) or in the retina upon treatment of neonatal mice with DAPT (Figures 5E–5H).

PFKFB3 Blockade Amplifies the Antiangiogenic Effect of VEGFR Blockers

VEGF blockade is a clinically approved antiangiogenic strategy. The VEGFR tyrosine kinase inhibitor SU5416 caused dose-dependent vascular defects in zebrafish embryos, characterized by progressive impairment and stalling of ISVs and lack of DLAV formation. At a maximal concentration (1 μM), SU5416 prevented the outgrowth of ~30% of the ISVs (Figure 5I). These defects were not only more severe, but also occurred at a higher incidence when increasing the dose of SU5416 (Figure 5I).

To evaluate if PFKFB3 blockade enhanced the antiangiogenic effect of VEGFR inhibition, we treated embryos with suboptimal doses of SU5416 (0.1 or 0.5 μM) and 3PO (20 or 30 μM), which alone only induced a negligible impairment of ISV outgrowth in a minority of embryos (Figures 5J–5L). However, the combination of both compounds at suboptimal doses aggravated the vessel defects in most embryos (Figures 5I and 5M). Even when a high dose of SU5416 (1 μM) was used that prevented the formation of half of the ISVs, the combination with 3PO (30 μM) further aggravated this phenotype, abrogating ISV development in nearly all embryos (Figure 5I). Overall, blockade of glycolysis amplified the efficacy of targeted VEGF inhibition in blocking angiogenesis.

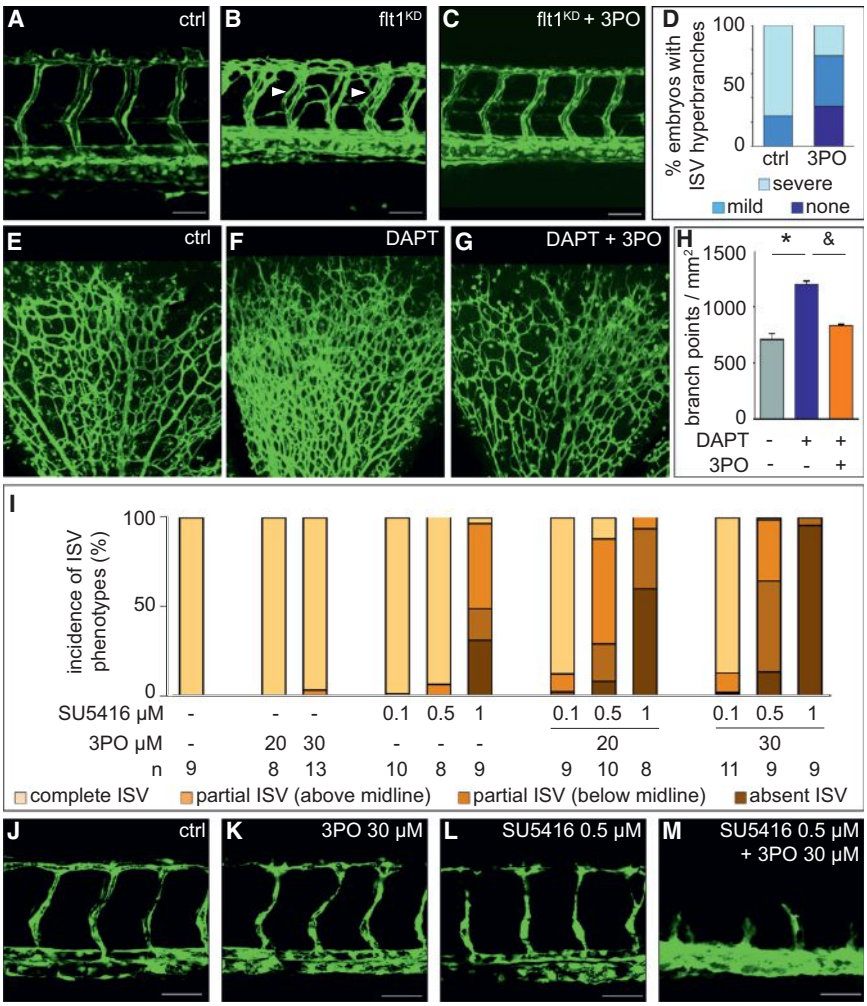

Figure 5. PFKFB3 Blockade Inhibits Vascular Hyperbranching In Vivo

(A–D) Confocal images of 72 hpf *fli1:EGFP*^{y1} embryos. As compared to the normally patterned ISV in a control embryo (A), ISVs hyperbranch in *flt1*^{KD} embryos (arrowheads in B). Treatment of *flt1*^{KD} embryos with 3PO (30 µM) largely normalized the vascular hyperbranching phenotype (C). Shown in (D) is the incidence of *flt1*^{KD} embryos with no, mild, or severe vascular hyperbranching, revealing that 3PO reduced vascular hyperbranching (n = 12; *p < 0.00001). Scale bars: 50 µm.

(E–G) Confocal images of the retinal vasculature after treatment with control (E), DAPT (F), or DAPT + 3PO (G), showing that DAPT increased the number of branch points and that 3PO abolished the hyperbranching induced by DAPT.

(H) Quantification of the number of branches (mean ± SEM; n = 5 for DAPT and 3PO+DAPT, n = 8 for ctrl; *p < 0.001 versus control (gray), &p < 0.05 versus DAPT).

(I) Quantification of the average incidence of indicated ISV phenotypes for 10 ISVs scored per embryo upon single or combined treatment with the indicated doses of 3PO and/or SU5416. Complete ISV, ISVs formed normally and completely; partial ISV (above midline), ISVs formed at least until or partially above the horizontal midline without reaching the dorsal roof level; partial ISV (below midline), ISVs were severely underdeveloped and failed to reach the horizontal midline; absent ISV, ISVs completely failed to sprout. n values per condition are indicated under the bars.

(J–M) Confocal images of GFP$^+$ vessels in 35 hpf *fli1:EGFP*^{y1} embryos, showing a control embryo (J) and a minor impairment of ISV development when treating embryos with a submaximal dose of 3PO (K) or the VEGFR tyrosine kinase inhibitor SU5416 (L) but severe vascular defects and near-complete abrogation of ISV formation in embryos treated with the combination of both inhibitors (M). Scale bars: 50 µm. See also Figure S5.

Blockade of PFKFB3 Reduces Pathological Angiogenesis

We tested if PFKFB3 blockade inhibited choroidal neovascularization (CNV), a model of age-related macular degeneration (AMD) (Van de Veire et al., 2010). The lesions in this model are largely vascular in nature, allowing us to assess antiangiogenic effects of 3PO. Starting from 1 day after laser burn injury of the Bruch's membrane to induce CNV, mice received a daily dose of vehicle or 3PO. Quantification of CNV lesions upon injection with fluorescein isothiocyanate (FITC)-conjugated dextran at 14 days after laser injury showed that 3PO dose dependently reduced the CNV lesion volume (Figures 6A–6C). We also evaluated if 3PO amplified the antiangiogenic activity of the anti-VEGFR2 monoclonal antibody (mAb) DC101 (Van de Veire et al., 2010). When using a suboptimal dose of DC101 (12.5 mg/kg, 3× per week), CNV was reduced by 38%, while the combination of DC101 plus 3PO caused a decrease of CNV by 67% (Figure 6D).

We confirmed the antiangiogenic activity of 3PO by using other models of pathological angiogenesis. We first used the oxygen-induced model of retinopathy of prematurity (ROP), which is based on the exposure of mouse pups to hyperoxia during a phase when their retinal vasculature is still developing, from P7–P12. This causes capillary depletion and vascular rarefication and, upon return to room air, results in retinal ischemia and, subsequently, in the formation of proliferative vascular tufts by P17–P21 (Scott and Fruttiger, 2010). Like in CNV, the lesions in the ROP model are primarily vascular in nature. Treatment of pups with 3PO during the phase of vascular proliferation from P12 to P17 reduced the formation of vascular tufts at P17 (Figures 6E–6G).

We also used two inflammation models, e.g., a skin psoriasis model and an inflammatory bowel disease model, since inflammatory disorders are characterized by increased angiogenesis (Wynn et al., 2013). A previous study reported that 3PO treatment reduced skin epithelial hyperplasia and inflammation, induced by local application of the immune activator imiquimod (IMQ), but this study did not analyze the effects on angiogenesis (Telang et al., 2012). Confirming previous findings, 3PO reduced the epidermal hyperplasia (Figure S6A), the spleen weight, another measure of inflammation (Figure S6B), and the number of CD3$^+$ lymphocytes in the lesions (Figure S6C). Importantly, 3PO also decreased the density of CD105$^+$ vessels in the epidermal lesions (Figures 7A–7D).

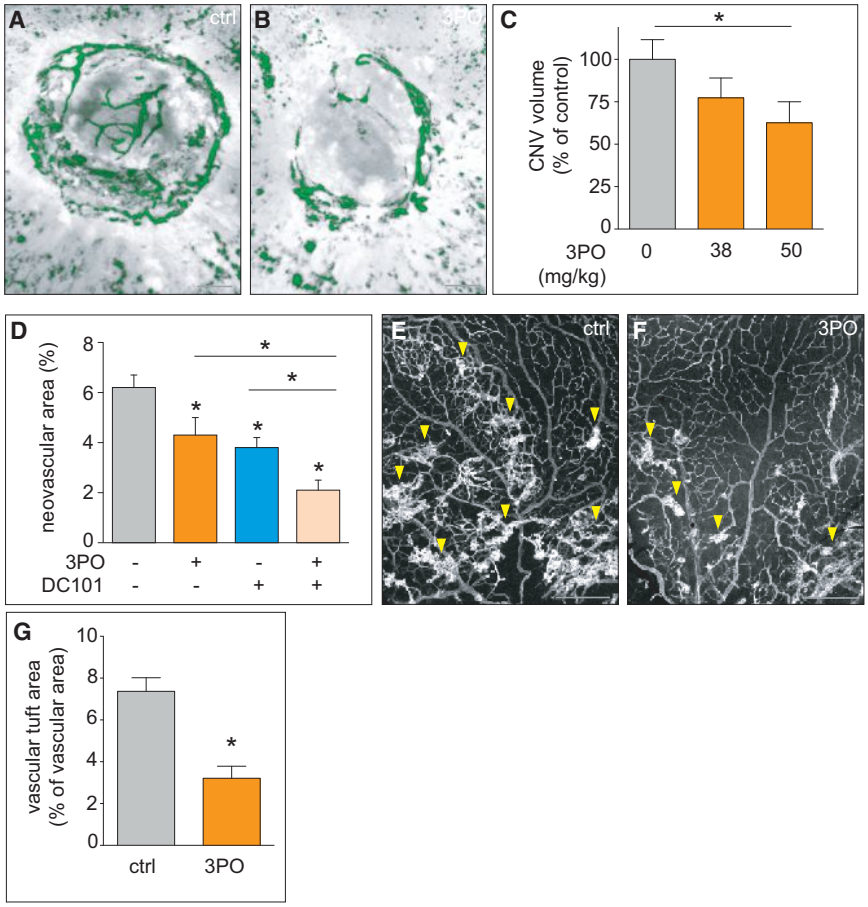

Figure 6. Blockade of PFKFB3 Reduces Pathological Angiogenesis: Ocular Models

(A and B) FITC-dextran choroidal flatmounts of control (A) or 3PO-treated mice (B), revealing fewer choroidal neovessels after 3PO treatment (B). The images are 3D isosurface renderings from z stacks of all individual optical sections through the neovascular lesion, as made by confocal laser scanning microscopy. Scale bars: 50 μm.

(C) 3PO dose dependently reduced CNV volume (estimated marginal mean ± SEM; n = 16 for ctrl, n = 16 for 38 mg/kg 3PO, and n = 14 for 50 mg/kg 3PO; two independent experiments; *$p < 0.04$ by general linear model univariate analysis, considering experiment as covariate).

(D) The combination treatment of 3PO (50 mg/kg) plus a submaximal dose of the anti-VEGFR2 mAb DC101 reduced the CNV neovascular area more than each monotherapy alone (mean ± SEM; n = 18 for ctrl, n = 7 for 3PO, n = 9 for DC101, and n = 8 for 3PO+DC101; *$p < 0.05$ versus ctrl or as indicated).

(E and F) Retinal flatmounts of ROP mice treated with DMSO (E) or 3PO (F) (70 mg/kg) and stained for isolectin B4, revealing reduced formation of vascular tufts (arrowheads) after 3PO (70 mg/kg) (F). Scale bars: 50 μm.

(G) Quantification of the vascular tuft area (mean ± SEM; n = 11 for ctrl, n = 9 for 3PO; *$p < 0.001$).

Inflammatory bowel disease, induced by administration of dextrane sulfate sodium (DSS), is also characterized by pathological angiogenesis (Hindryckx et al., 2010). Quantification of the disease activity index (DAI), which scores body weight loss, stool consistency, and blood in the stool and anal region, revealed that 3PO reduced disease severity (Figure 7H). Hematoxylin and eosin staining (H&E) showed that 3PO-treated mice had less-severe acute colitis (Figures 7E–7G). To quantify the histological signs of colitis, we used a histologic scoring method, taking into account the severity of inflammatory cell infiltration (dispersed, focal, or widespread), the extent of injury (mucosal, submucosal, or transmural), and crypt damage (basal, luminal, or entire crypt loss) (Cummins et al., 2008). This analysis confirmed that 3PO reduced the severity of colitis (histological score, median value: 10 for control versus 6 for 3PO; n = 11 for control and n = 10 for 3PO; $p = 0.0004$), and decreased $CD45^+$ cell infiltration in the (sub)mucosa and muscularis externa (Figure 7I). 3PO also decreased the area of $CD105^+$ vessels in the inflamed mucosa, submucosa, and muscularis externa (Figures 7J–7M).

DISCUSSION

Glycolysis: An Overlooked Target in Angiogenesis?

ECs rely on glycolysis and derive up to 85% of their ATP from glycolysis, while PFKFB3-driven glycolysis regulates EC proliferation and migration (De Bock et al., 2013b). We now also show that ECs increase glycolysis when shifting from quiescence to proliferation and migration. Glycolysis is required for cell proliferation, not only by providing ATP, but also by generating glycolytic intermediates that are used for the synthesis of macromolecules necessary for cell mass duplication during division (Lunt and Vander Heiden, 2011). In addition, glycolysis is required for EC motility, in part by compartmentalizing PFKFB3 and other glycolytic enzymes in lamellipodia and by concentrating these glycolytic enzymes with F-actin at leading membrane ruffles (De Bock et al., 2013b). The high glycolytic flux in ECs, their dependence on this pathway to generate most of the ATP, and the increased glycolysis during EC proliferation and migration, together with the genetic findings that loss of PFKFB3 in ECs affects tip and stalk cells (De Bock et al., 2013b), render glycolysis an attractive target for therapeutic inhibition of angiogenesis.

PFKFB3 Blockade Reduces Physiological and Pathological Angiogenesis

We previously reported that genetic silencing of PFKFB3 reduces vessel formation in physiological conditions (De Bock et al., 2013b), but it remained untested if pharmacological blockade of PFKFB3 could also impair pathological angiogenesis. 3PO phenocopied the effects of PFKFB3 silencing in ECs in vitro and of PFKFB3 inactivation in ECs in vivo (De Bock et al., 2013b). Indeed, 3PO impaired vessel sprouting in EC spheroids by reducing EC proliferation and migration, impeded filopodia formation, and EC accumulation in ISVs in zebrafish and caused vascular hypobranching and outgrowth in the

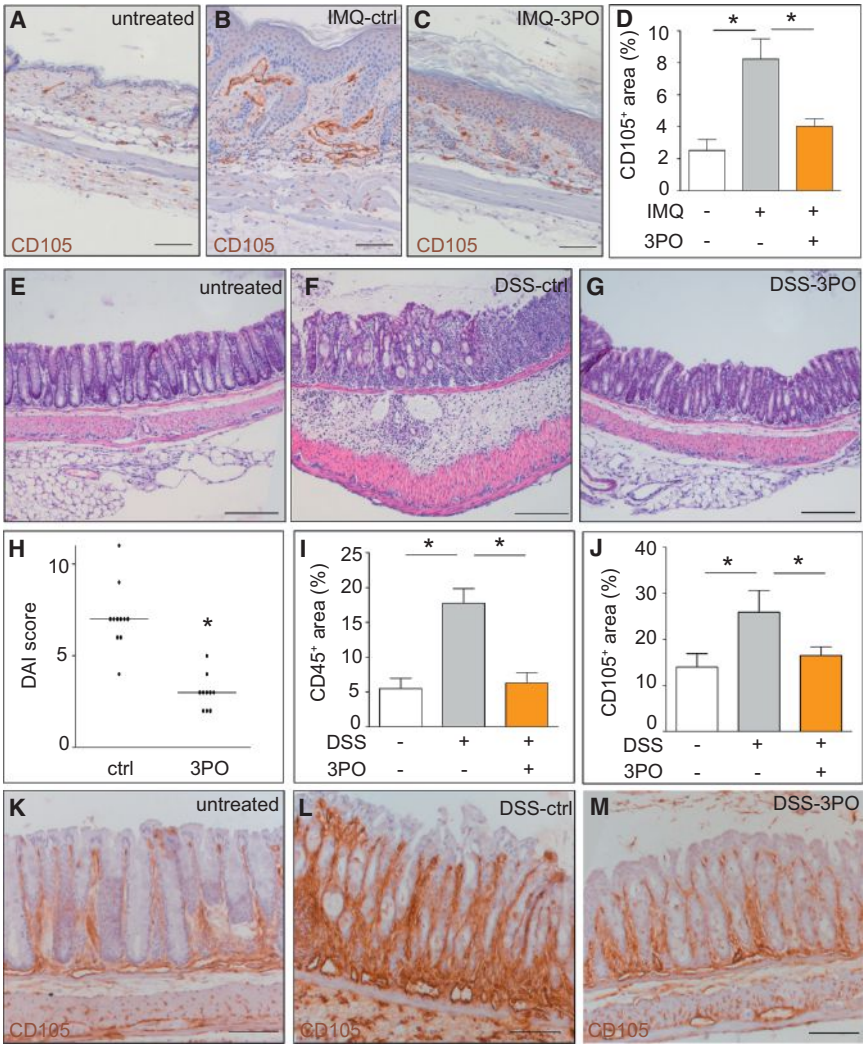

Figure 7. PFKFB3 Blockade Reduces Pathological Angiogenesis: Inflammation Models

(A–C) Representative images of CD105 staining of untreated skin (A), IMQ-DMSO-treated skin (ctrl) (B), and IMQ-3PO-treated skin (3PO) (C). Scale bars: 100 μm.

(D) Reduced CD105$^+$ vascular area in the dermis upon 3PO treatment (mean ± SEM; n = 7 for untreated, n = 9 for IMQ-DMSO and IMQ-3PO; *p < 0.001).

(E–M) DSS-induced colitis model. Representative H&E images of untreated healthy colon (E), DSS-DMSO-treated colon (DSS-ctrl) (F), and DSS-3PO-treated colon (50 mg/kg) (G). Scale bars: 200 μm. (H) Reduced disease activity index (DAI) score upon 3PO treatment (median; n = 11 for DSS-DMSO, n = 10 for DSS-3PO; *p < 0.0001). (I) Reduced CD45$^+$ area in the mucosa, submucosa, and muscularis externa of the colon upon 3PO treatment (mean ± SEM; n = 3 for untreated, n = 11 for control, and n = 10 for 3PO; *p < 0.003). (J) Reduced CD105$^+$ vascular area in the mucosa, submucosa, and muscularis externa of the colon upon 3PO treatment (mean ± SEM; n = 3 for untreated, n = 11 for DSS-DMSO, and n = 10 for DSS-3PO; *p < 0.004). Representative images of CD105 staining of untreated healthy colon (K), DSS-DMSO-treated colon (DSS-ctrl) (L), and DSS-3PO-treated colon (M). Scale bars: 100 μm. See also Figure S6.

mouse retina by decreasing EC proliferation and tip cell behavior. The finding that 3PO impaired lumen formation (a process requiring actin cytoskeleton changes; Sacharidou et al., 2012) is in agreement with findings that PFKFB3 regulates actin cytoskeleton remodeling processes (De Bock et al., 2013b).

3PO also reduced vascular hyperbranching induced by inhibition of Notch or VEGFR1 signaling in zebrafish embryos. In addition, 3PO largely normalized vascular hypersprouting in EC spheroids and the mouse retina, induced by the Notch signaling blocker DAPT. Moreover, 3PO reduced pathological neovascularization in ocular and inflammatory models in the mouse and amplified the antiangiogenic activity of a VEGF receptor tyrosine kinase inhibitor and anti-VEGF receptor 2 in the zebrafish and CNV mouse model, respectively. Together, inhibition of PFKFB3 by 3PO reduces vessel formation in physiological and pathological conditions in the models tested.

Partial and Transient Reduction of Glycolysis

Previous antiglycolytic anticancer strategies attempted to block glycolysis completely and permanently, but these approaches also caused adverse effects (Granchi and Minutolo, 2012). In agreement, our 2DG experiments show that more complete, sustained inhibition of glycolysis induces toxic effects in cultured ECs. In contrast, 3PO reduced glycolysis only partially, inducing EC quiescence without causing EC death in vitro. Likewise, 3PO reduced glycolysis only partially and transiently in vivo, but without inducing permanent refractoriness, since a second 3PO administration 24 hr later reduced glycolysis again to the same level as the first treatment. Thus, a partial and daily transient decrease of glycolysis sufficed to suppress pathological neovascularization. It remains to be studied whether 3PO treatment in vivo has acceptable tolerability.

The transient effect of 3PO is in agreement with its short half-life (30 min), rapid clearance (2,312 ml/kg/min), low Cmax (113 ng/ml) and low area under the concentration-time curve from zero to infinity ($AUC_{0\text{-inf}}$; 36 ng/hr/ml) ($AUC_{0\text{-inf}}$ refers to the actual body exposure to 3PO after administration of a dose of 3PO) (Clem et al., 2013). With the concentrations used, 3PO blocked PFKFB3 completely, since 3PO failed to further reduce glycolysis in ECs in which PFKFB3 was silenced to nearly undetectable levels. Despite full blockade of PFKFB3, glycolysis was only decreased by 35%–40%. Similar data were obtained when silencing PFKFB3 (De Bock et al., 2013b). The reason for the partial effect likely relates to the fact that 3PO blocks an activator of a key enzyme in glycolysis (e.g., PFK-1). Hence, PFKFB3 blockade has a ceiling level in its ability to inhibit glycolysis.

PFKFB3 Blockade: A Different Therapeutic Antiglycolytic Paradigm

Past antiglycolytic therapies faced challenges of cross-inhibition of other glycolytic targets, off-target effects, poor membrane permeability, and inability of compounds to efficiently antagonize abundant glycolytic substrates (Granchi and Minutolo, 2012). For instance, 2DG must compete with mM levels of glucose in the blood, necessitating delivery of high (toxic) amounts (Granchi and Minutolo, 2012). Nonetheless, cancer patients receiving 2DG had a progressive disease and suffered adverse effects (Granchi and Minutolo, 2012; Raez et al., 2013). Some of the side effects were attributed to the fact that these strategies block not only glycolysis, but also other glucose metabolism pathways (Granchi and Minutolo, 2012). Another reason is that these approaches inhibit glycolysis nearly completely and permanently, inducing ATP depletion and toxicity (Granchi and Minutolo, 2012). Indeed, human genetic studies reveal that a decrease in glycolysis due to hereditary mutations in glycolytic genes is well tolerated, as long as the decreased glycolysis levels do not deplete ATP levels (Climent et al., 2009).

PFKFB3 blockade by 3PO differs from these antiglycolytic approaches in various aspects. Firsty, it inhibits a defined intracellular enzyme, requiring much lower (μM) inhibitor concentrations than the high (mM) concentrations of 2DG needed to compete with the mM plasma glucose levels (François et al., 1987). Second, unlike 2DG and related drugs, which block glucose metabolism high up in the pathway, PFKFB3 blockade inhibits a defined downstream target, which specifically reduces glycolytic flux, without abrogating glycolytic side pathways such as the oxidative PPP (oxPPP), necessary for the production of NADPH to secure redox homeostasis. In fact, 3PO increased the oxPPP flux, but this change did not explain the antiangiogenic activity of 3PO. Third, 3PO and YN1 did not inhibit other glycolytic enzymes, tested by using recombinant enzymes or 3PO-treated EC extracts. Fourth, the K_M of PFKFB3 for its substrate fructose-6-phosphate (F6P) is 97 μM, while the K_i for competitive inhibition by 3PO is 25 μM, and 3PO has no effect on PFK-1, which shares an identical substrate, F6P (Clem et al., 2008). Fifth, 3PO did not cause EC death.

3PO Blocks Hyperglycolysis during EC Proliferation and Migration

Of the maximal amount of glycolysis that ECs can generate, they use 40% to proliferate and migrate, reserving 60% for maintenance homeostasis, in line with findings that proliferation only requires 30% of ATP production (Locasale and Cantley, 2010). Lowering glycolysis by 40% through 3PO treatment impaired EC proliferation and migration. This, however, did not cause EC death, but promoted reversible quiescence. PFKFB3 blockade thus reduced the hypermetabolism that is induced when ECs switch from quiescence to proliferation and migration.

Possible Medical Implications

PFKFB3 blockade decreased pathological angiogenesis in inflammatory and ocular disease models. Choroidal neovascularization (a preclinical model of wet AMD) and retinopathy of prematurity are blinding disorders, caused by excessive growth of retinal vessels (Cavallaro et al., 2013; Miller et al., 2013; Stewart, 2012). Anti-VEGF therapy has beneficial effects in AMD and ROP patients, but does not attain durable treatment-free cessation of the disease (Darlow et al., 2013; Niranjan et al., 2012; Rofagha et al., 2013). In addition, one-third of patients with wet AMD have poor visual outcome, and ~13% lost more vision after intraocular anti-VEGF treatment (Lalwani et al., 2009). Our findings that 3PO reduces vascular lesions in both ocular disorders and enhances the antiangiogenic effect of the anti-VEGFR2 in the CNV model may warrant further study of a possible therapeutic use of PFKFB3 blockers.

EXPERIMENTAL PROCEDURES

More detailed methods are described in the Supplemental Experimental Procedures.

Cellular Assays

Freshly isolated primary HUVECs were used for evaluation of metabolism, proliferation, migration, matrigel assay, spheroid capillary sprouting assays, and cell cycle status. Except for Figure 1A, we used the maximal concentration of 3PO that reversibly impaired in vitro EC responses, ranging between 15 and 20 μM.

RNA Expression Analysis

RNA expression analysis was performed by TaqMan qRT-PCR or in situ hybridization.

Metabolism Assays

Glycolysis, glucose incorporation into RNA, and oxidative pentose phosphate pathway flux were determined by incubating cells with radioactive-labeled tracer glucose. Briefly, ^3H_2O formation was a measure for glycolytic flux. $^{14}CO_2$ production was a measure for oxidative pentose phosphate pathway flux, and ^{14}C counts in isolated RNA was a measure for glucose incorporation. Fructose-2,6-bisphosphate levels in cell lysates were determined as described (Van Schaftingen et al., 1982). Oxygen consumption and lactate production were measured using the Seahorse XF24 analyzer. Energy balance was calculated as ([ATP] + ½[ADP]) / ([ATP] + [ADP] + [AMP]) based on high-performance liquid chromatography (HPLC) measurement of AMP, ADP, and ATP levels in cell extracts.

Proliferation

Proliferation was quantified by incubating cells with [^{3}H]-thymidine. The amount of [^{3}H]-thymidine incorporated into DNA was measured by scintillation counting.

Migration

Migration was evaluated using scratch wound or Boyden chamber migration assays. To evaluate responses in the absence of proliferation, MitoC-treated ECs (0.5–1 μg/ml for 24 hr) were used.

Spheroid Capillary Sprouting Assay

ECs were incubated overnight in hanging drops to form spheroids, embedded in collagen, and cultured for 24 hr (with addition of compounds as indicated) to induce sprouting. Cultures were fixed with 4% paraformaldehyde (PFA) and analyzed.

Matrigel Assay

ECs were plated on top of polymerized Matrigel Basement Membrane Matrix in M119 full medium containing 3PO or vehicle. After 6 hr, the network was fixed using 4% PFA.

Cell Cycle Analysis

Cell cycle analysis was determined by flow cytometry based on the DNA and RNA content as stained for with Hoechst and Pyronin Y.

In Vivo Metabolism

Glycolytic flux in vivo was assessed by mass spectrometry detection of ^{13}C-lactate in the plasma, collected 10 min after tail vein injection of [U-^{13}C] glucose. Glucose uptake in vivo was assessed by measuring the radiolabel content of the heart and diaphragm, harvested 1 hr after intravenous bolus injection of the mice with 2-deoxy-D-glucose, 2-[1-^{14}C].

Angiogenesis Models

Zebrafish

Tg(fli1:EGFP)^{y1} or *Tg(fli1:nEGFP)^{y7}* zebrafish were subjected to morpholino oligonucleotide injection of Dll4 or Flt1 or to treatment with inhibitors (3PO, YN1, SU5416). Assessment of sprouting and hyperbranching of ISVs, imaging, and morphometric quantitation was as detailed in the Supplemental Experimental Procedures.

Mouse Models of Ocular Angiogenesis

CNV was induced in C57BL/6 mice by laser burn. Mice were injected intraperitoneally (i.p.) with 38–50 mg/kg PFKFB3 inhibitor 3PO daily with or without treatment with anti-VEGFR2 DC101 (12.5 mg/kg i.p., 3× per week). Eyes were enucleated 2 weeks after the laser treatment and processed for immunohistochemistry and neovascular morphometric analysis as described in the Supplemental Experimental Procedures. Oxygen-induced retinopathy was induced by exposing C57BL/6 pups to 70% oxygen from P7–P12. Pups were then returned to normoxia and injected daily with 70 mg/kg 3PO and euthanized at P17. Retinal flat mounts were analyzed as described in the Supplemental Experimental Procedures. For analysis of neonatal retinal angiogenesis, mice were injected with 50 mg/kg 3PO or vehicle between P2 and P4 and euthanized at P4 or P5; eyes were enucleated and fixed, and retinal flat mounts were prepared for vascular analysis as described in the Supplemental Experimental Procedures.

Mouse Models of Inflammation

Skin inflammation was induced by daily topical application of 5% imiquimod cream on the back of BALB/c mice. Mice received a daily i.p. dose of 50 mg/kg 3PO. After 4 days, skins were resected for analyses as described in the Supplemental Experimental Procedures. Acute colitis was induced with 2.5% dextran sodium sulfate (DSS) in the drinking water for 6 days. Mice received a daily i.p. dose of 50mg/kg 3PO. Histological scoring was as detailed in the Supplemental Experimental Procedures. All experimental animal procedures were approved by the Institutional Animal Care and Research Advisory Committee of the University of Leuven.

Statistics

Data represent mean ± SEM of representative experiments, unless otherwise stated. For all in vitro and in vivo experiments, every experiment was performed at least three times. For analysis of the mouse models of angiogenesis, the investigator assessing the outcome was blinded to the group allocation; for analysis of zebrafish models of angiogenesis, assessment was done by an investigator ignorant of potential outcome. Unless otherwise indicated, statistical significance between groups was calculated by standard t test with F testing to confirm equality of variance (Prism v4.0b). Phenotype severity distributions were analyzed by chi-square test. Statistical significance of DAI and histological scoring data were determined by Mann-Whitney test. $p < 0.05$ was considered statistically significant.

SUPPLEMENTAL INFORMATION

Supplemental Information includes Supplemental Experimental Procedures, six figures, and one movie and can be found with this article online at http://dx.doi.org/10.1016/j.cmet.2013.11.008.

AUTHOR CONTRIBUTIONS

P.C., S.S., K.D.B., A.R.C., and M.G. conceived and designed the experiments. S.S. and A.R.C. performed the inflammation and ocular models of angiogenesis. All in vitro experiments were performed by S.S., K.D.B., A.R.C., and M.G. The manuscript was written by P.C., S.S., and K.D.B.

ACKNOWLEDGMENTS

We acknowledge the work of Leen Notebaert for help with the illustrations. K.D.B., A.R.C., and B.G. are Postdoctoral Fellows of the Research Foundation-Flanders (FWO); M.G. and S.S. received funding as Emmanuel Vanderschueren fellows of the Flemish Association against Cancer (VLK); and S.S. was funded by the Institution of Research and Innovation (IWT). The work of P.C. is supported by a Federal Government Belgium grant (IUAP7/03), long-term structural Methusalem funding by the Flemish Government, a Concerted Research Activities Belgium grant (GOA2006/11), grants from the FWO (G.0532.10, G.0817.11, G.0834.13, 1.5.202.10N, G.0764.10N, and 1.5.142.13N Krediet aan navorsers), the Foundation Leducq Transatlantic Network (ARTEMIS), the Foundation against Cancer, and the ERC Advanced Research Grant (EU-ERC269073). M.D. is supported by FWO grant G.0598.12. M.C. is supported by the Spanish Government and the European Union FEDER funds (SAF2011-25726), Generalitat de Catalunya-AGAUR (2009SGR1308), and the "ICREA Academia prize." P.C. declares being named as inventor on patent applications claiming subject matter related to the results described in this paper. J.C. is coinventor of US patent #8,088,385 (PFKFB3 inhibitors for the treatment of proliferative cancer).

Received: June 14, 2013
Revised: October 21, 2013
Accepted: November 6, 2013
Published: December 12, 2013

REFERENCES

Cavallaro, G., Filippi, L., Bagnoli, P., La Marca, G., Cristofori, G., Raffaeli, G., Padrini, L., Araimo, G., Fumagalli, M., Groppo, M., et al. (2013). The pathophysiology of retinopathy of prematurity: an update of previous and recent knowledge. Acta Ophthalmol. (Copenh.). Published online April 26, 2013. http://dx.doi.org/10.1111/aos.12049.

Chesney, J., Mitchell, R., Benigni, F., Bacher, M., Spiegel, L., Al-Abed, Y., Han, J.H., Metz, C., and Bucala, R. (1999). An inducible gene product for 6-phosphofructo-2-kinase with an AU-rich instability element: role in tumor cell glycolysis and the Warburg effect. Proc. Natl. Acad. Sci. USA *96*, 3047–3052.

Clem, B., Telang, S., Clem, A., Yalcin, A., Meier, J., Simmons, A., Rasku, M.A., Arumugam, S., Dean, W.L., Eaton, J., et al. (2008). Small-molecule inhibition of 6-phosphofructo-2-kinase activity suppresses glycolytic flux and tumor growth. Mol. Cancer Ther. *7*, 110–120.

Clem, B.F., O'Neal, J., Tapolsky, G., Clem, A.L., Imbert-Fernandez, Y., Kerr, D.A., 2nd, Klarer, A.C., Redman, R., Miller, D.M., Trent, J.O., et al. (2013). Targeting 6-phosphofructo-2-kinase (PFKFB3) as a therapeutic strategy against cancer. Mol. Cancer Ther. *12*, 1461–1470.

Climent, F., Roset, F., Repiso, A., and Pérez de la Ossa, P. (2009). Red cell glycolytic enzyme disorders caused by mutations: an update. Cardiovasc. Hematol. Disord. Drug Targets *9*, 95–106.

Cummins, E.P., Seeballuck, F., Keely, S.J., Mangan, N.E., Callanan, J.J., Fallon, P.G., and Taylor, C.T. (2008). The hydroxylase inhibitor dimethyloxalylglycine is protective in a murine model of colitis. Gastroenterology *134*, 156–165.

Darlow, B.A., Ells, A.L., Gilbert, C.E., Gole, G.A., and Quinn, G.E. (2013). Are we there yet? Bevacizumab therapy for retinopathy of prematurity. Arch. Dis. Child. Fetal Neonatal Ed. *98*, F170–F174.

De Bock, K., Georgiadou, M., and Carmeliet, P. (2013a). Role of endothelial cell metabolism in vessel sprouting. Cell Metab. *18*, 634–647.

De Bock, K., Georgiadou, M., Schoors, S., Kuchnio, A., Wong, B.W., Cantelmo, A.R., Quaegebeur, A., Ghesquière, B., Cauwenberghs, S., Eelen, G., et al. (2013b). Role of PFKFB3-driven glycolysis in vessel sprouting. Cell *154*, 651–663.

Ebos, J.M., and Kerbel, R.S. (2011). Antiangiogenic therapy: impact on invasion, disease progression, and metastasis. Nat Rev Clin Oncol *8*, 210–221.

François, J., Eraso, P., and Gancedo, C. (1987). Changes in the concentration of cAMP, fructose 2,6-bisphosphate and related metabolites and enzymes in Saccharomyces cerevisiae during growth on glucose. Eur. J. Biochem. *164*, 369–373.

Geudens, I., and Gerhardt, H. (2011). Coordinating cell behaviour during blood vessel formation. Development *138*, 4569–4583.

Granchi, C., and Minutolo, F. (2012). Anticancer agents that counteract tumor glycolysis. ChemMedChem *7*, 1318–1350.

Harjes, U., Bensaad, K., and Harris, A.L. (2012). Endothelial cell metabolism and implications for cancer therapy. Br. J. Cancer *107*, 1207–1212.

Hellström, M., Phng, L.K., Hofmann, J.J., Wallgard, E., Coultas, L., Lindblom, P., Alva, J., Nilsson, A.K., Karlsson, L., Gaiano, N., et al. (2007). Dll4 signalling through Notch1 regulates formation of tip cells during angiogenesis. Nature *445*, 776–780.

Herrero-Mendez, A., Almeida, A., Fernández, E., Maestre, C., Moncada, S., and Bolaños, J.P. (2009). The bioenergetic and antioxidant status of neurons is controlled by continuous degradation of a key glycolytic enzyme by APC/C-Cdh1. Nat. Cell Biol. *11*, 747–752.

Hindryckx, P., Waeytens, A., Laukens, D., Peeters, H., Van Huysse, J., Ferdinande, L., Carmeliet, P., and De Vos, M. (2010). Absence of placental growth factor blocks dextran sodium sulfate-induced colonic mucosal angiogenesis, increases mucosal hypoxia and aggravates acute colonic injury. Lab. Invest. *90*, 566–576.

Krueger, J., Liu, D., Scholz, K., Zimmer, A., Shi, Y., Klein, C., Siekmann, A., Schulte-Merker, S., Cudmore, M., Ahmed, A., and le Noble, F. (2011). Flt1 acts as a negative regulator of tip cell formation and branching morphogenesis in the zebrafish embryo. Development *138*, 2111–2120.

Lalwani, G.A., Rosenfeld, P.J., Fung, A.E., Dubovy, S.R., Michels, S., Feuer, W., Davis, J.L., Flynn, H.W., Jr., and Esquiabro, M. (2009). A variable-dosing regimen with intravitreal ranibizumab for neovascular age-related macular degeneration: year 2 of the PrONTO Study. Am. J. Ophthalmol. *148*, 43–58, e1.

Leopold, J.A., Walker, J., Scribner, A.W., Voetsch, B., Zhang, Y.Y., Loscalzo, A.J., Stanton, R.C., and Loscalzo, J. (2003). Glucose-6-phosphate dehydrogenase modulates vascular endothelial growth factor-mediated angiogenesis. J. Biol. Chem. *278*, 32100–32106.

Locasale, J.W., and Cantley, L.C. (2010). Altered metabolism in cancer. BMC Biol. *8*, 88.

Lunt, S.Y., and Vander Heiden, M.G. (2011). Aerobic glycolysis: meeting the metabolic requirements of cell proliferation. Annu. Rev. Cell Dev. Biol. *27*, 441–464.

Miller, J.W., Le Couter, J., Strauss, E.C., and Ferrara, N. (2013). Vascular endothelial growth factor a in intraocular vascular disease. Ophthalmology *120*, 106–114.

Niranjan, H.S., Benakappa, N., Reddy, K.B., Nanda, S., and Kamath, M.V. (2012). Retinopathy of prematurity promising newer modalities of treatment. Indian Pediatr. *49*, 139–143.

Potente, M., Gerhardt, H., and Carmeliet, P. (2011). Basic and therapeutic aspects of angiogenesis. Cell *146*, 873–887.

Raez, L.E., Papadopoulos, K., Ricart, A.D., Chiorean, E.G., Dipaola, R.S., Stein, M.N., Rocha Lima, C.M., Schlesselman, J.J., Tolba, K., Langmuir, V.K., et al. (2013). A phase I dose-escalation trial of 2-deoxy-D-glucose alone or combined with docetaxel in patients with advanced solid tumors. Cancer Chemother. Pharmacol. *71*, 523–530.

Rofagha, S., Bhisitkul, R.B., Boyer, D.S., Sadda, S.R., and Zhang, K.; SEVEN-UP Study Group (2013). Seven-Year Outcomes in Ranibizumab-Treated Patients in ANCHOR, MARINA, and HORIZON: A Multicenter Cohort Study (SEVEN-UP). Ophthalmology *120*, 2292–2299.

Sacharidou, A., Stratman, A.N., and Davis, G.E. (2012). Molecular mechanisms controlling vascular lumen formation in three-dimensional extracellular matrices. Cells Tissues Organs (Print) *195*, 122–143.

Scott, A., and Fruttiger, M. (2010). Oxygen-induced retinopathy: a model for vascular pathology in the retina. Eye (Lond.) *24*, 416–421.

Seo, M., Kim, J.D., Neau, D., Sehgal, I., and Lee, Y.H. (2011). Structure-based development of small molecule PFKFB3 inhibitors: a framework for potential cancer therapeutic agents targeting the Warburg effect. PLoS ONE *6*, e24179.

Singh, M., and Ferrara, N. (2012). Modeling and predicting clinical efficacy for drugs targeting the tumor milieu. Nat. Biotechnol. *30*, 648–657.

Stewart, M.W. (2012). The expanding role of vascular endothelial growth factor inhibitors in ophthalmology. Mayo Clin. Proc. *87*, 77–88.

Telang, S., Clem, B.F., Klarer, A.C., Clem, A.L., Trent, J.O., Bucala, R., and Chesney, J. (2012). Small molecule inhibition of 6-phosphofructo-2-kinase suppresses t cell activation. J. Transl. Med. *10*, 95.

Van de Veire, S., Stalmans, I., Heindryckx, F., Oura, H., Tijeras-Raballand, A., Schmidt, T., Loges, S., Albrecht, I., Jonckx, B., Vinckier, S., et al. (2010). Further pharmacological and genetic evidence for the efficacy of PlGF inhibition in cancer and eye disease. Cell *141*, 178–190.

Van Schaftingen, E., Lederer, B., Bartrons, R., and Hers, H.G. (1982). A kinetic study of pyrophosphate: fructose-6-phosphate phosphotransferase from potato tubers. Application to a microassay of fructose 2,6-bisphosphate. Eur. J. Biochem. *129*, 191–195.

Wynn, T.A., Chawla, A., and Pollard, J.W. (2013). Macrophage biology in development, homeostasis and disease. Nature *496*, 445–455.

Yalcin, A., Telang, S., Clem, B., and Chesney, J. (2009). Regulation of glucose metabolism by 6-phosphofructo-2-kinase/fructose-2,6-bisphosphatases in cancer. Exp. Mol. Pathol. *86*, 174–179.

Cell Press content is widely accessible

At Cell Press we place a high priority on ensuring that all of our journal content is widely accessible and on working with the community to develop the best ways to achieve that goal.

Here are just some of those initiatives...

Open archives

We provide free access to Cell Press research journals 12 months following publication

Access for developing nations

We provide free & low-cost access through programs like Research4Life

Open access journal

We launched Cell Reports - a new Open Access journal spanning the life sciences

Funding body agreements

We work cooperatively and successfully with major funding bodies

Public access

Full-text online via ScienceDirect is also available to the public via walk in user access from any participating library

Submission to PubMed Central

Cell Press deposits accepted manuscripts on our authors' behalf for a variety of funding bodies, including NIH and HHMI, to PubMed Central (PMC)

www.cell.com/cellpress/access

Cell PRESS

Cell Metabolism
Short Article

Irisin and FGF21 Are Cold-Induced Endocrine Activators of Brown Fat Function in Humans

Paul Lee,[1] Joyce D. Linderman,[1] Sheila Smith,[1] Robert J. Brychta,[1] Juan Wang,[1] Christopher Idelson,[1] Rachel M. Perron,[1] Charlotte D. Werner,[1] Giao Q. Phan,[2] Udai S. Kammula,[2] Electron Kebebew,[3] Karel Pacak,[4] Kong Y. Chen,[1] and Francesco S. Celi[1,*]

[1]Diabetes, Endocrinology, and Obesity Branch, National Institute of Diabetes and Digestive and Kidney Diseases
[2]Surgery Branch
[3]Endocrine Oncology Branch
[4]National Cancer Institute and Program in Reproductive and Adult Endocrinology, Eunice Kennedy Shriver National Institute of Child Health and Human Development
National Institutes of Health, Bethesda, MD 20892, USA
*Correspondence: fsceli@vcu.edu
http://dx.doi.org/10.1016/j.cmet.2013.12.017

SUMMARY

Rediscovery of cold-activated brown adipose tissue (BAT) in humans has boosted research interest in identifying BAT activators for metabolic benefits. Of particular interest are cytokines capable of fat browning. Irisin, derived from FNDC5, is an exercise-induced myokine that drives brown-fat-like thermogenesis in murine white fat. Here we explored whether cold exposure is an afferent signal for irisin secretion in humans and compared it with FGF21, a brown adipokine in rodents. Cold exposure increased circulating irisin and FGF21. We found an induction of irisin secretion proportional to shivering intensity, in magnitude similar to exercise-stimulated secretion. FNDC5 and/or FGF21 treatment upregulated human adipocyte brown fat gene/protein expression and thermogenesis in a depot-specific manner. These results suggest exercise-induced irisin secretion could have evolved from shivering-related muscle contraction, serving to augment brown fat thermogenesis in concert with FGF21. Irisin-mediated muscle-adipose crosstalk may represent a thermogenic, cold-activated endocrine axis that is exploitable in obesity therapeutics development.

INTRODUCTION

Cold-induced thermogenesis (CIT) is the increase in heat production in response to acute ambient temperature reduction. It comprises nonshivering thermogenesis (NST) and shivering thermogenesis (ST). In rodents, the chief tissue mediating NST is brown adipose tissue (BAT), which releases heat through the action of uncoupling protein 1 (UCP1) (Cannon and Nedergaard, 2004). Heat demand not met by NST recruits ST, thereby generating heat from muscle contractions. Long-term cold exposure reduces shivering, conceivably a result of NST enhancement from cold acclimatization (Davis, 1961). In humans, the rediscovery of cold-activated BAT suggests a possible regulatory role of BAT in NST (Cypess et al., 2009; Saito et al., 2009; van Marken Lichtenbelt et al., 2009; Virtanen et al., 2009). However, the physiologic cues orchestrating NST and ST recruitment are unclear.

While adequate shelter and clothing in modern society have minimized the hazards of cold temperatures, the obesity epidemic has reignited interest into exploring whether harnessing BAT may benefit weight control (Yoneshiro et al., 2013). Activated BAT may contribute up to 20% of CIT following mild cold exposure (Chen et al., 2013), representing a proportion of total energy expenditure (EE) sufficient to impact long-term energy balance. Identification of BAT endocrine activators may open new directions in obesity therapeutics development (Lee et al., 2013b).

Irisin is an exercise-induced myokine that is secreted into the circulation following proteolytic cleavage from its cellular form, fibronectin-type III domain-containing 5 (FNDC5) (Boström et al., 2012). It reverses diet-induced obesity and diabetes by stimulating thermogenesis in rodents through increasing brown adipocyte-like cell abundance (brite [Petrovic et al., 2010]/beige [Wu et al., 2012] adipocytes) within white fat. As it appears paradoxical that exercise should increase secretion of a thermogenic hormone, it has been hypothesized that the mechanism evolved from shivering-related muscle contraction to augment NST through BAT expansion (Boström et al., 2012).

In this study, we tested this hypothesis by investigating the impact of cold exposure in healthy adults on irisin secretion and compared its excursion with the sympatho-thyroid-adrenal axes, principal regulators of CIT (Celi et al., 2010), as well as fibroblast growth factor 21 (FGF21), a recently identified brown adipokine that predicts NST response in humans (Lee et al., 2013a, 2013c). Finally, we examined in vitro the bioenergetic profiles of FNDC5- and FGF21-treated human adipocytes to determine their thermogenic significance.

RESULTS AND DISCUSSION

Irisin Detection in Human Serum

Circulating irisin, cleaved from FNDC5, is heavily glycosylated, and multiple bands are visible on serum immunoblot against anti-FNDC5 antibody (Boström et al., 2012). Because of the recent controversy over the circulating form of irisin (Erickson,

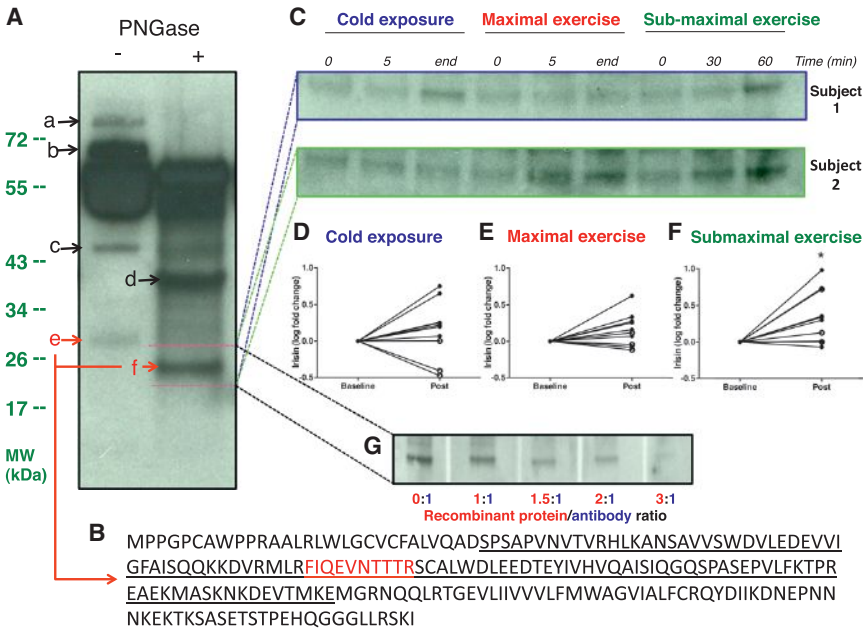

Figure 1. Validation of Immunoblot-Detected Irisin by Mass Spectrometry

(A) Immunoblot of paired serum samples following albumin/immunoglobulin depletion against anti-FNDC5 antibody revealed multiple distinct bands (a–f). PNGase treatment reduced size of band e (~32 kDa) to band f (~24 kDa).

(B) Shown is the amino acid sequence of full-length FNDC5 with the secreted irisin segment underlined. Mass spectrometry analysis of all bands (a–f) identified a specific peptide (in red), unique to irisin, only in band e and band f, with molecular weights matching those of glycosylated and deglycosylated irisin, respectively.

(C) Shown are representative immunoblots of serum irisin for fold change quantification from two subjects during cold exposure, maximal exercise, and submaximal exercise. Subject 1 shivered during cold exposure, while subject 2 did not. Accordingly, deglycosylated irisin band (~24 kDa) was stronger at the end of cold exposure only in subject 1. In contrast, irisin band was stronger after submaximal exercise in both subjects. Full-sized blots are shown in Figure S1.

(D–F) Graphical representation of serum irisin fold changes during cold exposure, maximal, and submaximal exercise tests, respectively, of all ten subjects. "Post" indicates the average band intensity of irisin extracted from the mid and final blood samples of each clinical test. Similar results were obtained when analysis was conducted comparing irisin band intensity between baseline and final sample alone. Irisin level rose significantly following sub-maximal exercise (F) and trended higher ($p = 0.07$) after maximal exercise (E). Irisin levels increased only in the seven subjects who shivered (closed circles, D), but not those who did not (open circles, D).

(G) Neutralization of anti-FNDC5 antibody by FNDC5 recombinant protein. FNDC5 antibody mixture in increasing ratio resulted in quenching of western signal in a dose-dependent manner by excess FNDC5 recombinant protein. *$p < 0.05$. Data are presented as mean ± SD.

2013), we first determined the identity of FNDC5-immunoreactive bands detectable in human serum by mass spectrometry (MS).

Consistent with previous reports, immunoblot of albumin/immunoglobulin-depleted serum revealed multiple bands reactive to anti-FNDC5 antibody. Deglycosylation reduced the size of a 32 kDa band to 24 kDa, corresponding to reported molecular weights (MWs) of glycosylated and deglycosylated irisin, respectively (Figure 1A) (Boström et al., 2012; Schumacher et al., 2013). MS analysis identified a unique peptide, mapped to the known sequence of irisin, only within the 32 kDa and 24 kDa bands (Figure 1B). These results thus validated immunoblot identification of circulating irisin in humans. To further ascertain specificity of antibody used, we also demonstrated successful quenching of irisin signal by excess recombinant protein (Figure 1G).

Exercise Increases Serum Irisin Levels in Humans

To understand the interrelationships between exercise, cold exposure, and irisin, we compared irisin secretion in ten healthy adults (four females, 27 ± 5 years old, body mass index [BMI] 22 ± 2 kg/m^2, body fat (BF) 24% ± 9%) following graded, stepwise cold exposure (27°C–12°C, see Figure S1 available online) with two forms of standard exercise tests: exercise on cycloergometer to maximal capacity (VO_{2max}) and submaximal exercise test at 40% VO_{2max} for 1 hr.

Serum irisin levels trended higher ($p = 0.07$) after maximal exercise (Figures 1C and 1E). After 60 min of submaximal exercise, irisin levels rose by 3.1- ± 2.8-fold ($p < 0.05$) (Figures 1C and 1F). These results thus replicated the known stimulatory effect of exercise on irisin secretion (Boström et al., 2012; Huh et al., 2012). The greater irisin increase during submaximal exercise compared to maximal exercise suggests endurance exercise maybe a more potent stimulus of irisin secretion, consistent with the finding of higher FNDC5 expression in oxidative versus glycolytic muscle fibers (Wrann et al., 2013).

Shivering Is an Afferent Signal of Irisin Secretion

We next determined the impact of cold temperature on irisin changes. Upon cold exposure, skin temperature decreased in all subjects ($p < 0.0001$) while core temperature was preserved (Table 1; Figure 2A). Arm-to-hand, skin-to-core, and supraclavicular-to-chest temperature gradients increased by 13% ± 18% ($p = 0.01$), 45% ± 15% ($p < 0.0001$), and 4% ± 3% ($p < 0.0001$), signifying vasoconstrictive, insulative, and thermogenic responses, respectively. EE rose by 48% ± 37% ($p < 0.01$), representing CIT response (Figure 2A). Seven subjects reported shivering, and shivering activity, quantified by surface electromyography (EMG), increased during cold exposure ($p < 0.01$) (Table 1). The increase in EMG activity was 88% ± 80% in individuals who shivered and 13% ± 9%, among those who did not ($p < 0.05$). Our cooling protocol thus elicited the full spectrum of CIT response, allowing the interrogation of irisin-CIT interrelationships. Irisin changes correlated the strongest with shivering among all CIT components (Table S1). Circulating irisin rose in the seven subjects who shivered (Figures 1C and 1D), and changes in irisin levels correlated positively with shivering activity ($r = 0.91$, $p < 0.001$) (Figure 2B). To ensure accuracy of our quantification, we also demonstrated concordant irisin changes measured with a commercially available irisin enzyme-linked immunosorbant assay (Figures 2E and

Table 1. Physiologic Changes during Cold Exposure and Hormonal Profile during Cold Exposure and Exercise Tests in Ten Subjects

Physiologic Variables						
Body Temperature (°C)	27°C	18°C	16°C	14°C	12°C	Trend p Value
Core	36.9 ± 0.2	36.9 ± 0.2	36.9 ± 0.2	36.9 ± 0.2	36.9 ± 0.2	0.65
Skin	32.1 ± 0.5	31.7 ± 0.7	31.1 ± 0.8	30.7 ± 0.9	30.0 ± 1.0	<0.0001
Gradient, core-to-skin	4.5 ± 0.8	4.8 ± 0.9	5.4 ± 1.1	5.9 ± 1.2	6.5 ± 1.2	<0.0001
Gradient, arm-to-hand	−6.7 ± 1.7	−7.1 ± 1.8	−7.4 ± 1.8	−7.2 ± 1.8	−7.3 ± 1.5	0.01
Gradient, supraclavicular-to-chest	1.04 ± 0.03	1.05 ± 0.03	1.06 ± 0.04	1.07 ± 0.05	1.09 ± 0.06	<0.0001
Resting EE (kcal/day)	1,488 ± 196	1,731 ± 337	1,926 ± 673	2,100 ± 785	2,235 ± 738	0.007
Respiratory quotient	0.78 ± 0.03	0.85 ± 0.07	0.79 ± 0.07	0.77 ± 0.07	0.79 ± 0.08	0.001
Surface electromyography ($\times 10^{-6}$ RMS)	2.5 ± 5.7	3.1 ± 2.1	4.0 ± 4.0	4.7 ± 3.6	4.9 ± 3.3	0.044

Hormonal Variables	Cold Exposure		Maximal Exercise		Submaximal Exercise	
	Baseline	End	Baseline	End	Baseline	End
Epinephrine (pg/ml)	38 ± 25	110 ± 73[a]	237 ± 418	300 ± 316	180 ± 406	311 ± 558 [a]
Norepinephrine (pg/ml)	658 ± 306	1,101 ± 449[a]	727 ± 264	1,568 ± 541[a]	714 ± 173	974 ± 209[a]
Glucose (mg/dL)	84 ± 3	86 ± 2	91 ± 6	117 ± 22[a]	87 ± 4	90 ± 10
Insulin (U/L)	4.2 ± 1.1	5.3 ± 1.1	6.8 ± 3.6	21.4 ± 22.6[a]	6.6 ± 3.5	7.9 ± 5.2
HOMA IR	1.0 ± 0.8	1.3 ± 0.8	1.5 ± 0.9	6.5 ± 6.7[a]	1.4 ± 0.8	1.8 ± 1.2
NEFA (μEq/L)	0.55 ± 0.07	0.57 ± 0.07	0.49 ± 0.19	0.45 ± 0.19	0.47 ± 0.23	0.65 ± 0.22[a]
TSH (mIU/L)	1.9 ± 0.3	2.1 ± 0.3	2.1 ± 0.7	2.5 ± 0.9[a]	1.9 ± 0.6	1.9 ± 0.7
Free T4 (ng/dL)	1.0 ± 0.0	1.0 ± 0.0	1.0 ± 0.1	1.0 ± 0.1	1.0 ± 0.1	1.0 ± 0.1
Free T3 (pg/dL)	320 ± 17	346 ± 13	299 ± 43	296 ± 47	312 ± 45	311 ± 41
Total T3 (ng/dL)	134 ± 22	139 ± 17	115 ± 29	114 ± 16	121 ± 23	117 ± 17
ACTH (pg/ml)	17 ± 9	19 ± 6	27 ± 16	156 ± 133[a]	19 ± 10	37 ± 31[a]
Cortisol (μg/dL)	12 ± 3	15 ± 5	16 ± 5	18 ± 6	14 ± 4	16 ± 5
FGF21 (pg/ml)	129 ± 76	98 ± 90	135 ± 80	102 ± 97	119 ± 79	97 ± 85

Data are presented as mean ± SD.
[a]$p < 0.05$ compared to baseline.

S1D–S1F), which has been validated against immunoblotting (Wen et al., 2013).

As exercise is the only known activator of irisin secretion, we compared cold- and exercise-induced irisin changes. The increment in irisin was similar during the two tests (Figure 2C). However, the increase in EE was significantly greater during maximal exercise, compared to cold exposure (9.8- ± 2.4-fold versus 1.5- ± 0.4-fold, $p < 0.0001$). The dissociation between irisin and EE responses suggests additional cold-specific signals, unrelated to muscle contraction, potentiating irisin secretion during shivering. As NST, mediated by BAT (Cannon and Nedergaard, 2004) and muscle (Bal et al., 2012), is activated with ST, we explored whether FGF21, a brown adipokine in rodents (Chartoumpekis et al., 2011; Hondares et al., 2011) and humans (Lee et al., 2013c), relates to shivering-induced irisin secretion.

Distinct Involvement of Irisin and FGF21 during Shivering and Nonshivering Thermogenesis

In agreement with known diurnal reduction in circulating FGF21 levels in humans (Yu et al., 2011), FGF21 concentration trended lower during all three tests (cold exposure and exercise tests) undertaken between 8:00 and 10:00 a.m. (Table 1). Greater FGF21 reduction was associated with more intense shivering, although it did not reach significance ($p = 0.08$) (Figure 2D). We interpret a greater reduction in FGF21 levels as lesser FGF21 secretion, indicating a lower NST response (Lee et al., 2013a) and leading to ST recruitment for additional heat generation. This is corroborated by a positive correlation observed between supraclavicular skin temperature (i.e., an index of BAT activity [Lee et al., 2011]) and FGF21 changes (Table S1; Figure 2F). To further substantiate our interpretation of cold-induced FGF21 secretion, we undertook two additional experiments in separate groups of subjects to characterize (1) relationships between BAT and FGF21 and (2) temperature dependency of FGF21 diurnal rhythm.

First, to elucidate whether BAT is a significant source of cold-augmented FGF21 secretion, we profiled FGF21 excursions in five men (21 ± 2 years old; BMI, 22 ± 1 kg/m^2; BF, 21% ± 2%) stratified to BAT status during 5 hr of either mildly cold, nonshivering condition (19°C) versus thermoneutrality (24°C) (Figures 2G and 2H). FGF21 diurnal reduction was blunted at 19°C in the group as a whole by 23% ± 17% ($p < 0.05$). However, the blunting effect was markedly greater in BAT-positive, compared to BAT-negative, subjects (Figures 2K and 2L), translating to a total FGF21 output more than 6-fold higher in BAT-positive individuals. Since the subjects were of similar age and leanness and differed only by BAT status, these associative

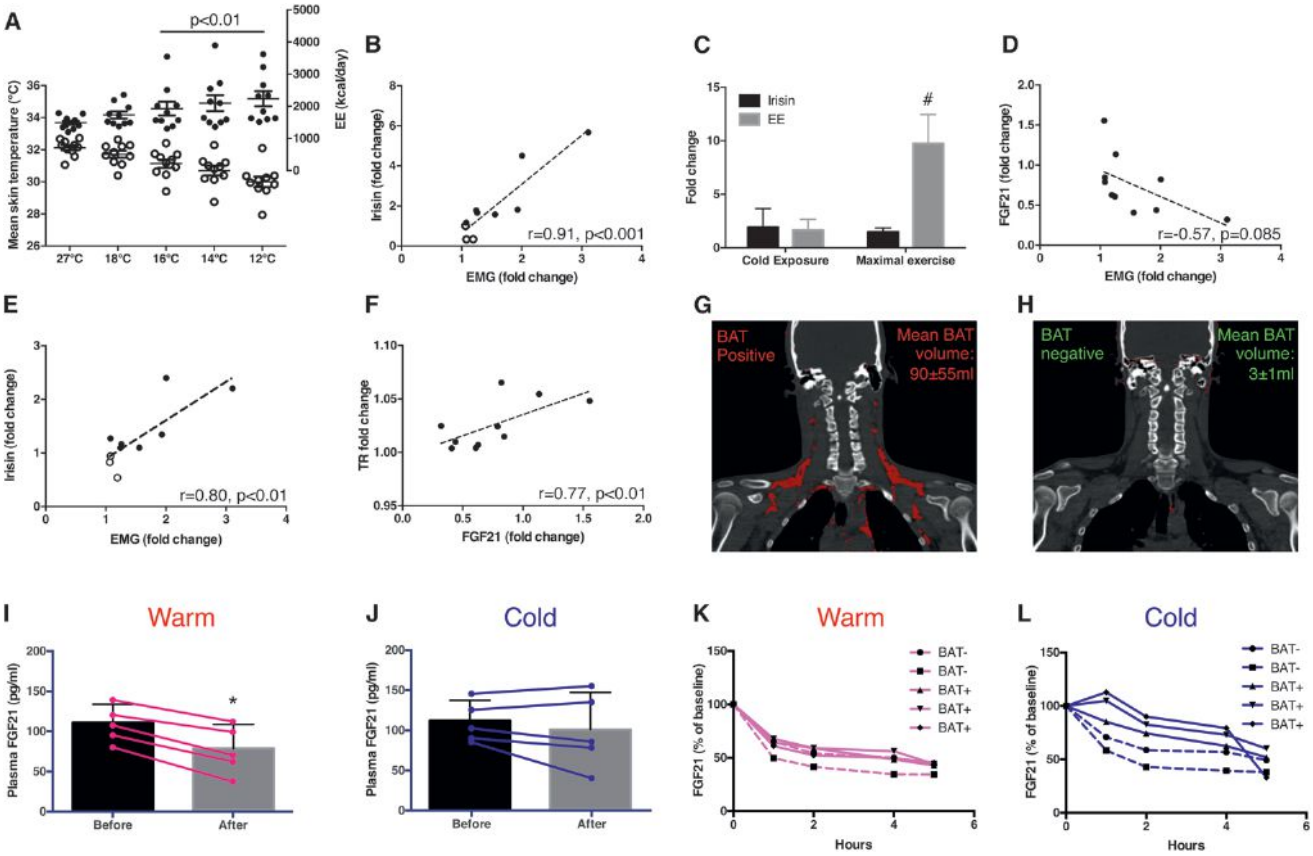

Figure 2. Relationship between Irisin, FGF21, BAT, and Temperature

Cold exposure resulted in reduction in skin temperature (open circles, A), accompanied by a rise in energy expenditure (EE) (closed circles), both reaching significance from 16°C to 12°C. Panels (B) (by immunoblot) and (E) (by ELISA) show positive associations between irisin and EMG fold changes during cold exposure. Panel (C) compares irisin and EE fold changes during cold exposure with maximal exercise test. Changes in FGF21 levels correlated negatively with shivering (D) but positively with thermogenic response (TR; difference between supraclavicular skin and chest T°C) (F). In (G) and (H), representative PET-CT images of BAT-positive (n = 3) and -negative (n = 2) individuals are shown, respectively (BAT in red). FGF21 diurnal reduction was more markedly blunted in BAT-positive (solid lines) compared to BAT-negative (dashed lines) individuals at 19°C (L) versus 24°C (K). Panels (I) and (J) compared FGF21 changes (n = 5) measured between 8 and 10 a.m. at either warm (27°C) or shivering (12°C) conditions. FGF21 reduction was significantly blunted in the cold. *p < 0.05 compared to warm condition; #p < 0.001 compared to cold exposure. Data are presented as mean ± SD.

results support BAT as a source of FGF21 during cold exposure in humans.

Second, to verify that FGF21 diurnal rhythm is indeed temperature sensitive, we measured FGF21 changes in another five men (26 ± 6 years old; BMI, 23 ± 2 kg/m^2; BF, 19% ± 3%) under the same shivering-inducing cold exposure employed in the main study but on a separate day exposed the same subjects to a warm temperature (27°), during which FGF21 was measured at matching time points. Cold exposure blunted FGF21 diurnal reduction by 28% ± 23% (p = 0.02) (Figures 2I and 2J). Pooling the results in these five subjects with the ten subjects originally studied, we observed a significant positive association between FGF21 diurnal reduction and shivering intensity (r = 0.53, p < 0.05).

Collectively, our findings indicate concerted stimulated secretion of FGF21 and irisin during NST and ST, respectively. In other words, shivering stimulates irisin secretion in a FGF21-primed milieu, through a mechanism mimicked by muscle contraction during exercise, which offers a plausible reconciliation for the paradox of why exercise, an energy-dissipating process, should stimulate the release of a thermogenic hormone.

FNDC5/FGF21 Induce Expression of Beige Gene Transcriptome in Human Neck Adipocytes

These results led us to probe the biological significance underlying enhanced irisin and FGF21 secretion during cold exposure. We hypothesize the two hormones are cold activated to boost whole-body thermogenic capacity by switching on brown-fat-like program in white fat. We thus examined in vitro the bioenergetic profiles of FNDC5- and FGF21-treated primary human adipocytes established from neck fat biopsies, a location known to be enriched with beige adipocytes.

While stimulated beige adipocytes manifest thermogenic capacity similar to that of classic brown adipocytes, they are characterized by a distinct gene signature (Cypess et al., 2013; Jespersen et al., 2013; Sharp et al., 2012; Wu et al., 2012). We therefore first determined the impact of FNDC5 and/or FGF21 treatment on classic brown and beige gene expression in human

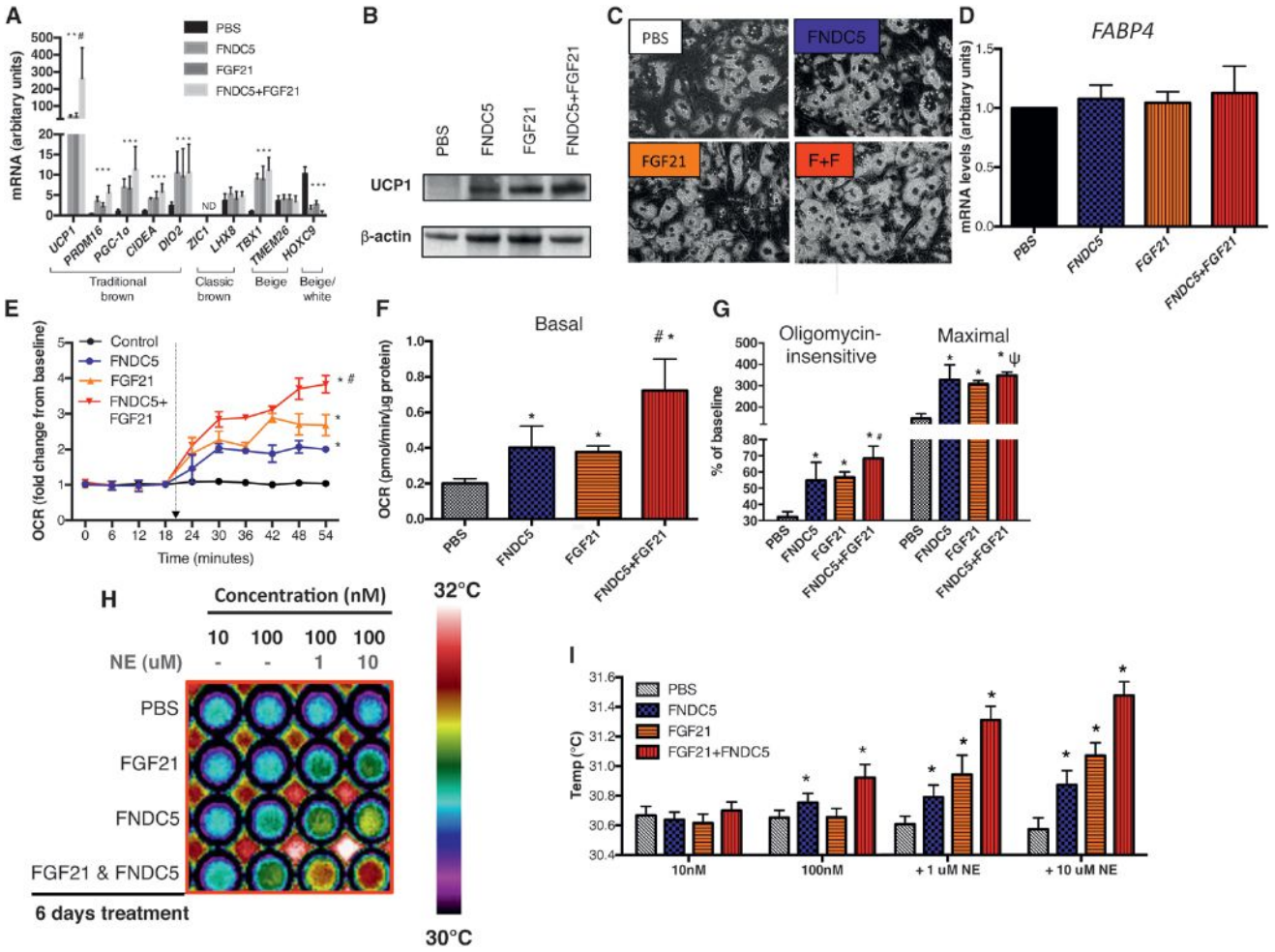

Figure 3. Effects of FNDC5 and/or FGF21 Treatment on Gene/Protein Expression and Bioenergenetics of Neck Adipocytes

(A) Effects of FGF21 and/or FNDC5 treatment on BAT/beige/white gene markers in neck adipocytes (n = 6). UCP1 protein was absent in PBS-treated adipocytes but was detected following FGF21 and/or FNDC5 treatment (B). UCP1 protein was highest in adipocytes treated with dual FGF21/FNDC5. Neck adipocytes displayed multilobulated lipid droplets (40×), similar before and after treatment (C, F+F = FNDC5+FGF21 treatment). Expression of *FABP4*, a general adipogenic gene, was not different following treatment (D). Induction of UCP1 was accompanied by upregulation of basal (F), oligomycin-insensitive, maximal uncoupled (G), and norepinephrine-induced (E) oxygen consumption, most robust in dual FGF21/FNDC5-treated adipocytes (n = 4). (H) Infrared thermographic images of adipocytes in microplates treated with PBS, FGF21, and/or FNDC5 (n = 4). The temperature scale showed color representation of temperature variation. Heat production was increased in the basal state by FNDC5 but not FGF21. Addition of norepinephrine (NE) increased heat production in increasing magnitude in FGF21-, FNDC5-, and dual FGF21/FNDC5-treated adipocytes. These results are displayed in graphical format in (I). *$p < 0.05$ compared to PBS; #$p < 0.05$ compared to FNDC5- or FGF21-treated adipocytes; $^{\Psi}p < 0.05$ compared to FGF21-treated adipocytes. Data are presented as mean ± SD.

neck adipocytes. FNDC5 and/or FGF21 treatment increased general BAT and beige gene expression without altering those belonging to the classic brown fat lineage (Figure 3A). UCP1 protein, absent in untreated adipocytes, became strongly expressed following FNDC5 and/or FGF21 treatment (Figure 3B). Pre- and posttreatment adipocytes displayed similar morphology, lipid accumulation, and general adipogenic gene expression (Figures 3C and 3D), indicating thermogenic gene upregulation was not a result of more efficient differentiation.

Bioenergetic Activation of Human Neck Adipocytes by FNDC5/FGF21

We next investigated the functional impact of FNDC5 and FGF21 on adipocyte thermogenic function. We chose a treatment duration of 6 days, as guided by previous studies reporting a reduction of shivering in cold acclimatized humans after 1 week (Davis, 1961). FNDC5 and/or FGF21 enhanced adipocyte basal oxygen consumption rate (OCR) (Figure 3F), as measured using an extracelluar fluid bioanalyzer. Pharmacological interrogation of mitochondrial respiration revealed augmentation of both forms of respiratory uncoupling (oligomycin-insensitive and maximal) by FNDC5 and FGF21 treatment (Figure 3G). To mimic cold exposure in vitro, we measured norepinephrine-induced thermogenesis. While untreated adipocytes did not respond to norepinephrine, FNDC5 and FGF21 both induced a robust increase in OCR upon norepinephrine exposure (Figure 3E) and thus recapitulated the observed cold-induced hormonal response in vivo. Combined FNDC5/FGF21 treatment produced greater

responses than either hormone alone (Figure 3). Treating adipocytes with irisin instead of FNDC5 resulted in a similar extent of fat browning on gene, protein, and functional levels (Figures S2A and S2C–S2E), consistent with previous findings in murine fat cells (Wu et al., 2012), and suggests both FNDC5 and irisin in the circulation could be biologically active at adipose tissue.

FNDC5/FGF21 Increases Human Neck Adipocyte Heat Production

As the primary function of BAT is to generate heat, we next quantified heat production from adipocytes directly by infrared thermography (IRT) (Figure S2G). FNDC5 treatment enhanced adipocyte heat production dose dependently (Figures 3H and 3I), which was further augmented by norepinephrine. In contrast, FGF21 increased heat production only after norepinephrine exposure. Additive effects were again observed following combined FNDC5/FGF21 treatment.

Taken together, these in vitro experiments provide mechanistic insight into our in vivo observations. It is conceivable that shivering-stimulated irisin, in concert with FGF21, phenotypically transforms white adipocytes to BAT-like cells to expand overall thermogenic capacity. This heat-generating hormonal response may confer an evolutionary advantage in the defense against environmental hypothermic challenges by boosting the more energy-efficient NST response over shivering.

Fat Depot-Specific Effects of FNDC5/FGF21

From a clinical perspective, a 2- to 3-fold increase in adipocyte OCR following FNDC5/FGF21 treatment, if extrapolated to the whole-body EE level, could be substantial. However, the in vivo relevance is dependent on the generalizability of our findings to other fat depots. We therefore repeated FNDC5/FGF21 experiments in primary human subcutaneous and visceral adipocytes. FNDC5/FGF21 enhanced BAT-like thermogenic program in subcutaneous but not omental adipocytes, and the magnitude of thermogenic activation was less compared to those observed in neck adipocytes (Figures S3 and S2F). Beige gene expression was either low (subcutaneous adipocytes) or absent (omental adipocytes). In rodents, irisin treatment only increased UCP1 in beige fat gene-expressing adipocytes (Wu et al., 2012). Lower or absent beige gene expression in subcutaneous and omental adipocytes may account for the modest or lack of response of these adipocytes to FNDC5/FGF21.

Metabolic Significance and Clinical Implications

Although our sample size is relatively small, our results are physiologically and clinically relevant. First, they uncover an intriguing evolutionary interconnection between exercise and shivering, juxtaposing at the muscle-fat interface through cold-induced endocrine BAT activators. As irisin levels were higher in shivering subjects, we hypothesize muscle to be the main contributor to the observed irisin rise, although adipose-derived irisin cannot be excluded (Roca-Rivada et al., 2013). Second, while the sympathetic nervous system (SNS) is the best-known mediator of CIT, recent evidence points to the existence of specific cold-induced neuroendocrine signals in animals, whose actions are highly fat specific, without undesirable global SNS activation (Villarroya and Vidal-Puig, 2013). Our study provides evidence supporting similar fat browning capacity of two of these cytokines, irisin and FGF21. Third, our irisin detection validation clarifies recent concerns over specificity of irisin immunoblotting (Erickson, 2013). Although the antibody used recognizes a peptide present in FNDC5, which is theoretically lost during irisin-specific proteolytic cleavage, it is possible that shivering induces release of FNDC5 fragments that harbor the antibody-reactive peptide. While the dynamics of irisin secretion remain to be clarified in future studies, identification of the same peptide sequence shared by circulating irisin (shown in our clinical study) and recombinant FNDC5/irisin proteins used in our in vitro experiments offers renewed perspective over controversy on the relevance of irisin in human biology (Atherton and Phillips, 2013). Fourth, our finding of fat depot-specific browning by FNDC5 suggests adipocyte browning potential may impact response to FNDC5/irisin and may account for negative results utilizing solely subcutaneous adipocytes (Raschke et al., 2013). Finally, long-term maintenance of regular exercise is challenging, and natural human tendency for thermal comfort limits cold exposure in contemporary society. Irisin and FGF21 may represent endocrine mimics of these thermogenic stimuli and are therefore potential therapeutic targets to attain weight control and to improve overall metabolic profile.

EXPERIMENTAL PROCEDURES

Clinical Studies

Healthy volunteers provided written informed consent. The NIDDK-NIAMS institutional review board approved the studies (http://clinicaltrials.gov, NCT00521729 and NCT01730105). We conducted three sets of studies. (1) Main Study consisted of three experiments: cold exposure, maximal, and submaximal exercise tests; (2) PET-CT Study involved FGF21 profiling in volunteers stratified to BAT status; and (3) Temperature Study determined temperature dependence of FGF21 diurnal rhythm.

Main Study

These tests allowed comparison of hormone/substrate profiles during active muscle contractions with cold-induced shivering. Volunteers were admitted after an overnight fast (September 2012–March 2013) for each test, performed at least 3 days apart.

Cold Exposure Test

Ten volunteers wearing hospital scrubs rested in beds in a room at 24°C. Two water-infused thermoblankets (Gaymar Medi Therm) were used to adjust rapidly temperature exposure (Figure S1A). Thirty minutes of resting EE measurement was obtained by indirect calorimetry when water temperature was at 27°C, after which it was cooled to 18°C, then further lowered by 2°C every 3 min until 12°C was reached. EE measurement continued throughout this period, and the test concluded after 5 min at 12°C. Shivering intensity was measured by surface electromyography (EMG) (Trigno, DelSys Inc.).

Exercise Tests

Maximal exercise test was performed on a mechanically braked cycle ergometer (Ergomedic 839E, Monark Exercise). A stepwise incremental exercise test was performed to assess maximal aerobic capacity (VO_{2max}) using breath-by-breath analysis. For the submaximal exercise test, volunteers cycled for 1 hr at an intensity of 40% of VO_{2max}.

Laboratory Measurements

Three blood samples were obtained during each test for hormone/substrate measurements: baseline, 5 min after the start of cooling or maximal exercise, and at the conclusion of the test. For the submaximal exercise test, samples were obtained at baseline, 30 min into, and at the end of the test. Serum irisin was measured by western blotting (Boström et al., 2012) and plasma FGF21 by enzyme immunoabsorbant assays.

PET-CT Study

Five subjects were studied after an overnight fast. They were exposed to either 24 hr of mild cold (19°C) or thermoneutral temperature (24°C). Blood samples were obtained at 08:00, 09:00, 10:00, 12:00, and 13:00, corresponding to 0, 1, 2, 4, and 5 hr after exposure to testing temperature. FGF21 levels were measured by same ELISA as in Main Study. At the end of 24 hr exposure to 19°C, each subject received a 5 mCi dose of ^{18}flurodeoxyglucose (FDG) at 08:00 and underwent PET-CT scanning.

Temperature Study

Five subjects underwent the same cold exposure study as those in Main Study. Blood samples were obtained at baseline and at the end of the cold exposure study for FGF21 measurements and correlation with shivering activity. On a separate day, subjects returned and were exposed to a constant warm temperature at 27°C for the same duration as the cold exposure testing period. Blood samples were obtained at matching time points for FGF21 measurements to directly compare with levels obtained during cold exposure.

In Vitro Studies

Adipocyte Culture

Thermogenic effects of FNDC5/FGF21 were tested on primary adipocytes established from human cervical, subcutaneous, and omental fat, as previously described (Lee et al., 2013c).

Gene/Protein Expression and Thermogenesis

Standard techniques were used for RNA/protein extraction and analysis by semiquantitative real-time PCR and immunoblotting. Cellular respiration was measured by XF24-3 extracellular flux analyzer (Seahorse Bioscience). Heat production was measured by IRT (FLIR Systems), as previously described (Lee et al., 2013c).

Additional clinical/laboratory experimental details and PET-CT scanning analytical methods are available in the Supplemental Information.

Statistical Analysis

Statistical analysis was performed using SPSS 20.0 (SPSS, Inc.). Data are expressed as mean ± SD. Comparisons between results during graded cold exposure (Main Study) and FGF21 time course (PET-CT Study) were performed using repeated-measure ANOVA with Bonferroni's correction. Paired t test was used for comparison of measurements at 24°C and 19°C. Data not normally distributed were log transformed before analysis but are presented in the text nontransformed. Pearson correlation coefficients were used to examine linear relations between variables. Areas under the curve were calculated using the trapezoidal rule. An α error of 0.05 was considered the threshold for statistical significance.

SUPPLEMENTAL INFORMATION

Supplemental Information includes Supplemental Experimental Procedures, one table, and three figures and can be found with this article at http://dx.doi.org/10.1016/j.cmet.2013.12.017.

ACKNOWLEDGMENTS

P.L. was supported by an Australian National Health Medical Research Council (NHMRC) Early Career Fellowship; the Royal Australasian College of Physicians (RACP) Foundations Diabetes Australia Fellowship and Bushell Travelling Fellowship; and the School of Medicine, University of Queensland, Australia. This study was supported by the Intramural Research Program of NIDDK, programs Z01-DK047057-02, Z01-DK071044, Z01-DK071013, and Z01-DK071014.

Received: September 6, 2013
Revised: November 20, 2013
Accepted: December 20, 2013
Published: February 4, 2014

REFERENCES

Atherton, P.J., and Phillips, B.E. (2013). Greek goddess or Greek myth: the effects of exercise on irisin/FNDC5 in humans. J. Physiol. *591*, 5267–5268.

Bal, N.C., Maurya, S.K., Sopariwala, D.H., Sahoo, S.K., Gupta, S.C., Shaikh, S.A., Pant, M., Rowland, L.A., Bombardier, E., Goonasekera, S.A., et al. (2012). Sarcolipin is a newly identified regulator of muscle-based thermogenesis in mammals. Nat. Med. *18*, 1575–1579.

Boström, P., Wu, J., Jedrychowski, M.P., Korde, A., Ye, L., Lo, J.C., Rasbach, K.A., Boström, E.A., Choi, J.H., Long, J.Z., et al. (2012). A PGC1-α-dependent myokine that drives brown-fat-like development of white fat and thermogenesis. Nature *481*, 463–468.

Cannon, B., and Nedergaard, J. (2004). Brown adipose tissue: function and physiological significance. Physiol. Rev. *84*, 277–359.

Celi, F.S., Brychta, R.J., Linderman, J.D., Butler, P.W., Alberobello, A.T., Smith, S., Courville, A.B., Lai, E.W., Costello, R., Skarulis, M.C., et al. (2010). Minimal changes in environmental temperature result in a significant increase in energy expenditure and changes in the hormonal homeostasis in healthy adults. Eur. J. Endocrinol. *163*, 863–872.

Chartoumpekis, D.V., Habeos, I.G., Ziros, P.G., Psyrogiannis, A.I., Kyriazopoulou, V.E., and Papavassiliou, A.G. (2011). Brown adipose tissue responds to cold and adrenergic stimulation by induction of FGF21. Mol. Med. *17*, 736–740.

Chen, K.Y., Brychta, R.J., Linderman, J.D., Smith, S., Courville, A., Dieckmann, W., Herscovitch, P., Millo, C.M., Remaley, A., Lee, P., and Celi, F.S. (2013). Brown fat activation mediates cold-induced thermogenesis in adult humans in response to a mild decrease in ambient temperature. J. Clin. Endocrinol. Metab. *98*, E1218–E1223.

Cypess, A.M., Lehman, S., Williams, G., Tal, I., Rodman, D., Goldfine, A.B., Kuo, F.C., Palmer, E.L., Tseng, Y.H., Doria, A., et al. (2009). Identification and importance of brown adipose tissue in adult humans. N. Engl. J. Med. *360*, 1509–1517.

Cypess, A.M., White, A.P., Vernochet, C., Schulz, T.J., Xue, R., Sass, C.A., Huang, T.L., Roberts-Toler, C., Weiner, L.S., Sze, C., et al. (2013). Anatomical localization, gene expression profiling and functional characterization of adult human neck brown fat. Nat. Med. *19*, 635–639.

Davis, T.R. (1961). Chamber cold acclimatization in man. J. Appl. Physiol. *16*, 1011–1015.

Erickson, H.P. (2013). Irisin and FNDC5 in retrospect: an exercise hormone or a transmembrane receptor? Adipocyte *2*, 289–293.

Hondares, E., Iglesias, R., Giralt, A., Gonzalez, F.J., Giralt, M., Mampel, T., and Villarroya, F. (2011). Thermogenic activation induces FGF21 expression and release in brown adipose tissue. J. Biol. Chem. *286*, 12983–12990.

Huh, J.Y., Panagiotou, G., Mougios, V., Brinkoetter, M., Vamvini, M.T., Schneider, B.E., and Mantzoros, C.S. (2012). FNDC5 and irisin in humans: I. Predictors of circulating concentrations in serum and plasma and II. mRNA expression and circulating concentrations in response to weight loss and exercise. Metabolism *61*, 1725–1738.

Jespersen, N.Z., Larsen, T.J., Peijs, L., Daugaard, S., Homøe, P., Loft, A., de Jong, J., Mathur, N., Cannon, B., Nedergaard, J., et al. (2013). A classical brown adipose tissue mRNA signature partly overlaps with brite in the supraclavicular region of adult humans. Cell Metab. *17*, 798–805.

Lee, P., Ho, K.K., Lee, P., Greenfield, J.R., Ho, K.K., and Greenfield, J.R. (2011). Hot fat in a cool man: infrared thermography and brown adipose tissue. Diabetes Obes. Metab. *13*, 92–93.

Lee, P., Brychta, R.J., Linderman, J., Smith, S., Chen, K.Y., and Celi, F.S. (2013a). Mild cold exposure modulates fibroblast growth factor 21 (FGF21) diurnal rhythm in humans: relationship between FGF21 levels, lipolysis, and cold-induced thermogenesis. J. Clin. Endocrinol. Metab. *98*, E98–E102.

Lee, P., Swarbrick, M.M., and Ho, K.K. (2013b). Brown adipose tissue in adult humans: a metabolic renaissance. Endocr. Rev. *34*, 413–438.

Lee, P., Werner, C.D., Kebebew, E., and Celi, F.S. (2013c). Functional thermogenic beige adipogenesis is inducible in human neck fat. Int. J. Obes. Published online May 10, 2013. http://dx.doi.org/10.1038/ijo.2013.82.

Petrovic, N., Walden, T.B., Shabalina, I.G., Timmons, J.A., Cannon, B., and Nedergaard, J. (2010). Chronic peroxisome proliferator-activated receptor gamma (PPARgamma) activation of epididymally derived white adipocyte cultures reveals a population of thermogenically competent, UCP1-containing

adipocytes molecularly distinct from classic brown adipocytes. J. Biol. Chem. *285*, 7153–7164.

Raschke, S., Elsen, M., Gassenhuber, H., Sommerfeld, M., Schwahn, U., Brockmann, B., Jung, R., Wisløff, U., Tjønna, A.E., Raastad, T., et al. (2013). Evidence against a beneficial effect of irisin in humans. PLoS ONE *8*, e73680.

Roca-Rivada, A., Castelao, C., Senin, L.L., Landrove, M.O., Baltar, J., Belén Crujeiras, A., Seoane, L.M., Casanueva, F.F., and Pardo, M. (2013). FNDC5/irisin is not only a myokine but also an adipokine. PLoS ONE *8*, e60563.

Saito, M., Okamatsu-Ogura, Y., Matsushita, M., Watanabe, K., Yoneshiro, T., Nio-Kobayashi, J., Iwanaga, T., Miyagawa, M., Kameya, T., Nakada, K., et al. (2009). High incidence of metabolically active brown adipose tissue in healthy adult humans: effects of cold exposure and adiposity. Diabetes *58*, 1526–1531.

Schumacher, M.A., Chinnam, N., Ohashi, T., Shah, R.S., and Erickson, H.P. (2013). The structure of irisin reveals a novel intersubunit β-sheet fibronectin type III (FNIII) dimer: implications for receptor activation. J. Biol. Chem. *288*, 33738–33744.

Sharp, L.Z., Shinoda, K., Ohno, H., Scheel, D.W., Tomoda, E., Ruiz, L., Hu, H., Wang, L., Pavlova, Z., Gilsanz, V., and Kajimura, S. (2012). Human BAT possesses molecular signatures that resemble beige/brite cells. PLoS ONE *7*, e49452.

van Marken Lichtenbelt, W.D., Vanhommerig, J.W., Smulders, N.M., Drossaerts, J.M., Kemerink, G.J., Bouvy, N.D., Schrauwen, P., and Teule, G.J. (2009). Cold-activated brown adipose tissue in healthy men. N. Engl. J. Med. *360*, 1500–1508.

Villarroya, F., and Vidal-Puig, A. (2013). Beyond the sympathetic tone: the new brown fat activators. Cell Metab. *17*, 638–643.

Virtanen, K.A., Lidell, M.E., Orava, J., Heglind, M., Westergren, R., Niemi, T., Taittonen, M., Laine, J., Savisto, N.J., Enerbäck, S., and Nuutila, P. (2009). Functional brown adipose tissue in healthy adults. N. Engl. J. Med. *360*, 1518–1525.

Wen, M.S., Wang, C.Y., Lin, S.L., and Hung, K.C. (2013). Decrease in irisin in patients with chronic kidney disease. PLoS ONE *8*, e64025.

Wrann, C.D., White, J.P., Salogiannnis, J., Laznik-Bogoslavski, D., Wu, J., Ma, D., Lin, J.D., Greenberg, M.E., and Spiegelman, B.M. (2013). Exercise induces hippocampal BDNF through a PGC-1α/FNDC5 pathway. Cell Metab. *18*, 649–659.

Wu, J., Boström, P., Sparks, L.M., Ye, L., Choi, J.H., Giang, A.H., Khandekar, M., Virtanen, K.A., Nuutila, P., Schaart, G., et al. (2012). Beige adipocytes are a distinct type of thermogenic fat cell in mouse and human. Cell *150*, 366–376.

Yoneshiro, T., Aita, S., Matsushita, M., Kayahara, T., Kameya, T., Kawai, Y., Iwanaga, T., and Saito, M. (2013). Recruited brown adipose tissue as an anti-obesity agent in humans. J. Clin. Invest. *123*, 3404–3408.

Yu, H., Xia, F., Lam, K.S., Wang, Y., Bao, Y., Zhang, J., Gu, Y., Zhou, P., Lu, J., Jia, W., and Xu, A. (2011). Circadian rhythm of circulating fibroblast growth factor 21 is related to diurnal changes in fatty acids in humans. Clin. Chem. *57*, 691–700.

Cell Metabolism
Short Article

Local Proliferation of Macrophages Contributes to Obesity-Associated Adipose Tissue Inflammation

Shinya U. Amano,[1,2] Jessica L. Cohen,[1,2] Pranitha Vangala,[1] Michaela Tencerova,[1] Sarah M. Nicoloro,[1] Joseph C. Yawe,[1] Yuefei Shen,[1] Michael P. Czech,[1,*] and Myriam Aouadi[1,*]
[1]Program in Molecular Medicine, University of Massachusetts Medical School, Worcester, MA 01605, USA
[2]These authors contributed equally to this work
*Correspondence: michael.czech@umassmed.edu (M.P.C.), myriam.aouadi@umassmed.edu (M.A.)
http://dx.doi.org/10.1016/j.cmet.2013.11.017

SUMMARY

Adipose tissue (AT) of obese mice and humans accumulates immune cells, which secrete cytokines that can promote insulin resistance. AT macrophages (ATMs) are thought to originate from bone-marrow-derived monocytes, which infiltrate the tissue from the circulation. Here, we show that a major fraction of macrophages unexpectedly undergo cell division locally within AT, as detected by Ki67 expression and 5-ethynyl-2′-deoxyuridine incorporation. Macrophages within the visceral AT (VAT), but not those in other tissues (including liver and spleen), displayed increased proliferation in obesity. Importantly, depletion of blood monocytes had no impact on ATM content, whereas their proliferation in situ continued. Treatment with monocyte chemotactic protein 1 (MCP-1) induced macrophage cell division in AT explants, whereas *mcp-1* deficiency in vivo decreased ATM proliferation. These results reveal that, in addition to blood monocyte recruitment, in situ proliferation driven by MCP-1 is an important process by which macrophages accumulate in the VAT in obesity.

INTRODUCTION

Obesity can induce an insulin-resistant state in adipose tissue (AT), liver, and skeletal muscle and is a strong risk factor for the development of type 2 diabetes (Guilherme et al., 2008; Olefsky and Glass, 2010). It is increasingly appreciated that the accumulation of macrophages and other immune cell types in AT correlates with a chronic inflammatory state that ultimately impairs adipocyte function and may contribute to the development of insulin resistance (Aouadi et al., 2013;Olefsky and Glass, 2010; Weisberg et al., 2003).

The origin of macrophages in AT has previously been attributed to the recruitment of blood monocytes into AT on the basis of one study using irradiation followed by bone marrow transplant (Weisberg et al., 2003). Therefore, strategies to decrease AT macrophage (ATM) accumulation have been particularly focused on decreasing macrophage migration into the AT by depleting blood monocytes or genes encoding chemokines that attract macrophages into the AT (Feng et al., 2011; Kanda et al., 2006; Nomiyama et al., 2007; Weisberg et al., 2006). However, studies using these approaches do not address whether migration is the only process contributing to macrophage accumulation in the AT. The present study was designed to determine whether significant macrophage cell division also occurs within visceral AT (VAT) in mice.

RESULTS AND DISCUSSION

Macrophages Proliferate Locally within the Adipose Tissue

To confirm macrophage accumulation in AT of obese mice, we used 8- to 12-week-old genetically obese (*ob/ob*) male mice and their lean control wild-type (WT) littermates. The stromal-vascular fraction (SVF) from VAT and subcutaneous AT (SAT) was stained with antibodies against macrophage markers, F4/80 and CD11b, an eosinophil marker, Siglec-F, and a neutrophil marker, Gr-1, and analyzed with flow cytometry. The macrophage population in the AT was defined as $F4/80^{+}/CD11b^{+}/Siglec\text{-}F^{-}/Gr\text{-}1^{-}$ (for the complete gating scheme, see Figure S1A available online). Consistent with published studies (Weisberg et al., 2003; Xu et al., 2003), macrophage content was significantly increased in the VAT of *ob/ob* in comparison to WT mice (*ob/ob* $959 \pm 69 \times 10^3$ versus WT $140 \pm 35 \times 10^3$ macrophages per g of VAT, $p < 0.001$; Figures 1A and 1B). The number as well as the percentage of macrophages was also increased in the SAT of *ob/ob* in comparison to WT mice but to a lower extent than in VAT (*ob/ob* $192 \pm 31 \times 10^3$ versus WT $109 \pm 12 \times 10^3$ macrophages per g of SAT, $p = 0.04$; Figure S1B). These results confirmed that macrophages accumulate mostly in the VAT in mice in response to obesity.

To test whether ATM proliferation increases in the inflammatory setting of obesity, SVF cells from WT and *ob/ob* mice were stained with an antibody against the proliferation marker Ki67, which is a protein expressed during all active phases of the cell cycle (Scholzen and Gerdes, 2000). Ki67 signal was detected in approximately 2.3% of ATMs from VAT of lean WT mice and in 10% of ATMs of *ob/ob* mice (*ob/ob* $94 \pm 7 \times 10^3$ versus WT $7.6 \pm 3.2 \times 10^3$ macrophages per g of VAT, $p < 0.001$; Figures 1C and 1D). The percentage of $Ki67^{+}$ macrophages was also increased in the SAT from *ob/ob* in comparison to WT mice (Figure S1C). However, the number of $Ki67^{+}$ macrophages was lower in SAT in comparison to VAT in *ob/ob* mice (SAT $20.0 \pm 3.3 \times 10^3$ versus VAT $94 \pm 7 \times 10^3$ macrophages per g, $p < 0.001$). This suggests that macrophages preferentially

accumulate and proliferate in the VAT of obese mice. Consistent with the flow cytometry analysis, immunofluorescence microscopy on SVF cells and VAT of *ob/ob* mice showed macrophages expressing Ki67 in their nuclei (Figures 1E and 1F). Interestingly, most of the Ki67 staining was observed in macrophages in a region of the VAT rich in macrophages termed crown-like structures (CLSs) (Figure 1F).

Similar to genetically induced obesity, diet-induced obesity increased macrophage content in the AT (Figures 1G and 1H). ATM number was significantly higher in SVF of VAT in mice fed a high-fat diet (HFD) in comparison to normal chow diet (ND) (HFD $1,045 \pm 131 \times 10^3$ versus ND $140 \pm 35 \times 10^3$ macrophages per g of VAT, $p < 0.001$). More importantly, in mice fed an HFD, 17% of ATMs were $Ki67^+$ in comparison to 3% in mice fed an ND (HFD $183 \pm 21 \times 10^3$ versus ND $7.6 \pm 3.2 \times 10^3$ macrophages per g of VAT, $p < 0.001$; Figures 1 I and 1J). Consistent with published data (Bourlier et al., 2008), and as suggested by gene expression profile analysis of human ATMs (Mayi et al., 2012), flow cytometry analysis of SVF stained with Ki67 antibody showed that approximately 8% of ATMs proliferate in AT (7.7% ± 1.9%, n = 5; Figure 1K). Altogether, with the use of flow cytometry and microscopic analysis, these results show that macrophages express the proliferation marker Ki67 in the AT in mice and humans and, to a higher degree, in response to obesity caused by either genetic manipulation or an HFD in mice.

Next, we tested whether fasting-induced weight loss also regulates ATM proliferation. After a 24 hr fast, mice lost an average of 5 percent body weight (data not shown). Although the percentage of ATM was slightly decreased, the number of ATM was significantly decreased in VAT of mice fed an HFD after a 24 hr fast (Figures 1L and 1M). Although this could be explained by a concomitant decrease in nonmacrophage cells, it has been shown that fasting induces the formation of lipid-laden macrophages attached to the adipocyte fraction (Kosteli et al., 2010). Interestingly, ATM proliferation was significantly decreased after a 24 hr fast, suggesting a correlation between macrophage content and proliferation in the AT (Figure 1N).

It is interesting to note that fasting had no effect on the proliferation of $F4/80^-/CD11b^-$ cells, which could include cell types that have been shown to proliferate in situ in the AT, including T cells (Morris et al., 2013a) and adipocyte progenitors (Lee et al., 2012) (Figure 1O). Altogether, these results suggest that changes occurring during AT mass regulation selectively affect proliferation of specific cell types in AT, including macrophages.

Obesity Stimulates Macrophage Proliferation Specifically in the Adipose Tissue

To test whether macrophage proliferation increases with obesity in tissues other than AT, we analyzed the proliferation rate of macrophages in the spleen and liver after a 3 hr pulse of the nucleoside analog to thymidine, 5-ethynyl-2′-deoxyuridine (EdU), which is incorporated into DNA only during the S phase. Approximately 1% of ATMs in lean mice and about 4.5% of the macrophages in the obese mice were in S phase during the pulse of EdU (Figure 2A), confirming that obesity increases ATM proliferation. In contrast, less than 2% of all cells, including macrophages, were EdU^+ in spleen and liver, and there was no difference in EdU^+ cells between lean and obese mice in these tissues (Figures 2B and 2C). This striking specificity for increased macrophage proliferation in AT in obesity implies that the AT microenvironment is important for macrophage proliferation.

Monocytes failed to display detectable EdU incorporation within the 3 hr pulse in lean or obese mice, suggesting that EdU^+ macrophages observed in the AT are not recently recruited blood monocytes (Figure 2D). Importantly, obesity did not affect the EdU incorporation rate in spleen, liver, or blood macrophages (Figure 2E). Interestingly, macrophage content increased with obesity in AT (Figure 1A), whereas there was no change or a slight decrease in spleen or liver in *ob/ob* mice in comparison to WT mice (Figure 2F). Furthermore, this confirms a correlation between macrophage accumulation and proliferation in tissues and suggests that AT provides a unique environment facilitating macrophage proliferation.

In order to study the selective effect of obesity on immune cell proliferation, we analyzed Ki67 staining in eosinophils and neutrophils, whose content in the AT has been shown to be regulated by obesity (Talukdar et al., 2012; Wu et al., 2011). Consistent with a prior report (Wu et al., 2011), we found that eosinophil content relative to macrophages in the AT decreased with obesity (Figures S2A–S2C). Neutrophil content in AT was not significantly different between WT and *ob/ob* mice (Figures S2D–S2F). Although both eosinophils and neutrophils have been shown to have some proliferative capacity outside of the bone marrow (Bjornson et al., 1985; Yang and Renzi, 1993), we failed to detect any EdU incorporation into these cells within AT (Figures S2C and S2F). Our results suggest that obesity does not stimulate the proliferation of all cells in the AT but selectively stimulates the proliferation of specific cell types, including macrophages.

Macrophage Proliferation Contributes to Adipose Tissue Inflammation Independently of Monocyte Recruitment

Next, to further ensure that the proliferating macrophages in the AT were not recently recruited EdU^+ blood monocytes, we studied the capacity of ATMs to proliferate ex vivo. SVF cells isolated from VAT of lean and obese mice were plated and treated with EdU for 3 hr. Approximately 0.3% of the ATMs from lean mice were EdU^+, whereas >2% were positive in macrophages from obese mice (Figures S3A and S3B). These results suggest that ATMs have the inherent capacity to proliferate ex vivo independently of blood monocyte recruitment. To test this hypothesis, we depleted blood monocytes in *ob/ob* mice by intravenous (i.v.) injection of clodronate-loaded liposomes (Clod-Lipo), which induce apoptosis once ingested by monocytes (Feng et al., 2011). Consistent with published studies, Clod-Lipo i.v. injection depleted about 80% of blood monocytes 16 hr after injection in comparison to a PBS-liposome (PBS-Lipo) injection (Figures 3A and 3B). Then, we injected *ob/ob* mice every 16 hr with Clod-Lipo in order to maintain blood monocyte depletion and measured macrophage content in the VAT. Unexpectedly, ATM absolute number (48 hr, PBS-Lipo 3.78 ± 0.37 versus Clod-Lipo 3.88 ± 0.35; 96 hr, PBS-Lipo 4.54 ± 0.60 versus Clod-Lipo 3.36 ± 0.11 $\times 10^6$ cells per g of VAT) and ATM percentage in the SVF were unchanged with Clod-Lipo treatment even after prolonged blood monocyte depletion (Figure 3C). These data raised the possibility that the increase in macrophages that occurs during obesity was largely the result of the

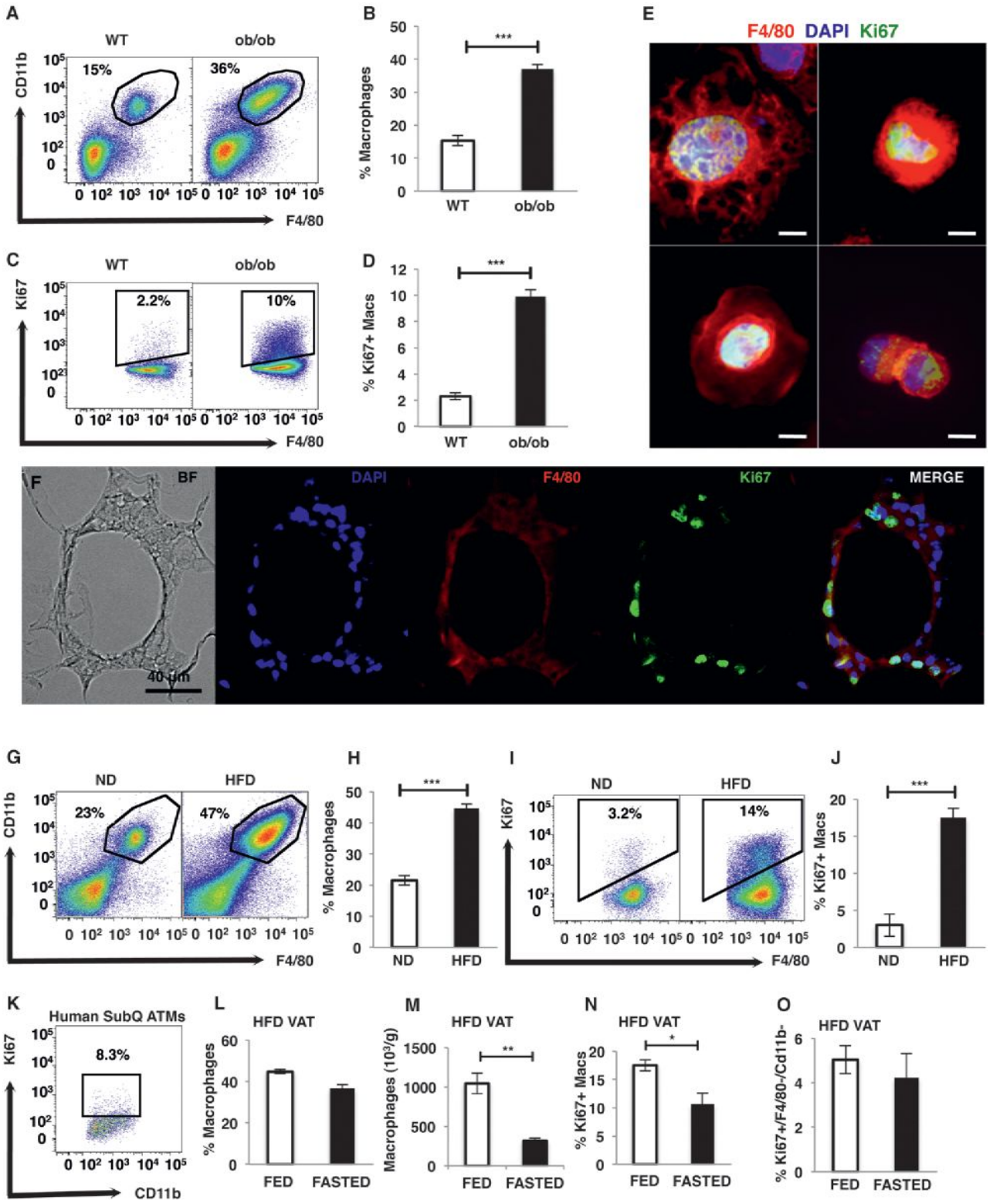

Figure 1. Adipose Tissue Macrophages Express the Cell Division Marker Ki67

SVF from VAT of WT and ob/ob mice was isolated and analyzed by flow cytometry.

(A) Representative flow cytometry dot plots.

(B) Percentage of macrophages in SVF.

(C) Representative flow cytometry dot plots of ATMs stained with Ki67.

(legend continued on next page)

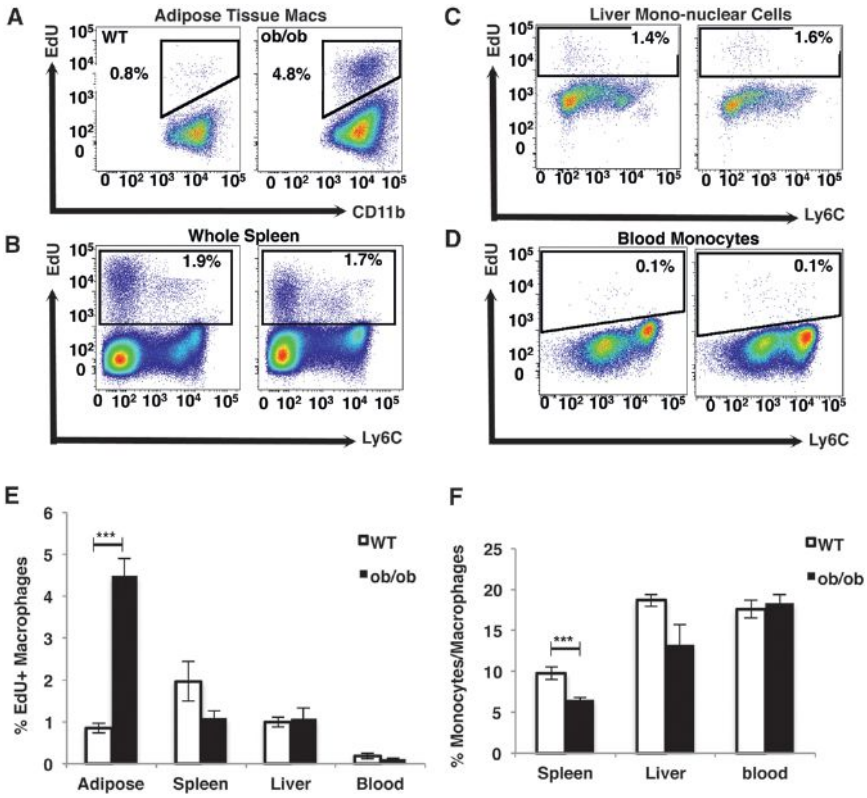

Figure 2. Obesity Increases Macrophage Proliferation Specifically in Adipose Tissue

(A–D) WT and *ob/ob* mice were intraperitoneal injected with EdU, and AT (A), spleen (B), liver (C), and blood (D) were collected and digested 3 hr after treatment. All cells were stained and analyzed by flow cytometry. Representative dot plots depict the EdU incorporation into all cells of the respective tissues or blood monocytes.

(E) Mean percentage of EdU incorporation rate of the macrophages of each tissue ± SEM.

(F) Percentage of macrophages in each tissue. n = 14–15 from three independent experiments for AT and blood, and n = 9–10 from two independent experiments for spleen and liver. Statistical significance was determined by a Student's t test. ***$p < 0.001$.

See also Figure S2.

proliferation of the resident population. Therefore, *ob/ob* mice were given EdU in drinking water during monocyte depletion, as depicted in the diagram in Figure 3D. About half of the macrophages in the AT of *ob/ob* mice injected with PBS-Lipo had incorporated EdU 80 hr after EdU exposure (Figures 3E and 3F). Importantly, the depletion of blood monocytes had no effect on macrophage proliferation, as observed by the EdU incorporation in the VAT of *ob/ob* mice injected with Clod-Lipo (Figures 3E and 3F). Interestingly, no difference in EdU incorporation was observed in macrophages in SAT of *ob/ob* in comparison to WT mice after 80 hr of EdU exposure (Figure 3G). This suggested that macrophage proliferation plays a major role in VAT macrophage expansion in obesity independently of monocyte recruitment. However, recently recruited macrophages may also proliferate in AT of obese mice, given that a recent study showed that 5% of labeled blood monocytes transferred from donor into recipient mice express Ki67 in the host AT 2 days after transfer (Oh et al., 2012).

Although macrophage subpopulations in the AT may have overlapping marker expression profiles, it is generally thought that CD11c expression is characteristic of proinflammatory macrophage subtypes (Lumeng et al., 2008). Therefore, we analyzed the rate of proliferation of proinflammatory ($CD11c^+$) and anti-inflammatory ($CD11c^-$) macrophages (Figure S3C). We failed to observe any difference in the rate of proliferation of macrophage population subtypes. This suggests that obesity increases macrophage proliferation rate independently of their inflammatory state. It has been previously shown that CLS density is higher in the VAT in comparison to SAT in obese mice (Murano et al., 2008). Interestingly, microscopic analysis of VAT sections showed that EdU was mostly incorporated in macrophages in CLS (Figure 3H). Altogether, these results suggest that ATM proliferation occurs at a high rate in the VAT, where macrophage content and CLS density are greatly increased by obesity.

(D) Percentage of macrophages expressing Ki67. n = 30–31 from six independent experiments.

(E) Microscopy of plated SVF stained with antibodies against F4/80 (red) and Ki67 (green). Nuclei were stained with DAPI (blue). 63× magnification images. The scale bar represents 5 μm.

(F) VAT of *ob/ob* mice containing CLS stained with antibodies against F4/80 (red) and Ki67 (green). Nuclei were stained with DAPI (blue). 20× magnification images. The scale bar represents 40 μm.

(G) SVF from VAT of mice fed an ND or HFD for 7 weeks was isolated and analyzed by flow cytometry. Representative flow cytometry dot plots.

(H) Mean percentage of macrophages in SVF.

(I) Representative flow cytometry dot plots of ATMs stained with Ki67.

(J) Percentage of macrophages expressing Ki67. n = 30–31 from six independent experiments.

(K) Representative dot plot of SVF from human SAT stained with Ki67.

(L) Percentage of macrophages in SVF from VAT of mice fed an HFD for 7 weeks and fasted for 24 hr. n = 8–18.

(M) Number of macrophages in SVF from VAT of mice fed an HFD and fasted for 24 hr. n = 5.

(N) Percentage of macrophages expressing Ki67 in fasted mice. n = 8–18.

(O) Percentage of nonmacrophages ($CD11b^-/F4/80^-$) expressing Ki67. n = 8–18. All graphs are expressed as mean ± SEM. Statistical significance was determined by a Student's t test. ***$p < 0.001$; **$p < 0.01$; *$p < 0.05$.

See also Figure S1.

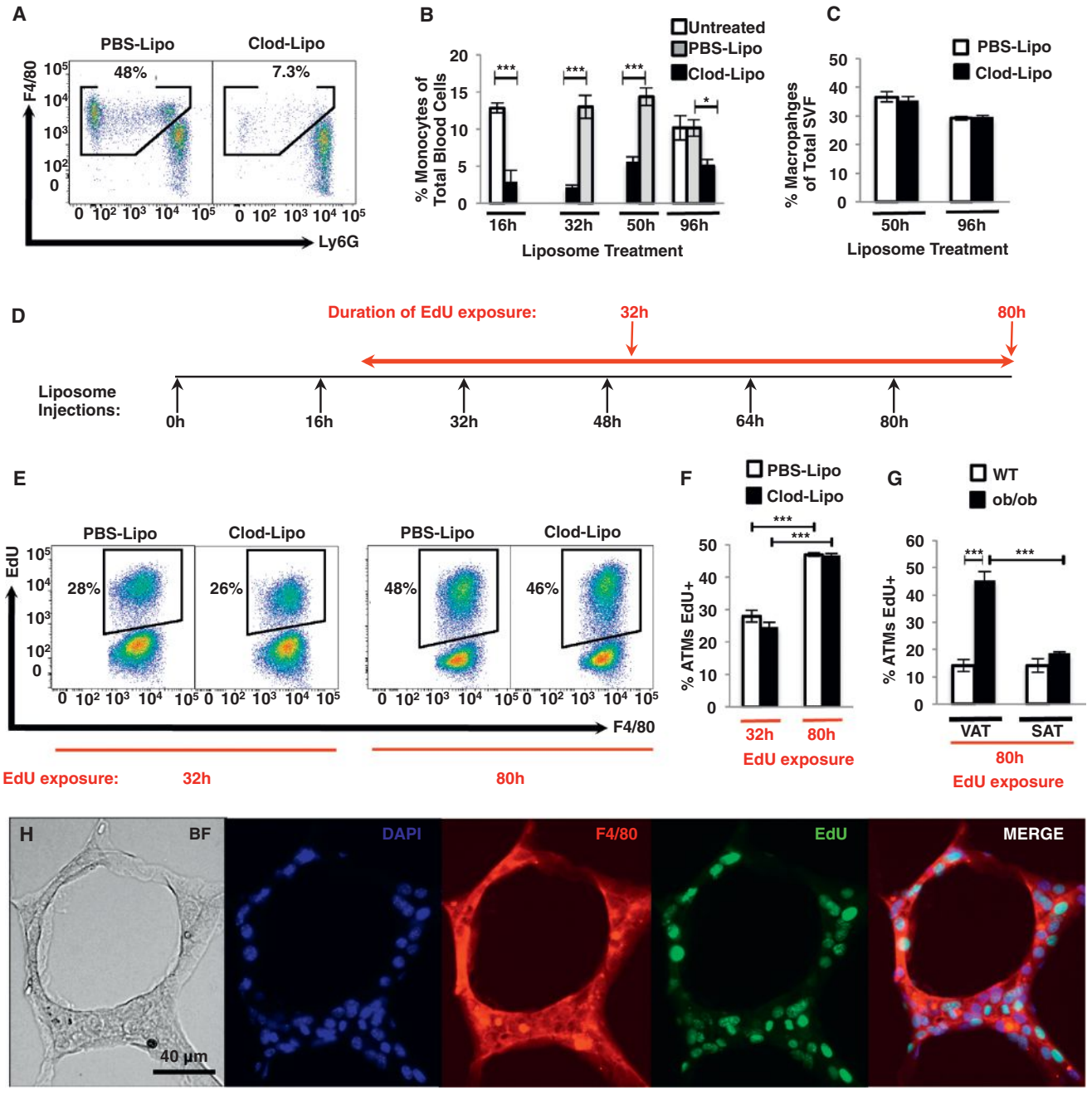

Figure 3. Adipose Tissue Macrophages Proliferate Independently of Monocyte Recruitment

(A and B) Example flow cytometry dot plots of $CD11b^{+}$ blood cells show the depletion of monocytes.

(B) The quantitation of blood monocytes expressed as a percentage of total blood cells. n = 10 for 16–48 hr of liposome treatment, and n = 4–5 for the 96 hr time point.

(C) Macrophage content in the AT of PBS-Lipo- and Clod-Lipo-treated *ob/ob* mice. n = 5 mice per group. 18 hr after initial injection, the mice were given drinking water containing EdU.

(D) Diagram representing the experimental design of the treatment.

(E and F) Representative flow cytograms (E) and quantificationn (F) of EdU incorporation into ATMs during 32 and 80 hr of exposure to EdU drinking water in PBS-Lipo-treated and monocyte-depleted Clod-Lipo-treated *ob/ob* mice.

(G) Quantification of EdU incorporation into ATMs during 80 hr of exposure to EdU drinking water in VAT and SAT in lean WT and *ob/ob* obese mice. n = 5 mice per group. All graphs are expressed as mean ± SEM. Statistical significance was determined by a Student's t test or two-way ANOVA followed by a Tukey post hoc test. ***$p < 0.001$; **$p < 0.01$; *$p < 0.05$.

(H) VAT of *ob/ob* mice containing CLS stained with antibodies against F4/80 (red) and EdU (green). Nuclei were stained with DAPI (blue). 20× magnification images. The scale bar represents 40 µm.

ob/ob mice were i.v. injected with either PBS-Lipo or Clod-Lipo every 16 hr. See also Figure S3.

MCP-1 Stimulates Adipose Tissue Macrophage Proliferation

To investigate the mechanism by which obesity stimulates macrophage proliferation selectively in the AT, we measured the expression of multiple cytokines known to play a role in macrophage proliferation and infiltration in the AT and liver of lean (ND and WT) and obese (HFD and *ob*/*ob*) mice. These included interleukin 4 (IL-4) (Jenkins et al., 2011), macrophage colony-stimulating factor (M-CSF) (Hashimoto et al., 2013), osteopontin (OPN) (Nomiyama et al., 2007), and monocyte chemotactic protein (also referred to as chemokine [C-C motif] ligand 2 [CCL2/MCP-1]) (Kanda et al., 2006; Weisberg et al., 2006) (Figures 4A–4D and S4A–S4D). Only *opn* and MCP-1 expression were significantly increased with obesity (Figures 4A–4D and S4A–S4D). As described in Figures 1 and 2, macrophage proliferation was mainly increased in VAT in obese mice compared to lean mice; therefore, we measured the expression of *opn* and *mcp-1* in this fat depot in comparison to SAT and liver, where ATM proliferation is minimal (Figures 4E and 4F). Although *opn* expression was unchanged in SAT with obesity, it was significantly increased in the liver (Figure 4E). In addition, *opn* expression was similar in liver and VAT in mice fed an HFD (Figure 4E). In contrast, *mcp-1* expression was significantly higher in VAT in comparison to liver and SAT in obese mice (Figure 4F). In addition, MCP-1 was the only cytokine that was decreased with fasting, which was consistent with a recent study (Asterholm et al., 2012) (Figures 4G and S4E). This suggests a positive correlation between *mcp-1* expression and macrophage proliferation in mice.

On the basis of the above analysis, the expression of *mcp-1* in adipocytes and SVF from VAT of mice fed an HFD was measured. Although *mcp-1* expression was high in both fractions, it was significantly higher in the adipocytes (Figure S4F). Interestingly the MCP-1 receptor, chemokine (C-C motif) receptor 2 (CCR2), has been shown to be mostly expressed in macrophages in CLS where most of proliferating ATMs were observed (Lumeng et al., 2008). These results suggest that MCP-1 released by adipocytes in CLS could stimulate the proliferation of surrounding ATMs.

In order to test whether MCP-1 regulates ATM proliferation, mice lacking the *mcp-1* gene and their WT littermates were fed an HFD and ATM content, and proliferation was measured in the VAT after 30 hr of EdU administration in drinking water (Figures 4H–4K). HFD-induced obesity significantly increased ATM content, whereas fasting decreased the percentage of macrophages in the VAT (Figures 4H and 4I). Most importantly, we observed a significant decrease in the percentage and number of macrophages in the VAT from MCP-1 knockout (KO) in comparison to WT (Figures 4H and 4I). RT-PCR analysis revealed that *emr1* and *cd11b* expression was decreased in the VAT of MCP-1 KO in comparison to WT mice fed an HFD, confirming the decreased ATM content (Figure S4G). In addition, *mcp-1* deficiency was associated with a decrease in the total number of SVF cells (WT-HFD, 1,836.78 ± 256.77 versus MCP-1 KO, 287.96 ± 74.40), suggesting a general effect of MCP-1 on immune cell accumulation in AT, as suggested in other tissues (Allavena et al., 1994; Jimenez et al., 2010). On the other hand, macrophages in the adipose tissue have been shown to play the role of antigen-presenting cells able to induce T cell proliferation (Morris et al., 2013b), suggesting that the decreased ATM accumulation observed in MCP-1 KO mice could result in decreased T cell proliferation. Interestingly, fasting had no additional effect on ATM content in MCP-1 KO, suggesting that MCP-1 could be a major regulator of macrophage content in the VAT (Figures 4H and 4I). EdU staining analysis showed that the percentage and number of EdU^+ ATMs decreases with fasting and *mcp-1* deficiency, suggesting that the decrease in ATM content observed in MCP-1 KO mice could be due to a decreased rate of proliferation (Figures 4J and 4K). Interestingly, *mcp-1* deficiency had no effect on the percentage of macrophages in liver and SAT, confirming the selective role of MCP-1 in the regulation of macrophage content in the VAT (Figure S4H).

Although MCP-1 has been shown to stimulate proliferation of multiple cell types (Hinojosa et al., 2011; Sager et al., 2010), it has been extensively described as a chemokine attracting macrophages from the blood to the AT in obese mice (Kanda et al., 2006; Weisberg et al., 2006). Thus, to test whether MCP-1 regulates ATM proliferation independently of macrophage recruitment, the monocyte content in the blood of MCP-1 KO and WT mice was analyzed (Figure 4L). We observed an increase in circulating monocytes in control mice with HFD in comparison to ND (Figure 4L), suggesting that monocyte recruitment contributes to macrophage accumulation in the AT. However, monocyte number in the blood remained the same in fed and fasted states in MCP-1 KO and WT mice, indicating that fasting-associated MCP-1 decrease or MCP-1 deficiency lowers ATM content mostly by decreasing proliferation (Figure 4L). To test this hypothesis, we measured EdU incorporation in ATM in VAT explants from *ob*/*ob* mice treated with MCP-1. Consistent with the hypothesis that MCP-1 regulates the accumulation of multiple cell types, the treatment of explants with MCP-1 ex vivo increased the total number of SVCs (untreated, 1,961.15 ± 788.00 versus MCP1 [10 ng/ml], 4,404.80 ± 353.66). Importantly, MCP-1 treatment significantly increased the number of ATMs and EdU incorporation (Figures 4M and 4N). Although proliferation may be regulated by multiple factors, MCP-1 plays a major role in regulating macrophage proliferation in the AT of obese mice independently of monocyte recruitment. However, these data do not exclude the contribution of monocyte recruitment and subsequent proliferation in the AT in obesity.

Next, body weight, glucose tolerance, and fasting glycaemia were measured in MCP-1 KO and WT mice fed an HFD in order to assess the metabolic consequences of a decreased ATM proliferation (Figures 4O–4Q). The body weight of MCP-1 KO was slightly, but not significantly, higher than WT mice fed an HFD, and both were significantly higher than WT mice fed an ND (Figure 4O). Surprisingly, although *mcp-1* deficiency led to a lower rate of macrophage proliferation in the AT and consequently a decreased ATM content, glucose intolerance was exacerbated in MCP-1 KO in comparison to WT mice (Figure 4P). Similarly, fasting blood glucose levels were significantly elevated in MCP-1 KO in comparison to WT mice (Figure 4Q). This result corroborated data from a previous study showing that MCP-1 KO mice fed an HFD are more glucose intolerant that their WT littermates (Inouye et al., 2007). However, Inouye et al. (2007) showed that macrophage content is slightly increased in the

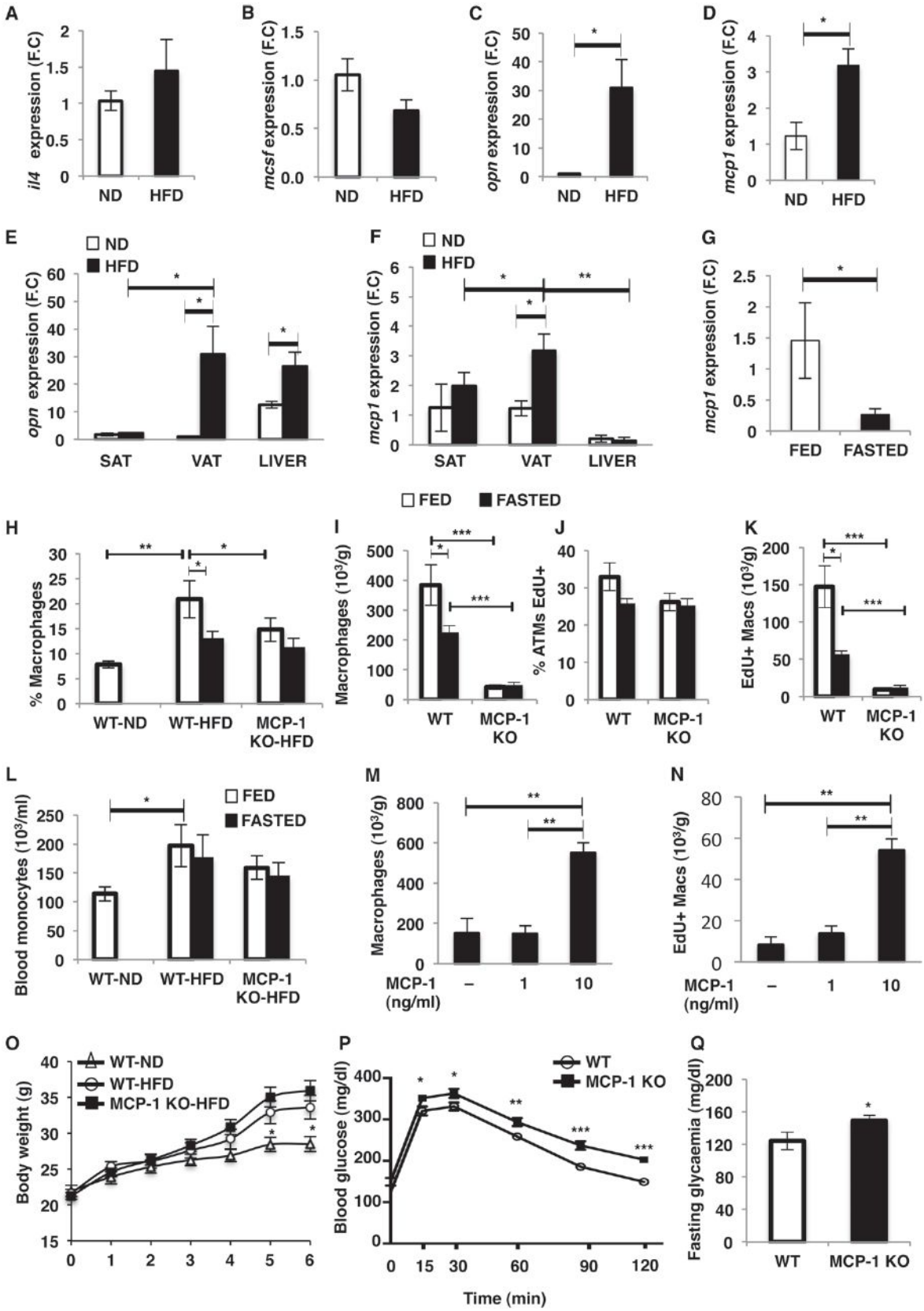

(legend on next page)

VAT of MCP-1 KO in comparison to WT mice. One of the reasons for this discrepancy could be the gating scheme used to define macrophages in the AT. In our study, macrophages were defined as F4/80$^+$/CD11b$^+$/Siglec-F$^-$/Gr1$^-$ (see the gating scheme in Figure S1) versus F4/80$^+$/CD11b$^+$, which includes eosinophils and neutrophils in Inouye et al. (2007).

Altogether, these results show that a decreased ATM proliferation is associated with exacerbated glucose intolerance. Although much of the relevant literature suggests that macrophages in AT are inhibitory to adipose function (Olefsky and Glass, 2010), some data indicate a beneficial role, for example, in increasing adipose lipid storage or clearance of dead cells in AT (Kosteli et al., 2010; Murano et al., 2008). Although MCP-1 deficiency could regulate glucose tolerance independently of an effect on ATM proliferation, such as increased body weight or decreased accumulation of multiple immune cell types, our results indicate that proliferation may be a mechanism mediating the accumulation of ATM beneficial for glucose tolerance.

In summary, we show that macrophage proliferation within VAT is a dynamic mechanism that increases with obesity and decreases during acute weight loss. Given the high proportion of macrophages (about 50%) that incorporate EdU over 80 hr, proliferation most likely contributes significantly, in addition to recruitment, to the accumulation of macrophages in the AT in obesity. At the molecular level, this study reveals MCP-1 as a potential stimulus for macrophage proliferation in obese AT.

EXPERIMENTAL PROCEDURES

Animals

We obtained 8- to 12-week-old male WT C57BL/6J and B6.V-*Lepob*/J (*ob/ob*) mice from Jackson Laboratory and maintained on a 12 hr light/dark cycle. Animals were given free access to food and water. WT C57BL/6J mice were fed an HFD (45% calories from lipids; D12451, Research Diets) for 7 weeks. All other mice were fed normal chow diet (Prolab 5P76 Isopro RMH 3000, LabDiet). We obtained 6-week-old male MCP-1 KO and WT mice on a C57BL/6J background from the Jackson Laboratory. Mice were fed an HFD (60% calories from lipids; D12492, Research Diets) for 6 weeks. All procedures were performed in accordance with protocols approved by the University of Massachusetts Medical School's Institutional Animal Care and Use Committee.

Isolation of Macrophages from Human and Mouse Adipose Tissue

All protocols were approved by the UMass Institutional Review Board. Human SAT was obtained from discarded tissue of five patients undergoing panniculectromy at UMass Memorial Hospital. Adipose tissue SVF cells were prepared from collagenase-digested adipose tissue. In brief, fat pads were digested with 2 mg/ml collagenase (Sigma-Aldrich) at 37°C for 45 min, filtered through 100 μm BD Falcon cell strainers, and spun at 300 × *g* for 10 min at room temperature. The adipocyte layer and the supernatant were aspirated, and the pelleted cells were collected as the SVF.

Liver and Spleen Cell Isolation

Liver cells were isolated as previously described (Page and Garvey, 1979). Spleens were manually dissociated, and the resultant cell suspension was centrifuged at 500 × *g*.

Flow Cytometry

For mice, cells were resuspended in PBS containing 1% BSA (fluorescence-activated cell sorting buffer) and Fc Block (eBioscience) and allowed to block nonspecific binding for 15 min at 4°C. Then, cells were counted and incubated for an additional 20 min in the dark at 4°C with fluorophore-conjugated primary antibodies or isotype control antibodies. See the Supplemental Experimental Procedures for a complete list of the antibodies used.

For the EdU experiments, cells were surface stained according to manufacturer's instructions. After incubation with primary antibodies, cells were washed and fixed with Fixation/Permeabilization Concentrate buffer (eBioscience) and then permeabilized with permeabilization buffer (eBioscience). EdU was chemically conjugated to Alexa 405 or Alexa 647 fluorophore according to the instructions of the manufacturer (Invitrogen). Sample data were acquired on a BD LSRII flow cytometer (BD Biosciences) and analyzed with FlowJo (Tree Star).

Liposome Preparation and Depletion of Blood Monocytes

PBS and clodronate-loaded liposomes were prepared in a precisely scaled-down version of a method previously described (van Rooijen and van Kesteren-Hendrikx, 2003). *ob/ob* mice were i.v. injected with 200 μl of clodronate-loaded liposomes or an equal volume of PBS-loaded liposomes every 16 hr. Small amounts of blood were taken at the end of several of the 16 hr periods and immediately before subsequent liposome injection in order to ensure that monocyte depletion was continuous. Untreated mice did not receive any injections. The mice were given drinking water containing 1 mg/ml EdU 18 hr after the initial liposome injection. ATM content and EdU incorporation into ATMs were assessed by flow cytometric analysis 32 and 80 hr after exposure to EdU drinking water.

Explants and Treatments

Pieces (1–2 mm^3) of VAT from *ob/ob* mice were treated with 10 μM EdU and 1 or 10 ng/ml of MCP-1 (Invitrogen). After 48 hr of treatment, SVF cells were isolated, counted, and analyzed by flow cytometry.

Immunohistochemistry

Adipose tissue SVF cells and sections were stained and analyzed by fluorescent microscopy as previously described (Aouadi et al., 2013).

Isolation of RNA and Real Time PCR

RNA isolation was performed according to the Trizol Reagent Protocol (Invitrogen). cDNA was synthesized from 0.5–1 μg of total RNA with an iScript cDNA Synthesis Kit (Bio-Rad) according to the manufacturer's instructions. For real-time PCR, synthesized cDNA forward and reverse primers along with the iQ SYBR Green Supermix were run on the CFX96 Touch Real-Time PCR Detection System (Bio-Rad). The ribosomal mRNA 36B4 was used as an internal loading control.

Figure 4. MCP-1 Is Required for Optimal Adipose Tissue Macrophage Proliferation

(A–D) *il4* (A), *mcsf* (B), *opn* (C), and *mcp-1* (D) expression was measured by RT-PCR. n = 5.
(E and F) Expression of *opn* (E) and *mcp-1* (F) in SAT, VAT, and liver from mice fed an ND or HFD for 7 weeks. n = 5.
(G) Expression of *mcp-1* in VAT of mice fed an HFD for 7 weeks and fasted for 24 hr.
(H and I) Percentage (H) and number (I) of macrophages in SVF from VAT of MCP-1 KO and WT mice fed an HFD for 6 weeks and fasted for 18 hr. n = 5.
(J and K) Percentage (J) and number (K) of EdU$^+$ macrophages in AT of MCP-1 KO and WT mice.
(L–N) Number of blood monocytes in MCP-1 KO and WT mice (L). Explants from VAT of five *ob/ob* mice were treated with 1 and 10 ng/ml of MCP-1 in presence of 10 μM of EdU for 48 hr. Graph represents the number of macrophages (M) and EdU$^+$ (N) macrophages in explants.
(O) Body weight of MCP-1 KO and WT mice fed an HFD for 6 weeks.
(P and Q) GTT (P) and fasting glycaemia (Q). All graphs are expressed as mean ± SEM. Statistical significance was determined by a Student's t test or two-way ANOVA followed by a Tukey post hoc test. ***p < 0.001; **p < 0.01; *p < 0.05.
VAT was isolated from mice fed am ND or HFD for 7 weeks. See also Figure S4.

Statistical Analysis

All values are shown as means ± SEM. A Student's t test for two-tailed distributions with equal variances was used for comparison between two groups. $p \leq 0.05$ was considered significant. Statistical analyses were performed with GraphPad Prism 5.

Please see the Supplemental Information for detailed experimental procedures and additional data.

SUPPLEMENTAL INFORMATION

Supplemental Information contains Supplemental Experimental Procedures and four figures and can be found with this article online at http://dx.doi.org/10.1016/j.cmet.2013.11.017.

ACKNOWLEDGMENTS

We thank Drs. S. Corvera, H. Kornfeld, S. Levitz, D. Greiner, J. Harris, and J. Virbasius and members of our laboratory group for excellent discussion of the data in this paper. We also appreciate the help of R. Konz and the staff of Flow Cytometry and Morphology Cores in the University of Massachusetts. These studies were supported by grants to M.P.C. from the NIH (DK085753 and AI046629), a grant from the International Research Alliance at Novo Nordisk Foundation Center for Metabolic Research, a grant from the JDRF (17-2009-546), and the Core Facilities in the University of Massachusetts Diabetes and Endocrinology Research Center also funded by the NIH (DK325220). J.L.C. is supported by the NIDDK of the NIH under NRSA postdoctoral fellowship F32DK098879.

Received: August 22, 2012
Revised: June 4, 2013
Accepted: November 15, 2013
Published: December 26, 2013

REFERENCES

Allavena, P., Bianchi, G., Zhou, D., van Damme, J., Jílek, P., Sozzani, S., and Mantovani, A. (1994). Induction of natural killer cell migration by monocyte chemotactic protein-1, -2 and -3. Eur. J. Immunol. *24*, 3233–3236.

Aouadi, M., Tencerova, M., Vangala, P., Yawe, J.C., Nicoloro, S.M., Amano, S.U., Cohen, J.L., and Czech, M.P. (2013). Gene silencing in adipose tissue macrophages regulates whole-body metabolism in obese mice. Proc. Natl. Acad. Sci. USA *110*, 8278–8283.

Asterholm, I.W., McDonald, J., Blanchard, P.G., Sinha, M., Xiao, Q., Mistry, J., Rutkowski, J.M., Deshaies, Y., Brekken, R.A., and Scherer, P.E. (2012). Lack of "immunological fitness" during fasting in metabolically challenged animals. J. Lipid Res. *53*, 1254–1267.

Bjornson, B.H., Harvey, J.M., and Rose, L. (1985). Differential effect of hydrocortisone on eosinophil and neutrophil proliferation. J. Clin. Invest. *76*, 924–929.

Bourlier, V., Zakaroff-Girard, A., Miranville, A., De Barros, S., Maumus, M., Sengenes, C., Galitzky, J., Lafontan, M., Karpe, F., Frayn, K.N., and Bouloumié, A. (2008). Remodeling phenotype of human subcutaneous adipose tissue macrophages. Circulation *117*, 806–815.

Feng, B., Jiao, P., Nie, Y., Kim, T., Jun, D., van Rooijen, N., Yang, Z., and Xu, H. (2011). Clodronate liposomes improve metabolic profile and reduce visceral adipose macrophage content in diet-induced obese mice. PLoS ONE *6*, e24358.

Guilherme, A., Virbasius, J.V., Puri, V., and Czech, M.P. (2008). Adipocyte dysfunctions linking obesity to insulin resistance and type 2 diabetes. Nat. Rev. Mol. Cell Biol. *9*, 367–377.

Hashimoto, D., Chow, A., Noizat, C., Teo, P., Beasley, M.B., Leboeuf, M., Becker, C.D., See, P., Price, J., Lucas, D., et al. (2013). Tissue-resident macrophages self-maintain locally throughout adult life with minimal contribution from circulating monocytes. Immunity *38*, 792–804.

Hinojosa, A.E., Garcia-Bueno, B., Leza, J.C., and Madrigal, J.L. (2011). CCL2/MCP-1 modulation of microglial activation and proliferation. J. Neuroinflammation *8*, 77.

Inouye, K.E., Shi, H., Howard, J.K., Daly, C.H., Lord, G.M., Rollins, B.J., and Flier, J.S. (2007). Absence of CC chemokine ligand 2 does not limit obesity-associated infiltration of macrophages into adipose tissue. Diabetes *56*, 2242–2250.

Jenkins, S.J., Ruckerl, D., Cook, P.C., Jones, L.H., Finkelman, F.D., van Rooijen, N., MacDonald, A.S., and Allen, J.E. (2011). Local macrophage proliferation, rather than recruitment from the blood, is a signature of TH2 inflammation. Science *332*, 1284–1288.

Jimenez, F., Quinones, M.P., Martinez, H.G., Estrada, C.A., Clark, K., Garavito, E., Ibarra, J., Melby, P.C., and Ahuja, S.S. (2010). CCR2 plays a critical role in dendritic cell maturation: possible role of CCL2 and NF-kappa B. J. Immunol. *184*, 5571–5581.

Kanda, H., Tateya, S., Tamori, Y., Kotani, K., Hiasa, K., Kitazawa, R., Kitazawa, S., Miyachi, H., Maeda, S., Egashira, K., and Kasuga, M. (2006). MCP-1 contributes to macrophage infiltration into adipose tissue, insulin resistance, and hepatic steatosis in obesity. J. Clin. Invest. *116*, 1494–1505.

Kosteli, A., Sugaru, E., Haemmerle, G., Martin, J.F., Lei, J., Zechner, R., and Ferrante, A.W., Jr. (2010). Weight loss and lipolysis promote a dynamic immune response in murine adipose tissue. J. Clin. Invest. *120*, 3466–3479.

Lee, Y.H., Petkova, A.P., Mottillo, E.P., and Granneman, J.G. (2012). In vivo identification of bipotential adipocyte progenitors recruited by β3-adrenoceptor activation and high-fat feeding. Cell Metab. *15*, 480–491.

Lumeng, C.N., DelProposto, J.B., Westcott, D.J., and Saltiel, A.R. (2008). Phenotypic switching of adipose tissue macrophages with obesity is generated by spatiotemporal differences in macrophage subtypes. Diabetes *57*, 3239–3246.

Mayi, T.H., Daoudi, M., Derudas, B., Gross, B., Bories, G., Wouters, K., Brozek, J., Caiazzo, R., Raverdi, V., Pigeyre, M., et al. (2012). Human adipose tissue macrophages display activation of cancer-related pathways. J. Biol. Chem. *287*, 21904–21913.

Morris, D.L., Cho, K.W., Delproposto, J.L., Oatmen, K.E., Geletka, L.M., Martinez-Santibanez, G., Singer, K., and Lumeng, C.N. (2013a). Adipose tissue macrophages function as antigen-presenting cells and regulate adipose tissue CD4+ T cells in mice. Diabetes *62*, 2762–2772.

Morris, D.L., Cho, K.W., Delproposto, J.L., Oatmen, K.E., Geletka, L.M., Martinez-Santibanez, G., Singer, K., and Lumeng, C.N. (2013b). Adipose tissue macrophages function as antigen-presenting cells and regulate adipose tissue CD4+ T cells in mice. Diabetes *62*, 2762–2772.

Murano, I., Barbatelli, G., Parisani, V., Latini, C., Muzzonigro, G., Castellucci, M., and Cinti, S. (2008). Dead adipocytes, detected as crown-like structures, are prevalent in visceral fat depots of genetically obese mice. J. Lipid Res. *49*, 1562–1568.

Nomiyama, T., Perez-Tilve, D., Ogawa, D., Gizard, F., Zhao, Y., Heywood, E.B., Jones, K.L., Kawamori, R., Cassis, L.A., Tschöp, M.H., and Bruemmer, D. (2007). Osteopontin mediates obesity-induced adipose tissue macrophage infiltration and insulin resistance in mice. J. Clin. Invest. *117*, 2877–2888.

Oh, D.Y., Morinaga, H., Talukdar, S., Bae, E.J., and Olefsky, J.M. (2012). Increased macrophage migration into adipose tissue in obese mice. Diabetes *61*, 346–354.

Olefsky, J.M., and Glass, C.K. (2010). Macrophages, inflammation, and insulin resistance. Annu. Rev. Physiol. *72*, 219–246.

Page, D.T., and Garvey, J.S. (1979). Isolation and characterization of hepatocytes and Kupffer cells. J. Immunol. Methods *27*, 159–173.

Sager, H.B., Middendorff, R., Rauche, K., Weil, J., Lieb, W., Schunkert, H., and Ito, W.D. (2010). Temporal patterns of blood flow and nitric oxide synthase expression affect macrophage accumulation and proliferation during collateral growth. J Angiogenes Res *2*, 18.

Scholzen, T., and Gerdes, J. (2000). The Ki-67 protein: from the known and the unknown. J. Cell. Physiol. *182*, 311–322.

Talukdar, S., Oh, Y., Bandyopadhyay, G., Li, D., Xu, J., McNelis, J., Lu, M., Li, P., Yan, Q., Zhu, Y., et al. (2012). Neutrophils mediate insulin resistance in mice fed a high-fat diet through secreted elastase. Nat. Med. *18*, 1407–1412.

van Rooijen, N., and van Kesteren-Hendrikx, E. (2003). "In vivo" depletion of macrophages by liposome-mediated "suicide". Methods Enzymol. *373*, 3–16.

Weisberg, S.P., McCann, D., Desai, M., Rosenbaum, M., Leibel, R.L., and Ferrante, A.W., Jr. (2003). Obesity is associated with macrophage accumulation in adipose tissue. J. Clin. Invest. *112*, 1796–1808.

Weisberg, S.P., Hunter, D., Huber, R., Lemieux, J., Slaymaker, S., Vaddi, K., Charo, I., Leibel, R.L., and Ferrante, A.W., Jr. (2006). CCR2 modulates inflammatory and metabolic effects of high-fat feeding. J. Clin. Invest. *116*, 115–124.

Wu, D., Molofsky, A.B., Liang, H.E., Ricardo-Gonzalez, R.R., Jouihan, H.A., Bando, J.K., Chawla, A., and Locksley, R.M. (2011). Eosinophils sustain adipose alternatively activated macrophages associated with glucose homeostasis. Science *332*, 243–247.

Xu, H., Barnes, G.T., Yang, Q., Tan, G., Yang, D., Chou, C.J., Sole, J., Nichols, A., Ross, J.S., Tartaglia, L.A., and Chen, H. (2003). Chronic inflammation in fat plays a crucial role in the development of obesity-related insulin resistance. J. Clin. Invest. *112*, 1821–1830.

Yang, J.P., and Renzi, P.M. (1993). Interleukin-2 and lymphocyte-induced eosinophil proliferation and survival in asthmatic patients. J. Allergy Clin. Immunol. *91*, 792–801.

Introducing the China Gateway

The home for Chinese scientists

The new Cell Press China Gateway is the ultimate destination for Chinese scientists. Now highlights of the latest research, regional events, and featured content from Cell Press are accessible online, on a single webpage.

The Cell Press China Gateway was designed with you in mind. We hope you'll make yourself at home.

Visit us at **www.cell.com/china**

CellPress

SnapShot: Sirtuins, NAD, and Aging

Takashi Nakagawa[1] and Leonard Guarente[2]
[1]Frontier Research Core for Life Sciences, University of Toyama, Toyama 930-0194, Japan
[2]Paul F. Glenn Laboratory for the Science of Aging and Department of Biology, and The Koch Institute, Massachusetts Institute of Technology, Cambridge, MA 02139, USA

Cell Metabolism

TARGETS OF SIRTUINS

nucleus cytoplasm mitochondria

SIRT6

cMyc	CtIP
H3K9	GCN5
H3K56	SNF2H
HIF1α	G3BP
NF-κB	FoxO3
TNFα	PARP1
SREBP1/2	

SIRT1

H3K9	HDAC1	PPARα	HNF4α	Rb	TFAM	eNOS	Atg7
H3K56	PGC1α	PPARγ	HIF1α	NBS1	NF-κB	LKB1	Atg8
H4K16	FoxO1	LXR	HIF2α	XPA	MyoD	Smad7	14-3-3ζ
H1K26	FoxO3a	FXR	PARP1	WRN	Nhlh2	β-catenin	PGAM1
Suv39h1	Foxa2	RARβ	p53	CREB	cMyc	Survivin	AceCS1
p300	CRTC1	SREBP1c	Ku70	Nkx2-1	UCP2	Akt	PTP1B
PCAF	CRTC2	SREBP2	E2F1	STAT3	TSC2	Atg5	S6K1

SIRT7

cMyc	CUL4B
H3K18	ELK4
PAF53	RNA Pol I
HIF1α	Mybbp1a
HIF2α	TFIIIC2
DCAF1	mTOR
DDB1	p53

SIRT4

GDH
MCD
IDE
SLC25A5

SIRT3

LCAD	AceCS2	OTC
VLCAD	GDH	CypD
HMGCS2	IDH2	OPA1
NDUFA9	MRPL10	PDH
Skp2	PDP1	FoxO3
SDHA	SOD2	

SIRT5

CPS1
HMGCS2
PDH
SDH
SOD1

SIRT2

H4K16	NF-κB
H3K56	HIF1α
H3K18	CDK9
FoxO1	Cdc20
FoxO3a	APC
p300	

SIRT2

Tubulin	Keratin8
G6PD	PRLR
LDH	MEK1
PEPCK1	ITPK1
ACYL	S6K1
Par3	

	Enzymatic Activities	Physiological Functions
SIRT1	Deacetylase ADP-ribosylase (weak)	SIRT1 orthologs extend life span in yeast, worms, flies, and mice. SIRT1 also protects against metabolic disorders, such as obesity, insulin resistance, and hepatic steatosis, as well as aging-related neuronal diseases, by deacetylating histones and many transcription factors and cofactors.
SIRT2	Deacetylase	SIRT2 primarily resides in cytoplasm but also relocates to nucleus upon stress and during mitosis. Nuclear SIRT2 deacetylates histones and various transcription factors and regulates cell-cycle progression and cell differentiation. SIRT2 also regulates various metabolic enzymes in the cytosol.
SIRT3	Deacetylase	The major mitochondrial deacetylase SIRT3 affects acetylation of hundreds of mitochondrial proteins and regulates many metabolic enzymes through deacetylation, including LCAD (β-oxidation). SIRT3 KO mice develop hepatic steatosis and insulin resistance on high-fat diet. SIRT3 also acts as a tumor suppressor by reducing ROS and its loss reprograms cellular metabolism in various human cancers.
SIRT4	Deacetylase (malonyl CoA decarboxylase) ADP-ribosylase	SIRT4 is involved in amino acid metabolism by ADP-ribosylating GDH. SIRT4 KO mice manifest hyperinsulinemia due to the constitutive activation of GDH. SIRT4 is also a tumor suppressor and regulates glutamine metabolism in cancer cells via GDH. SIRT4 KO mice are prone to lung cancer.
SIRT5	Deacylase (Succinyl, malonyl, glutaryl groups) Deacetylase (weak)	Loss of SIRT5 leads to hypersuccinylation and malonylation of mitochondrial proteins and inhibition of β-oxidation and ketogenesis. SIRT5 KO mice also manifest elevated ammonia level due to the lack of CPS1 activation during fasting.
SIRT6	Deacylase (long-chain fatty acyl groups) Deacetylase (weak) ADP-ribosylase (weak)	Overexpression of SIRT6 extends life span in mice. Deletion of SIRT6 results in hypoglycemia and aging-like phenotypes in mice, including lymphopenia, kyphosis, and loss of fat pads. SIRT6 has various roles in transcription, genome stability, and metabolic regulation. SIRT6 efficiently removes long-chain fatty acids from lysine and thus promotes TNFα secretion. SIRT6 acts as a corepressor for HIF-1α and cMYC and, thus, inhibits tumorigenesis.
SIRT7	Deacetylase	In cancer cells, SIRT7 deacetylates H3K18 and represses the transcription of tumor-suppressor genes. SIRT7 is also involved in lipid metabolism, and SIRT7 KO mice are resistant to diet-induced obesity and fatty liver.

NAD METABOLISM

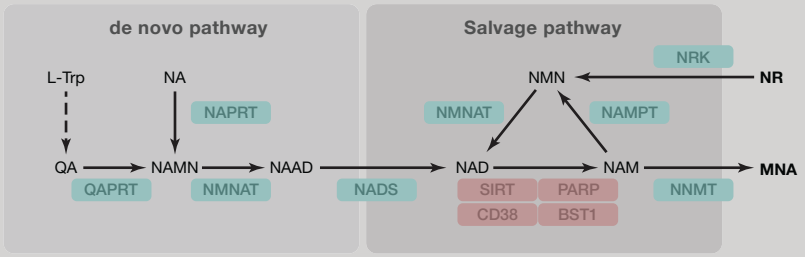

Enzymes	Physiological functions
Nampt	Insulin secretion, Circadian rhythm, Cancer metabolism
Nmnat1	Leber congenital amaurosis Wallerian degeneration
Nmnat2	Axonal development Protection from axonal injury
Nmnat3	Hemolytic anemia Protection from axonal injury
NNMT	Obesity, Tumorigenesis Longevity in *C. elegans*
CD38	Immune response Oxytocin secretion

 DOI http://dx.doi.org/10.1016/j.cmet.2014.06.001

See online version for legends and references

With Cell Press Reviews

Insight and perspective is a powerful combination. That's why we offer readers a critical examination of the evidence that provokes thought and facilitates discussion within scientific communities.

To propel your research forward, faster, turn to Cell Press Reviews. Our insightful, authoritative reviews—published across the life sciences in our primary research and *Trends* journals—go beyond synthesis and offer a point of view.

Find your way with Cell Press Reviews

www.cell.com/reviews

CellPress
Your work is our life

Develop a greater understanding of

THE ROLE OF CELL METABOLISM IN

aging and neurodegenerative diseases

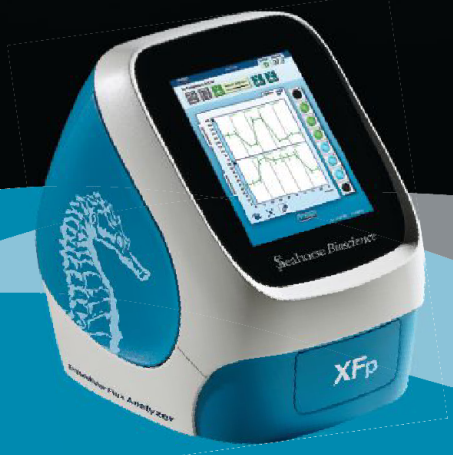

The Seahorse XFp Extracellular Flux Analyzer

The compact XFp Analyzer is built on innovative and proven XF technology, and is ideal for use in **pairwise comparisons**, **phenotyping** and with **patient-derived samples**. The XFp Analyzer delivers the Gold Standard assays that are providing scientists with the necessary functional data that is enabling a greater understanding of cell metabolism.

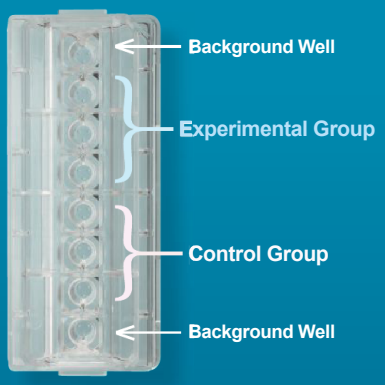

See what's possible.

Scan this QR code to view videos and see what the XF technology can achieve. Visit www.seahorsebio.com/cellmetab for more information!

Seahorse *Bioscience*